Breakup of the Gondwana supercontinent: East African perspectives from the Early Jurassic to Cretaceous

PHETHEAN, JORDAN,JERAD,JOHN

Breakup of the Gondwana supercontinent: East African perspectives from the Early Jurassic to Cretaceous

Durham University

Jordan Jerad John Phethean

A thesis submitted in partial fulfilment of the requirements for the degree of Doctor of Philosophy at Durham University

Department of Earth Sciences

October, 2017

Abstract

Accurate mapping of first-order tectonic features such as oceanic fracture zones and continental margins is vital for the production of reliable plate reconstructions. These reconstructions allow for a better understanding of the palaeo-configuration of continental fragments within Gondwana and ultimately provide insight into how and why supercontinents break apart. Detection of spreading lineaments within the heavily sedimented Western Somali Basin (WSB) has been achieved using a novel technique based on directional derivatives of free-air gravity. This new lineament dataset allows for the construction of a high-resolution plate tectonic reconstruction of the WSB, which is in good agreement with ocean magnetic data and the position of the abandoned WSB spreading centre. The model also reveals a change in spreading direction, from NNW-SSE to N-S, during the Late Jurassic. This controversial spreading direction change places the origin of Madagascar within the Tanzania Coastal Basin (TCB), inboard of the Davie Fracture Zone (DFZ), which was previously believed to be the continent-ocean transform margin of the WSB. This tight-fit of Gondwana fragments prior to continental breakup necessitates a reassessment of both the crustal nature of the TCB, which is shown to be partly oceanic in nature, and of the nature of the margins surrounding the WSB. The northern margins of the WSB are likely orthogonally rifted margins. However, the western margins are likely highly segmented and/or obliquely rifted margins. The model also predicts a large transform offset along the Rovuma Basin.

Systematic gravity modelling and combined seismic investigations along the Rovuma basin reveals the 'Rovuma Transform Margin', which offsets the obliquely rifted margins of northeast Mozambique and Tanzania. The discovery of this transform margin confirms the initial SSE plate motion predicted from gravity lineament analysis and plate reconstructions, and shows that the breakup of the Gondwana supercontinent occurred not just along pre-existing lithospheric weaknesses associated with the Karoo rift system, but also along newly developed highly oblique deformation zones as well. The final breakup of the Gondwana supercontinent, which followed extensive and episodic Karoo aged rifting, was coincident with extensive magmatism in Mozambique and may therefore have been triggered by the interaction of several facilitators of continental breakup (i.e. oblique rifting, pre-existing weaknesses, and magmatism).

The oblique breakup of Gondwana along the TCB led to the development of a segmented mid-ocean ridge system within this basin, offset by SSE trending fracture zones. These fracture zones were incompatible with the N-S spreading that followed the Late Jurassic change in plate motion, resulting in the abandonment of mid-ocean ridge segments and compression within this basin. This compression led to the formation of the 250 km long Tanzania Coastal Basin thrust belt, the largest intraplate oceanic thrust belt yet discovered. The cessation of compression within the TCB followed the development of the DFZ, which propagated from south to north. This structure was subsequently dominated by transpression throughout its history, suggesting it was not perfectly compatible with plate driving forces. Formation of the DFZ along aligned weak rifted margins and young oceanic crust may have resulted in the mismatch of plate motions and driving forces, and also suggests a first order 'top-down' control on plate motions during the breakup of Gondwana.

Contents

List of figures

Declaration

I declare that this thesis, which I submit for the degree of Doctor of Philosophy at Durham University, is my own work and not substantially the same as any which has previously been submitted at this or any other university.

Jordan J. J. Phethean

Durham University

October 2017

Signed: ________________

Jordan Phethean

Date: ________________

Acknowledgements

I am very thankful to my supervisory team, whose endless support, encouragement, and expert training has enabled me to make it this far. Firstly, I would like to give special thanks to Jeroen van Hunen for his truly invaluable guidance and advice in all matters, both academic and beyond. In all circumstances, Jeroen makes time for his students and without his constant positive outlook some obstacles would have seemed unsurmountable. I would also like to thank Lara Kalnins for taking me under her wing and providing me with outstanding technical guidance when it was needed most. She is an exceptional and rigorous scientist, whose input has improved the quality of my work to no end. Thanks also go to Ken McCaffrey for his academic insights, which are always delivered with a chuckle, and to Paolo G. Biffi for his great observations and ability to keep my best interests at heart. Finally, I would like to thank Richard Davies for believing in me and for his endless 'can-do' attitude that led to this project.

I would also like to thank my friends and colleagues at ENI who made me feel so welcome in a place so far from home, particularly Dorina Testi.

Colin Reeves and David Boote provided insightful discussions, which proved extremely useful to me, and I hope they continue in the coming years.

Special thanks go to my parents, John and Kath, whose encouragement, guidance, and help throughout my life has helped me reach where I am today. I would also like to thank my Nana, Grandad, Aunti Guina, and Uncle Donald for their support both before and during this project. My brother James, niece Beth, and Jade are thanked for the good times gone and those yet to come.

I would like to thank my friends in Durham and elsewhere for their kindness and for making life so much fun. The list is large, and you know who you are, so I'm going to spare us all. However, in particular I would like to thank Alex Peace, Bob Jamieson, Chris Harbord, Matt Keeves, Kate Horan and Sarah Clancy, with whom I have a particularly large number of fond memories.

1. Introduction

1.1. Motivation and methods summary

Rifted margins are of significant interest as they provide insight into the causes and mechanisms of supercontinent breakup (e.g. Bercovici and Long, 2014). But besides this academic interest, they have also provided a reliable worldwide source of hydrocarbon resources for over 30 years (Levell et al., 2010) and economic and political forces have recently driven a strong shift towards the exploration of deep-water (500-2500 m below sea level) regions of these margins (White et al., 2003). A wealth of research, focused on the evolution of volcanic and magma-poor rifted margins (e.g. Afilhado et al., 2008; Brune et al., 2013; Geoffroy et al., 2015; Manatschal, 2004; Reston and Mcdermott, 2014), shows that the extent of continental crust and the nature of the continent-ocean transition in these deep-water settings are highly variable (e.g. Stab et al., 2016; Unternehr et al., 2010), and have strong impacts on the presence and maturation of source rocks (e.g. Waples, 2002). Transform margins, on the other hand, have been relatively poorly studied (Mercier de Lépinay et al., 2016) and, in the past, have not presented a major target for the hydrocarbon industry. The 2007 discovery of the Jubilee field along the West Africa transform margin (Dailly et al., 2013), however, opened up a new play type and dramatically increased interest in transform margins. East Africa is, at a basic level, understood to represent such a transform margin, and as such new interest in the region is rapidly growing. However, the details of kinematic and dynamic margin development, as well as the extent of continental crust is poorly understood along the East African margins and at transform margins in general.

Reducing these uncertainties invites further interest in the exploration of the East African rifted margins for hydrocarbon resources, and is crucial for the successful discovery and development of said resources. In order for East Africa to benefit economically from its potential natural resources, and to allow associated benefits of development opportunities, stability, and prosperity to East Africa, it is therefore necessary to constrain these unknowns.

Plate motions during Gondwana disassembly, and the initial configuration of continental fragments and deformation zones in Gondwana, are a matter of particular controversy (e.g. Bunce and Molnar, 1977; Coffin and Rabinowitz, 1987; Davis et al., 2016; Gaina et al., 2013; Klimke et al., 2017; Lawver and Scotese, 1987; Norton and Sclater, 1979; Pinna, 1995; Project, 2015; Reeves, 2014; Scrutton et al., 1981; Sègoufin and Patriat, 1980;

Shackleton, 1996; Smith and Hallam, 1970; Windley et al., 1994), and so the development of accurate and reliable plate tectonic models for the region is fundamental before more detailed understanding of the margin can be attempted. In order to constrain the plate motions during the disruption of Gondwana we apply novel processing techniques to recently available and highly accurate marine satellite gravity data. This successfully allows us to develop a highly accurate plate reconstruction for the region that, due to the nature of continental margins being dependant on plate motions relative to zones of lithospheric deformation (e.g. Basile and Braun, 2016), indicates which styles of continental margin should develop along different regions of the East Africa coast; a crucial step in the development of our understanding of this enigmatic region.

The extent of continental crust along rifted margins is another key parameter in resource prospectivity, however, is not well constrained by such kinematic plate tectonic reconstructions. We therefore also perform rigorous 2D gravity modelling of the margin structure to locate the boundary between oceanic and continental crust. This confirms the proposed natures of the East African margins gained from Plate tectonic modelling.

Finally, in order to better understand transform margin development in general, which can not only reduce risk and interest in the study region but can also contribute to our understanding of transform margins worldwide, we perform a detailed study of the structural development of this margin through the interpretation of high quality deep imaging seismic reflection data. This interpretation allows for a model of the development of the East African margins to be constructed, which bears strong similarities to other transform systems worldwide (e.g. Whittaker et al., 2016; Schiffer et al., 2017) and may therefore contribute to a unified understanding of transform margin processes.

1.2. Plate tectonics, the Wilson cycle, and what drives them

The theory of plate tectonics was formulated in 1968 (Morgan, 1968) and is one of the fundamental principles on which the work presented herein relies. The roots of this theory, however, lie much earlier.

As early as 1596, the ‘lock and key’ geometry of Africa-Europe and America (Figure 1.1) was noted by the Flemish-Dutch cartographer Abraham Ortelius in ‘Thesaurus Geographicus’ (Ortelius, 1596). He went on to propose that the continents were “torn away…by earthquakes and floods”. This remarkable insight was, however, ahead of its time and it was not until 1912 that the German meteorologist Alfred Wegener developed the hypothesis for ‘continental drift’. Importantly, Wegener used observations from the geologic, climatic, fossil, and palaeo-topographic records to support the argument for an original connection of the continents in his seminal work ‘Die Entstehung der Kontinente’ (‘The Origin of the Continents’) (Wegener, 1912).

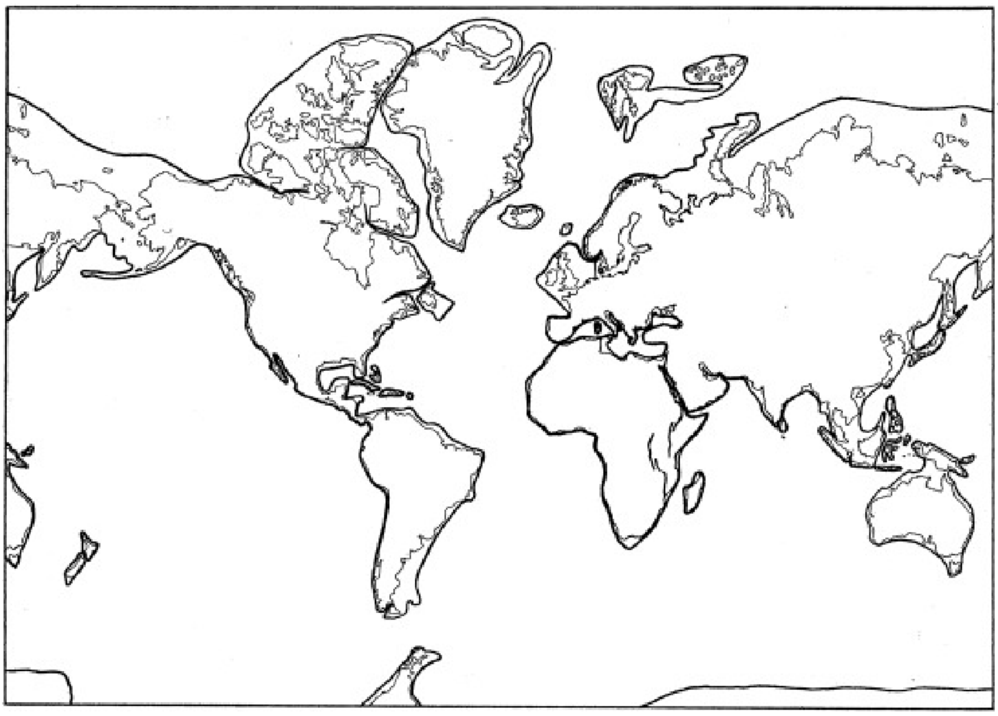

Figure 1.1. Known distribution of landmasses (thin black lines) and continental shelf edges (thick black lines), in 1912, showing the similarity in the outlines of the east and west Atlantic margins. Image extract from Wegener (1912).

At first, this paradigm shifting hypothesis was strongly opposed by many due to the lack of a viable mechanism by which the continents could ‘plough through’ solid oceanic crust (e.g. Frankel, 1990). And at the time ‘Geosynclinal Theory’, developed in the 1800’s by James Hall and James Dwight Dana (e.g. Knopf, 1948), was able to explain the major observations from orogenic belts and sedimentary basins, as well as ocean development.

Support for continental drift, nonetheless, built throughout the 20th century, attested by the publication of ‘Our Wandering Continents: An Hypothesis of Continental Drift’ by Alex du Toit in 1937 (Du Toit, 1937). This shift was assisted by several key events that paved the way for plate tectonics:

- 1931: Arthur Holmes hypothesises the occurrence of thermal convection within the Earth due to the heat generated by radioactive decay, providing a driving mechanism for plate motions (Holmes, 1931).
- 1935: Haskell determines the fluid behaviour of the mantle from the study of glacial rebound, allowing for the drift of continents (Haskell, 1935).

- 1949: Benioff discovers Wadati-Benioff zones, suggesting a solution to space problems associated with drifting continents and shrinking oceans (Benioff, 1949).
- 1962: Harry Hess proposes 'seafloor spreading' to occur along mid-ocean rises (Hess, 1962).
- 1963: Vine and Matthews prove the occurrence of seafloor spreading using linear magnetic reversals recorded in the oceanic crust 'tape recorder' (Vine and Matthews, 1963).
- 1965: Runcorn uses polar wander to support the motion of the continents through geologic time (Runcorn, 1965), and Wilson proposes the 'transform fault', the "missing" type of plate boundary (Wilson, 1965).
- 1968: Jason Morgan coins the term 'plate tectonics', or the theory that 'the surface of the Earth is composed of several rigid plates all in relative motion about each other as a natural consequence of thermal convection in the mantle' (Figure 1.2), and describes the motion of plates on the globe about poles of rotation (Morgan, 1968; Figure 1.3).

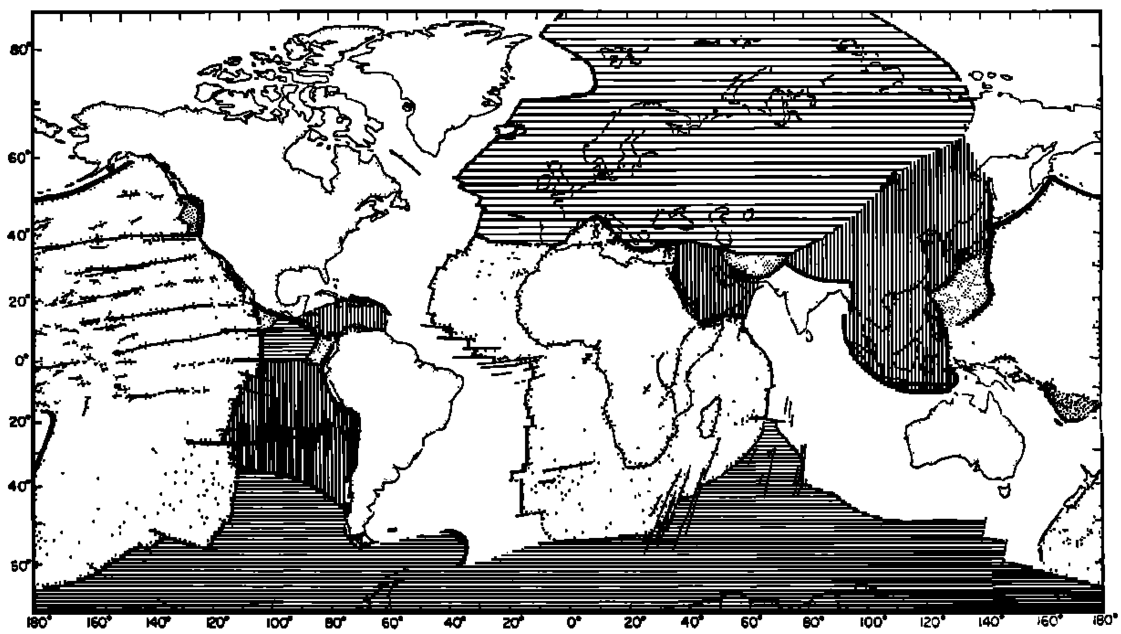

Figure 1.2. Configuration of the tectonic plates as initially described by Morgan (1968). The boundaries between tectonic plates are seafloor spreading centres, ocean trenches (subduction zones), and transform faults. Image from Morgan (1968).

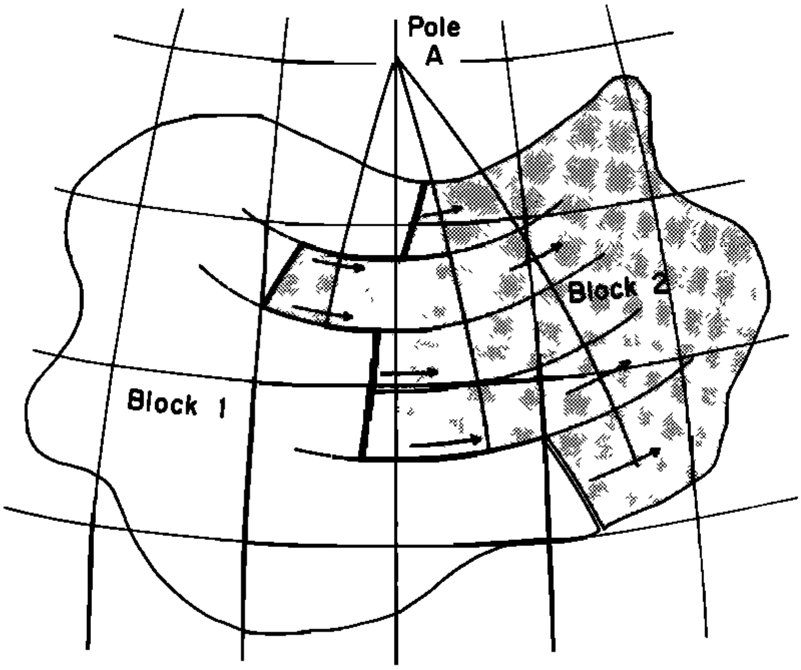

Figure 1.3. The motions of tectonic plates (Block 1 and Block 2) on the surface of a sphere must follow small circles about a pole of rotation (Pole A). Image from Morgan (1968).

Around this time it was also discovered that not only do tectonic plates collide and rift apart from each other, but that this process was cyclic. Careful analysis of the distribution of faunal realms on either side of the Atlantic Ocean by Wilson (1966) showed that a ‘proto-Atlantic’ must have opened and closed prior to the opening of the present day Atlantic Ocean. This cycle of rifting, continental breakup, ocean spreading, subduction initiation, ocean closing, and continental collision thus became known as the Wilson Cycle.

An inherent periodicity to such events of mountain building, sea level change, magmatism, climate, and even evolution was documented as early as the 1940’s by Umbgrove in “The Pulse of the Earth” (Umbgrove, 1947), however, it was not until 1984 that Worsley recognised these cycles as the manifestation of supercontinent assembly and breakup (Worsley et al., 1984). Regular episodes of continental collision and breakup related mafic magmatism throughout Earth’s history had been recognised through Rb/Sr and K/Ar dating (Condie, 1976; Windley, 1977) and were shown to occur at roughly 500 m.y. intervals (Figure 1.4). Subsequently, 4 or 5 supercontinent amalgamations have been proposed prior to the most recent assembly of Pangea.

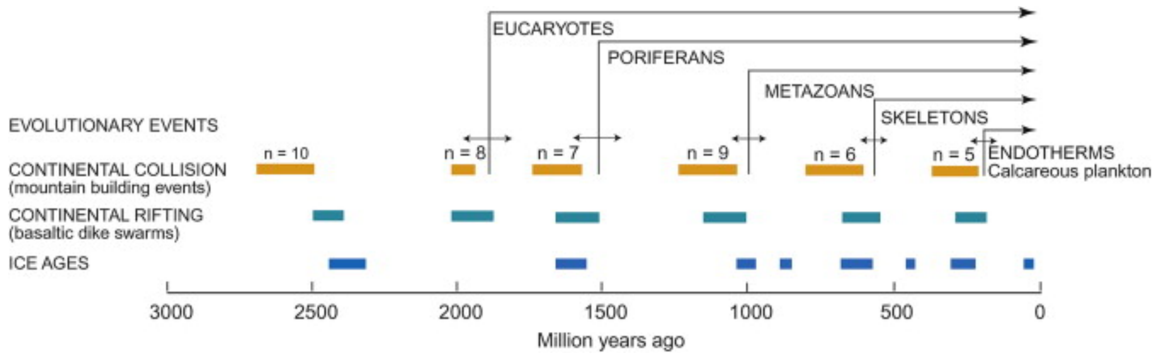

Figure 1.4. Periodic events linked to the Wilson Cycle throughout Earth's history (Worsley et al., 1984). Image from Nance and Murphy (2013).

The driving force behind the Wilson (supercontinent) Cycle is, however, still a matter of debate today, and, whilst mantle convection is still generally recognised as an important factor in controlling plate motions (e.g. Ziegler, 1993), other drivers have been proposed to also play important roles. Common suggestions include ridge-push and slab-pull (e.g. Lithgow-Bertelloni, 2014), gravitational collapse along orogenic belts (e.g. Rey et al., 2001), and mantle plumes (a special case of mantle convection; e.g Larson, 1991). The coincidence of many continental breakups with large igneous provinces has been used to support the role of hot mantle plumes in this phase of the Wilson Cycle (e.g. White and McKenzie, 1989). Examples of continental breakup lacking evidence for abnormal mantle temperatures during breakup, however, preclude the ubiquitous involvement of mantle plumes in this process (e.g. Storey, 1995). A distinction has therefore arisen between 'active' and 'passive' rifting to explain the generic observations from rifted margins: uplift, magmatism, and extension. During active rifting, uplift and melting are attributed to the impingement of a mantle plume or convection cell on the base of the lithosphere resulting in extension. During passive rifting, extension is attributed to an alternative driving force and results in the uplift and melting observed during rifting (e.g. Turcotte and Emerman, 1983).

1.3. Passive continental margins

Both active and passive rifting may result in a complete thinning of the continental lithosphere and the onset of seafloor spreading. This transition is termed continental breakup, and the zone of recently rifted continental crust becomes a passive margin. These features form 105,000 km of the world's continental margins, almost twice the length of convergent boundaries (53,000 km; Bradley, 2008), where one tectonic plate subducts beneath another. The term 'passive margin' may, however, be misleading as these types of margins are more and more commonly being found to undergo significant tectonic inversion, resulting from compression, and uplift, possibly due to mantle dynamics, during their 'passive' stage (e.g. Japsen et al., 2012; Yamato et al., 2013). The causes of continental rifting and the subsequent reactivation of passive margins are still a matter of debate and form a key area of research today (e.g. Geoffroy et al., 2015; Rabineau et al., 2015)

Depending on the stress conditions under which they form, two endmember groups of passive margins can develop. Where the trend of a deforming lithospheric zone is closely orthogonal to the extension direction across it, divergent (rifted) margins are formed. When the extension direction is closely parallel to the overall trend of a lithospheric deformation zone, transform margins develop. Between these two endmembers, oblique margins may develop and strain may be accommodated along transtensional normal faults, or may become partitioned onto alternating divergent and transform segments (Basile and Braun, 2016).

1.3.1. Divergent Margins

Divergent margins are commonly categorised by two end-member extremes. These are volcanic rifted margins and magma-poor rifted margins, and are commonly distinguished by the volume of syn-rift igneous rocks emplaced. Following breakup, passively upwelling mantle replaces material that moves laterally away from an ocean spreading centre, and consistently results in decompression melting, which produces an ~7 km thick crust (e.g. Katz et al., 2003; White et al., 1992). Generally, an elevated mantle temperature, due to continental insulation (e.g. Brandl et al., 2013) or mantle plumes (e.g. White and McKenzie, 1989), is invoked to explain the greater melt volumes observed at some volcanic rifted margins. Several alternative hypotheses have, however, also been proposed including; rifting speed (van Wijk et al., 2001), small-scale convection (SSC; Boutilier and Keen, 1999; Mutter et al., 1988; Simon et al., 2009), chemical enrichment of the mantle (Lizarralde et al., 2007), and rifting history (Armitage et al., 2010). The development of magma-poor rifted margins may therefore be explained as the result of rifting away from mantle thermal anomalies (e.g. Reston, 2009), although depth-dependent stretching of the lithosphere (e.g. Huismans and Beaumont, 2011) and presence of a partially depleted sub-lithospheric mantle (e.g. Pérez-Gussinyé et al., 2006) have also been proposed to control their development. Significant variations in magmatism and rifting style over different length scales (e.g. Behn and Lin, 2000; Franke et al., 2007; Lizarralde et al., 2007) precludes one single causal mechanism, and demonstrates our incomplete understanding of the development of rifted margins. In reality, a spectrum between the two endmember rifted margin types likely exist (Franke, 2013) as the natural result of interplay between different mechanisms.

1.3.2. Transform and oblique Margins

In cases of continental rifting where the extension direction is not perpendicular to a lithospheric deformation zone, oblique and/or transform margins develop. Following breakup, mature ocean spreading centres predominantly accommodate extension in a fully partitioned manner, i.e. along extension-perpendicular rifts connected by extension-parallel transform faults. Exceptions are limited to slow and very slow spreading centres, e.g. the Mohns (Dauteuil and Brun, 1996) and Reykjanes (Peyve, 2009) ridges, where oblique oceanic accretion occurs. Strain partitioning thus occurs at the majority of plate boundaries that developed in an oblique setting. The timing of this partitioning (i.e. transform fault development) is, however, variable and several possible scenarios have been described by Basile (2015) and are summarised below.

1.3.2.1. Transform development at the onset of rifting or shortly after

Where extension is closely parallel to pre-existing lithospheric weaknesses, such weaknesses may be reactivated as transform faults at the onset of rifting (Figure 1.5a). This has been proposed for several instances where oceanic transform faults are aligned with an onshore tectonic structure such as in the South Atlantic (e.g. Wright, 1976) and Gulf of Aden (Bellahsen et al., 2013). Alternatively, where a deformation zone is at low angles to the extension direction (Figure 1.5b), or where narrow rifts predominate (Figure 1.5c), individual rift segments do not overlap and may be connected by transform faults at the onset of rifting or shortly thereafter.

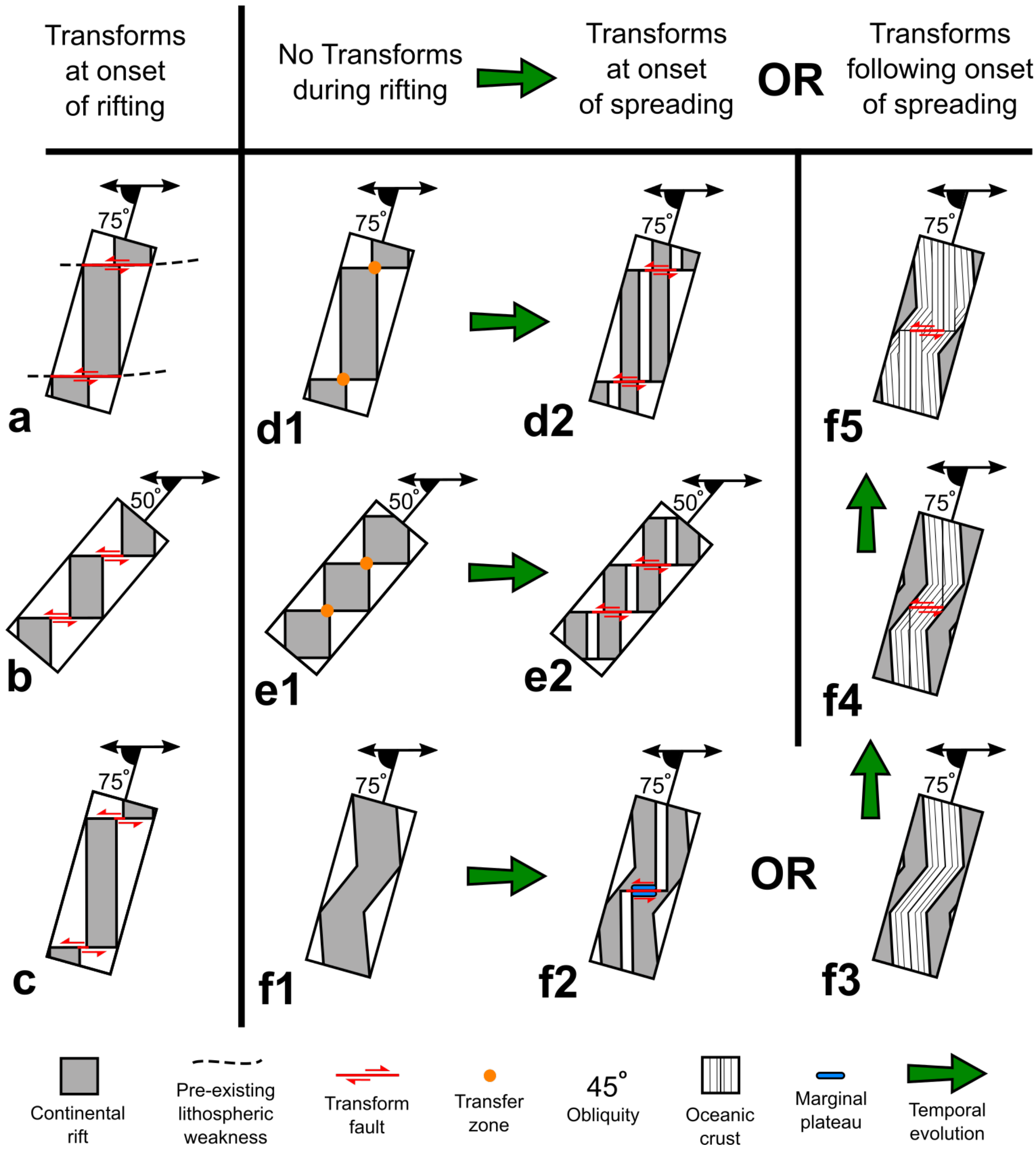

Figure 1.5. Development of transform and oblique margins. Left column: transform faults may be present at the onset of rifting along pre-existing lithospheric weaknesses (a) or between non-overlapping rift segments, which may result from a high obliquity (b) or narrow rift segments (c). Other columns: transform faults may not develop during rifting if rift segments overlap, which may occur in low obliquity settings (d1) or where wide rifts predominate (e1), or if transtensional rifting occurs (f1). In these cases, strain partitioning generally occurs at the onset of oceanic spreading (d2, e2, and f2) and new transform faults cut older rift structures in the continental crust. In the case of transtensional rifting, partitioning may also occur after a phase of oblique spreading (f3-5), in which case transforms may not develop in the continental crust and no transform margin will result. Figure after Basile (2015).

1.3.2.2. Transform development at the onset of spreading or later

Where a deformation zone lies at high angles to the extension direction (Figure 1.5d1), or where wide rifts develop in more oblique settings (Figure 1.5e1), individual rift segments may overlap. In this setting, transfer fault zones (e.g. Basile, 2015; Milani and Davison, 1988) separate rift segments and may accommodate the offset without the need for transform faults. Common structures forming interbasin transfer zones include interbasinal ridges, antithetic interference zones, transfer faults, and relay ramps (e.g. Gawthorpe and Hurst, 1993; Figure 1.6). Transtensional rifting is also able to accommodate oblique extension without the need for transform faults (Figure 1.5f1). In these cases, strain partitioning onto transforms may occur at the onset of oceanic spreading (Figure 1.5d2-f2; e.g Taylor et al., 2009), in which case transform faults cut older rift structures and may result in the development of marginal plateaus (Mercier de Lépinay et al., 2016). Alternatively, for the case of transtensional rifting, partitioning may also occur after a phase of oblique spreading. In this instance transform faults may not be present in the continental domain of an oblique rifted margin (Figure 1.5f3-5).

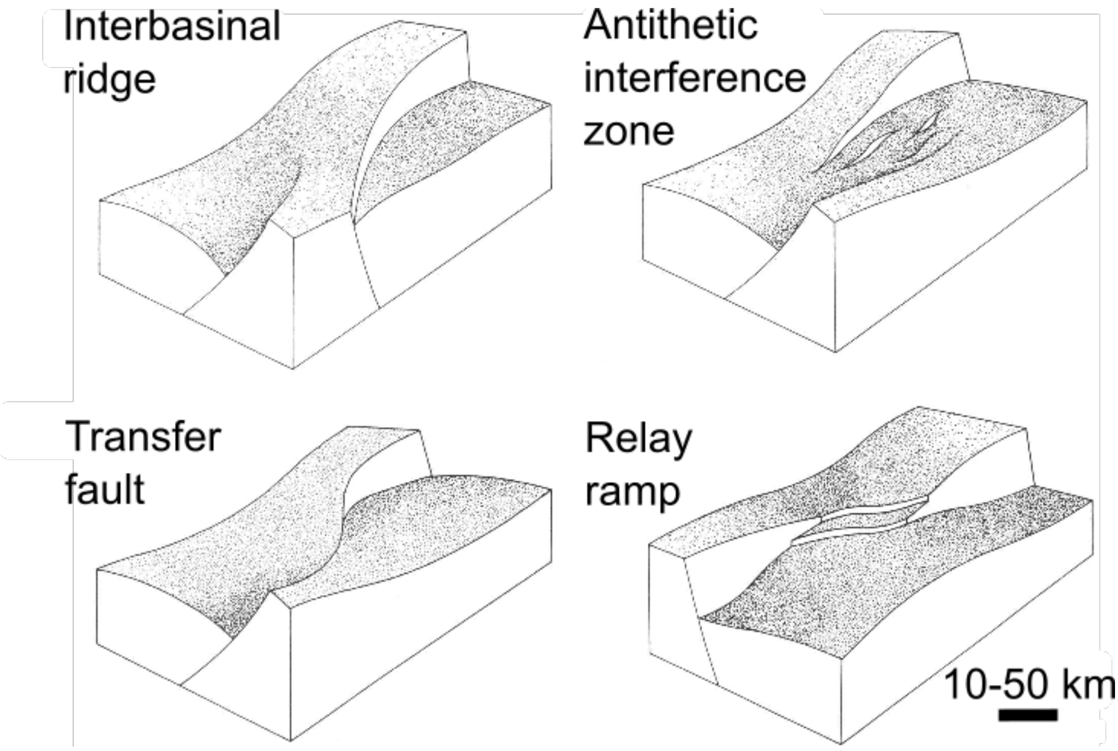

Figure 1.6. Interbasinal transfer zone geometries that may link offset, but overlapping, rift systems without the need for transform faults. The vertical scale is greatly exaggerated. Image from Gawthorpe and Hurst (1993).

1.3.3. Characterisation of passive margins

Each margin type is characterised by features that develop under the different rifting regimes. Identification of these features, through the use of geophysical methods, can allow for a robust differentiation between divergent and transform type margins. The main distinguishing features of the different categories of passive margin are summarised below and are shown in Figure 1.7.

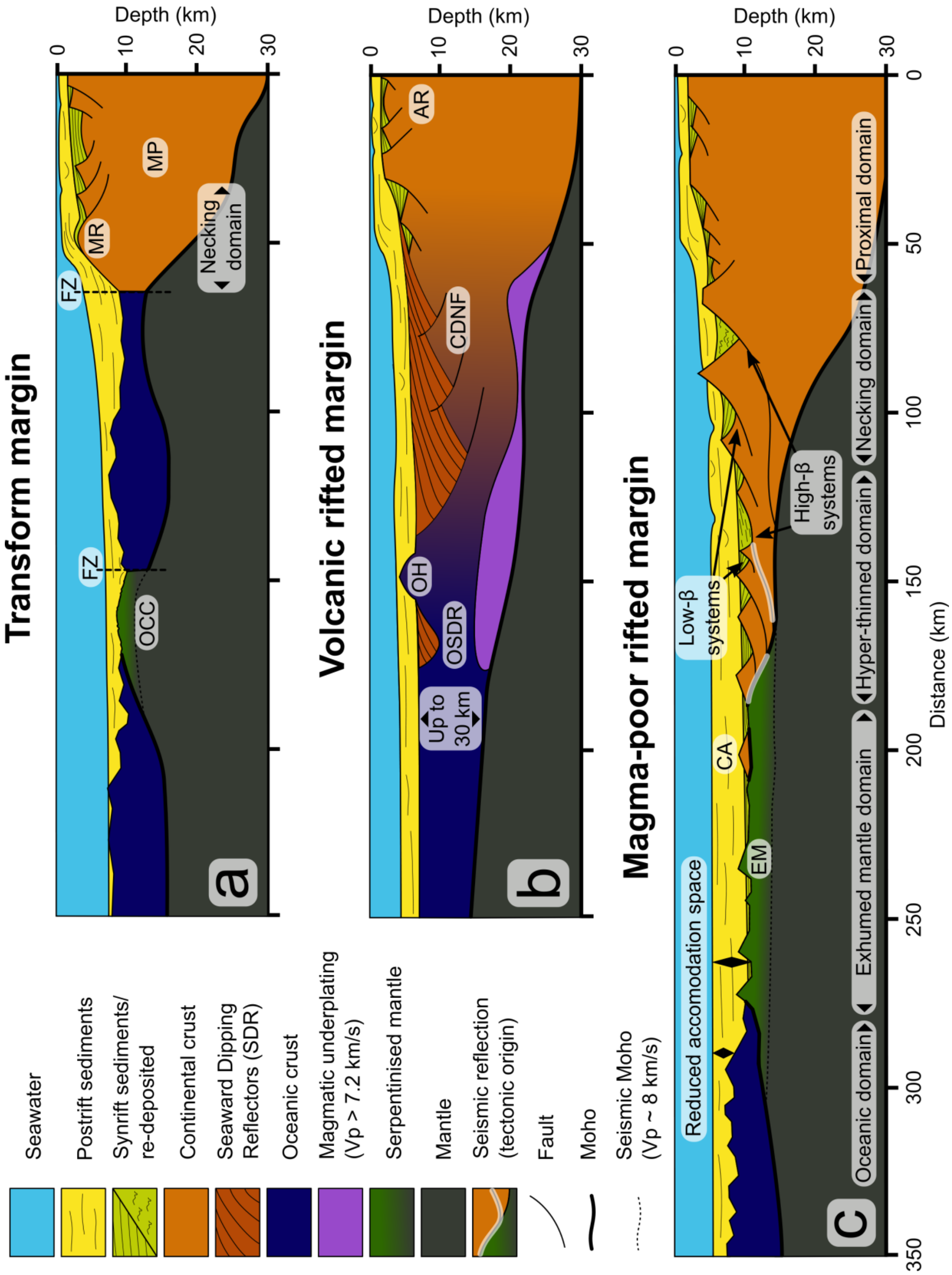

Figure 1.7. Key characteristics of each margin type as described in Section 1.2. (a) Transform margins commonly exhibit: narrow necking domains of the Moho and basement, marginal plateaus, marginal ridges, adjacent thin oceanic crust and exhumed mantle at oceanic core complex. (b) Volcanic rifted margins often show: continentward dipping normal faults, adjacent abandoned rifts, SDRs, underplated high velocity lower crust, initially thick ocean crust. (c) Magma-poor rifted margins generally display: up to 200 km of thinned crust, both low-β and high-β fault systems, high amplitude seismic reflections along low angle faults, exhumed and serpentinised mantle, initially thin oceanic crust. AR: abandoned rift; CA: continental allochthon; CDNF: continentward dipping normal faults; EM: exhumed mantle; FZ: fracture zone; MP: marginal plateau; MR: marginal ridge; OCC: ocean core complex; OH: outer high; OSDR: outer seaward dipping reflectors.

1.3.3.1. Volcanic rifted margins

Where large volumes of melt are emplaced during rifting, volcanic rifted margins develop (Figure 1.7b), and may indicate the breakup of the lithospheric mantle before or at the same time as that of the crust (Franke, 2013). This magmatism manifests itself as thick wedges of volcanic flows, identified in seismic reflection data as seaward dipping reflectors (SDRs), and magmatic underplating, identified in seismic refraction studies as high velocity (>7.2 km/s) lower crustal bodies (Franke, 2013). As these margins develop and become submerged, the introduction of water may results in explosive volcanism resulting in the formation of an outer high, beyond which outer SDRs may develop as deep sea volcanic sheet flows before the onset of normal oceanic crust production (Planke et al., 2000). The enhanced melt production during breakup often also results in an initially over-thickened oceanic crust up to 30 km thick (Geoffroy, 2005).

Crustal thinning at volcanic rifted margins often occurs adjacent to previous sedimentary basins and is quite abrupt, occurring over 50-100 km (Figure 1.7b). Continentward dipping normal faults may also accommodate the extension, although the large volumes of extrusive volcanic rocks at these margins often masks rift structures making accurate identifications of the last continental crust and the COT difficult (Stab et al., 2016). The considerable amounts of intrusive magmatism and magmatic underplating also alter Moho geometries, which therefore provide little insight into the structure of the continental crust as a result of rifting.

1.3.3.2. Magma-poor rifted margins

Where exhumation of the mantle occurs and limited melt is produced during rifting, magma-poor passive margins develop (Figure 1.7c), indicating a complete thinning of the crust before the breakup of the lithospheric mantle (Franke, 2013). These margins typically display five domains. Starting from the continent and moving oceanwards, these are: 1) proximal domain, where crustal thinning and accommodation space are minimal; 2) necking domain, where the crust is thinned most intensively resulting in the steepest Moho slopes; 3) hyper-thinned domain, where thinned continental crust (sometimes less than 10 km thick) forms an extensive continental rise; 4) exhumed mantle domain, where complete thinning of the crust occurs and lithospheric mantle is exhumed along detachment faults and becomes partially serpentinised ; and 5) oceanic domain, where following sufficient thinning of the lithosphere, mantle melting occurs to produce oceanic crust (Reston, 2009; Tugend et al., 2015).

Crustal thinning at magma-poor rifted margins occurs through both low-β and high-β extensional systems, where β is the crustal extension factor. Low-β systems accommodate small amounts of extension through high-angle normal faults, forming classic half-graben structures with wedge-shaped sedimentary fills (Figure 1.7c). This type of extensional system can occur all along the margin (Tugend et al., 2015), and most magma-poor rifted margins display well defined fault blocks of this type (Reston, 2009). High-β systems allow large amounts of extension to be accommodated through long-offset normal faults. These detachment faults exhume the underlying footwall over large areas forming smooth fault-related topography and hyperextended sag basins. These basins often contain syn-rift sediments that gently onlap the low-angle basement, or that have been redeposited due to significant fault block rotation (Wilson et al., 2001), losing their initial syn-rift sedimentary wedge configuration. Where the low angle faults of high-β systems are intracrustal, or form the boundary between crust and mantle, they are commonly imaged as high amplitude seismic reflections (e.g. Davy et al., 2016; Dean et al., 2008). High-β systems tend to develop in the necking, hyperthinned, and exhumed mantle domains alongside low-β systems (Tugend et al., 2015). These extensional systems lead to complete crustal thinning, from a thickness of ~30 km, over a long distance of 100-200 km (Figure 1.7c), with most of the crustal thinning (from ~20-10 km) occurring in the necking zone (Reston, 2009). This region of sharp crustal thinning generally has average Moho slopes of between 5° - 25°, although average Moho slopes across the necking zone have reached 33 and 36 degrees across the Porcupine Basin (O'Reilly et al., 2006) and Newfoundland margin, respectively. In the latter example, however, the steepness is thought to have been influenced by lower crustal gabbroic lenses localising deformation (Van Avendonk et al., 2009).

Following complete crustal thinning, partially serpentinised peridotites of the exhumed mantle domain form the OCT (Tugend et al., 2015). In these domains no clear Moho reflection is present due to the gradual downward decrease in the amount of serpentinisation (Gillard et al., 2015). The onset of magmatism and production of oceanic crust marks the beginning of the oceanic domain. Oceanic crust is often initially thin (e.g. (Davy et al., 2016)) but its presence is often marked by (sometimes weak) Moho reflections. The boundary between the oceanic and exhumed mantle domains may correspond to a step in the basement topography and smaller accommodation space within the oceanic domain (Figure 1.7c) due to the relative buoyancy of the oceanic crust over mantle (Tugend et al., 2015).

1.3.4. Characterisation of Transform Margins

When oblique extension is partitioned onto transform and divergent margins early enough, transform faults cut the continental crust and lithosphere, facilitating plate separation and forming transform margins (Figure 1.7a; Basile, 2015). As the transform faults of the lithospheric deformation zone at transform margins are sub-vertical, extremely narrow 'necking zones', typically 50 km wide, develop (Mercier de Lépinay et al., 2016). This sharp zone of crustal thinning is accompanied by the development of steep average Moho slopes, commonly between 8° - 40°, although sub-vertical Moho slopes have been observed at the Côte d'Ivoire-Ghana transform margin (Sage et al., 2000). At the oceanward edge of the necking zone, a steep basement slope may also be present, the base of which often coincides with the COT. The Falkland escarpment basement slope lies at 13 degrees (Lorenzo and Wessel, 1997), Ghana at 12 degrees (Sage et al., 2000), the Northern Demerara and French Guiana margins show slopes of 24 and 13 degrees respectively (Greenroyd et al., 2008), and the Newfoundland Fracture Zone basement slope forms a slope of ~40 degrees (Keen et al., 1990). Rift basins are generally not seen within this slope region, although any present may not have been clearly imaged using seismic reflection techniques due to the slope steepness.

The presence of thick continental lithosphere adjacent to MORs at transform margins results in a high thermal contrast between the continental and oceanic lithospheres. Thin oceanic crust may therefore be formed adjacent to transform margins due to heat conduction away from the spreading centre, resulting in reduced melting (e.g., Ghana: 4 km (White et al., 1992); Agulas-Falkland FZ: 4 km (Becker et al., 2012)). This process is analogous to those occurring at long offset transform faults in the oceanic domain. In these settings, the reduced melt supply results in tectonic accommodation of extension and lower crust or mantle rocks may be exhumed to the surface at oceanic core complexes up to 50 km wide (e.g. Karson, 1999). The high thermal contrast across transform margins also results in differential subsidence, and where the oceanic and continental plates are coupled flexural downwarping of the continental side may occur (Lorenzo and Wessel, 1997; Mercier de Lépinay et al., 2016).

Marginal plateaus, possibly inherited from continental thinning prior to the partitioning of oblique strain onto transform faults (Basile, 2015)(Figures 1.5f1-2), are also commonly observed adjacent to transform margins (Mercier de Lépinay et al., 2016). A marginal ridge (e.g. Bird, 2001), where crust or pre/syn-rift sediments are elevated linearly along the margin near the top of the continental slope, may also be present (Figure 1.7a). However, the mechanisms for forming marginal ridges are still under debate and possibly diverse in origin; for a full review the reader is referred to (Basile, 2015).

1.4. Gondwana assembly and breakup

The paleomagnetic, stratigraphic, and tectonic records of the continental crust span Earth's almost entire history, as they are not systematically destroyed like those of the oceanic crust, which is subducted comparatively soon after its formation (e.g. Roberts et al., 2015). They therefore make a useful tool for reconstructing Wilson Cycles that occurred before the formation of the Earth's present day oceanic crust. The formation of the supercontinent Gondwana, a long lived accumulation of much of the earths continental lithosphere into one landmass, represents such a cycle. Gondwana was reconstructed from the lithospheric mega-plates formed during the disintegration of the previous supercontinent Rodinia between 1000 and 700 Ma (Veevers, 2004). These plates were reunited during the Pan-African orogeny between 650 and 500 Ma, which brought together the present day landmasses of Africa, Antarctica, Australia, India, the Middle East, North America, South America, and also briefly North America (Laurentia). The return of Laurentia with Baltica and Siberia, together forming Laurasia, to Gondwana at ~320 Ma resulted in the Variscan orogeny along the north-eastern margin of Gondwana, and formation of the supercontinent Pangea. Gondwana remained intact within Pangea and was surrounded by the near global Panthalassas Ocean, which by ~300 Ma had renewed subduction beneath the southern margin of Gondwana (Veevers, 2004).

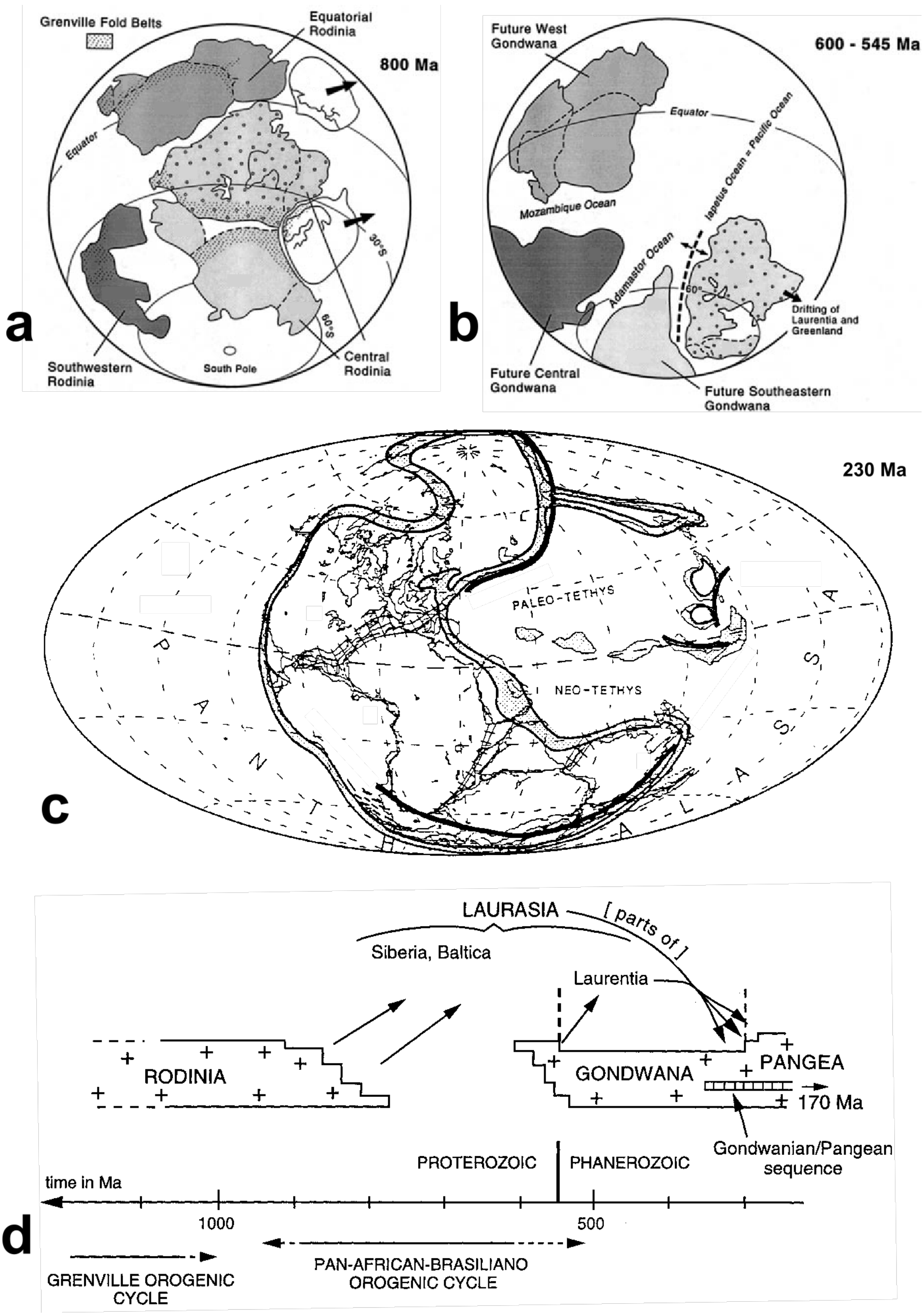

Figure 1.8. Disassembly of Rhodinia (a) and reassembly into Gondwana (b). Later merging of Gondwana with Laurasia forms Pangea, surrounded by the Panthalassas Ocean (c and d). Images a, b, and d are modified from Trompette (2000), image c is modified from Veevers (2004).

This subduction and accretion led to the development of foreland basins and the Cape Fold Belt in South Africa between 220 and 290 Ma (Frimmel et al., 2001) with fluctuating deformation intensity. This compression became more widespread, also affecting South America to the west, at ~258 Ma (Veevers, 2004). The episodic and changeable development of the Karoo rift system (Hankel, 1994; Schandelmeier et al., 2004) across Gondwana at this time (Reeves et al., 2016) may therefore be the result of this compression (Delvaux, 2001a), which varied temporally in orientation and intensity, reactivating pre-existing basement weaknesses along the northern parts of the Karoo rift system (Reeves, 2014). Studies of Karoo rifts, which predominantly follow a NW-SE trend (Delvaux, 2001b) or a NE-SW trend (Schandelmeier et al., 2004) in the present day East Africa region, show the general progression:

1) Sinistral strike-slip along NE-SW trending basins with local deposition in left lateral step-over basins. Extension along NW-SE trending basins with strike-slip deformation along E-W trending offsets in the rift system. This phase of rifting led to the deposition of Sakoa aged deposits between ~265 Ma and ~300 Ma (Figure 1.9), which are capped by the Vohitolia marine limestones (Hankel, 1994) suggesting a connection to the NeoTethys Ocean in the north at this time.
2) After a brief pause in rifting, a reconfiguration occurred between ~259 and ~264 Ma (Hankel, 1994), coincident with the broadening and intensification of compression along southern Gondwana (Veevers, 2004). The onset of rapid subsidence in NE-SW trending basins (Schandelmeier et al., 2004), along with strike slip deformation along formerly extensional NW-SE trending basins and compression along their E-W trending offsets, resulted in deposition of Sakamena aged deposits (Figure 1.9).
3) A second larger pause in rifting occurred around ~249 Ma, and was followed by a rejuvenation of rifting along NE-SW trending rifts at ~242 Ma with little activity along NW-SE trending rifts, which led to the development of Isalo aged deposits until ~210 Ma (Figure 1.9; Hankel, 1994).

Following the cessation of compression along the cape fold belt, a substantial period of quiescence along the Karoo rifts ensued (Geiger et al., 2004). Rejuvenation of rifting did not occur until the Early Jurassic (Toarcian), coincident with eruption of the Karoo large igneous province in Mozambique. This Early Jurassic rifting at ~182 Ma culminated in the breakup of East and West Gondwana, which had thus remained intact for over 520 Myr. The kinematics and dynamics during this drifting apart of East and West Gondwana form the main focus of this thesis.

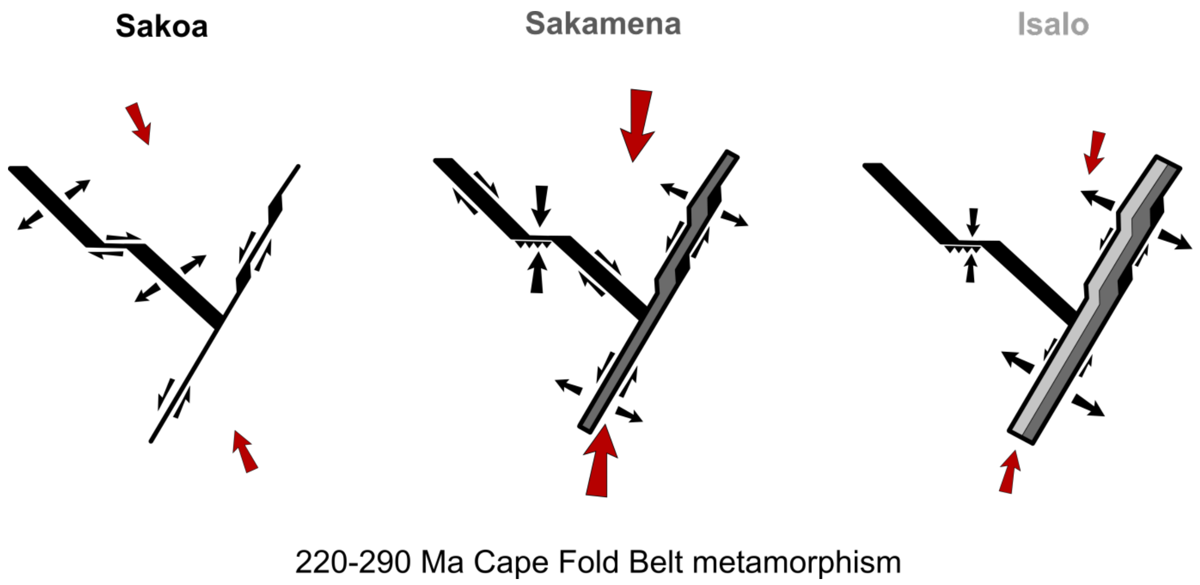

Figure 1.9. Schematic of Karoo rift development in East Africa, possibly in response to varying intensities and orientations of compression along the Cape Fold Belt. The distributions Sakoa aged deposits are shown in black, Sakamena deposits in dark grey, and Isalo deposits in light grey.

1.5. Thesis outline

Chapters 2 to 4 of this thesis are the results chapters of this thesis. They are presented as three 'journal-style' academic papers or manuscripts, and as such are designed to be stand-alone. Nonetheless, they contain a through-going theme and are further tied together in the conclusions chapter at the end of this thesis.

Each results chapter has either been published in, or is intended for submission to, a relevant academic journal within the field of Earth Sciences. These papers are multi-authored and as such my contributions to each chapter are outlined below:

Chapter 2 - 'Madagascar's escape from Africa: A high-resolution plate reconstruction for the Western Somali Basin and implications for supercontinent dispersal: this chapter has been published in *Geochemistry, Geophysics, Geosystems* in 2016. As first author of this paper my contributions included: concept design, gravity modelling, plate tectonic modelling, and manuscript preparation. Co-authors have contributed training, useful discussion, and editorial assistance.

Chapter 3 - 'The Rovuma Transform Margin: Pinning down the East African continent-ocean transform margin using seismic and gravity methods': this chapter is intended for submission to *Tectonics*. As first author of this paper my contributions included: Moho and bathymetry data digitisation, seismic interpretation, Matlab code development, gravity modelling, manuscript preparation. Concept design was joint between myself and co-authors. Co-authors have contributed training, useful discussion, and editorial assistance.

Chapter 4 – 'Compressional consequences of complex spreading: Formation of the Tanzania Coastal Basin and Davie Fracture Zone during the Mesozoic East Africa breakup': this chapter is also intended for submission to *Tectonics*. As first author of this paper my contributions included: analysis of satellite image data, seismic interpretation, regional tectonic model development, and manuscript preparation. Co-authors have contributed training, useful discussion, and editorial assistance.

1.6. References

Afilhado, A., Matias, L., Shiobara, H., Hirn, A., Mendes-Victor, L., Shimamura, H., 2008. From unthinned continent to ocean: The deep structure of the West Iberia passive continental margin at 38°N. Tectonophysics 458, 9–50. doi:10.1016/j.tecto.2008.03.002

Armitage, J.J., Collier, J.S., Minshull, T.A., 2010. The importance of rift history for volcanic margin formation. Nature 465, 913–917. doi:10.1038/nature09063

Basile, C., 2015. Transform continental margins - part 1: Concepts and models. Tectonophysics 661, 1–10. doi:10.1016/j.tecto.2015.08.034

Basile, C., Braun, J., 2016. The initiation of pull-apart basins and transform continental margins: Results from numerical experiments of kinematic partitioning in divergent settings. Terra Nov. 28, 120–127. doi:10.1111/ter.12198

Becker, K., Franke, D., Schnabel, M., Schreckenberger, B., Heyde, I., Krawczyk, C.M., 2012. The crustal structure of the southern Argentine margin. Geophys. J. Int. 189, 1483–1504. doi:10.1111/j.1365-246X.2012.05445.x

Behn, M.D., Lin, J., 2000. Segmentation in gravity and magnetic anomalies along the U.S. East Coast passive margin: Implications for incipient structure of the oceanic lithosphere. J. Geophys. Res. 105, 25769. doi:10.1029/2000JB900292

Bellahsen, N., Leroy, S., Autin, J., Razin, P., d'Acremont, E., Sloan, H., Pik, R., Ahmed, A., Khanbari, K., 2013. Pre-existing oblique transfer zones and transfer/transform relationships in continental margins: New insights from the southeastern Gulf of Aden, Socotra Island, Yemen. Tectonophysics 607, 32–50. doi:10.1016/j.tecto.2013.07.036

Benioff, H., 1949. Seismic evidence for the fault origin of oceanic deeps. Bull. Geol. Soc. Am. 60, 1837–1866.

Bercovici, D., Long, M.D., 2014. Slab rollback instability and supercontinent dispersal. Geophys. Res. Lett. 41, 6659–6666. doi:10.1002/2014GL061251

Bird, D., 2001. Shear margins: Continent-ocean transform and fracture zone boundaries. Lead. Edge 20, 150. doi:10.1190/1.1438894

Boutilier, R.R., Keen, C.E., 1999. Small-scale convection and divergent plate boundaries. J. Geophys. Res. 104, 7389. doi:10.1029/1998JB900076

Bradley, D.C., 2008. Passive margins through earth history. Earth-Science Rev. 91, 1–26. doi:10.1016/j.earscirev.2008.08.001

Brandl, P.A., Regelous, M., Beier, C., Haase, K.M., 2013. High mantle temperatures following rifting caused by continental insulation. Nat. Geosci. 6, 391–394. doi:10.1038/ngeo1758

Brune, S., Heine, C., Pérez-gussinyé, M., Sobolev, S., 2013. High resolution 2D numerical models from rift to break-up : Crustal hyper-extension , Margin asymmetry , Sequential faulting 15, 6015.

Bunce, E.T., Molnar, P., 1977. Seismic reflection profiling and basement topography in the somali basiin: possible fracture sones between Madagascar and Africa. J. Geophys. Res. 82, 5305–5311.

Coffin, M.F., Rabinowitz, P.D., 1987. Reconstruction of Madagascar and Africa: Evidence From the Davie Fracture Zone and Western Somali Basin 92, 9385–9406.

Condie, K.C., 1976. Palte Tectonics and Crustal Evolution. Chem. … 294.

Dailly, P., Henderson, T., Hudgens, E., Kanschat, K., Lowry, P., 2013. Exploration for Cretaceous stratigraphic traps in the Gulf of Guinea, West Africa and the discovery of the Jubilee Field: a play opening discovery in the Tano Basin, Offshore Ghana. Geol. Soc. London, Spec. Publ. 369, 235–248. doi:10.1144/SP369.12

Damian Nance, R., Brendan Murphy, J., 2013. Origins of the supercontinent cycle. Geosci. Front. 4, 439–448. doi:10.1016/j.gsf.2012.12.007

Dauteuil, O., Brun, J.-P., 1996. Deformation partitioning in a slow spreading ridge undergoing oblique extension: Mohns Ridge, Norwegian Sea. Tectonics 15, 870–884. doi:10.1029/95TC03682

Davis, J.K., Lawver, L.A., Norton, I.O., Gahagan, L.M., 2016. New Somali Basin magnetic anomalies and a plate model for the early Indian Ocean. Gondwana Res. 34, 16–28. doi:10.1016/j.gr.2016.02.010

Davy, R.G., Minshull, T.A., Bayrakci, G., Bull, J.M., Klaeschen, D., Papenberg, C., Reston, T.J., Sawyer, D.S., Zelt, C.A., 2016. Continental hyperextension, mantle exhumation, and thin oceanic crust at the continent-ocean transition, West Iberia: New insights from wide-angle seismic 121, 3177–3199. doi:doi:10.1002/ 2016JB012825.

Dean, S.M., Minshull, T.A., Whitmarsh, R.B., 2008. Seismic constraints on the three-dimensional geometry of low-angle intracrustal reflectors in the Southern Iberia Abyssal Plain. Geophys. J. Int. 175, 571–586. doi:10.1111/j.1365-246X.2008.03869.x

Delvaux, D., 2001a. Tectonic and palaeostress evolution of the Tanganyika-Rukwa-Malawi rift segment, East African Rift System. Peri-Tethys Mem. 6 Peri-Tethyan Rift. Basins Passiv. Margins 545–567.

Delvaux, D., 2001b. Karoo rifting in western Tanzania: precursor of Gondwana break-up? Contrib. to Geol. Palaeontol. Gondwana honour Helmut Wopfner 111–125.

Du Toit, A.L., 1937. Our Wandering Continents: An Hypothesis of Continental Drifting. Edinburgh Oliver Boyd.

Franke, D., 2013. Rifting, lithosphere breakup and volcanism: Comparison of magma-poor and volcanic rifted margins. Mar. Pet. Geol. 43, 63–87. doi:10.1016/j.marpetgeo.2012.11.003

Franke, D., Neben, S., Ladage, S., Schreckenberger, B., Hinz, K., 2007. Margin segmentation and volcano-tectonic architecture along the volcanic margin off Argentina/Uruguay, South Atlantic. Mar. Geol. 244, 46–67. doi:10.1016/j.margeo.2007.06.009

Frankel, H., 1990. The development of plate tectonics by J. Morgan and D. McKenzie. Terra Nov. 2, 202–214. doi:10.1111/j.1365-3121.1990.tb00067.x

Frimmel, H.E., Fölling, P.G., Diamond, R., 2001. Metamorphism of the permo-triassic cape fold belt and its basement, South Africa. Mineral. Petrol. 73, 325–346. doi:10.1007/s007100170005

Gaina, C., Torsvik, T.H., van Hinsbergen, D.J.J., Medvedev, S., Werner, S.C., Labails, C., 2013. The African plate: A history of oceanic crust accretion and subduction since the Jurassic. Tectonophysics 604, 4–25. doi:10.1016/j.tecto.2013.05.037

Gawthorpe, R.L., Hurst, J.M., 1993. Transfer zones in extensional basins: their structural style and influence on drainage development and stratigraphy. J. Geol. Soc. London. 150, 1137–1152. doi:10.1144/gsjgs.150.6.1137

Geiger, M., Clark, D.N., Mette, W., 2004. Reappraisal of the timing of the breakup of Gondwana based on sedimentological and seismic evidence from the Morondava Basin, Madagascar. J. African Earth Sci. 38, 363–381. doi:10.1016/j.jafrearsci.2004.02.003

Geoffroy, L., 2005. Volcanic passive margins. Comptes Rendus - Geosci. 337, 1395–1408. doi:10.1016/j.crte.2005.10.006

Geoffroy, L., Burov, E.B., Werner, P., 2015. Volcanic passive margins: another way to break up continents. Sci. Rep. 5, 14828. doi:10.1038/srep14828

Gillard, M., Autin, J., Manatschal, G., Sauter, D., Munschy, M., Schaming, M., 2015. Tectonomagmatic evolution of the final stages of rifting along the deep conjugate Australian-Antarctic magma-poor rifted margins: Constraints from seismic observations 753–783. doi:10.1002/2015TC003850.

Greenroyd, C.J., Peirce, C., Rodger, M., Watts, A.B., Hobbs, R.W., 2008. Demerara Plateau - The structure and evolution of a transform passive margin. Geophys. J. Int. 172, 549–564. doi:10.1111/j.1365-246X.2007.03662.x

Hankel, O., 1994. Early Permian to Middle Jurassic rifting and sedimentation in East Africa and Madagascar. Geol. Rundschau 83, 703–710. doi:10.1007/BF00251069

Haskell, N.A., 1935. The motion of a fluid under a surface load. Physics (College. Park. Md). 6, 265–269.

Hess, H.H., 1962. History of Ocean Basins. Petrol. Stud. A Vol. to Honor A. F. Buddingt. 599–620.

Holmes, A., 1931. Radioactivity and earth movements. Trans. Geol. Soc. Glas. 18, 559–606.

Huismans, R., Beaumont, C., 2011. Depth-dependent extension, two-stage breakup and cratonic underplating at rifted margins. Nature 473, 74–78. doi:10.1038/nature09988

Japsen, P., Chalmers, J.A., Green, P.F., Bonow, J.M., 2012. Elevated, passive continental margins: Not rift shoulders, but expressions of episodic, post-rift burial and exhumation. Glob. Planet. Change 90–91, 73–86. doi:10.1016/j.gloplacha.2011.05.004

Karson, J.A., 1999. Geological investigation of a lineated massif at the Kane Transform Fault: implications for oceanic core complexes. Philos. Trans. R. Soc. a-Mathematical Phys. Eng. Sci. 357, 713–736. doi:10.1098/rsta.1999.0350

Katz, R.F., Spiegelman, M., Langmuir, C.H., 2003. A new parameterization of hydrous mantle melting. Geochemistry, Geophys. Geosystems 4, 1–19. doi:10.1029/2002GC000433

Keen, C.E., Kay, W.A., Roest, W.R., 1990. Crustal anatomy of a transform continental margin. Tectonophysics 173. doi:10.1016/0040-1951(90)90244-3

Klimke, J., Franke, D., Mahanjane, E.S., Leitchenkov, G., 2017. Tie-points for Gondwana reconstructions from a structural interpretation of the Mozambique Basin, East Africa, and the Riiser-Larsen Sea, Antarctica. Solid Earth Discuss. 1–28.

Knopf, A., 1948. The Geosynclinal Theory. Bull. Geol. Soc. Am. 59, 649–670.

Larson, R.L., 1991. Geological consequences of superplumes. Geology 19, 963–966. doi:10.1130/0091-7613(1991)019<0963:GCOS>2.3.CO

Lawver, L.A., Scotese, C.R., 1987. A revised reconstruction of Gondwanaland. Geophys. Monogr. Ser. 40, 17–23.

Levell, B., Argent, J., Fraser, S., 2010. Session : Passive Margins. Pet. Geol. Conf. Ser. 823–830. doi:10.1144/0070823

Lithgow-Bertelloni, C., 2014. Driving Forces: Slab Pull, Ridge Push BT - Encyclopedia of Marine Geosciences, in: Harff, J., Meschede, M., Petersen, S., Thiede, J. (Eds.), . Springer Netherlands, Dordrecht, pp. 1–6. doi:10.1007/978-94-007-6644-0_105-1

Lizarralde, D., Axen, G.J., Brown, H.E., Fletcher, J.M., González-Fernández, A., Harding, A.J., Holbrook, W.S., Kent, G.M., Paramo, P., Sutherland, F., Umhoefer, P.J., 2007. Variation in styles of rifting in the Gulf of California. Nature 448, 466–469. doi:10.1038/nature06035

Lorenzo, J.M., Wessel, P., 1997. Flexure across a continent-ocean fracture zone: the northern Falkland/Malvinas Plateau, South Atlantic. Geo-Marine Lett. 17, 110–118. doi:10.1007/s003670050015

Lottes, A.L., Rowley, D.B., 1990. Reconstruction of the Laurasian and Gondwanan segments of Permian Pangaea. Geol. Soc. Mem. 12, 383–395.

Manatschal, G., 2004. New models for evolution of magma-poor rifted margins based on a review of data and concepts from West Iberia and the Alps. Int. J. Earth Sci. 93, 432–466. doi:10.1007/s00531-004-0394-7

Mercier de Lépinay, M., Loncke, L., Basile, C., Roest, W.R., Patriat, M., Maillard, A., De Clarens, P., 2016. Transform continental margins – Part 2: A worldwide review. Tectonophysics 693, 96–115. doi:10.1016/j.tecto.2016.05.038

Milani, E.J., Davison, I., 1988. Basement control and transfer tectonics in the Reconcavo-Tucano-Jatoba rift, Northeast Brazil. Tectonophysics 154. doi:10.1016/0040-1951(88)90227-2

Morgan, W.J., 1968. Rises, Trenches, Great Faults and Crustal Blocks. J. Geophys. Res. 73, 1959–1982.

Mutter, J.C., Buck, W.R., Zehnder, C.M., 1988. Convective partial melting: 1. A model for the formation of thick basaltic sequences during the initiation of spreading. J. Geophys. Res. 93, 1031–1048. doi:10.1029/JB093iB02p01031

Norton, I.O.I., Sclater, J.G., 1979. A model for the evolution of the Indian Ocean and the breakup of Gondwanaland. J. Geophys. Res. 84, 6803–6830.

O'Reilly, B.M., Hauser, F., Ravaut, C., Shannon, P.M., Readman, P.W., 2006. Crustal thinning, mantle exhumation and serpentinization in the Porcupine Basin, offshore Ireland: evidence from wide-angle seismic data. J. Geol. Soc. London. 163, 775–787. doi:10.1144/0016-76492005-079

Ortelius, A., 1596. Thesaurus geographicus.

Pérez-Gussinyé, M., Morgan, J.P., Reston, T.J., Ranero, C.R., 2006. The rift to drift transition at non-volcanic margins: Insights from numerical modelling. Earth Planet. Sci. Lett. 244, 458–473. doi:10.1016/j.epsl.2006.01.059

Peyve, A.A., 2009. Accretion of oceanic crust under conditions of oblique spreading. Geotectonics 43, 87–99. doi:10.1134/S0016852109020022

Pinna, P., 1995. On the dual nature of the Mozambique Belt, Mozambique to Kenya. J. African Earth Sci. 21, 477–480. doi:10.1016/0899-5362(95)00077-7

Planke, S., Symonds, P.A., Alvestad, E., Skogseid, J., 2000. Seismic volcanostratigraphy of large-volume basaltic extrusive complexes on rifted margins. J. Geophys. Res. Solid Earth 105, 19335–19351. doi:10.1029/1999JB900005

Rabineau, M., Cloetingh, S., Kuroda, J., Aslanian, D., Droxler, A., Gorini, C., Garcia-Castellanos, D., Moscariello, A., Burov, E., Sierro, F., Lirer, F., Roure, F., Pezard, P.A., Matenco, L., Hello, Y., Mart, Y., Camerlenghi, A., Tripati, A., 2015. Probing connections between deep earth and surface processes in a land-locked ocean basin transformed into a giant saline basin: The Mediterranean GOLD project#. Mar. Pet. Geol. 66, 6–17. doi:10.1016/j.marpetgeo.2015.03.018

Reeves, C., 2014. The position of Madagascar within Gondwana and its movements during Gondwana dispersal. J. African Earth Sci. 94, 45–57. doi:10.1016/j.jafrearsci.2013.07.011

Reeves, C. V, Teasdale, J.P., Mahanjane, E.S., 2016. Insight into the Eastern Margin of Africa from a new tectonic model of the Indian Ocean. Geol. Soc. London, Spec. Publ. 431, 1–24. doi:10.1144/SP431.12

Reston, T., Mcdermott, K., 2014. An assessment of the cause of the “extension discrepancy” with reference to the west Galicia margin. Basin Res. 26, 135–153. doi:10.1111/bre.12042

Reston, T.J., 2009. The structure, evolution and symmetry of the magma-poor rifted margins of the North and Central Atlantic: A synthesis. Tectonophysics 468, 6–27. doi:10.1016/j.tecto.2008.09.002

Rey, P., Vanderhaeghe, O., Teyssier, C., 2001. Gravitational collapse of continental crust: definitions, regimes, mechanisms and modes. Tectonophysics 342, 435–449.

Roberts, N.M.W., Van Kranendonk, M.J., Parman, S., Clift, P.D., 2015. Continent formation through time. Geol. Soc. London, Spec. Publ. 389, 1–16. doi:10.1144/SP389.13

Runcorn, S.K., 1965. Palaeomagnetic Comparisons between Europe and North America. Philos. Trans. R. Soc. London. Ser. A, Math. Phys. Sci. 258, 1–11.

Sage, F., Basile, C., Mascle, J., Pontoise, B., Whitmarsh, R.B., 2000. Crustal structure of the continent-ocean transition off the Cote d’Ivoire-Ghana transform margin: Implications for thermal exchanges across the palaeotransform boundary. Geophys. J. Int. 143, 662–678. doi:10.1046/j.1365-246X.2000.00276.x

Schandelmeier, H., Bremer, F., Holl, H.G., 2004. Kinematic evolution of the Morondava rift basin of SW Madagascar - From wrench tectonics to normal extension. J. African Earth Sci. 38, 321–330. doi:10.1016/j.jafrearsci.2003.11.002

Schiffer, C., Peace, A., Phethean, J., Gernigon, L., McCaffrey, K.J.W., Petersen, Kenni, D., Foulger, G., n.d. The Jan Mayen Microplate Complex and the Wilson Cycle. Geol. Soc. London, Spec. Publ.

Scrutton, R.A., Heptonstall, W.B., Peacock, J.H., 1981. Constraints on the motion of Madagascar with respect to Africa. Mar. Geol. 43, 1–20. doi:10.1016/0025-3227(81)90126-2

Sègoufin, J., Patriat, P., 1980. Existence d’anomalies mésozoïques dans le bassin de Somalie. Implications pour les relations Afrique-Antarctique-Madagascar. Comptes Rendus l’Académie des Sci. 291, 85–88.

Shackleton, R.M., 1996. The final collision zone between East and West Gondwana: where is it? J. African Earth Sci. 23, 271–287.

Simon, K., Huismans, R.S., Beaumont, C., 2009. Dynamical modelling of lithospheric extension and small-scale convection: Implications for magmatism during the formation of volcanic rifted margins. Geophys. J. Int. 176, 327–350. doi:10.1111/j.1365-246X.2008.03891.x

Smith, A.G., Hallam, A., 1970. The Fit of the Southern Continents. Nature 225, 139–144.

Stab, M., Bellahsen, N., Pik, R., Quidelleur, X., Ayalew, D., Leroy, S., 2016. Modes of rifting in magma-rich settings: Tectono-magmatic evolution of Central Afar. Tectonics 35, 2–38. doi:10.1002/2015TC003893

Storey, B.C., 1995. The role of mantle plumes in continental breakup: case histories from Gondwanaland. Nature. doi:10.1038/377301a0

Taylor, B., Goodliffe, A., Martinez, F., 2009. Initiation of transform faults at rifted continental margins. Comptes Rendus - Geosci. 341, 428–438. doi:10.1016/j.crte.2008.08.010

Tugend, J., Manatschal, G., Kusznir, N.J., Masini, E., 2015. Characterizing and identifying structural domains at rifted continental margins: application to the Bay of Biscay margins and its Western Pyrenean fossil remnants. Geol. Soc. London, Spec. Publ. 413, 171–203. doi:10.1144/SP413.3

Turcotte, D.L., Emerman, S.H., 1983. Mechanisms of active and passive rifting. Dev. Geotecton. 19, 39–50. doi:10.1016/B978-0-444-42198-2.50010-9

Umbgrove, J.M.F., 1947. The Pulse of the Earth. Martinus Nijhoff, The Hague, Netherlands.

Unternehr, P., Peron-Pinvidic, G., Manatschal, G., Sutra, E., 2010. Hyper-extended crust in the South Atlantic: in search of a model. Pet. Geosci. 16, 207–215. doi:10.1144/1354-079309-904
Van Avendonk, H.J.A., Lavier, L.L., Shillington, D.J., Manatschal, G., 2009. Extension of continental crust at the margin of the eastern Grand Banks, Newfoundland. Tectonophysics 468, 131–148. doi:10.1016/j.tecto.2008.05.030
van Wijk, J.W., Huismans, R.S., ter Voorde, M., Cloetingh, S.A.P.L., 2001. Melt generation at volcanic continental margins: No need for a mantle plume? Geophys. Res. Lett. 28, 3995–3998. doi:10.1029/2000GL012848
Veevers, J.J., 2004. Gondwanaland from 650-500 Ma assembly through 320 Ma merger in Pangea to 185-100 Ma breakup: Supercontinental tectonics via stratigraphy and radiometric dating. Earth-Science Rev. 68, 1–132. doi:10.1016/j.earscirev.2004.05.002
Vine, F.J., Matthews, D.H., 1963. Magnetic Anomalies Over Oceanic Ridges. Nature 199, 947–949.
Waples, D.W., 2002. A new model for heat flow in extensional basins: estimating radiogenic heat production. Nat. Resour. Res. 11, 125–133. doi:10.1023/A:1015568119996
Wegener, A., 1912. Die Entstehung der Kontinente. Dr. A. Petermanns Mitteilungen aus Justus Perthes' Geogr. Anstalt 63, 185–195, 253–256, 305–309.
White, N., Thompson, M., Barwise, T., 2003. deep-water continental margins 426.
White, R., McKenzie, D., 1989. Magmatism at rift zones: The generation of volcanic continental margins and flood basalts. J. Geophys. Res. 94, 7685. doi:10.1029/JB094iB06p07685
White, R.S., McKenzie, D., O'Nions, R.K., 1992. Oceanic crustal thickness from seismic measurements and rare earth element inversions. J. Geophys. Res. 97, 19683–19715. doi:10.1029/92JB01749
Whittaker, J.M., Williams, S.E., Halpin, J.A., Wild, T.J., Stilwell, J.D., Jourdan, F., Daczko, N.R., 2016. Eastern Indian Ocean microcontinent formation driven by plate motion changes. Earth Planet. Sci. Lett. 454, 203–212. doi:10.1016/j.epsl.2016.09.019
Wilson, J.T., 1965. A New Class of Faults and their Bearing on Continental Drift. Nature 207, 343–347. doi:10.1038/207343a0
Wilson, R.C.L., Manatschal, G., Wise, S., 2001. Rifting along non-volcanic passive margins: stratigraphic and seismic evidence from the Mesozoic successions of the Alps and western Iberia. Geol. Soc. London, Spec. Publ. 187, 429–452. doi:10.1144/GSL.SP.2001.187.01.21
Wilson, T.J., 1966. Did the Atlantic close and then re-open? Nature 211, 676–681.
Windley, B.F., 1977. The evolving continents. Geol. J.
Windley, B.F., Razafiniparany, A., Razakamanana, T., Ackermand, D., 1994. Tectonic framework of the Precambrian of Madagascar and its Gondwana connections: a review and reappraisal. Geol. Rundschau 83, 642–659. doi:10.1007/BF00194168
Worsley, T.R., Nance, D., Moody, J.B., 1984. Global tectonics and eustasy for the past 2 billion years. Mar. Geol. 58, 373–400. doi:10.1016/0025-3227(84)90209-3
Wright, J.B., 1976. kacture systems in Nigeria and initiation of fracture zones in the South Atlantic Figure 1 represents the convergence of two quite different lines of evidence which together make a compelling case for proposing that initiation of the Romanche and Chain fr. Atlantic 34, 43–47.
Yamato, P., Husson, L., Becker, T.W., Pedoja, K., 2013. Passive margins getting squeezed in the mantle convection vice. Tectonics 32, 1559–1570. doi:10.1002/2013TC003375
Ziegler, P.A., 1993. Plate-moving mechanisms: their relative importance. J. Geol. Soc. London. 150, 927–940. doi:10.1144/gsjgs.150.5.0927

2. Madagascar's escape from Africa: A high-resolution plate reconstruction for the Western Somali Basin and implications for supercontinent dispersal

Abstract

Accurate reconstructions of the dispersal of supercontinent blocks are essential for testing continental breakup models. Here, we provide a new plate tectonic reconstruction of the opening of the Western Somali Basin during the breakup of East and West Gondwana. The model is constrained by a new comprehensive set of spreading lineaments, detected in this heavily sedimented basin using a novel technique based on directional derivatives of free-air gravity anomalies. Vertical gravity gradient and free-air gravity anomaly maps also enable the detection of extinct mid-ocean ridge segments which can be directly compared to several previous ocean magnetic anomaly interpretations of the Western Somali Basin. The best-matching interpretations have basin symmetry around the M0 anomaly; these are then used to temporally constrain our plate tectonic reconstruction. The reconstruction supports a tight fit for Gondwana fragments prior to breakup, and predicts that the continent-ocean transform margin lies along the Rovuma Basin, not along the Davie Fracture Zone (DFZ) as commonly thought. According to our reconstruction, the DFZ represents a major ocean-ocean fracture zone formed by the coalescence of several smaller fracture zones during evolving plate motions as Madagascar drifted southwards, and offshore Tanzania is an obliquely rifted, rather than transform, margin. New seismic reflection evidence for oceanic crust inboard of the DFZ strongly supports these conclusions. Our results provide important new constraints on the still enigmatic driving mechanism of continental rifting, the nature of the lithosphere in the Western Somali Basin, and its resource potential.

2.1. Introduction

Continental breakup is a fundamental, but poorly understood, part of the plate tectonic cycle. Our understanding of the conditions needed for successful rift formation is particularly limited. Besides pre-existing weak zones (Ziegler and Cloetingh, 2004) and thermal weakening due to rifting-related magmatism (Buck, 2007), it has also recently been shown that oblique rifting is an important mechanism to facilitate the breakup (Brune et al., 2012). To further investigate these concepts, accurate reconstructions of rifting events with high spatial resolution are essential to enable detailed comparisons between models and observations (Nance and Murphy, 2013). Detailed history of rifted margin evolution is also key in hydrocarbon exploration by enabling the prediction of the petroleum potential for conjugate basins with similar tectonostratigraphic histories (Beglinger et al., 2012). Some of the most significant rifting episodes in Earth's history occurred during supercontinent breakup, e.g. rifting between East and West Gondwana, which spanned many of our present day continents.

Gondwana was assembled between 600 and 500 Ma in the Pan-African orogeny (e.g. Trompette, 2000; Van Hinsbergen et al., 2011). Beginning in the Jurassic the subsequent breakup of East and West Gondwana carried Madagascar approximately southwards, as shown by ocean magnetic anomalies (Sègoufin and Patriat, 1980; Rabinowitz et al., 1983; Cochran, 1988; Eagles and König, 2008; Davis et al., 2016), forming the Western Somali Basin (WSB) (Coffin and Rabinowitz 1987; Geiger et al., 2004). Knowledge of Madagascar's former position within Gondwana, and the path it followed during its southward drift, is crucial for creating accurate plate tectonic reconstructions of Gondwana's dispersal.

Paleogeographic reconstructions of Madagascar's position in Africa (Figure 2.1) have a large range of fits, suggesting significantly different locations for the continent-ocean transition. This is primarily due to the lack of fracture zone expressions in bathymetry data, where the characteristic fracture zone topography is commonly obscured by over 5 km of sediment (Coffin et al., 1986). The Davie Fracture Zone (DFZ), commonly assumed to form the western transform fault (Coffin et al., 1986) or continental ocean transform margin (e.g. Gaina et al., 2013) of the WSB, is one of the few fracture zones confidently identified. However, the DFZ is overlapped by several independently generated reconstructions (e.g. Smith and Hallam, 1970; Lottes and Rowley, 1990; Reeves, 2014). This puts our understanding of this feature into doubt, and highlights the need for the comprehensive detection of fracture zones to support plate tectonic reconstructions of the basin.

In this paper we present a detailed and self-consistent plate tectonic reconstruction of the WSB that can be used to further our understanding of the dynamics of continental breakup. We use a novel combination of free-air gravity, vertical gravity gradient and filtered free-air gravity directional derivatives to determine the location of the extinct mid-ocean ridge (MOR) segments and a comprehensive set of gravity lineaments related to fracture zones in the WSB. Using global gravity datasets with 1 arc-minute resolution captures the complexity of the breakup geometry and motion, beyond what can be seen in widely spaced shipboard magnetic profiles, and also constrains the history of the basin to the west of 43˚E where no magnetic anomaly identifications are available (e.g. Davis et al., 2016). These spreading-related features are tested against existing magnetic and seismic reflection data before being used to produce a high-resolution plate tectonic reconstruction.

The model provides new insight into Madagascar's position in Africa prior to Gondwana breakup, the nature of the DFZ, and the geometry and structure of the East African continental margin. This provides a significant advance towards a more comprehensive understanding of the nature of the margins and underlying lithosphere of the WSB, as well as a broader understanding of rifting events and continental breakup mechanisms.

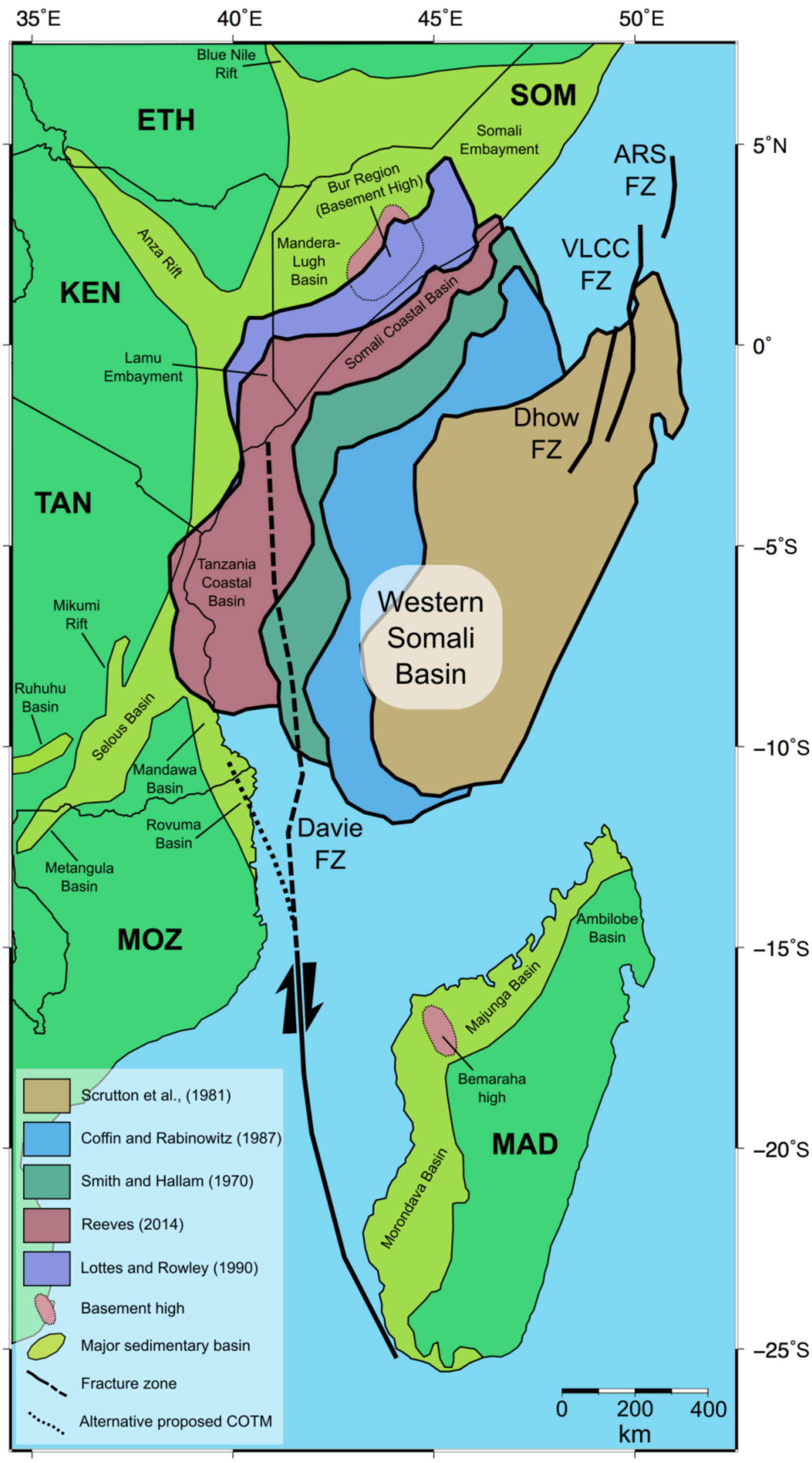

Figure 2.1. Published reconstructions for Madagascar's paleo-position in Africa are shown alongside major continental basins, basement highs, and previously identified oceanic fracture zones. ARS - Auxiliary Rescue and Salvage; VLCC - Very Large Crude Carrier; ETH - Ethiopia; KEN - Kenya; MAD - Madagascar; MOZ - Mozambique; SOM - Somalia; TAN - Tanzania; COTM – Continent-ocean transform margin.

2.2. Data and processing

In this study, we used the distribution and orientation of fracture zones (FZs) and extinct MORs to construct a plate tectonic model for the WSB. These tectonic features were detected using a combination of gravity, magnetic and seismic data.

2.2.1. Gravity data

We used version 23 of the Sandwell and Smith gravity model (Sandwell et al., 2014), which now has an accuracy of ~2 mGal (compared to 3-5 mGal in previous versions) following the addition of retracked CryoSat-2 and Jason-1 satellite altimetry data. This improvement allows detection of many buried structures, particularly short wavelength features such as extinct MORs and FZs (e.g. Sandwell et al., 2014). In addition to the widely-used free-air gravity anomaly, gradients such as the vertical gravity gradient (VGG) amplify short wavelength gravity signals, aiding the detection of relatively small features such as seamounts and ocean spreading structures (e.g. Kim and Wessel, 2011).

FZs are the inactive extensions of transform faults along the MOR, which run parallel to the spreading direction during their formation and therefore record plate motions. Oceanic plate ages, and thus seafloor depths, are offset across transform faults, causing a distinct bathymetric feature, which is permanently locked in by welding at ridge-transform intersections (Sandwell, 1984). Variations in crustal thickness due to melt supply (Blackman and Forsyth, 1991; Gente et al., 1995), transpression or transtension (Menard and Atwater, 1969), and thermal contraction (Collette, 1974) can also result in bathymetric expressions along fracture zones. The resulting linear ridges and troughs can be traced in bathymetric data in order to track the spreading history, which in turn may be used in constructing a plate tectonic model.

In heavily sedimented regions, however, spreading features may be completely buried. Fortunately, expressions of the spreading features are also preserved in gravity data, even when buried by sediments, due to lateral density contrasts between sediment, crust, and mantle across the structures. Gravity data therefore allows the derivation of paleo-spreading directions in heavily sedimented regions of the ocean (Sandwell et al., 2014).

2.2.1.1. Bandpass filtering and gravity gradients

We used a combination of directional derivatives and bandpass filtering to further enhance the portion of the gravity field associated with FZs. First, a Gaussian bandpass filter was used to remove short wavelength noise and shallow features within the sediment layer, together with long wavelength signals from deep mantle heterogeneities. Mulder and Collette (1984) found that most FZs produce anomalies with intermediate wavelengths between 50 and 200 km. We further refined these bounds empirically, looking for sharp, continuous linear anomalies parallel to the overall spreading direction derived from ocean magnetic anomalies, and found that wavelengths of 55-85 km best highlighted fracture zone structure.

After filtering, we exploited the linear nature of spreading features by taking directional gradients of the free-air gravity to emphasise lineations of a given orientation (e.g. Mitchell and Park, 2014). This procedure has similar advantages to illuminating a topographic map to highlight fault scarps (e.g. Arrowsmith and Zielke, 2009). In the case of the WSB, the ocean magnetic anomalies indicate an approximately N-S spreading direction. Therefore gradients taken along this strike would highlight spreading-perpendicular features, such as MOR segments, and those taken with an E-W strike would highlight spreading-parallel features, such as FZs. To account for local variability and changes in spreading direction, we took the directional gradient at 10° intervals between 30° clockwise and anti-clockwise of the chosen azimuth. This allowed near-perpendicular gradients to be sampled at all points along curved lineations, ensuring an unbiased sampling of the greatest gradient magnitudes. Examples showing the effect of changing the orientation and range of gradient sampling are provided in the supplementary material.

2.2.1.2. Testing the detection method

To check our methodology's usefulness in detecting spreading-related structures in buried oceanic crust, we tested it on a region of the Cape Basin, offshore South Africa (Figure 2.2a). Like the WSB this basin has a thick sedimentary cover (2-5+ km), resulting in enigmatic spreading features that are difficult to interpret from free-air gravity and VGG alone. The overall spreading rate is also similar to the WSB (e.g. Eagles, 2007) likely resulting in similar FZ morphology; making this a very good natural laboratory. The free-air gravity anomaly of the test region within the Cape Basin was compared to that of an unsedimented example location from the Central Atlantic (Figures 2.2b-c), demonstrating the masking effect of sedimentation on the spreading features: clear lineations are visible in the Central Atlantic (Figure 2.2b), but lineations are only poorly distinguishable in the Cape Basin (Figure 2.2c). In this case, the VGG does little to enhance the spreading lineations (Figure 2.2d). Derivatives of the gravity anomaly, perpendicular to the spreading direction for the Cape Basin, were taken after filtering to retain different wavelengths (Figures 2.2e-g) to check which wavelengths best enhance spreading features. Shorter wavelengths (25-55 km, Figure 2.2e) are noisy and reduce the continuity of spreading parallel anomalies, whilst longer wavelengths (85-115 km, Figure 2.2g) reduce the sharpness of individual lineations and can also merge anomalies into false lineations (example indicated by black arrows).

Intermediate wavelengths of 55-85 km give the best balance between noise reduction and imaging of sharp FZ-related anomalies.

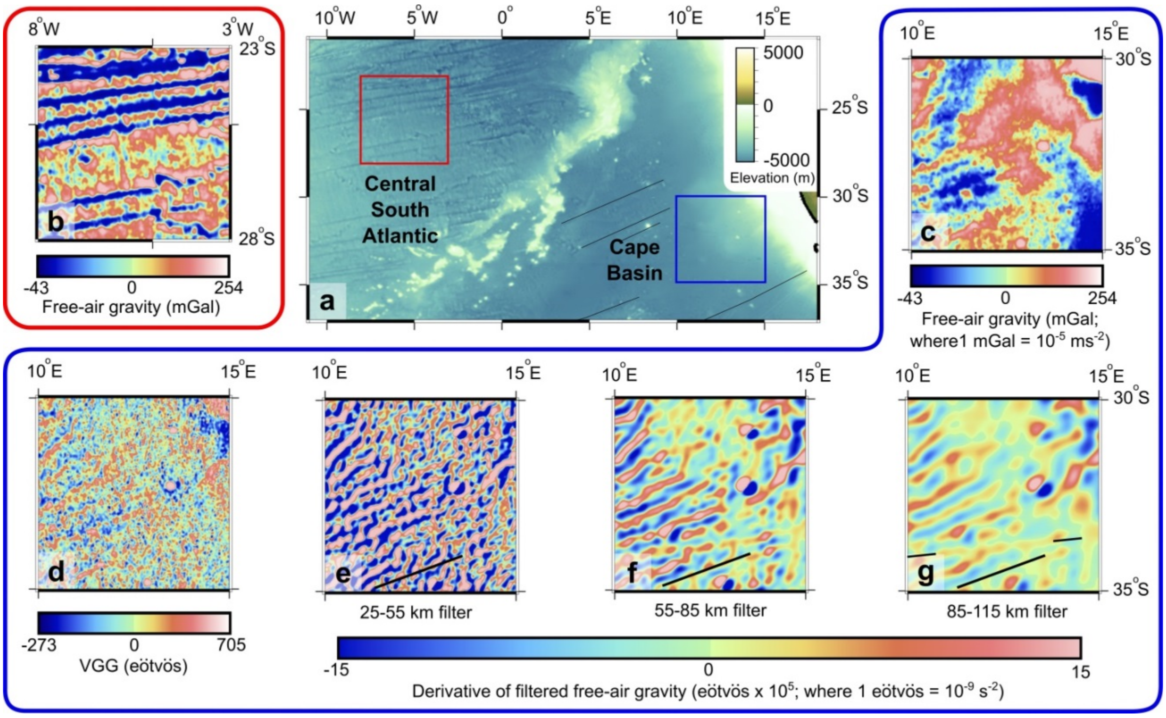

Figure 2.2. (a) Test location for the processing technique within the heavily sedimented Cape Basin, and an unsedimented example location in the Central South Atlantic. Major fracture zones of the Cape basin are marked as thin black lines. (b) Free-air gravity example of non-sedimented Central Atlantic spreading features. (c) Free-air gravity from the heavily sedimented test location. (d) VGG from the test location. (e-g) Spreading parallel derivatives of gravity after filtering to retain specified wavelength bands. Black lines indicate spreading direction as constrained by major FZs from elsewhere in the Cape Basin; arrows in g indicate merged anomaly lineations.

2.2.2. Magnetics

We used two primary magnetic data types to inform our final model: the Earth Magnetic Anomaly Grid (EMAG2 – Maus et al., 2009), and published ocean magnetic anomaly interpretations from ship-track data. EMAG2 (non-directionally gridded version) shows the large scale trend of magnetic anomalies in the WSB, where many individual linear ocean magnetic anomalies are identifiable. The requirement for orthogonality between these linear ocean magnetic anomalies and identified FZs allowed us to check our interpretation.

Of the published ocean magnetic anomaly interpretations, those by Sègoufin and Patriat (1980), Cochran (1988), and Davis et al. (2016) show strong similarities to each other, with the basin's centre of symmetry lying around the M0 ocean magnetic anomaly (125 Ma) and the oldest anomalies detected in the basin reaching between M21 and M24. Rabinowitz et al. (1983) and Eagles and König (2008) choose an alternative interpretation with the basin's centre of symmetry around M10, and located significantly farther south. We compare these lines of symmetry with MOR segments identified in the gravity data and used the best matching interpretations to temporally constrain our reconstruction. All interpretations suggest slow-intermediate spreading rates for the WSB

2.2.3. Seismic reflection data

The East AfricaSPAN seismic reflection lines were used to identify the nature of the top basement reflector and measure the crustal thickness, thus helping determine whether the underlying basement is continental, oceanic, or transitional in nature. In addition, faults associated with the tectonic fabric at mature slow/intermediate spreading centres dip towards the MOR (e.g. Carbotte and Macdonald, 1990; Behn and Ito, 2008). Therefore fault polarity switches were used to help constrain the location of the MOR to the east of the DFZ, when spreading ceased ~50 Ma after breakup.

2.3. Feature identification

Spreading features of the WSB, including the extinct MOR and FZs, must be detected in order to constrain plate tectonic reconstructions. To do this we identify the characteristics that define each group of features. We must, however, also be careful to avoid interpretation of areas modified by young rifts, such as the Quirimbas Graben, and post spreading magmatic additions, such as the Comoros Islands, Cosmoledo Group, and Wilkes Rise (e.g. Figure 2.3), which have strong expressions in the gravity data and mask the true nature of spreading features.

2.3.1. Mid-oceanic ridge segments

Extinct MOR segments have orientations perpendicular to the final spreading direction, and appear as a free-air gravity low due to a persistent low density gabbroic root (Jonas et al., 1991). These linear anomalies usually lie close to the basin's centre of symmetry, with the exception of basins undergoing subduction, such as the Pacific Ocean (Müller et al., 2008), or those having undergone spreading centre reorganisation and ridge jumps. To identify the extinct MOR from gravity anomalies, we therefore looked for three characteristics: 1) a linear free-air gravity low, 2) an orientation perpendicular to the approximately N-S paleo-spreading direction (e.g. Sègoufin and Patriat, 1980), and 3) a location close to the axis of symmetry for the WSB. Free-air gravity and VGG maps were used for this task.

Regions where only one gravity lineament with these characteristics was identified provided reliable MOR segment interpretations. These segments were therefore compared with the ocean magnetic anomaly interpretations of Sègoufin and Patriat (1980), Rabinowitz et al. (1983), Cochran (1988), Eagles and König (2008), and Davis et al. (2016) to assess confidence in these interpretations. Where multiple possible MOR anomalies existed, seismic reflection data were used to locate the MOR using basement fault polarity (e.g. Behn and Ito, 2008). If no seismic data were available, we chose the lineament that was most consistent with the ocean magnetic anomaly interpretations verified by our reliable MOR segments

2.3.2. Fracture zones

In the WSB, 2-5+ km of sediment have accumulated since the Jurassic (Coffin et al., 1986), removing most bathymetric expressions of FZs. A limited set of major lineations related to fracture zones can, however, be seen in the free-air gravity anomaly, reflecting crustal thickness variations, basement offsets, and infilling sediments along the FZs. We further highlighted FZ-related anomalies using a 55-85 km bandpass filter and an E-W directional derivative, orthogonal to the overall N-S spreading direction, as illustrated for the Cape Basin in Figure 2.2.

The resulting linear anomalies relating to the FZ trends are generally of low amplitude compared with those arising from volcanic edifices or active rifts. This is primarily the result of the FZs' comparatively small scale, greater depth, and lower density contrast across the structural boundary. However, to map FZs, we were primarily interested in fairly continuous linear anomalies that form a consistent pattern, even if low in amplitude due to the thick sedimentary cover. These lineations (e.g. Figure 2.2f) can be mapped along minima, maxima, or polarity changes in the gravity gradient; all have the same orientation and thus lead to the same plate tectonic model. However, for consistency, we have manually picked along the polarity change in the gravity gradient, except in cases where this is poorly defined and the maximum or minimum shows the orientation more clearly.

The Tanzania Coastal Basin, inboard of the DFZ, has previously been assumed to be underlain by continental crust. To determine whether to interpret any gravity lineations within this basin as continental shear zones or oceanic fracture zones, the East AfricaSPAN seismic reflection dataset was used to determine the nature of the crust. Oceanic crust was identified through the recognition of a rough high amplitude top reflector with a tectonic spreading fabric, lacking significant syn-rift deposits (Davies et al., 2005; Rodger et al., 2006) or by a hummocky reflector with continuous overlying sedimentary deposits (Soto et al., 2011), and, for normal oceanic crust, a two-way travel time (TWTT) between top basement and any Moho reflections of ~2 seconds (e.g. White et al., 1992).

2.4. Plate tectonic reconstruction

After establishing the FZ lineations for the WSB, we used the plate tectonic reconstruction software Gplates (e.g. Williams et al., 2012), populated with the plate polygons of Seton et al. (2012), to retrace Madagascar's path back to Africa. The previously identified Dhow and VLCC fracture zones (Bunce and Molnar, 1977) were not used as input to the model because Coffin and Rabinowitz (1987) suggested they may be the result of tectonic processes other than oceanic spreading. Once the general origin for Madagascar was established, its position was refined by aligning conjugate continental shear zones and sedimentary basins, following Windley et al. (1994) and Reeves (2014). Artificial flowlines were then seeded at the deepest points of the basins between Madagascar and Africa according to the CRUST1.0 model (Laske et al., 2013), assumed to be the original centre of symmetry for spreading. In an iterative process, the motion of Madagascar away from Africa was then refined by aligning model-generated flowlines with the interpreted fracture zone trends. The plate model was temporally constrained by the ocean magnetic anomaly interpretations of Cochran (1988) and Davis et al. (2016), whose centres of symmetry around M0 most reliably matched the observed MOR segments. However, no plate velocity constraints exist between the initiation of rifting in the Toarcian (182 Ma) and the oldest ocean magnetic anomaly detected in the basin (M22, 150.5 Ma – Cochran, 1988; Gradstein, 2012). Between the onset of rifting and breakup at 170 Ma in the Bajocian (Geiger et al., 2004) we imposed an extensional velocity of 3.3 mm/y. This was based on well constrained present day extension rates along the East African Rift System between Malawi and Afar (Saria et al., 2014) and may therefore represent a realistic estimate for Jurassic extensional rates during the rifting phase. Following this rifting episode ~390 km remained between the spreading centre and the M22 magnetic anomaly, which was bridged with a constant velocity of 40 mm/y.

2.5. Results

Using free-air gravity, VGG, and directional derivatives of filtered gravity from version 23 of the Sandwell and Smith gravity model, we have detected the extinct MOR segments and a comprehensive set of lineaments relating to spreading features in the Western Somali Basin. These features are tested against magnetic and seismic reflection data before being used to produce a high-resolution plate tectonic reconstruction of the basin.

2.5.1. MOR segment locations

Oceanic magnetic anomalies in the WSB show that spreading occurred in a generally N-S direction (Sègoufin and Patriat, 1980). Following this, and the NE-SW trends of the Kenya-Somalia and Northern Madagascar coastlines, we expect the extinct MOR to be composed of E-W trending segments with an overall NE-SW trend following the basins centre of symmetry. We identify short linear gravity lows following this pattern in both the free-air gravity anomaly (Figure 2.3a and b) and the VGG (Figure 2.3c and d). The MOR segments generally range from 30-100 km in length, with offsets between segments ranging from as little as 20 km up to 350 km between the two easternmost segments.

On the eastern side of the basin, single gravity lineaments point unambiguously to the MOR. This region is therefore used as an independent check of the previous ocean magnetic anomaly interpretations. This shows that interpretations with the basin's centre of symmetry based on M0 are most reliable, and therefore the ocean magnetic anomaly interpretations of Cochran (1988) and Davis et al. (2016) are used to temporally constrain our plate tectonic model. In the western region of the basin, close to the DFZ, two segments have several possible MOR anomalies identifiable in the gravity data (Figure 2.3 – dashed lines). For the westernmost segment, seismic reflection data covers the southern gravity lineament and shows a flip in half graben polarity centred at its location. The next segment to the east is covered by magnetic data along ship tracks and the verified ocean magnetic anomaly interpretations show the northern gravity lineament to be most consistent (Figure 2.3 – solid lines).

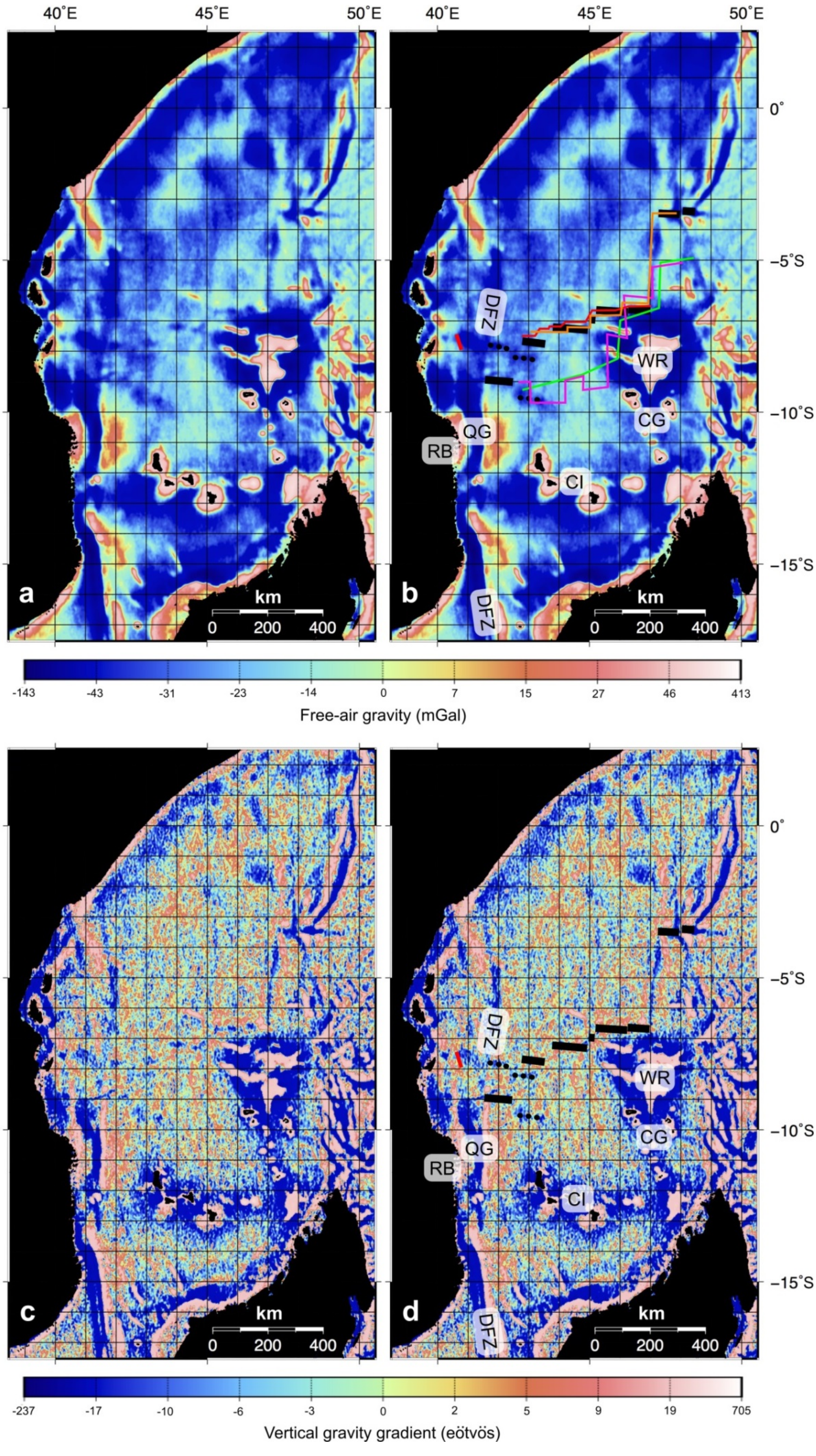
40˚E
45˚E
50˚E
0˚
−5˚S
−10˚S
−15˚S
a
b
c
d
km
0 200 400
DFZ
WR
CG
QG
RB
CI
-143 -43 -31 -23 -14 0 7 15 27 46 413
Free-air gravity (mGal)
-237 -17 -10 -6 -3 0 2 5 9 19 705
Vertical gravity gradient (eötvös)

Figure 2.3. (a) Free-air gravity anomaly. (b) Figure 2.3a overlain with the picked MOR (solid black lines) and alternative segment possibilities (dashed black lines). Location of the East AfricaSpan seismic reflection line shown in this study is indicated by the thick red line in the Tanzania Coastal Basin. Previously determined basin symmetries are shown as coloured lines where constrained by ocean magnetic anomalies. The interpretations of Cochran (1988 – orange) and Davis et al. (2016 – red) are centred on M0 and lie in good agreement with the MOR defined by gravity. The interpretations of Coffin and Rabinowitz (1987 - green) and Eagles and König (2008 - pink) are centred on M10 and deviate significantly from the gravity MOR. RB – Rovuma Basin; QG – Quirimbas graben (active rift). DFZ – Davie Fracture Zone; Post spreading volcanism: CI – Comoros islands; CG – Cosmoledo Group; WR – Wilkes Rise. (c) Vertical gravity gradient. (d) Figure 2.3c overlain with MOR picks and abbreviations as for Figure 2.3b.

2.5.2. Fracture zone trends

The free-air gravity anomaly shows a number of major lineaments in the Western Somali Basin, including the Davie, ARS, Dhow, and VLCC fracture zones, as well as number of more subtle lineaments with a similar trend (Figure 2.4). Fracture zones in the Indian Ocean, which has much thinner sediment cover (<1 km; Whittaker et al., 2013), are also clearly seen. These lineaments often display a significant anomaly in the gravity field, from ~20 mGal to over 100 mGal compared to their surroundings, and can be traced for several hundreds of kilometres, including over 1000 km in the case of the DFZ. They show an arcuate spreading pattern for the Western Somali Basin. This trend can not only be seen in the north of the basin, but is also defined by a striking bend in the DFZ located at 41° E, 14 ° S, which appears to deflect the trend of the continent-ocean transform margin onshore along the Rovuma Basin.

Lineaments detected only in the filtered and directionally differentiated gravity data are generally shorter and less continuous, ranging in length from less than 100 km up to approximately 600 km (Figure 2.5). In several instances, extensions to fracture zones detected in the free-air anomaly can be made, such as at 45° E 7° S, where a conjugate fracture zone to one detected in the north becomes apparent in the southern half of the basin. On the whole, these lineaments align with the framework laid out by anomalies detected in the free-air gravity and provide a comprehensive record of plate spreading directions. A few short lineaments, however, lie at significant angles to the general fabric. It is likely that these lineaments are the result of structures unrelated to spreading (which should produce a consistent and predictable network of FZs), such as small volcanic chains or large infilled submarine channels, producing gravity anomalies with a similar wavelength to those of spreading features.

The EMAG2 gridded magnetic dataset (Figure 2.6a) contains several linear magnetic trends within the central region of the WSB where the basement is oceanic in nature (Coffin et al., 1986). Away from magmatic structures such as the Wilkes Rise and Comoros Islands these anomalies should be due to magnetization of oceanic crust during seafloor spreading, producing ocean magnetic anomalies. Their orientation appears variable and they do not seem to define a consistent spreading direction. When, however, the magnetics are overlain by the FZ trends identified in the gravity data, the linear magnetic anomalies can be seen to lie consistently perpendicular to the arcuate fracture zone lineaments (Figure 2.6b), providing independent confirmation of our proposed fracture zone structure.

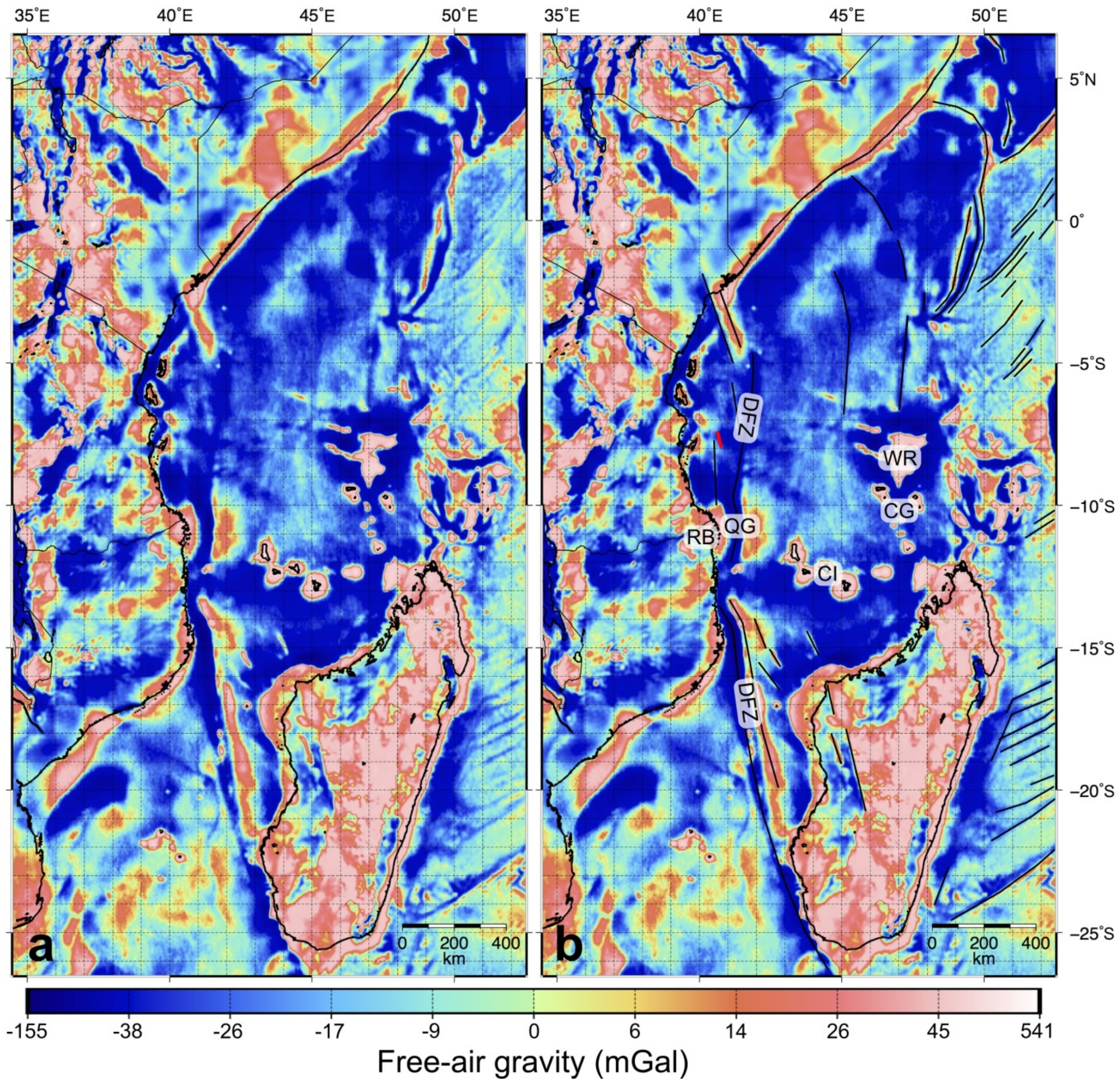

Figure 2.4. (a) Free-air gravity anomaly. (b) Figure 2.4a overlain with the linear anomalies related to potential fracture zones. Abbreviations as for Figure 2.3. Location of the East AfricaSPAN seismic reflection line shown in this study is indicated by the red line in the Tanzania Coastal Basin.

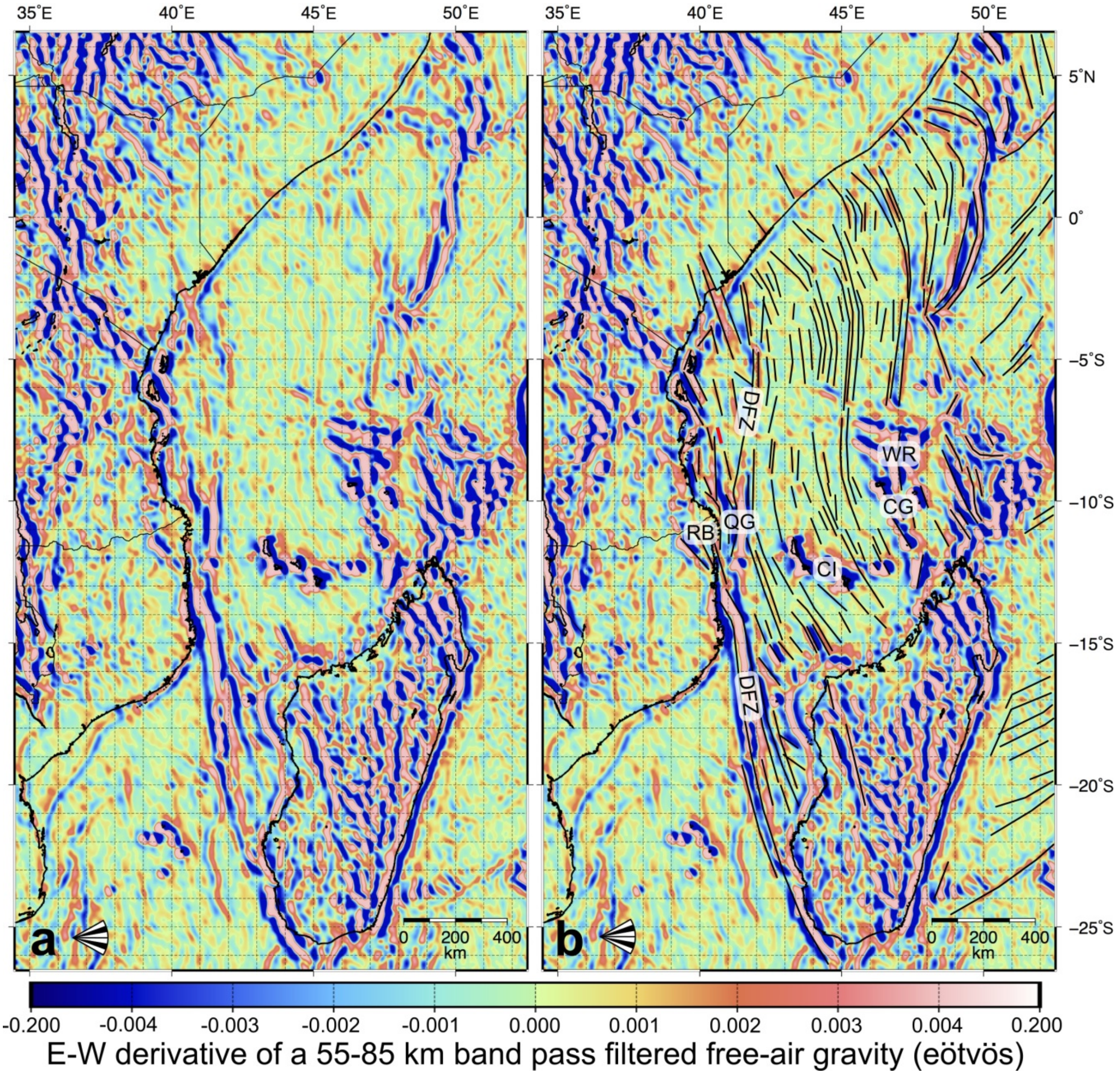

Figure 2.5. (a) E-W derivative of a Gaussian band-pass filtered free-air anomaly, 50% long and short wavelength cutoffs at 85 and 55 km, respectively, to best retain anomalies related to fracture zones. (b) Figure 2.5a overlain with the linear anomalies identified here and in Figure 2.4. Abbreviations as for Figure 2.3. Location of the East AfricaSpan seismic reflection line shown in this study is indicated by the red line in the Tanzania Coastal Basin

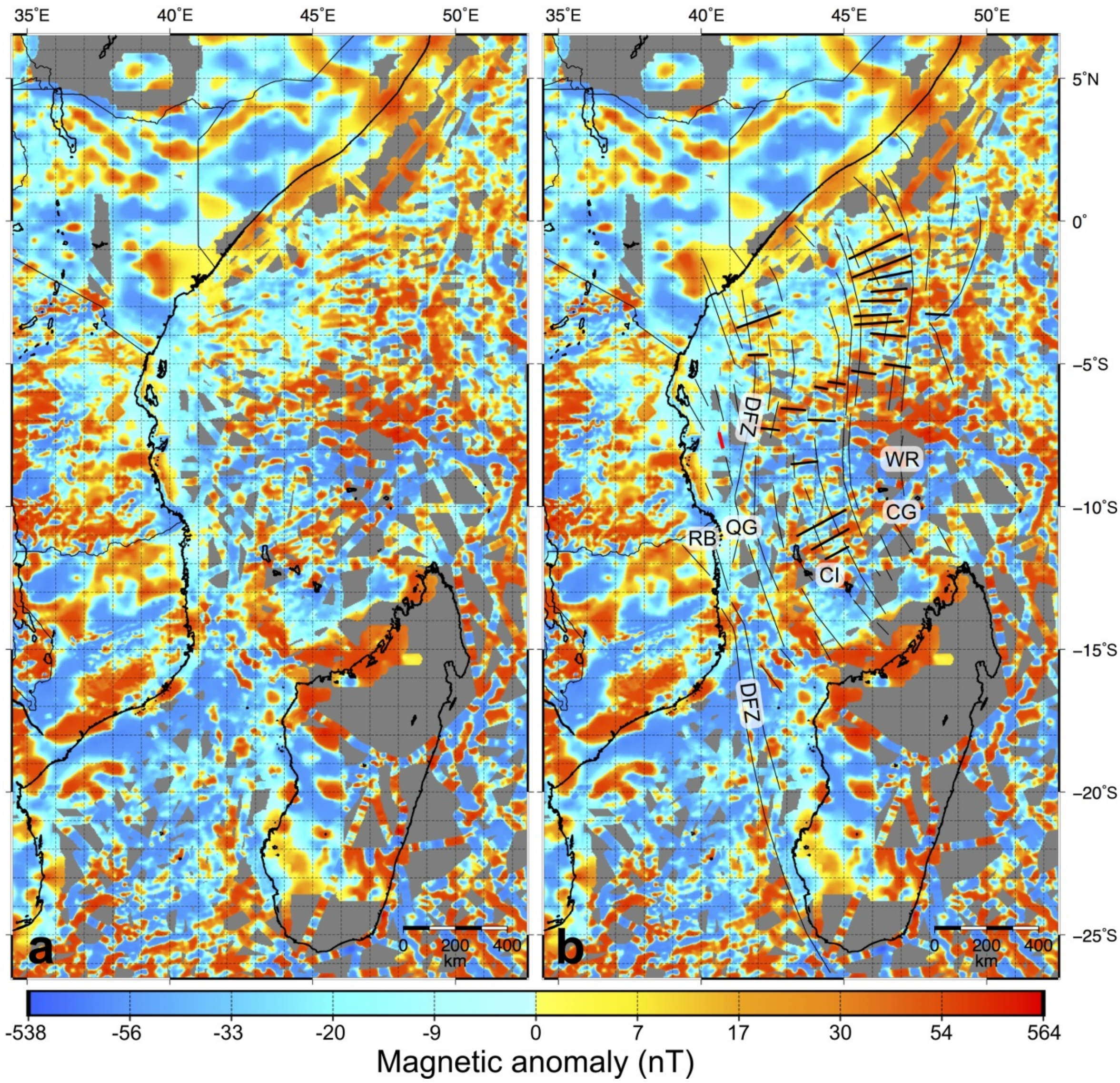

Figure 2.6. (a) The EMAG2 non-directionally gridded magnetic anomaly dataset. (b) Figure 2.6a with broadly E-W linear magnetic anomalies detected from unmodified oceanic crust (thick black lines) and fracture zones (thin black lines) marked, showing a consistently orthogonal relationship. Abbreviations as for Figure 2.3. Location of the East AfricaSpan seismic reflection line shown in this study is indicated by the red line in the Tanzania Coastal Basin.

2.5.3. Plate tectonic model

Using our new fracture zone lineaments, shear zone data from Reeves and De Wit (2000), and basin depth data from CRUST1.0, we developed a new plate tectonic reconstruction for Madagascar's separation from Africa (Figure 2.7).

An initial phase of continental rifting from 182 Ma leads to continental break up at approximately 170 Ma (Figure 2.7b-c). Oceanic spreading commences in a NNW-SSE direction and results in strike slip tectonics between Madagascar and northern Mozambique, forming the Rovuma Basin (Figure 2.7c-d). At ~150.5 Ma the spreading direction changes to almost N-S, resulting in the near alignment of several flow lines in the west of the basin (Figure 2.7d-e). After 136 Ma the spreading direction continues to rotate causing full convergence of the flow lines in the west of the basin along the trace of the DFZ. Faster spreading in the west compared to the east also results in an anti-clockwise rotation of Madagascar to its present day position, which was reached when oceanic spreading ceased in the basin at ~125 Ma (Figure 2.7e-f).

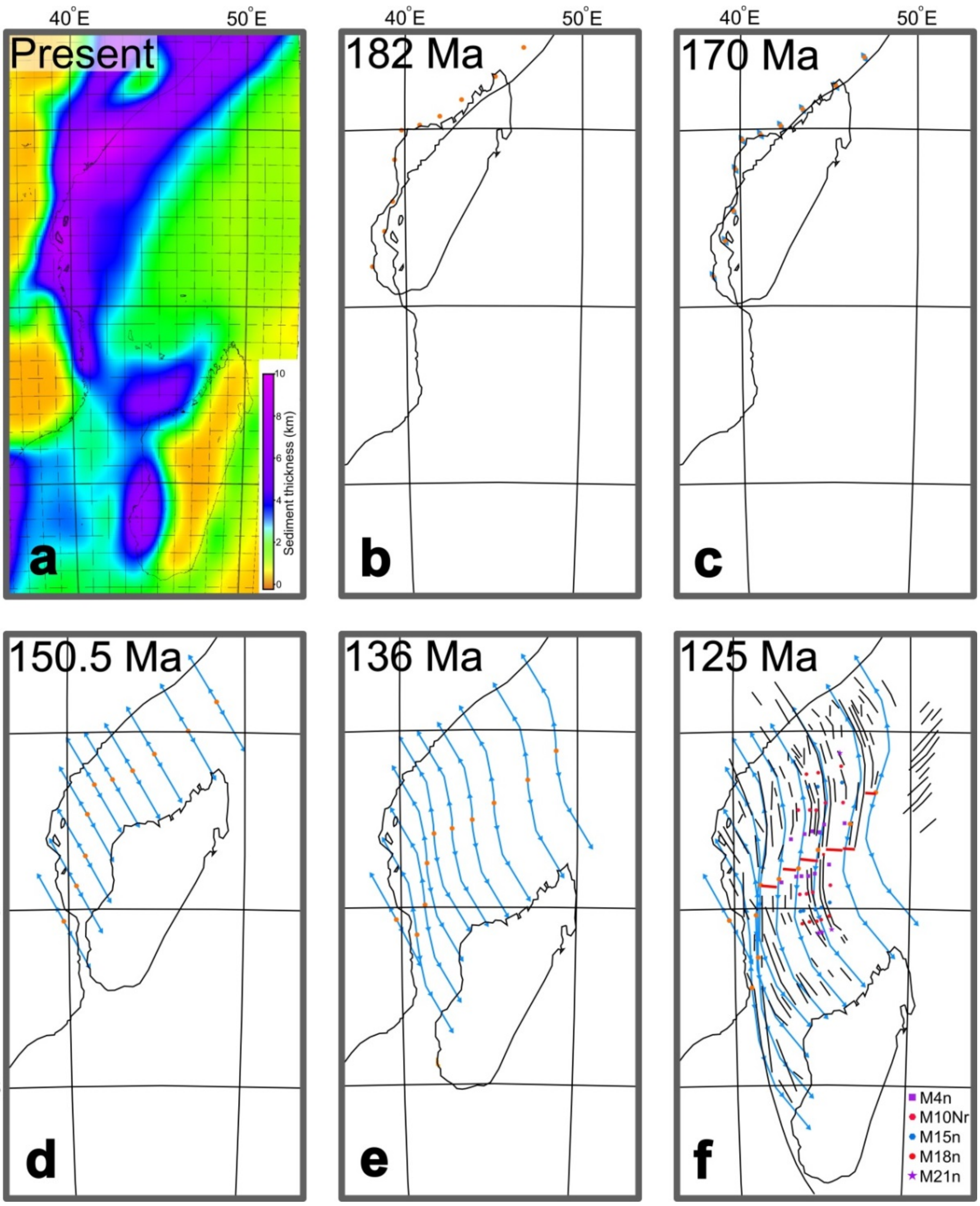

Figure 2.7. Plate tectonic reconstruction of Madagascar's escape from Africa from the Early Jurassic to the cessation of spreading in the Cretaceous. Madagascar is shown without the remainder of East Gondwana (India, Antarctica and Australia) attached. (a) Present day sediment thickness in the Western Somali Basin taken from the CRUST1.0 model. (b-e) The key stages of Madagascar's motion out of Africa. Modelled flowlines are shown as blue arrowed lines where the centre of symmetry is marked by orange circles. (f) Madagascar's present-day position, which is reached at around 125 Ma. Flowlines closely match the fracture zone pattern of the basin (additional black lines), and the basin's predicted final symmetry (orange circles) lies in good agreement with the interpreted extinct mid-ocean

ridge system (red lines). Locations of magnetic anomalies used to temporally constrain plate motions shown with symbols as interpreted by Davis et al. (2016).

2.6. Discussion

2.6.1. The nature of the WSB's margins and of gravity lineaments in the coastal basins

Modern concepts of passive margin formation define two end member types. 1) At volcanic rifted margins, crustal thinning occurs over relatively short distances (50-100 km (e.g. Franke, 2013)) and is accompanied by large volumes of magmatism. These are characterised by both thick wedges of volcanic flows that appear as seaward dipping reflectors in seismic reflection data (e.g. Planke and Eldholm, 1994; Geoffroy, 2005) and by high velocity underplating and heavily intruded crust identified in seismic refraction studies (e.g. Korenaga et al., 2000; Hirsch et al., 2009). 2) At magma-poor rifted margins, largely unthinned continental crust of the proximal domain passes into a hyperextended domain containing three sub domains (necking, hyperthinned, and exhumed mantle domains), before oceanic crust marks the onset of the oceanic domain (Tugend et al., 2015). The necking domain and hyperthinned domains accommodate most of the crustal thinning, containing continental crust of <10 km thick, and typically extend 100-200 km from the proximal domain (e.g. Reston, 2009; Sutra and Manatschal, 2012). The exhumed mantle domain forms the continent-ocean transition and is thought to consist of mantle material unroofed and serpentenised during extensional detachment faulting (e.g. Bayrakci et al., 2016; Gillard et al., 2016), which separates continental crust from oceanic crust. These margins characteristically experience limited magmatism during extension (Franke, 2013).

To understand the style of margin formation in the WSB, we draw together a combination of seismic, gravity, magnetic and geological evidence. Coffin et al. (1986) confirmed the existence of oceanic crust just offshore of the Kenya-Somalia border as far north and west as 42.05° E 2.52° S, but inboard of this within the Tanzania Coastal Basin and extending onshore within the Lamu Embayment, thin crust (<13 km thick; Reeves et al., 1987) of an ambiguous nature is covered by thick sediments (up to +12 km, Yuan et al., 2012 and references therein). Based on gravity and magnetic modelling, Reeves et al. (1987) proposed that this crust is oceanic in nature, consistent with observations of necking zones (as defined by Tugend et al., 2015) onshore along the western edge of the Lamu Embayment from seismic refraction data, which suggest a sharp crustal thinning from over 40 km to probably less than 15 km at this location (Prodehl et al., 1997). This implies that offshore seismic reflection data along the Tanzanian and Kenyan margins is located seaward of the necking zones. Ascertaining the margin nature is thus more difficult, since seaward dipping reflectors, which are characteristic of volcanic margins, form in vicinity to the necking zone and therefore may not be detected, whilst exhumed mantle domains, as seen at magma-poor margins, can be difficult to distinguish from oceanic crust formed at slow spreading centres when using seismic reflection data alone (e.g. Davy et al., 2016).

Furthermore, the already thin crust onshore within the Lamu Embayment suggests that the ‘shelf edge’ high, seen in the free-air gravity along the Somali coast east of the DFZ, is not indicative of crustal thinning, and may not coincide with the continent-ocean transition as proposed elsewhere (e.g. Bauer et al., 2000). The effects of increasing water depth and thick sedimentary accumulations can also produce this pattern of gravity anomalies without an additional contribution from decreasing crustal thickness (e.g. Walcott,1972; Watts & Stewart, 1998). Elsewhere, along the western margins of the WSB, no shelf edge gravity anomalies are present, possibly due to superimposed effects of active rifting in the area, providing little information as to the margin nature. However, as there is little evidence for Jurassic rift-related volcanic rocks exposed at the surface in Madagascar, Tanzania or Kenya (e.g. Guiraud et al., 2005), and neither have they been drilled onshore or offshore (despite the pervasive record of post-rift volcanics emplaced in the upper Cretaceous (Coffin and Rabinowitz, 1988) related to the breakup between Madagascar and India (e.g. Storey et al., 1995)), significant magmatism during rifting in the WSB seems unlikely. This apparent lack of rift related volcanism, the generally thin nature of the oceanic crust interpreted elsewhere within the WSB (5.22 $\pm$ 0.64 Km, Coffin et al., 1986), and the lack of any high velocity underplating interpreted around the necking zone from seismic refraction studies (Prodehl et al., 1997) make present observations from the margins of the WSB more consistent with the magma-poor endmember style of rifted margins.

The ambiguous crust within the Tanzania Coastal Basins and Lamu Embayment could therefore be either oceanic, formed after breakup, or hyperextended continental crust and mantle. Whilst the present-day high heatflow along the East African margin (attested by the significant gas discoveries in the region) possibly favours the presence of radiogenic continental crust (e.g. White et al., 2003), active lithospheric thinning along the offshore branch of the East African Rift System (e.g. Delvaux and Barth, 2010; Franke et al., 2015) would also act to increase regional heatflow. In the mid-Tanzania Coastal Basin, inboard of the DFZ, the East AfricaSPAN seismic reflection lines image a strong and continuous reflector at approximately 9.5 s TWTT, which is 1.5 to 2.3 s TWTT below the top basement (Figure 2.8). This is typical of slightly thin to normal oceanic crust (White et al., 1992), and is similar to the 1.17 to 2 s TWTT derived for oceanic crust elsewhere within the WSB

(Coffin et al., 1986). Several areas within the crust also have a low reflectivity character, often described within oceanic crust (e.g. Bécel et al., 2015).

The nature of the crust changes from NNW to SSE along the line. In the NNW, a smooth top basement reflector is imaged at 7.4 s TWTT, which is characteristic of oceanic crust formed by relatively robust magmatic accretion with little tectonic extension (e.g. Reston et al., 2004). Here an additional reflector can be seen at ~8.3 s TWTT (0.9 seconds below top basement) which delineates an upper and lower crustal layer. Elsewhere within the WSB, the oceanic layer 2 thickness has been derived as 0.93 s TWTT (Coffin et al., 1986), and so this reflector may represent the boundary between oceanic layers 2 and 3. The smooth top basement and Moho reflectors also extend ENE along the seismic cross line, perpendicular to the spreading direction, with a consistent offset of between 1.8 and 2 s TWTT, before eventually reaching the tectonically overprinted DFZ, where their character is lost. To the SSE in Figure 2.8, following a reduction in thickness of the crust demonstrated by the shallowing of the Moho reflector, the top basement gains a weak tectonic fabric. These observations are consistent with a reduction in magma supply and resulting increase in the tectonic extensional component of oceanic spreading (e.g. Reston et al., 2004).

Alternatively, the Moho reflector could represent a detachment fault formed between continental crust and mantle during hyper-extension (e.g. Tugend et al., 2015), such as the S reflector west of Galicia (Hoffmann and Reston, 1992) and H reflector in the Iberia Abyssal Plain (Dean et al., 2008). However, the smooth top basement reflector lacks the well-defined fault blocks often imaged in such hyper-extended domains (Reston, 2009). This suggests that extreme crustal extension is unlikely, especially as rift related volcanism, which could otherwise have masked fault block topography, is extremely limited during hyper-extension at magma-poor margins (Franke, 2013).

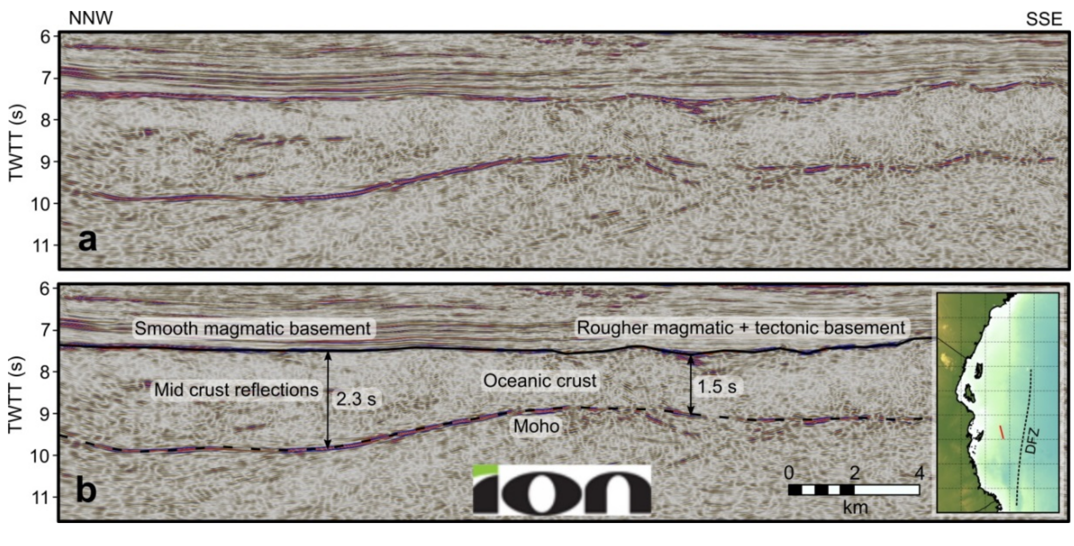

Figure 2.8. (a) Seismic reflection line from the East AfricaSPAN (Ion Geophysical) inboard of the DFZ. (b) Figure 2.8a with interpretation overlain. Inset shows location relative to the coastline and the DFZ.

All these observations thus support high levels of extension, probably including oceanic crust, in the mid-Tanzania coastal basin inboard of the DFZ. The DFZ cannot then be a simple continent-ocean transform margin. Instead, Madagascar must have originated from within the Tanzania Coastal Basins and Lamu Embayment, with the Rovuma Basin forming the continental-ocean transform margin. The onshore trend of this basin is closely aligned with the early SSE trending fracture zones detected in the gravity data (Figure 2.9b), and in fact, in our plate tectonic reconstructions, strike-slip motion of southern Madagascar along this basin is unavoidable. This is in good agreement with observations of dextral strike slip faults along the Rovuma Basin margin (Emmel et al., 2011) and an onshore sedimentary thickness of ~10 km in the northern Rovuma Basin that rapidly thins westward to <1 km (Key et al., 2008), consistent with a continent-ocean transform margin. As noted by Reeves (2014), the passage of Madagascar along the Rovuma Basin also allows for a much tighter and consistent fit of Gondwana fragments, reducing the need for gaps and non-smooth plate motions during Gondwana's disassembly.

2.6.2. Rifting mechanisms and Gondwana breakup

Rifting between East and West Gondwana began in the Toarcian (Geiger et al., 2004) and was probably initiated by the eruption of the Bouvet plume, resulting in a contemporaneous volcanic passive margin in Mozambique (Klausen, 2009). Here, an 8.5 km thick suite of rift-related basalts and rhyodacites defines a relatively narrow volcanic margin, where a magmatic mode of extension dominated in the lead-up to breakup (Klausen, 2009). This section of the rift system developed discordantly to the structural trend of Gondwana's sedimentary basins (Salman and Abdula, 1995), suggesting that pre-existing lithospheric structure was not a key parameter leading to breakup.

In the Western Somali basin, however, there is little evidence for a magmatic breakup as discussed earlier (Section 2.6.1.). This is most likely a function of the WSB's distance from the volcanic centre in Mozambique as seen in the Gulf of Aden. Here, volcanic margins formed close to the Afar hotspot, yet farther away, east of longitude 46° E, the margins are magma-poor (Leroy et al., 2012). Breakup along the Tanzanian-Kenyan and Kenyan-Somalian rift sections is therefore less likely to have been influenced by magmatism and thermal weakening of the lithosphere (Buck, 2007). It is apparent from the spreading lineaments detected in the WSB that initial spreading occurred in a NNW-SSE direction, in agreement with principal extensional stresses around the Mozambique basin (Le Gall et al., 2005). This is consistent with the occurrence of strike-slip tectonics along the NNW-SSE trending Rovuma Basin and oblique rifting along the N-S trending Kenya-Tanzania margin (Figure 2.9b), both of which are mechanically favourable (Emmel, 2011; Brune et al., 2012). This is similar to observations from the Gulf of California where oblique rifting assisted continental breakup through the efficient focusing of crustal thinning within pull-apart basins bounded by large offset strike-slip faults (Bennett and Oskin, 2014). If this mechanism was active during the Jurassic rifting along the Tanzania-Kenya margins, it may explain the possible margin segmentation suggested by the stepped shape of Madagascar's western coastline. Margin segmentation is common to many oblique passive margins worldwide (e.g. Leroy et al., 2012; Bennett and Oskin, 2014).

Conversely, the NE-SW trending Kenyan-Somalian rifted margin formed orthogonally to the breakup direction. Although the Rovuma basin shows little evidence of Karoo age rifting and sedimentation (Smelror et al., 2008), the Morondava, Majunga and Ambilobe basins of Madagascar all contain underlying Karoo sediments (e.g. Hankel, 1994). The conjugate margins on the mainland, the Tanzanian-Kenyan and Kenyan-Somalian rift systems, thus appear to have followed the pre-existing lithospheric structure of the Karoo rift system. A transition can therefore be proposed along the East African margin from dominant strike-slip tectonics and oblique rifting in the Rovuma Basin, progressing northwards to oblique rifting that also follows pre-existing lithospheric structures along the Tanzanian-Kenyan section, and finally, purely orthogonal rifting along a pre-existing lithospheric structure along the Kenyan-Somalian section. This is consistent with the obliqueness of rifting (Brune et al., 2012) and pre-existing lithospheric structure (e.g. Audet and Bürgmann, 2011) assisting supercontinent breakup.

The rifting between East and West Gondwana therefore provide a good natural laboratory for the study of the spatially variable interplay between different rifting mechanisms during supercontinent breakup. Examples where each of the proposed facilitating mechanisms (magmatism, oblique rifting, and pre-existing structure) appears to dominate during breakup can be seen along the Gondwana rift system between Mozambique and Somalia, with predominantly magmatic breakup in the Mozambique Basin, apparent strike-slip and oblique tectonics along the Rovuma Basin, and coincident pre-existing lithospheric structure along the Kenyan-Somalian coast. Analogy can be made to the opening of the South Atlantic during breakup of the supercontinent Pangea, where evidence supports similar regional variation in breakup mechanism. Here, a south to north transition from magmatically dominated breakup in the southern South Atlantic (e.g. Gibson et al., 2006), inheritance driven rifting in the central South Atlantic (e.g. Lentini et al., 2010), and strongly oblique rifting in the Equatorial Atlantic (Heine and Brune, 2014) is seen. Together, these margins suggest that rifting during supercontinent dispersal may often be facilitated by multiple mechanisms, with regional variation along the margin due to different pre-existing geological structures and changing tectonic geometry on length scales as short as a few hundred kilometres.

2.6.3. Plate tectonic reconstruction

For the initial rifting phase we impose a plate separation rate of 3.3 mm/y, similar to that of the present day East African Rift System between Malawi and Afar (Saria et al., 2014). Breakup occurred at approximately 170 Ma, as evidenced by the Early Bajocian break up unconformity identified in the Morondava Basin (Geiger et al., 2004) and the overwhelming transition to marine deposits along the East Africa margins at this time (Coffin and Rabinowitz, 1992). Between breakup and the earliest magnetic anomaly constraint (M22) an average full spreading rate of 40 mm/y therefore occurred, similar to the average full spreading rate of ~49 mm/y determined by ocean magnetic anomalies for the younger oceanic crust between M22 and M0 (Cochran, 1988; Davis et al., 2016).

Following this initial phase of spreading, which resulted in strike-slip motion between Madagascar and the Rovuma Basin, a rotation in the spreading direction occurred at ~150.5 Ma. The oldest conjugate pair of magnetic anomalies detected, M22 (Cochran, 1988; Davis et al., 2016), constrains the age of this rotation, which is contemporaneous with Madagascars exit from the SSE trending Rovuma Basin, after which it began to follow a N-S spreading direction. This rotation began the cessation of any oceanic spreading in the Tanzania Coastal basin and offshore Morondava Basin as flow lines began to align along what was to become the DFZ (Figure 2.7d-e). This alignment suggests strike-slip tectonics began to dominate along this zone, and it is therefore possible that the DFZ formed at this point as several fracture zones coalesced into one major oceanic fracture zone with a significant accumulated offset.

Following the first rotation in plate motions at 150.5 Ma, spreading continued relatively undisturbed in the Western Somali Basin until approximately 136 Ma, when a further change in plate motion occurred contemporaneous with Madagascar's departure from the Mozambique continental transform margin. This rotation further aligned the flowlines along the DFZ as it became the dominant strike slip fault in the basin. From here until the termination of oceanic spreading at M0 (125 Ma), Madagascar underwent a gentle anti-clockwise rotation to take its present day position relative to Africa.

The termination points for our model flowlines lie very close to the extinct MOR identified in the gravity data. We emphasise that this striking agreement is generated only from our fracture zone trends and initial seed points for the flowlines, which were chosen independently based on the CRUST1.0 dataset, and thus provides strong confirmation of the model. No ocean magnetic anomalies have been identified to help constrain the location of the westernmost segment of the MOR. However, seismic reflection data suggests a southerly location for the MOR segment in line with the symmetry predicted from the plate tectonic reconstruction.

A key result of the reconstruction is that the DFZ is shown to be a major ocean-ocean FZ, where oceanic crust has formed inboard of this feature within the Tanzania Coastal Basin. This challenges many plate tectonic reconstructions which, based on the previously available literature, have defined the DFZ as the continent-ocean transform margin of the Western Somali Basin (e.g. Gaina et al., 2013), an important constraint on spreading kinematics. As the DFZ is a predominantly straight feature, treating it as the continent-ocean transition naturally results in the prediction of a less complex spreading pattern (i.e. only ~N-S without an initial NNW-SSE component) and a looser fit of Gondwana fragments due to the inability to reconstruct continents inboard of the DFZ. However, by detailed analysis of spreading lineaments on a small scale, we have been able to resolve the initial NNE-SSW spreading stage. This is in agreement with NNW-SSE principal extensional stresses during breakup around the Mozambique basin, recorded from dyke dilation in the Okavango and Limpopo dyke swarms (Le Gall et al., 2005). This spreading pattern is also strikingly similar to spreading patterns extrapolated to the WSB basin from the Mozambique basin, where they were derived from magnetic anomalies and FZs (Eagles and König, 2008). This suggests that during the earlier stages of spreading, Madagascar and Antarctica shared a similar breakup history, and moved as a cohesive unit away from Africa, as opposed to an amalgamation of continental blocks with relative motions between them. This highlights the importance of basin scale reconstructions in deciphering supercontinent dispersal mechanisms, as well as their potential for constraining the histories of neighbouring basins that lack detailed kinematic indicators and for informing larger regional reconstructions.

The Dhow and VLCC fracture zones as interpreted by Bunce and Molnar (1977) were not used as input to the plate tectonic model since they may have formed by processes other than oceanic spreading (Coffin and Rabinowitz 1987). However, their trends are independently predicted by our plate model, so they are likely to have been originally formed as the result of plate spreading after all. Reactivation of these structures may have occurred during the breakup of Madagascar and India, resulting in their more prominent expression in the gravity data compared to other fracture zones in the WSB.

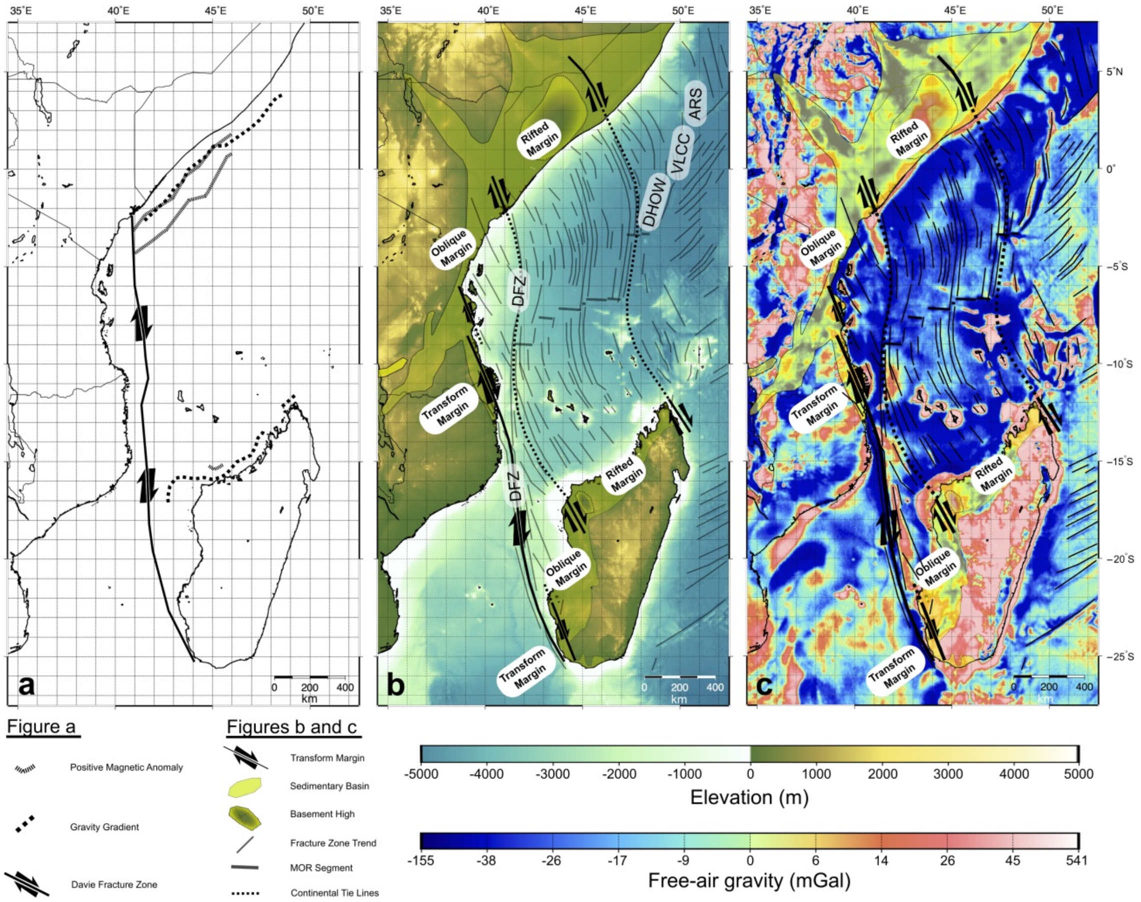

Figure 2.9. (a) Commonly interpreted basin configuration, where the continent-ocean transition is assumed to follow the DFZ (e.g. Bunce and Molnar, 1977; Coffin and Rabinowitz, 1987). (b) Schematic of the basin configuration suggested in this study, with strike slip tectonics dominating along the edge of the Rovuma Basin, while much of the Tanzania Coastal Basin should be considered as an obliquely rifted margin. The Davie Fracture Zone is a major ocean-ocean fracture zone, not the continent-ocean transform margin. DFZ – Davie Fracture Zone; DHOW – Dhow Fracture Zone; VLCC – Very Large Crude Carrier Fracture Zone; ARS – Auxiliary Rescue and Salvage Fracture Zone. (c) Free-air gravity overlain with interpretation as for Figure 2.9b.

2.7. Conclusions

Using new techniques to analyse the latest Sandwell and Smith gravity datasets (V23), we have detected the location of the extinct MOR segments and, for the first time, a comprehensive set of fracture zone lineaments within the Western Somali Basin. We have used these to constrain Madagascar's position in Africa prior to breakup, validate ocean magnetic anomaly interpretations for the WSB, and construct a well constrained, high resolution plate tectonic reconstruction for the region. This plate tectonic reconstruction bears strong similarities to reconstructions from the neighbouring Mozambique Basin, and may suggest that East Gondwana broke off from West Gondwana as a cohesive unit, rather than as an amalgamation of continental blocks with relative motions between them. During this disassembly, no single parameter leads to breakup along the entire margin, with thermal weakening due to magmatism, oblique rifting, and pre-existing structure apparently dominating in turn from south to north along the Jurassic Gondwana rifts.

The discovery of oceanic crust in the Tanzania Coastal Basin, fracture zone orthogonality to regional magnetic anomalies, and observations from the Rovuma Basin support this reconstruction, and show that the Davie Fracture Zone is a major ocean-ocean fracture zone, formed by the coalescence of several smaller fracture zones during changing spreading directions, and not a continent-ocean transform margin. The western edge of the basin is thus defined by a transform margin in the Rovuma Basin, whereas the Tanzanian and Kenyan margins formed in an oblique regime and are most likely segmented, magma-poor rifted margins. The change in the location and nature of the continent ocean transition has important implications for the nature of the lithosphere underlying the western portion of the basin, and thus for its thermal history and resource potential.

2.8. References

Arrowsmith, J.R., Zielke, O., 2009. Tectonic geomorphology of the San Andreas Fault zone from high resolution topography: An example from the Cholame segment. Geomorphology 113, 70-81.

Audet, P., Burgmann, R., 2011. Dominant role of tectonic inheritance in supercontinent cycles. Nature Geosci 4, 184-187.

Bayrakci, G., Minshull, T.A., Sawyer, D.S., Reston, T.J., Klaeschen, D., Papenberg, C., Ranero, C., Bull, J.M., Davy, R.G., Shillington, D.J., Perez-Gussinye, M., Morgan, J.K., 2016. Fault-controlled hydration of the upper mantle during continental rifting. Nature Geosci 9, 384-388.

Bécel, A., Shillington, D.J., Nedimović, M.R., Webb, S.C., Kuehn, H., 2015. Origin of dipping structures in fast-spreading oceanic lower crust offshore Alaska imaged by multichannel seismic data. Earth and Planetary Science Letters 424, 26-37.

Beglinger, S.E., Corver, M.P., Doust, H., Cloetingh, S., Thurmond, A.K., 2012. A new approach of relating petroleum system and play development to basin evolution: An application to the conjugate margin Gabon coastal and Almada-Camamu basins. AAPG Bulletin 96, 953-982.

Behn, M.D., Ito, G., 2008. Magmatic and tectonic extension at mid-ocean ridges: 1. Controls on fault characteristics. Geochemistry, Geophysics, Geosystems 9, n/a-n/a.

Bennett, S.E.K., Oskin, M.E., 2014. Oblique rifting ruptures continents: Example from the Gulf of California shear zone. Geology 42, 215-218.

Blackman, D.K., Forsyth, D.W., 1991. Isostatic compensation of tectonic features of the Mid-Atlantic Ridge: 25–27°30′S. Journal of Geophysical Research: Solid Earth 96, 11741-11758.

Brune, S., Popov, A.A., Sobolev, S.V., 2012. Modeling suggests that oblique extension facilitates rifting and continental break-up. Journal of Geophysical Research: Solid Earth 117, B08402.

Buck, W.R., 2007. Dynamic Processes in Extensional and Compressional Settings: The Dynamics of Continental Breakup and Extension, Treatise on Geophysics, Treatise on Geophysics. Elsevier, Amsterdam, pp. 335-376.

Bunce, E.T., Molnar, P., 1977. Seismic reflection profiling and basement topography in the Somali basin: possible fracture zones between Madagascar and Africa. Journal of Geophysical Research 82, 5305-5311.

Cochran, J.R., 1988. Somali Basin, Chain Ridge, and origin of the Northern Somali Basin gravity and geoid low. Journal of Geophysical Research: Solid Earth 93, 11985-12008.

Coffin, M.F., Rabinowitz, P.D., 1992. The Mesozoic East African and Madagascan Conjugate Continental Margins. American Association of Petroleum Geologists Memoir 53, 207-240.

Coffin, M.F., Rabinowitz, P.D., Houtz, R.E., 1986. Crustal structure in the Western Somali Basin. Geophysical Journal of the Royal Astronomical Society 86, 331-369.

Collette, B.J., 1974. Thermal contraction joints in a spreading seafloor as origin of fracture zones. Nature 251, 299-300.

Davies, R.J., MacLeod, C.J., Morgan, R., Briggs, S.E., 2005. Termination of a fossil continent-ocean fracture zone imaged with three-dimensional seismic data: The Chain Fracture Zone, eastern equatorial Atlantic. Geology 33, 641-644.

Davis, J.K., Lawver, L.A., Norton, I.O., Gahagan, L.M., 2016. New Somali Basin magnetic anomalies and a plate model for the early Indian Ocean. Gondwana Research 34, 16-28.

Dean, S.M., Minshull, T.A., Whitmarsh, R.B., 2008. Seismic constraints on the three-dimensional geometry of low-angle intracrustal reflectors in the Southern Iberia Abyssal Plain. Geophysical Journal International 175, 571-586.

Delvaux, D., Barth, A., 2010. African stress pattern from formal inversion of focal mechanism data. Tectonophysics 482, 105-128.

Eagles, G., 2007. New angles on South Atlantic opening. Geophysical Journal International 168, 353-361.

Eagles, G., König, M., 2008. A model of plate kinematics in Gondwana breakup. Geophysical Journal International 173, 703-717.

Emmel, B., Kumar, R., Ueda, K., Jacobs, J., Daszinnies, M.C., Thomas, R.J., Matola, R., 2011. Thermochronological history of an orogen-passive margin system: An example from northern Mozambique. Tectonics 30, TC2002.

Franke, D., 2013. Rifting, lithosphere breakup and volcanism: Comparison of magma-poor and volcanic rifted margins. Marine and Petroleum Geology 43, 63-87.

Franke, D., Jokat, W., Ladage, S., Stollhofen, H., Klimke, J., Lutz, R., Mahanjane, E.S., Ehrhardt, A., Schreckenberger, B., 2015. The offshore East African Rift System: Structural framework at the toe of a juvenile rift. Tectonics 34, 2086-2104.

Gaina, C., Torsvik, T.H., van Hinsbergen, D.J.J., Medvedev, S., Werner, S.C., Labails, C., 2013. The African Plate: A history of oceanic crust accretion and subduction since the Jurassic. Tectonophysics 604, 4-25.

Geiger, M., Clark, D.N., Mette, W., 2004. Reappraisal of the timing of the breakup of Gondwana based on sedimentological and seismic evidence from the Morondava Basin, Madagascar. Journal of African Earth Sciences 38, 363-381.

Gente, P., Pockalny, R.A., Durand, C., Deplus, C., Maia, M., Ceuleneer, G., Mével, C., Cannat, M., Laverne, C., 1995. Characteristics and evolution of the segmentation of the Mid-Atlantic Ridge between 20°N and 24°N during the last 10 million years. Earth and Planetary Science Letters 129, 55-71.

Gibson, S.A., Thompson, R.N., Day, J.A., 2006. Timescales and mechanisms of plume–lithosphere interactions: 40Ar/39Ar geochronology and geochemistry of alkaline igneous rocks from the Paraná–Etendeka large igneous province. Earth and Planetary Science Letters 251, 1-17.

Gillard, M., Manatschal, G., Autin, J., 2016. How can asymmetric detachment faults generate symmetric Ocean Continent Transitions. Terra Nova 28, 27-34.

Gradstein, F., Ogg, J., Schmitz, M., Ogg, G., 2012. The Geologic Time Scale 2012. Elselvier, 1144 p.

Guiraud, R., Bosworth, W., Thierry, J., Delplanque, A., 2005. Phanerozoic geological evolution of Northern and Central Africa: An overview. Journal of African Earth Sciences 43, 83-143.

Hankel, O., 1994. Early Permian to Middle Jurassic rifting and sedimentation in East Africa and Madagascar. Geol Rundsch 83, 703-710.

Heine, C., Brune, S., 2014. Oblique rifting of the Equatorial Atlantic: Why there is no Saharan Atlantic Ocean. Geology 42, 211-214.

Hirsch, K.K., Bauer, K., Scheck-Wenderoth, M., 2009. Deep structure of the western South African passive margin — Results of a combined approach of seismic, gravity and isostatic investigations. Tectonophysics 470, 57-70.

Hoffmann, H.-J., Reston, T.J., 1992. Nature of the S reflector beneath the Galicia Banks rifted margin: Preliminary results from prestack depth migration. Geology 20, 1091-1094.

Jonas, J., Hall, S., Casey, J.F., 1991. Gravity anomalies over extinct spreading centers: A test of gravity models of active centers. Journal of Geophysical Research: Solid Earth 96, 11759-11777.

Key, R.M., Smith, R.A., Smelror, M., Sæther, O.M., Thorsnes, T., Powell, J.H., Njange, F., Zandamela, E.B., 2008. Revised lithostratigraphy of the Mesozoic-Cenozoic succession of the onshore Rovuma Basin, northern coastal Mozambique. South African Journal of Geology 111, 89-108.

Kim, S.-S., Wessel, P., 2011. New global seamount census from altimetry-derived gravity data. Geophysical Journal International 186, 615-631.

Klausen, M.B., 2009. The Lebombo monocline and associated feeder dyke swarm: Diagnostic of a successful and highly volcanic rifted margin? Tectonophysics 468, 42-62.

Korenaga, J., Holbrook, W.S., Kent, G.M., Kelemen, P.B., Detrick, R.S., Larsen, H.C., Hopper, J.R., Dahl-Jensen, T., 2000. Crustal structure of the southeast Greenland margin from joint refraction and reflection seismic tomography. Journal of Geophysical Research: Solid Earth 105, 21591-21614.

Laske, G., Masters, G., Ma, Z., Pasyanos, M.E., 2013. Update on CRUST1.0: A 1-degree Global Model of Earth's Crust. Geophys. Res. Abstracts, 15, Abstract EGU2013-2658.

Le Gall, B., Tshoso, G., Dyment, J., Basira Kampunzu, A., Jourdan, F., Féraud, G., Bertrand, H., Aubourg, C., Vétel, W., 2005. The Okavango giant mafic dyke swarm (NE Botswana): its structural significance within the Karoo Large Igneous Province. Journal of Structural Geology 27, 2234-2255.

Lentini, M.R., Fraser, S.I., Sumner, H.S., Davies, R.J., 2010. Geodynamics of the central South Atlantic conjugate margins: implications for hydrocarbon potential. Petroleum Geoscience 16, 217-229.

Leroy, S., Razin, P., Autin, J., Bache, F., d'Acremont, E., Watremez, L., Robinet, J., Baurion, C., Denèle, Y., Bellahsen, N., Lucazeau, F., Rolandone, F., Rouzo, S., Kiel, J.S., Robin, C., Guillocheau, F., Tiberi, C., Basuyau, C., Beslier, M.-O., Ebinger, C., Stuart, G., Ahmed, A., Khanbari, K., Al Ganad, I., de Clarens, P., Unternehr, P., Al Toubi, K., Al Lazki, A., 2012. From rifting to oceanic spreading in the Gulf of Aden: a synthesis. Arabian Journal of Geosciences 5, 859-901.

Lottes, A.L., Rowley, D.B., 1990. Reconstruction of the Laurasian and Gondwanan segments of Permian Pangaea. Geological Society, London, Memoirs 12, 383-395.

Maus, S., Barckhausen, U., Berkenbosch, H., Bournas, N., Brozena, J., Childers, V., Dostaler, F., Fairhead, J.D., Finn, C., R.R.B., v.F., Gaina, C., Golynsky, S., Kucks, R., Lühr, H., Milligan, P., Mogren, S., Müller, D.R., Olesen, O., Pilkington, M., Saltus, R., Schreckenberger, B., Thébault, E., Caratori Tontini, F., 2009. EMAG2: A 2–arc min resolution Earth Magnetic Anomaly Grid compiled from satellite, airborne, and marine magnetic measurements. Geochemistry, Geophysics, Geosystems 10, Q08005.

Menard, H.W., Atwater, T., 1969. Origin of Fracture Zone Topography. Nature 222, 1037-1040.

Mitchell, N.C., Park, Y., 2014. Nature of crust in the central Red Sea. Tectonophysics 628, 123-139.

Mulder, T.F.A., Collette, B.J., 1984. Gravity anomalies over inactive fracture zones in the central North Atlantic. Marine Geophysical Researches 6, 383-394.

Müller, R.D., Sdrolias, M., Gaina, C., Roest, W.R., 2008. Age, spreading rates, and spreading asymmetry of the world's ocean crust. Geochemistry, Geophysics, Geosystems 9, Q04006.

Nance, D.R., Murphy, B.J., 2013. Origins of the supercontinent cycle. Geoscience Frontiers 4, 439-448.

Planke, S., Eldholm, O., 1994. Seismic response and construction of seaward dipping wedges of flood basalts: Vøring volcanic margin. Journal of Geophysical Research: Solid Earth 99, 9263-9278.

Prodehl, C., Ritter, J.R.R., Mechie, J., Keller, G.R., Khan, M.A., Jacob, B., Fuchs, K., Nyambok, I.O., Obel, J.D., Riaroh, D., 1997. The KRISP 94 lithospheric investigation of southern Kenya — the experiments and their main results. Tectonophysics 278, 121-147.

Rabinowitz, P.D., Coffin, M.F., Falvey, D., 1983. The Separation of Madagascar and Africa. Science 220, 67-69.

Reeves, C., 2014. The position of Madagascar within Gondwana and its movements during Gondwana dispersal. Journal of African Earth Sciences 94, 45-57.

Reeves, C., De Wit, M.J., 2000. Making ends meet in Gondwana: retracing the transforms of the Indian Ocean and reconnecting continental shear zones. Terra Nova 12, 272-280.

Reston, T.J., 2009. The structure, evolution and symmetry of the magma-poor rifted margins of the North and Central Atlantic: A synthesis. Tectonophysics 468, 6-27.

Reston, T.J., Ranero, C.R., Ruoff, O., Perez-Gussinye, M., Dañobeitia, J.J., 2004. Geometry of extensional faults developed at slow-spreading centres from pre-stack depth migration of seismic reflection data in the Central Atlantic (Canary Basin). Geophysical Journal International 159, 591-606.

Rodger, M., Watts, A.B., Greenroyd, C.J., Peirce, C., Hobbs, R.W., 2006. Evidence for unusually thin oceanic crust and strong mantle beneath the Amazon Fan. Geology 34, 1081-1084.

Salman, G., Abdula, I., 1995. Development of the Mozambique and Ruvuma sedimentary basins, offshore Mozambique. Sedimentary Geology 96, 7-41.

Sandwell, D.T., 1984. Thermomechanical evolution of oceanic fracture zones. Journal of Geophysical Research: Solid Earth 89, 11401-11413.

Sandwell, D.T., Müller, R.D., Smith, W.H.F., Garcia, E., Francis, R., 2014. New global marine gravity model from CryoSat-2 and Jason-1 reveals buried tectonic structure. Science 346, 65-67.

Saria, E., Calais, E., Stamps, D.S., Delvaux, D., Hartnady, C.J.H., 2014. Present-day kinematics of the East African Rift. Journal of Geophysical Research: Solid Earth 119, 3584-3600.

Scrutton, R.A., Heptonstall, W.B., Peacock, J.H., 1981. Constraints on the motion of Madagascar with respect to Africa. Marine Geology 43, 1-20.

Sègoufin, J., Patriat, P., 1980. Existence d'anomalies mésozoïques dans le bassin de Somalie. Implications pour les relations Afrique-Antarctique-Madagascar. Comptes Rendus de l'Académie des Sciences 291, 85-88.

Smelror, M., Key, R.M., Smith, R.A., Njange, F., 2008. Late Jurassic and Cretaceous Palynostratigraphy of the Onshore Rovuma Basin, Northern Mozambique. Palynology 32, 63-76.

Smith, A.G., Hallam, A., 1970. The Fit of the Southern Continents. Nature 225, 139-144.

Soto, M., Morales, E., Veroslavsky, G., de Santa Ana, H., Ucha, N., Rodríguez, P., 2011. The continental margin of Uruguay: Crustal architecture and segmentation. Marine and Petroleum Geology 28, 1676-1689.

Storey, M., Mahoney, J.J., Saunders, A.D., Duncan, R.A., Kelley, S.P., Coffin, M.F., 1995. Timing of Hot Spot—Related Volcanism and the Breakup of Madagascar and India. Science 267, 852-855.

Sutra, E., Manatschal, G., 2012. How does the continental crust thin in a hyperextended rifted margin? Insights from the Iberia margin. Geology 40, 139-142.

Trompette, R., 2000. Gondwana evolution; its assembly at around 600 Ma. Comptes Rendus de l'Académie des Sciences - Series IIA - Earth and Planetary Science 330, 305-315.

Van Hinsbergen, D.J.J., Buiter, S.J.H., Torsvik, T.H., Gaina, C., Webb, S.J., 2011. The formation and evolution of Africa from the Archaean to Present: introduction. Geological Society, London, Special Publications 357, 1-8.

Walcott, R.I., 1972. Gravity, Flexure, and the Growth of Sedimentary Basins at a Continental Edge. Geological Society of America Bulletin 83, 1845-1848.

Watts, A.B., Stewart, J., 1998. Gravity anomalies and segmentation of the continental margin offshore West Africa. Earth and Planetary Science Letters 156, 239-252.

White, N., Thompson, M., Barwise, T., 2003. Understanding the thermal evolution of deep-water continental margins. Nature 426, 334-343.

White, R.S., McKenzie, D., O'Nions, R.K., 1992. Oceanic crustal thickness from seismic measurements and rare earth element inversions. Journal of Geophysical Research: Solid Earth 97, 19683-19715.

Whittaker, J.M., Goncharov, A., Williams, S.E., Müller, R.D., Leitchenkov, G., 2013. Global sediment thickness data set updated for the Australian-Antarctic Southern Ocean. Geochemistry, Geophysics, Geosystems 14, 3297-3305.

Williams, S.E., Müller, D.R., Landgrebe, T.C.W., Whittaker, J.M., 2012. An open-source software environment for visualizing and refining plate tectonic reconstructions using high-resolution geological and geophysical data sets. GSA Today 22.

Windley, B.F., Razafiniparany, A., Razakamanana, T., Ackermand, D., 1994. Tectonic framework of the Precambrian of Madagascar and its Gondwana connections: a review and reappraisal. Geol Rundsch 83, 642-659.

Ziegler, P.A., Cloetingh, S., 2004. Dynamic processes controlling evolution of rifted basins. Earth-Science Reviews 64, 1-50.

2.9. Supplementary material

These supplementary images show the effect of changing key parameters during the gravity processing described in the main text. Free-air gravity data from the Western Somali Basin (WSB) has been processed to enhance the expression of fracture zones. First filtering was performed using a Gaussian bandpass filter with 50% cutoffs at 55 and 85 km wavelengths. Following this, directional derivatives of the gravity were taken perpendicular to the approximate N-S spreading direction, as determined from ocean magnetic anomalies from the WSB. Derivatives were taken at 10° intervals between 30° clockwise and anticlockwise of E-W. The greatest gradient magnitude recorded from this set of derivatives was stored for each grid element to form the final gradient anomaly map (Figure S2.1).

Supplementary Figures S2.2-4 show the effects of reducing the range of azimuths over which gradients are taken; the aim being to show that the process of taking several gradients assists in highlighting the trends of curved fracture zones. In the case of the WSB, the greatest improvements can therefore be seen closer to the continents where the spreading direction early in the basin history was ~NW-SE and not N-S.

Supplementary figures S2.5-8 show result of taking gradients over these same ranges of azimuths as in supplementary figures S2.1-4, but parallel to the spreading direction as opposed to perpendicular to it. This shows that lineations do not arise purely as a result of this processing without a geological driver.

1894

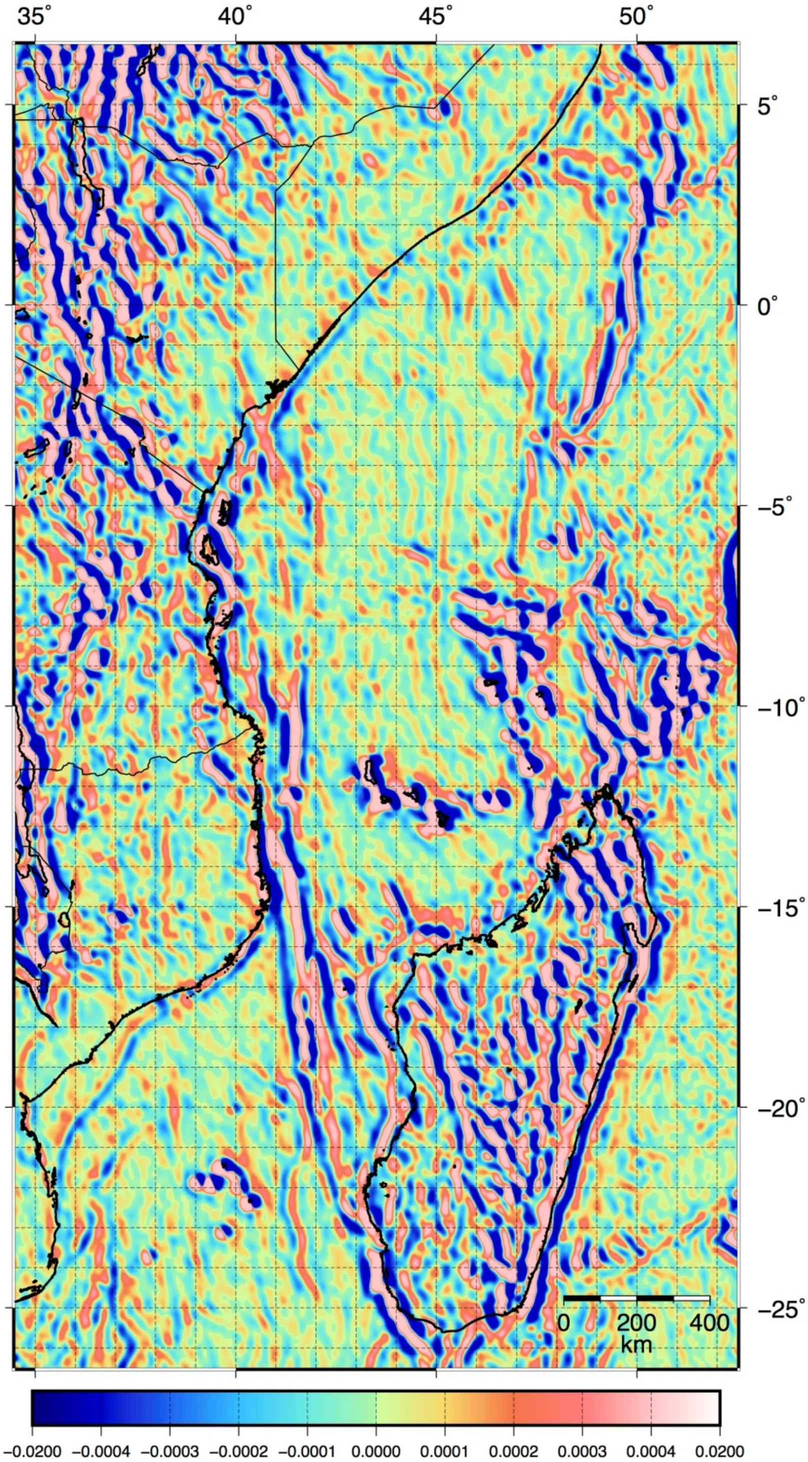

1895

1896 **Figure S2.1.** Maximum free-air gravity directional derivative from azimuths of
1897 240°/250°/260°/270°/280°/290°/300°. Units of scale are eötvös.

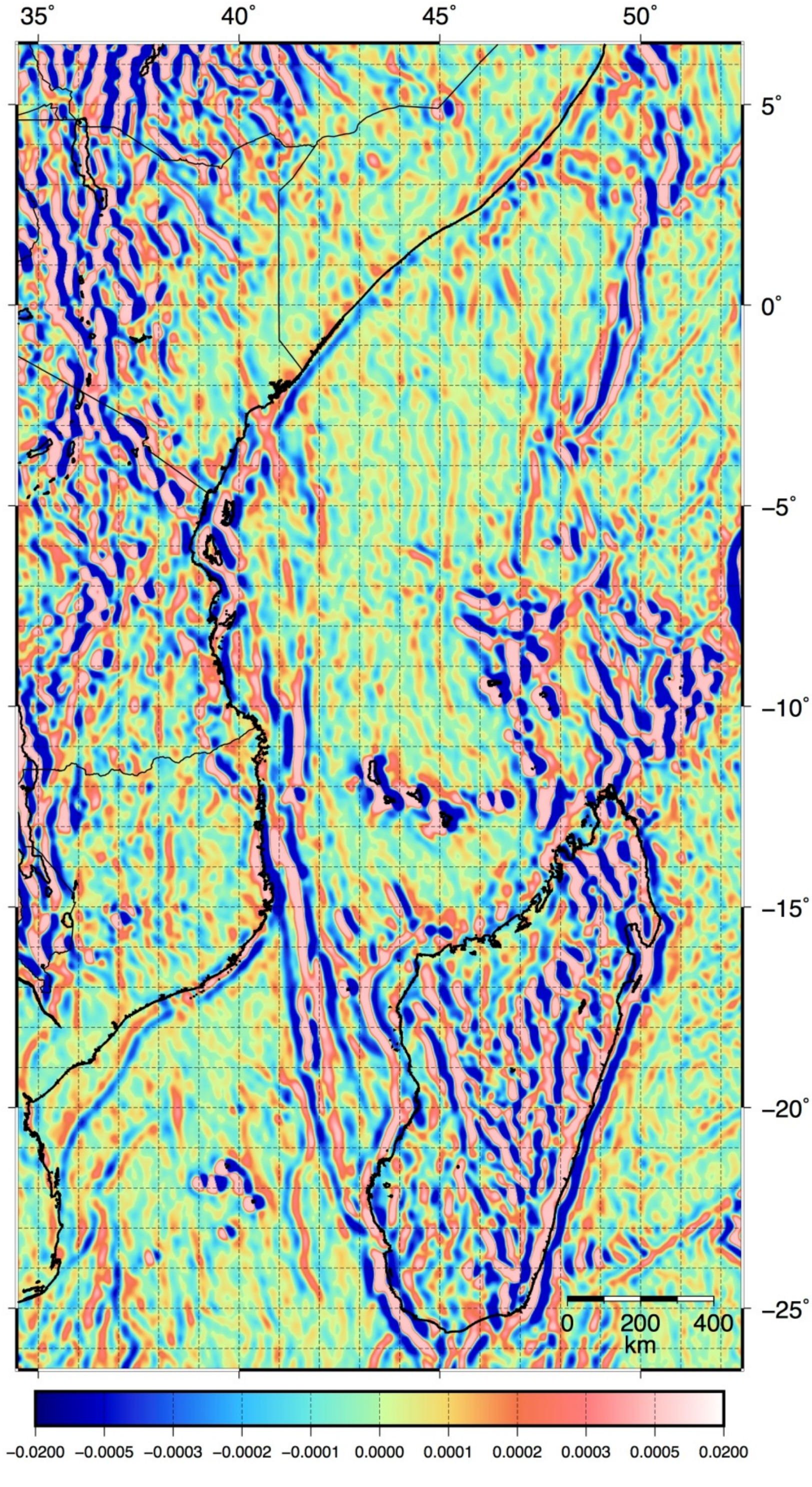

Figure S2.2. Maximum free-air gravity directional derivative from azimuths of 250°/260°/270°/280°/290°. Units of scale are eötvös.

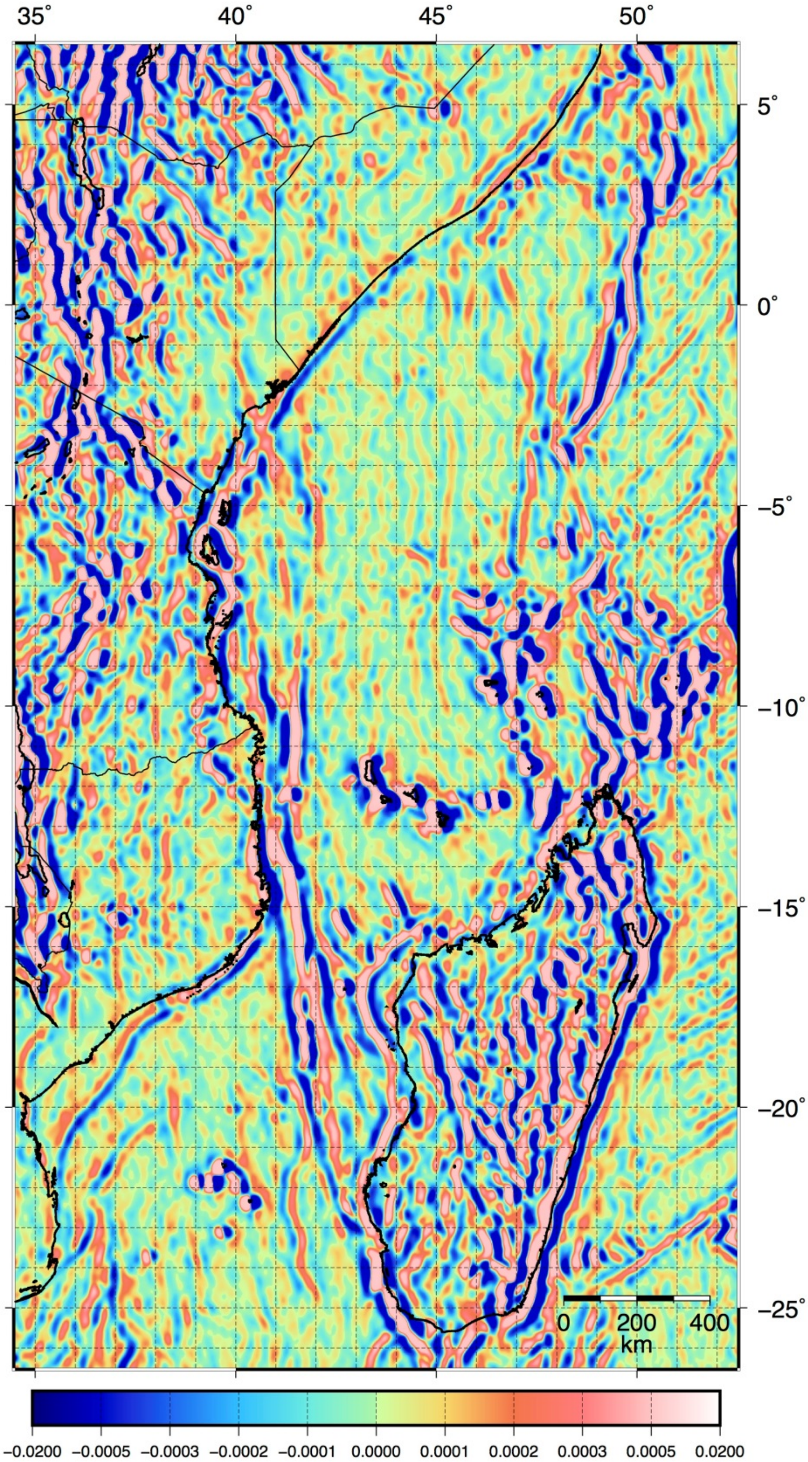

Figure S2.3. Maximum free-air gravity directional derivative from azimuths of 260°/270°/280°. Units of scale are eötvös.

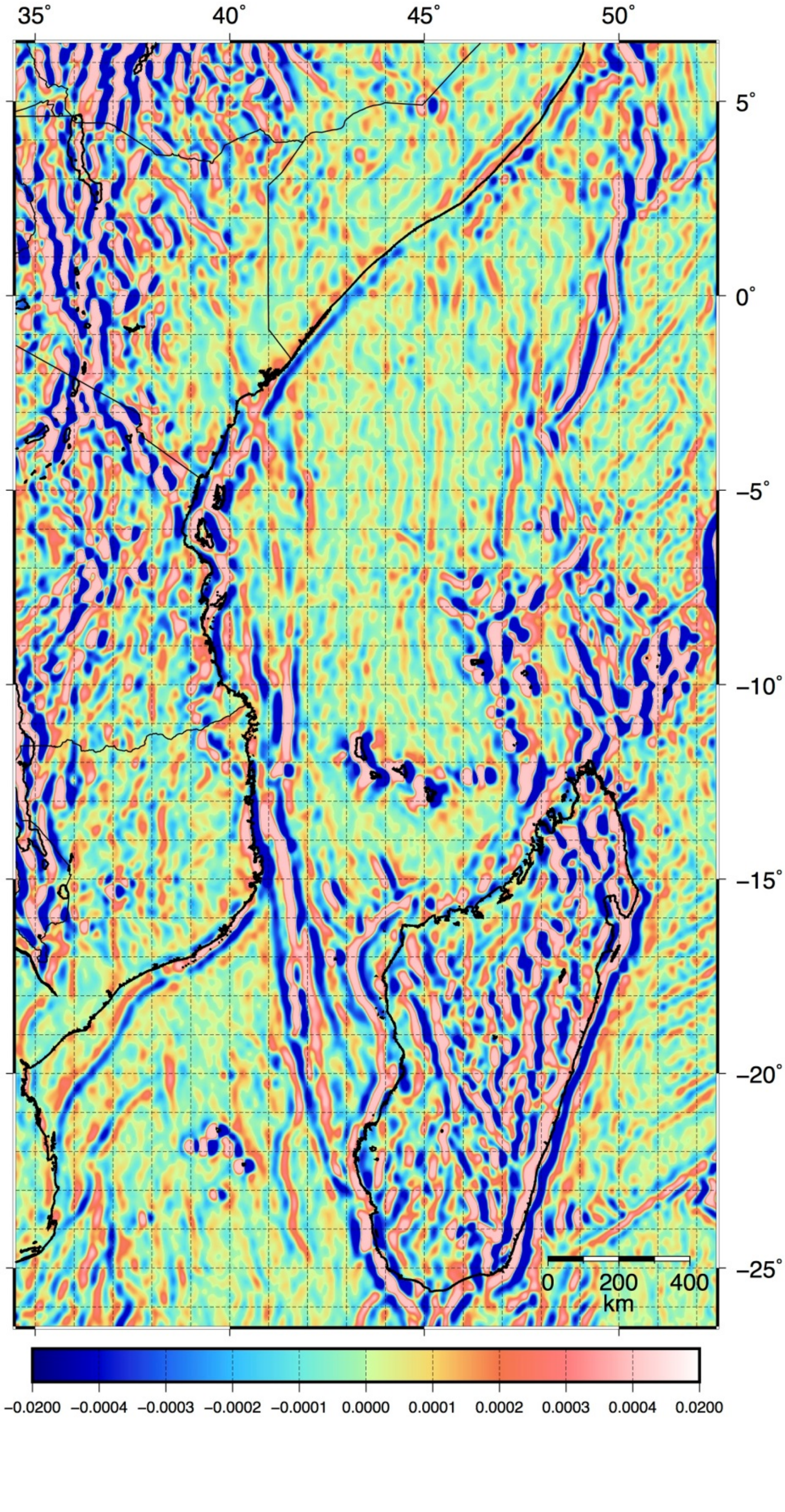

Figure S2.4. Free-air gravity directional derivative at an azimuth of 270°. Units of scale are eötvös.

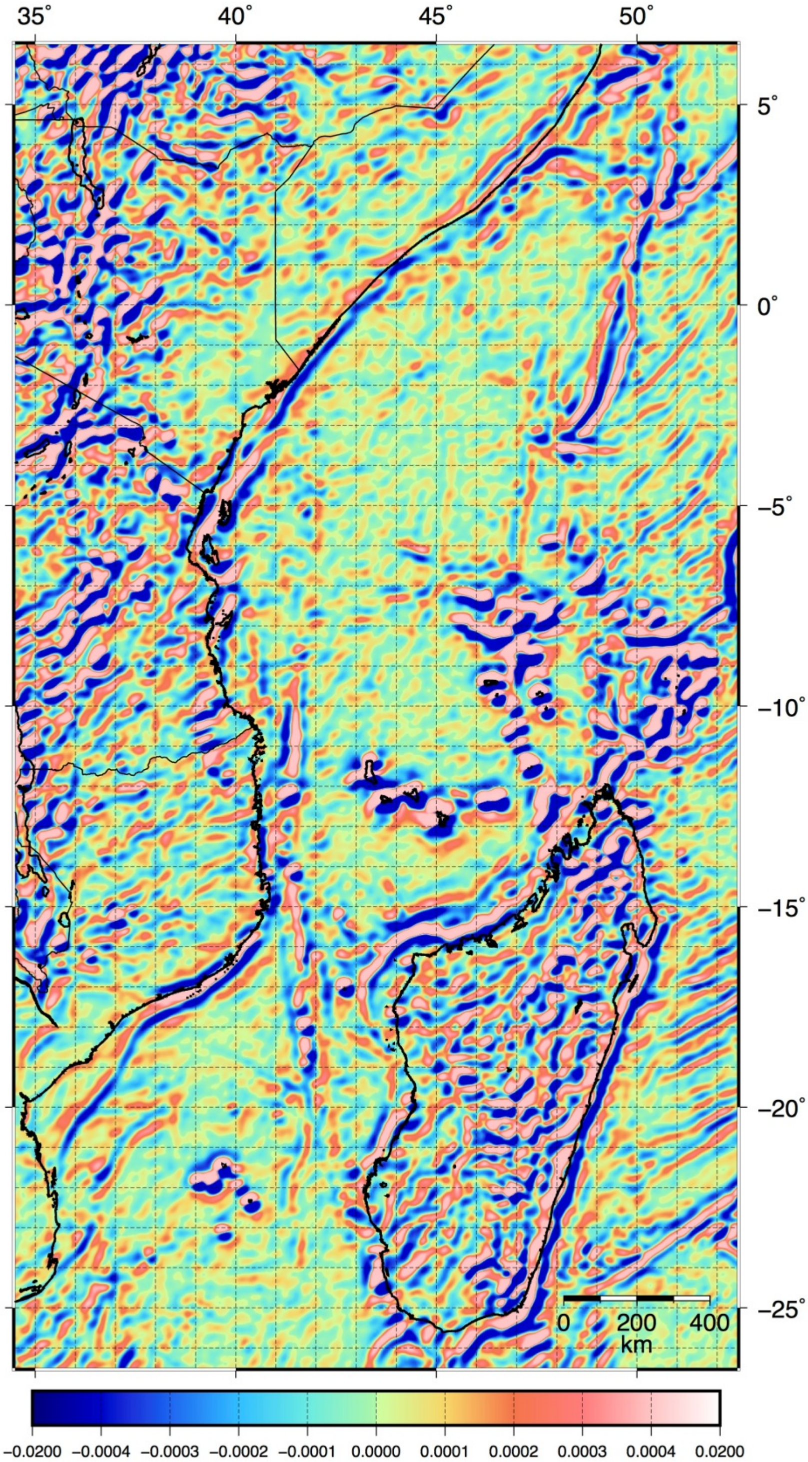

Figure S2.5. Maximum free-air gravity directional derivative from azimuths of 330°/340°/350°/0°/10°/20°/30°. Units of scale are eötvös.

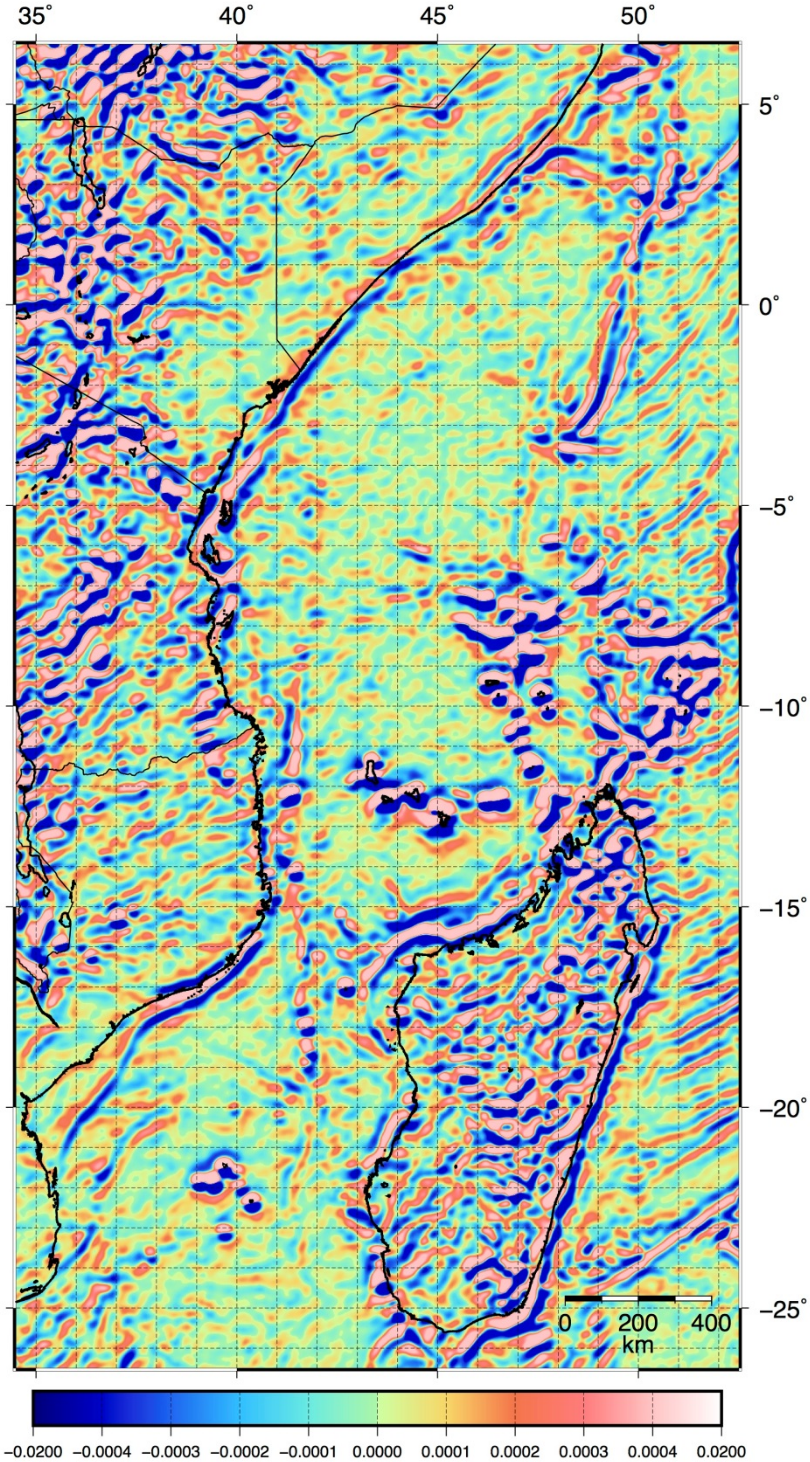

Figure S2.6. Maximum free-air gravity directional derivative from azimuths of 340°/350°/0°/10°/20°. Units of scale are eötvös.

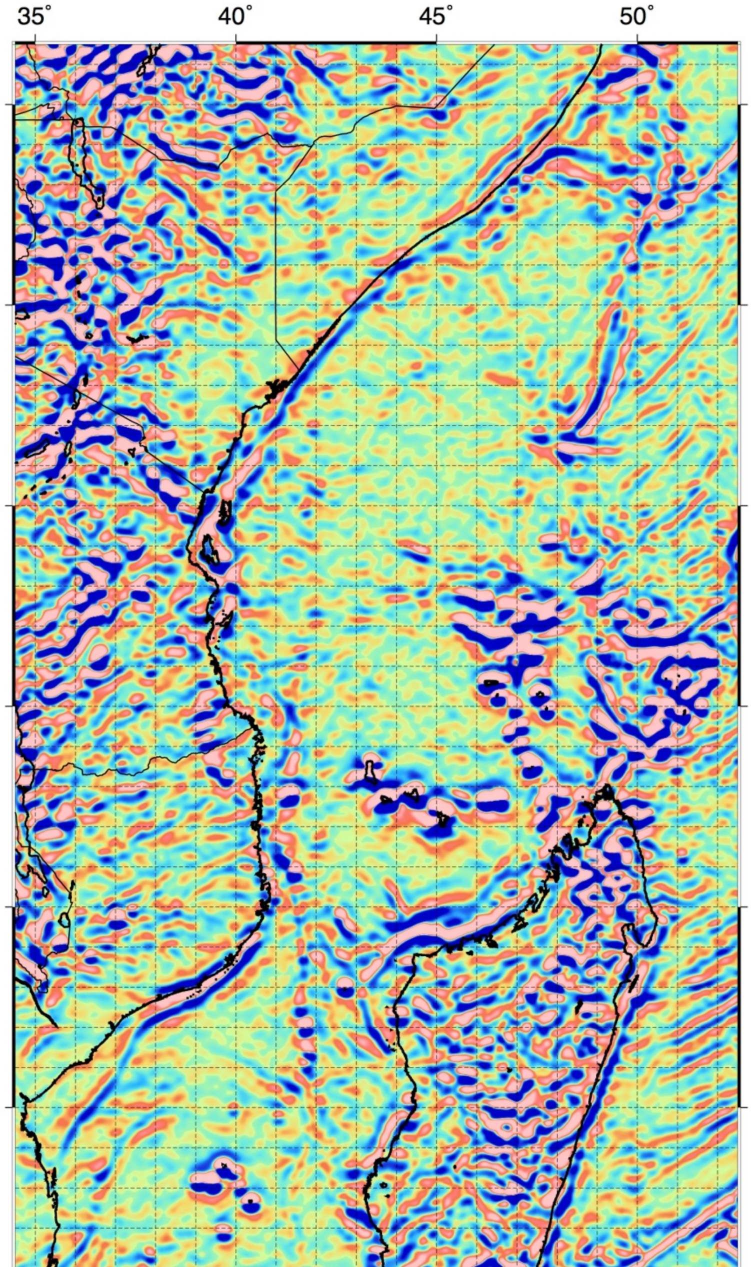

Figure S2.7. Maximum free-air gravity directional derivative from azimuths of 350°/0°/10°. Units of scale are eötvös.

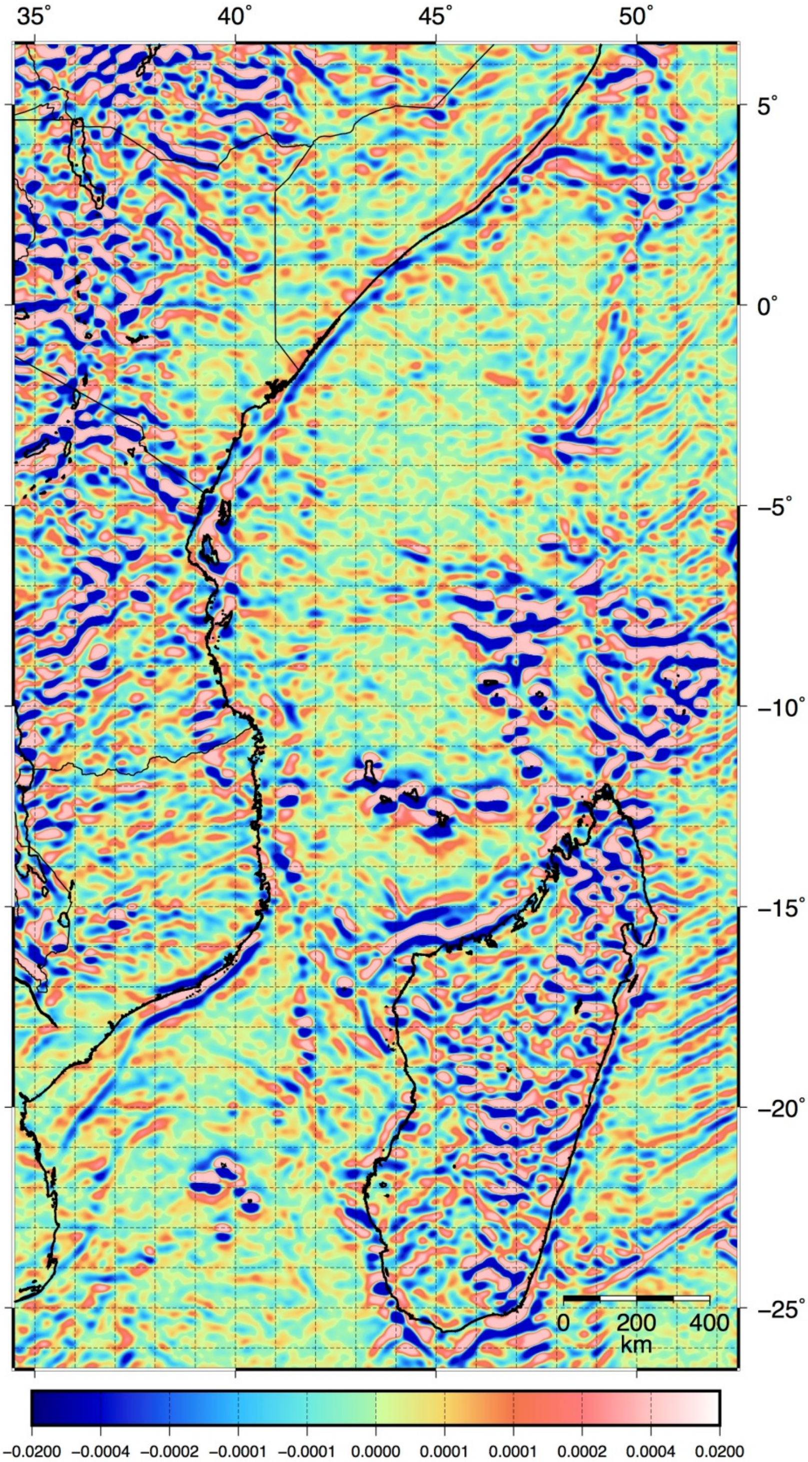

Figure S2.8. Free-air gravity directional derivative at an azimuth of 0°. Units of scale are eötvös.

3. The Rovuma Transform Margin: Pinning down the East African continent-ocean transform margin using seismic and gravity methods

Abstract

A firm knowledge of the nature and location of the continental margins of East Africa is crucial for producing accurate plate tectonic reconstructions of Gondwana, hydrocarbon resource exploration, and for developing our understanding of how supercontinents break apart. Here, we present evidence for a newly identified continent-ocean transform margin along the Rovuma Basin, identified using seismic and gravity data. The 'Rovuma Transform Margin' lies landward of the Davie Fracture Zone, which has previously been interpreted as the continent-ocean transform margin of the Western Somali basin, and trends in a NNW direction, following the onshore basement outcrop of the Rovuma Basin. The >400 km long transform margin connects the obliquely rifted Tanzania Coastal Basin in the north, with the Nacala and Mozambique basins in the south. This configuration supports an origin for Madagascar within the Tanzania Coastal Basin, and tight-fit reconstructions of Gondwana fragments prior to the Jurassic.

3.1. Introduction

Continental breakup occurs when a zone of continental lithosphere is thinned to the point of rupture due to the separation of tectonic plates (Ebinger, 2005). This results in partial melting of the asthenospheric mantle, leading to oceanic crust production and the localisation of strain at the mid-ocean ridge (MOR). At this time, the region where continental lithosphere is thinned (from ~30 to 0 km) may be referred to as a passive continental margin. Due to the relation between extension and accommodation space (Tugend et al., 2015), continental margins may be readily identified between the continents and ocean by using seismic reflection data to identify the great increase in sedimentary accommodation space that occurs across them. This increase is primarily due to the subsidence that occurs across passive margins as the result of isostatic compensation following thinning of the relatively buoyant crust.

The East Africa margins developed during the Early Jurassic, following the cessation of older Karoo rifting episodes (Geiger et al., 2004), by the breakup of East and West Gondwana (e.g. Reeves et al., 2016). The subsequent drift of East Gondwana (Madagascar, India, Antarctica, and Australia) away from West Gondwana (Africa, South America) generated the Western Somali Basin (WSB; e.g. Rabinowitz et al., 1983). Figure 3.1 summarises the two main groups of plate tectonic models have been proposed to describe plate motions during the formation of the WSB. 1) Direct N-S motion of East Gondwana away from West Gondwana, often assumed to follow the Davie Fracture Zone (DFZ) and requiring an initial 'loose' fit of Gondwana fragments (e.g. Coffin and Rabinowitz, 1987). 2) A similar pattern, but where an initial NW-SE (Klimke et al., 2017; Reeves et al., 2016) or NNW-SSE (Phethean et al., 2016) motion precedes N-S spreading allowing for a 'tight' initial configuration of Gondwana fragments.

Depending on the orientation of a margin relative to the extensional direction under which it forms, margins develop under different modes (i.e. divergent, transform, or oblique). The resulting geometries and structures are characteristic of each margin type, allowing us to differentiate between them. Due to the different initial extension directions used by the two groups of plate models, each group predicts that the margins of the curved WSB will develop differently. For example, models using N-S spreading predict transform margins with a N-S trend, whereas those using NNE-SSW spreading predict a NNE-SSW trend.

Understanding the mode of rifting and margin structures of the WSB is not only crucial for our understanding of how supercontinent dispersal occurs, but also has significant implications for the nature of the basement rocks surrounding the margins of East Africa and the location of the continent-ocean transition (COT), both important factors for hydrocarbon exploration. In this study we use seismic reflection data and gravity modelling to investigate the geometry, structure, and trend of the Rovuma continental margin (Northern Mozambique) in order to decipher: 1) the margin type and its mode of formation (divergent vs strike-slip), and 2) which group of plate tectonic models are best able to predict the observed structures and margin trend. For the first time, we unambiguously identify a transform continental margin in seismic reflection data from the southern Rovuma Basin and support our observations with rigorous gravity modelling. The identified margin is not coincident with the DFZ, which is often assumed to form the continent-ocean transform margin (COTM) of the WSB.

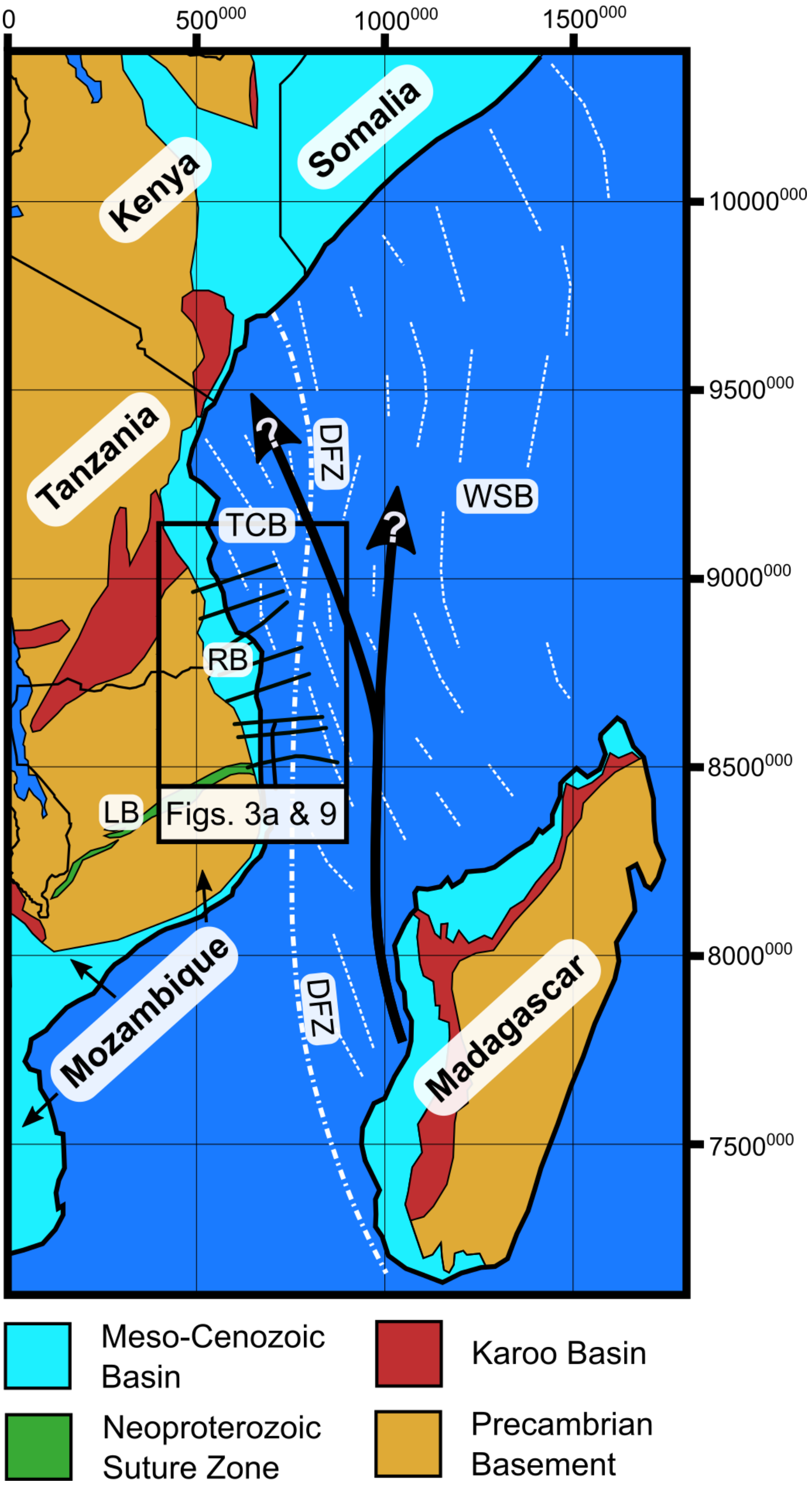

Figure 3.1. Map of the Western Somali Basin (WSB) showing the location of gravity profiles (black lines) studied in the Rovuma Basin (RB). Karoo and Jurassic aged sedimentary basins used to reconstruct the conjugate margins are shown. White dashed lines depict gravity lineaments related to the ocean spreading fabric of the basin (Phethean et al.,

2016). Large black arrows indicate the two main groups of reconstruction paths proposed for Madagascar. DFZ, Davie Fracture Zone; LB, Lurio Belt; TCB, Tanzania Coastal Basin.

3.2. Characterisation of passive continental margins

The angle between the lithospheric deformation zone and the regional extension direction (previously discussed in Chapter 1.2) controls which of the two endmember types of passive margins, divergent and transform margins, develops. Where the deformation zone lies almost perpendicular (~ > 80°) to the extension direction, divergent margins develop. Decreasing the obliquity between the extension direction and the deformation zone to between ~60° and ~80° results in the development of divergent margin segments linked by transfer zones. A further reduction to between ~20° and ~50° leads to the development of alternating divergent and transform margin segments, possibly connected through horsetail splay faults. Below ~20°, transform margins develop (Basile and Braun, 2016).

Harry et al., (2003) devised a method of differentiating between margin endmembers by comparison of crustal thickness variations across a margin to a compilation of well-studied examples. This compilation has since been updated by Mercier de Lépinay et al., (2016) and allows for a rapid identification of margin type and, therefore, mode of development.

This method of margin interpretation can also be supplemented through the identification of features characteristic of each margin type to provide a more robust differentiation between divergent and transform type margins. We use the main characteristics of passive margin endmembers summarised in Chapter 1.2 for this purpose. Furthermore, average Moho slopes across the necking zones of magma-poor divergent margins and transform margins show differing distributions (Figure 3.2) and may therefore be used to differentiate between the two margin types. Whilst the bulk of Moho slopes for both transform and magma-poor divergent margins overlap, transform margins with slopes less than 7° are yet to be identified, as are magma-poor divergent margins with slopes greater than 36°. Average Moho slopes across necking zones that are lower or higher than these values therefore imply a divergent or transform margin, respectively. As the crustal necking zones of volcanic divergent margins are modified by magmatic additions, the slope of the Moho across them may not be used to identify the margin as divergent or transform in nature. These margins are, however, readily identifiable by other characteristic features in seismic reflection data (e.g. Chapter 1.2) and do not require such Moho slope analysis for identification.

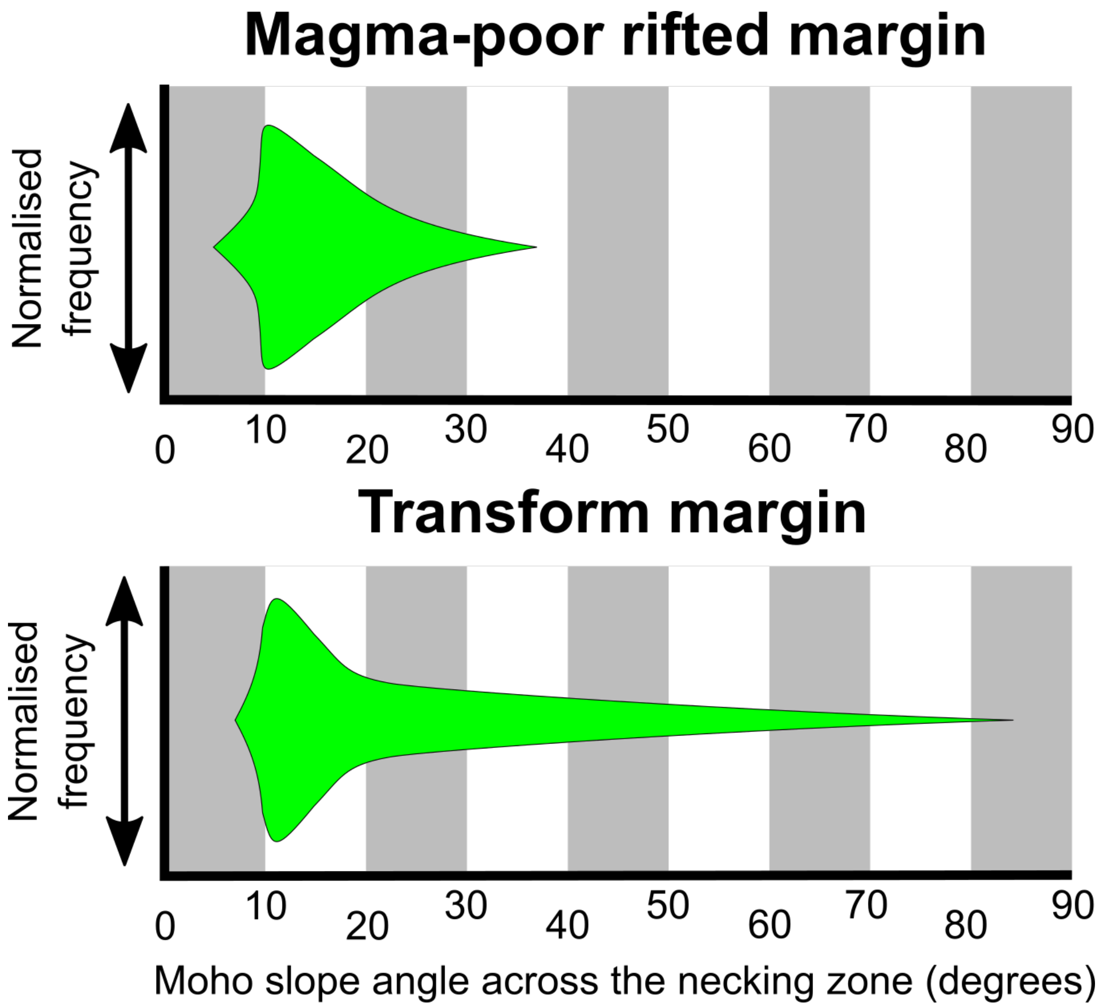

Figure 3.2. Normalised frequency distribution of average Moho slope angles across the necking zones of magma-poor rifted margins and transform margins respectively. Data is derived from: Reston (2009) and Van Avendonk (2009) for magma-poor rifted margins; and, Todd et al., (1988), Todd and Reid (1989), Barton et al., (1990), Keen et al., (1990), Edwards et al., (1997), Sage et al., (2000), Greenroyd et al., (2008), and Parsiegla et al., (2009) for transform margins.

3.3. Data and Methods

Seismic reflection data and 2D gravity modelling are used to investigate the Rovuma Basin margin geometry, structure, and trend in order to discern the margin type and therefore strain regime under which it formed. This allows for the comparison of predictions from different plate tectonic models with observations in order to determine which best accounts for the evolution of the WSB.

3.3.1. Seismic reflection data and interpretation

Multichannel seismic reflection data from the ION East AfricaSPAN and VEMA (leg 3618) cruises are used for the geological interpretation of basement structures around the continental margin of the Rovuma Basin (Figure 3.1), and to constrain 2D gravity models.

Three lines from the ION East AfricaSPAN PSDM (pre-stack depth migrated) dataset cross the continental margin of the Rovuma Basin at near perpendicular angles (Figure 3.3a). These lines are used to identify features of the Rovuma margin that are characteristic of the different endmember margin types (as described in Chapter 1.2). This assists in the interpretation of the margin type, helps to delineate the COT, and identifies the lateral position of the bottom of the basement slope, which is compared with those predicted by gravity modelling.

A fourth line from the ION East AfricaSPAN PSDM dataset crosses the continental margin at a highly oblique angle and captures continental Moho reflections. Moho slope angles measured across the necking zone on this line are therefore corrected to their true dip. For this purpose, the strike of the margin is assumed to follow the onshore basement outcrop of the Rovuma Basin.

3.3.2. Gravity data

Three different gravity datasets are used to constrain the gravity anomaly for gravity modelling. These include the Trident Bouguer onshore, free-air offshore anomaly dataset (Trident BAFA) provided by Getech (Fairhead et al., 2009), the Sandwell and Smith V24 free-air anomaly (SS24; Sandwell et al., 2014; Figure 3.3a), and the DTU15 free-air anomaly (Stenseng et al., 2015). Each dataset has its own strengths. For instance, the Trident BAFA dataset contains additional proprietary data onshore; SS24 has a 'rich' frequency content due to its use of residual slopes of sea surface height during gravity estimation (Pavlis et al., 2012); and DTU15 has been argued to have an increased accuracy in coastal regions due to its use of simply the residual sea surface heights in its estimation of gravity anomalies (Pavlis et al., 2012). Using the datasets together also allows a qualitative measure of uncertainty by comparing their variability and reduces the error produced by local deviations of any one dataset during modelling.

To reduce the errors associated with modelling a 3D interface in 2D, and to make all three gravity datasets BAFA and thus comparable, we perform Bouguer and terrain corrections on the SS24 and DTU15 datasets before 2D modelling. Those corrections were performed in GMT using the Okabe method, which is able to handle arbitrarily complex geometries. A resolution of 1 km was used for SRTM elevation data, and we assume a density for the upper crust of 2.67 g cm^{-3} to be consistent with the Trident BAFA dataset.

Following BAFA conversion, the three datasets can be directly compared. Onshore, both the DTU15 and SS24 datasets use the Earth Gravitational Model (EGM2008; Pavlis et al., 2012) solution, but where the additional proprietary data included in Trident result in significant local differences between this dataset and the others, we consider Trident more reliable. Offshore, the Trident dataset is produced primarily as a stacked solution of older versions of the SS and DTU anomalies, and so this dataset generally follows the trend of the DTU15 and SS24 anomalies. Where it does differ, it is deemed less reliable as it was produced before the addition of new CryoSat-2 and Jason-1 altimetry data. As, however, the DTU15 and SS24 datasets are produced using different methodologies, differences between these datasets represent real uncertainty in the gravity anomaly. To mitigate this problem, gravity profiles for 2D modelling are located away from any significant disagreements so that differences are generally < 10 mGal. Where onshore sections of gravity profiles must cross regions of significant disagreement between the Trident and SS24/DTU15 datasets, we replace the SS and DTU onshore data with that of the more reliable Trident dataset. A spline covering 10 km either side of the coastline is used to produce a smooth join between the datasets. A map showing the variations between datasets is provided in the supplementary material (Figure S3.1).

3.3.3. Gravity modelling

Three types of gravity modelling have been performed during this study in order to determine the margin type, the margin's trend, and the detailed crustal structure of the margin, respectively.

Firstly, a rigorous parameter space search investigating the preferred slope angle and location of a simple ramp-style Moho geometry is performed for the three profiles where coincident seismic data crossing the margin is available to constraint the seabed and basement interfaces (Figure 3.3b). This provides an understanding of the Moho geometry unbiased by human interpretation and is used to generate profiles of crustal thickness variation across the margin. These profiles are then compared to the global margin crustal thickness variation compilations of Harry et al., (2003), and Mercier de Lépinay et al., (2016), providing an independent interpretation of the Rovuma Basin margin type.

Secondly, the preferred Moho slope angles and locations derived for profiles 2 and 3 are used to produce a simplified average geometry of the margin. We then use this simplified geometry to find the best fitting margin location along gravity profiles 4-8, which have no seismic constraints. Profile 1, south of the Lurio belt, is used as an independent test profile for this method. These best fit locations constrain the margin trend and, in combination with the interpretation of the margin type, allow us to determine which group of plate tectonic models best predicts observations from the Rovuma Margin.

Following the first-order determination of the margin type, a final procedure involves detailed 2D forward gravity modelling of the three gravity profiles with coincident seismic data, using the commercial Interpex IX2D-GM software. This modelling allows for the addition of geologically plausible refinements to reduce misfit between the modelled gravity profile and data, where required. The resulting detailed crustal structure of the margin is then used to identify features characteristic of the different margin types, providing additional constraints for the interpretation of the margin.

3.3.3.1. Modelling type 1: Systematic investigation of Moho geometry

Gravity profiles with coincident seismic data crossing the margin's basement slope (Profiles 1,2, and 3; Figure 3.3a) were used to investigate the underlying Moho geometry using the accurate seismic constraints on the remaining density interfaces. Simple ramp-style Moho geometries were tested for slopes between 5 and 85 degrees over a 65 km distance around the bottom of the basement slope as identified from seismic data. An initial search at 5 degree and 5 km intervals covers the plausible parameter space with over 250 Moho geometry combinations (Figure 3.3b). This is then followed by a refined search around the initial parameter minimum at 1 degree and 1 km intervals. The root-mean-square fit between the calculated gravity anomalies and the three gravity datasets used in this study is then determined.

The 2D forward modelling was performed in Matlab using the analytical expression for the gravity effect of line elements with horizontal and vertical dimensions of 100 m and 20 m respectively. The model domain was extended 600 km beyond the extent of the gravity profile to mitigate boundary effects, whilst linear smoothing of density contrasts was performed laterally for 500 m on either side of a density interface to reduce artefacts resulting from gravity calculations of the rectangular grid elements across extremely shallow interfaces, such as outcropping basement.

The densities and geometries of the sediment and crustal layers used for all types of gravity modelling are constrained using a variety of Industry and academic data, as well as information from the literature. These are described below.

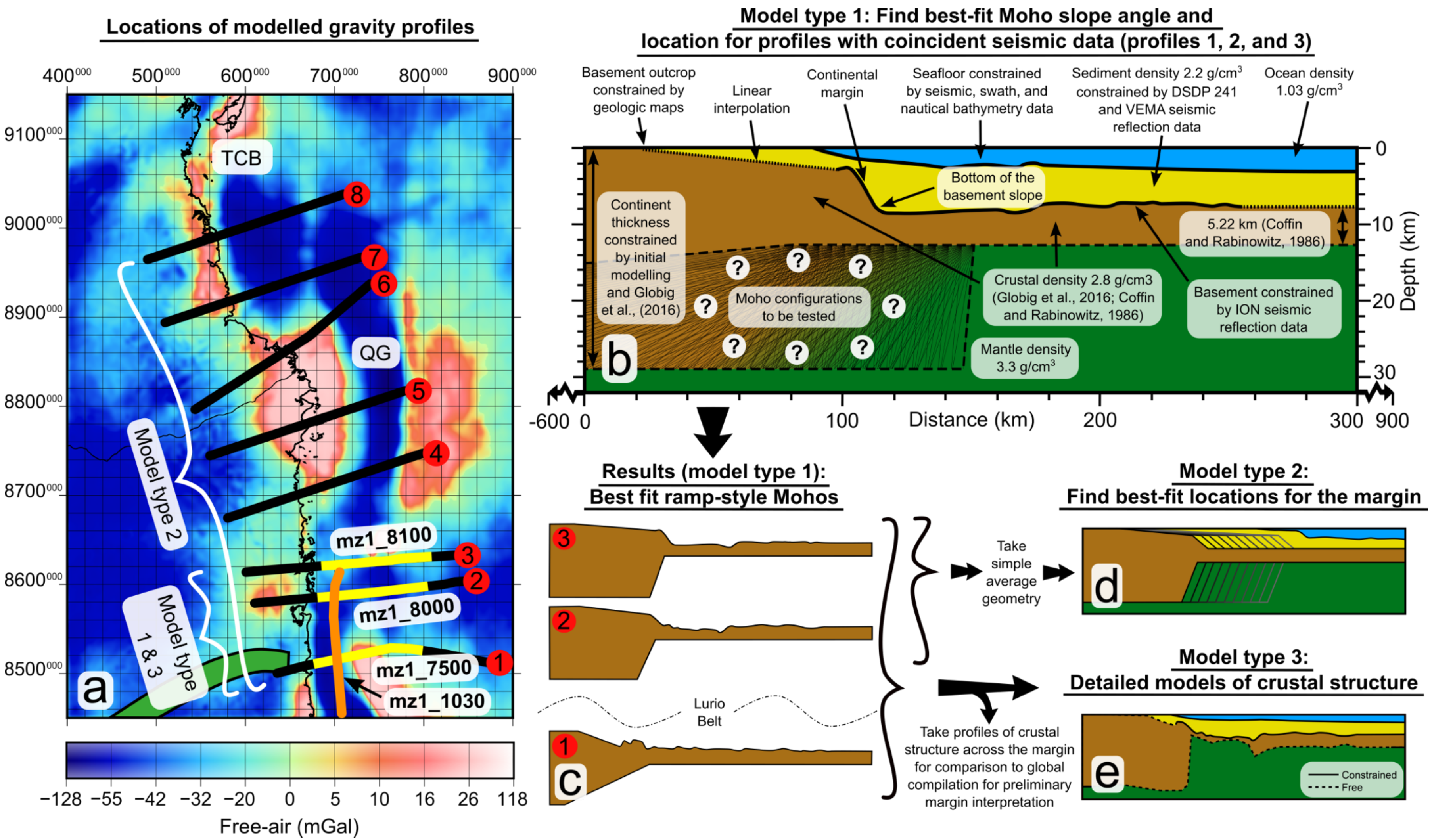

Locations of modelled gravity profiles
TCB
QG
Model type 2
Model type 1 & 3
mz1_8100
mz1_8000
mz1_7500
mz1_1030
a
Free-air (mGal)
Model type 1: Find best-fit Moho slope angle and location for profiles with coincident seismic data (profiles 1, 2, and 3)
Basement outcrop constrained by geologic maps
Linear interpolation
Continental margin
Seafloor constrained by seismic, swath, and nautical bathymetry data
Sediment density 2.2 g/cm3 constrained by DSDP 241 and VEMA seismic reflection data
Ocean density 1.03 g/cm3
Bottom of the basement slope
Continent thickness constrained by initial modelling and Globig et al., (2016)
Moho configurations to be tested
Crustal density 2.8 g/cm3 (Globig et al., 2016; Coffin and Rabinowitz, 1986)
5.22 km (Coffin and Rabinowitz, 1986)
Basement constrained by ION seismic reflection data
Mantle density 3.3 g/cm3
b
Distance (km)
Depth (km)
Results (model type 1): Best fit ramp-style Mohos
Lurio Belt
c
Take simple average geometry
Model type 2: Find best-fit locations for the margin
d
Take profiles of crustal structure across the margin for comparison to global compilation for preliminary margin interpretation
Model type 3: Detailed models of crustal structure
e
Constrained
Free

Figure 3.3. Locations of seismic and gravity profiles, and summary of gravity modelling methods (a) Sandwell and Smith free-air gravity anomaly map showing modelled gravity profiles, which are indicated by black lines with corresponding identification number in red circles. Coincident seismic profiles that cross the continental margin are marked in yellow. Seismic profile mz1_1030 (orange) runs highly obliquely to the margin trend. The Lurio Belt is marked by the green band. QG, Quirimbas Graben; TCB, Tanzania Coastal Basin. (b) Summary of type 1 modelling – Moho geometry investigations along seismically constrained profiles. Constrained density interfaces are shown as solid lines, assumed interfaces are shown as short dashed lines, and the region of Moho configurations to be tested around the margin is marked as long dashed lines. (c) The results from type 1 modelling on profiles 2 and 3 (situated to the north of the Lurio Belt) are used to generate an average margin geometry for use in type 2 models, with profile 1 used to test the method. Results from profiles 1, 2, and 3 are used as starting models for type 3 modelling. (d) Summary of type 2 modelling. The average margin geometry is modelled across the margin for all profiles (1-8) to find the best fit locations and determine the margin trend. (e) Summary of type 3 modelling. Seismically constrained lines are modelled in detail using Interpex IX2D-GM software. The Moho and unconstrained regions of the basement are allowed to move freely. Crustal thicknesses of 29 km and 5.22 km are used as continental and ocean boundary conditions, respectively.

3.3.3.1.1. Bathymetry surface

The seabed is a shallow interface with a high density contrast across it. Because of this, it is one of the major contributors to the gravity anomaly, and it must be well constrained to perform accurate gravity modelling. The ION seismic reflection lines provide an extensive and high quality seabed constraint for the region. However, as they sometimes do not cross the shelf edge, they are unable to fully constrain the geometry of this major shallow structure. We therefore supplement the ION seabed constraints with available ship-based singlebeam and multibeam bathymetry data extracted from the GEBCO and Sandwell and Smith global elevation datasets, as well as additional depth soundings taken from nautical charts for the region, which significantly increase the seabed constraints around the shelf break (Figure 3.4a). In places these additional constraints deviate from global elevation datasets by more than 500 m and represent a significantly more accurate constraint on the seabed for gravity modelling (Figure 3.4b).

As ship-based measurements are generally quite widely spaced, they can provide good constraints on the long wavelength information of the seabed, but provide little information on short wavelengths between data points. Following surfacing of the combined dataset (performed using Generic Mapping Tools (GMT; Wessel et al., 2013) with a tension factor of 0.25), we therefore apply a 15 km low-pass Gaussian filter and replace the short wavelengths with those of the Sandwell and Smith gravity-derived seabed dataset, which has full spatial coverage.

The seabed interface will thus inherently account for the vast majority of the very short wavelength (< 15 km) content of the gravity anomaly, allowing us to produce realistic models with a full range of wavelengths without affecting the modelling of the basement and Moho structures of interest, which inherently have longer wavelength gravity signatures due to upward continuation. A 15-km filter is used as it provides the best trade-off between increased continuity of structural seabed trends derived from the SS data and maximised accuracy in regions of data constraint. The resulting seabed surface is shown in Figure 3.4c. Examples using alternative filter cut-off wavelengths are presented in the supplementary material (Figures S3.2-5) .

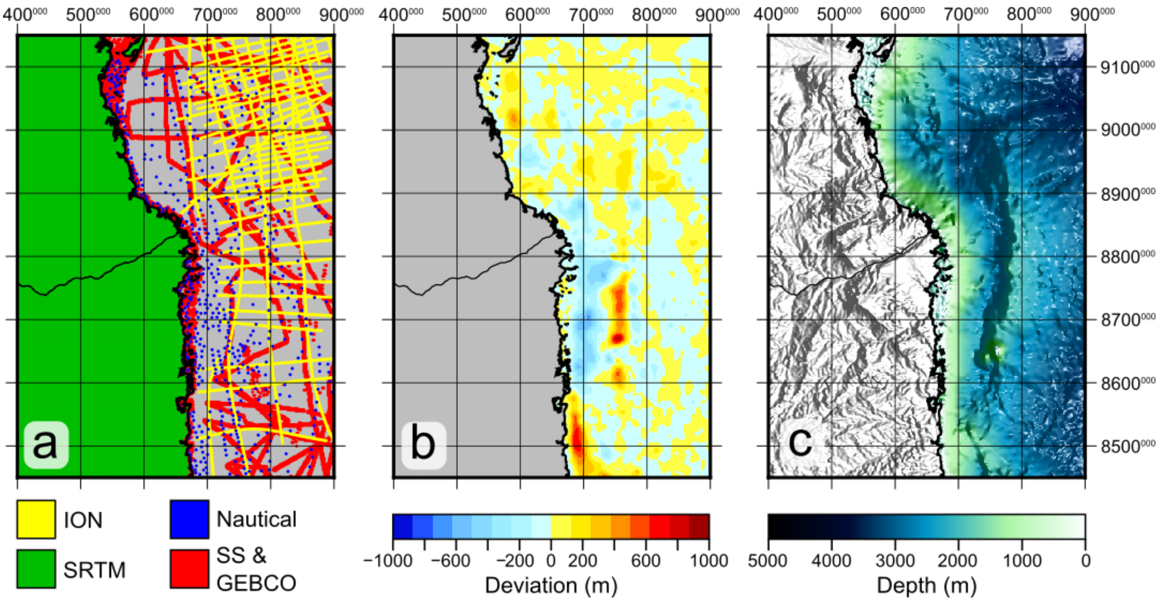

Figure 3.4. (a) Input data for the new bathymetry surface. (b) Difference between the new bathymetry surface and global elevation models. Offsets of almost 1 km can be seen and represent a significant improvement in the predicting capabilities of the dataset. (c) The new bathymetry surface, illuminated from the east.

3.3.3.1.2. Sediment density

We constrain the density of the sediment layer using seismic velocities derived during post stack migration processing of the multichannel seismic reflection line 84v, shot during the R/V *Vema* leg 3618. This line is situated in the north of the WSB, but is chosen due to the availability of coincident density measurements from the DSDP 241 borehole. The Nafe-Drake relation provides a good fit of densities derived from velocity conversion to densities measured at DSDP 241, where converted densities range from 1.62 to 2.38 g cm^{-3}, with a mean value of ~2.2 g cm^{-3}. Further information and figures on the derivation of the sediment density are provided in the supplementary material (Figures S3.6-8).

3.3.3.1.3. Sediment thickness

Offshore, where ION PSDM seismic reflection lines are coincident with gravity profiles, the top basement interface constrains the sediment thickness. Where possible, crosslines are used to check the interpretation of the top basement reflector. Where young volcanic edifices within the sediment layer obscure the basement interface, we linearly interpolate between basement picks.

Onshore, the basement outcrop is constrained using regional geological maps. Between the onshore basement outcrop and the seismically constrained basement offshore, we linearly interpolate the basement horizon. This is likely a gross simplification of the true geometry of the basement interface; however, it avoids the introduction of unjustified complexities in the gravity modelling. Sensitivity to this simple linear geometry was also tested by modelling alternative imposed geometries, such as simple basins or rises, within the unconstrained region.

3.3.3.1.4. Crustal density and thickness in the ocean and continent

In order to investigate the nature of the transition from continent to ocean, densities and thicknesses of the continental and oceanic crust on either side of the transition must first be constrained.

Offshore, (Coffin et al., 1986) used sonobuoy experiments to determine the thickness and velocity structure of oceanic crust in the WSB. They showed that the crust has an average thickness of 5.22 km, which we use to constrain the depth of the Moho below top basement at the seaward edge of the coincident seismic data. The crust has an average layer 2 thickness of 2.73 km with a velocity of 5.83 +/- 0.27 km/s, and a thin layer 3 averaging just 2.62 km thick with a velocity of 7.03 +/- 0.25 km/s. Using the Nafe-Drake relationship, we convert these seismic velocities to densities for the upper and lower bounds of the velocity estimate. We then average the densities of upper and lower crust weighted by the thickness of each layer to calculate an average crustal density for the oceanic crust. Due to the dense layer 3 being thin compared to most estimates from normal oceanic crust, the average oceanic crustal density is also low at between 2.76 and 2.89 g/cm3.

Onshore, a recent study by Globig et al. (2016) incorporating a comprehensive dataset of Moho depths showed that the average crustal density of the African continent is 2.79 g/cm^3. The continent-scale study also predicted crustal thicknesses along the Rovuma basin as low as 30 km. To determine the final crustal thickness to be used, we initially perform modelling phase 1 using crustal thicknesses between 20 and 35 km, with testing at 1 km intervals for all profiles between 27 and 31 km, and selected the thickness consistently resulting in the lowest RMSD for use in the final models. The full results from this testing are presented in the supplementary material (Figure S3.9).

As the average density of the continental crust falls within the range for the oceanic crust, we model both using a single density of 2.8 g/cm^3. This provides several advantages: Firstly, there is no imposed lateral density contrast between the ocean and continent. This allows us to avoid any circularity in determining the location of the COB from crustal thickness, which would be influenced by the chosen location of a lateral density contrast. Secondly, by not differentiating between upper and lower crusts, we avoid the introduction of an additional unconstrained interface into the model. A disadvantage of this method is that the basement-sediment interface may be modelled using a slightly higher density contrast than might be present at these depths.

3.3.3.2. Model type 2: Determining the margin trend

To determine the along-strike trend of the margin, we generate a simplified average margin geometry and model its best fit location along gravity profiles that cross the continental margin to the north of the Lurio Belt (Figure 3.3d). We use the Matlab code previously described in section 3.3.3.1, and the best fit location is again determined by calculating the RMSD between the modelled gravity anomaly and the three gravity datasets.

The simplified average margin basement geometry is generated from seismic and geological map constraints of the basement interface along profiles 2 and 3, and is defined by 3 inflection points along the basement interface (Figure 3.3c-d). From onshore seaward the inflection points are: 1) the onshore basement surface outcrop, where the basement interface begins to dip gently seaward; 2) the top of the basement slope, at a depth of 2.8 km, after which the basement interface dips steeply at 21°, until; 3) the bottom of the basement slope, at a depth of 7.8 km, after which the basement interface returns to horizontal. A ramp-style Moho geometry, determined from the type 1 modelling, defines the base of the crust and has a slope of 67°, the top of which is positioned 8 km landward and 5.22 km below the bottom of the basement slope.

Only profiles 2 and 3 are used for the generation of the average margin geometry for two main reasons. Firstly, it allows us to use profile 1 to test the search algorithm's ability to correctly locate the base of the basement slope on a profile with coincident seismic data. Secondly, profile 1 is located to the south of the Lurio Belt, an ENE-WSW trending

Neoproterozoic suture zone separating the northern and southern basement complexes of northern Mozambique (Emmel et al., 2011), across which basement structure differs (Franke et al., 2015). The geometry of profile 1 is therefore less likely to be representative of the margin to the north, making it a poor contribution to the average geometry of the margin. It does, however, therefore serve as a demanding test for the search algorithm allowing an assessment of the techniques robustness. We quantify the accuracy of type 2 modelling by measuring the offset between its predicted margin location and the Moho and basement slopes determined from seismic data and type 1 modelling. We also perform further testing of the search algorithm's sensitivity to the inputted average margin geometry, along with checks on the geological plausibility of required adjustments to type 2 model output in order to satisfy gravity data.

3.3.3.3. Model type 3: Detailed 2D gravity models

Following systematic investigation of preferred Moho geometries using a simple ramp-style Moho slope, more complex 2D forward modelling is performed with full freedom of the Moho interface and, within its unconstrained region, top basement interface. This modelling is performed using Interpex's IX2d-GM software.

This investigates the detailed crustal structure along the profiles, allowing for the identification of features characteristic of different margin types. Key features that could be identified by this modelling include: a) marginal ridges or complex rift structures within the region of unconstrained basement, characteristic of some transform margins and rifted margins respectively; b) complex Moho geometries, some of which may influence Moho slope angles determined across the necking zone from type 1 modelling; c) margin flexure, found at transform margins with mechanically coupled ocean and continental domains, and d; hyper-thinned continental crust and exhumed mantle found at magma-poor rifted margins, or exhumed mantle and thin oceanic crust found at transform margins and ocean fracture zones.

The same layer densities as for type 1 and 2 modelling are used, although we also test layered sediment densities and two layer crustal densities. The same crustal thicknesses as for type 1 and 2 modelling are also imposed at the ends of the gravity profiles as boundary conditions.

3.4. Results

3.4.1. Seismic reflection observations

The location of the four seismic reflection lines from the ION East AfticaSPAN dataset are shown in Figure 3.3. Three of the lines cross the continental margin perpendicularly. Results for these lines (from north to south: mz1_8100, mz1_8000, and mz1_7500) are shown in Figure 3.5. A fourth line, mz1_1030, runs perpendicular to the three previous lines and also crosses the continental margin at a highly oblique angle, and results for this line are shown in Figure 3.6.

3.4.1.1. Mz1_8100

At the western edge of line mz1_8100, a massive 6 km increase in accommodation space occurs over an extremely short distance of ~17 km (Figure 3.5a and d). The large increase in accommodation space indicates that the continental crust has been thinned and that this structure represents the continental margin. No faults are imaged within the steep 24° basement slope, which is instead onlapped by steeply dipping parallel sequences of post rift sediments. Immediately at the base of the margin slope a crossline confirms the top basement pick, which becomes obscured slightly eastwards due to the St Lazare volcanic edifice. East of St Lazare and of the DFZ, which is obscured by the above volcanics, the top basement is again imaged and has a hummocky character commonly associated with oceanic crust. No continuous reflections define the Moho surface for any region of this line and no evidence for syn-rift volcanics is present, despite extensive post breakup volcanism.

3.4.1.2. Mz1_8000

Approximately 35 km to the south a similar setting is observed (Figure 3.5b and e). Again a steep basement slope, here 18°, defines a large 5 km increase in accommodation space and is void of any faults. The presence of limited post rift volcanics allows the top basement to be traced across the entirety of this line. To the west of the DFZ this surface lies at ~7.3 s TWTT, and shows a rough and hummocky character. No Moho reflections are visible anywhere to the west of the DFZ, but recent faulting of the overlying sediments may partially obscure the deep structure of some of this region due to the disruption of seismic energy by such faults before the basement is imaged and by tectonic overprinting of the original basement structure. The DFZ itself is defined by a rise in the top basement, and possible weak Moho reflections define a crustal thickness of ~2.4 s TWTT. To the east of the DFZ, the top basement is well defined and lies at ~6.8 s TWTT, 0.5 s above that to the west, and is defined by a hummocky character. In the vicinity of the DFZ, Moho reflections have a sudden onset and clearly define an average crustal thickness of ~1.8 s TWTT until the end of the profile.

Aligning the base of the basement slopes (black stars on Figure 3.5) of these two similar margin profiles (mz1_8100 and mz1_8000) defines a slightly NNW-SSE trend of the margin, at 172°.

3.4.1.3. Mz1_7500

Moving 70 km farther southwards, and crossing the offshore extension of the Lurio Belt, a change in the margin architecture occurs. On the west, rift grabens filled with divergent wedges of synrift sediment are bounded by continentward-dipping normal faults, possibly forming the northern continuation of the Angoche Basin (e.g. Mahanjane, 2014; Figure 3.5c and f). These half grabens sit at a depth of approximately 4 s TWTT, substantially above the basement to the east, which lies at between 5 and 7 s TWTT. This is consistent with a thicker crust beneath this region providing isostatic support, and with a continental origin of this basement. This faulted crust is bounded seaward by a large horst block, sitting up to 1.5 km above the half grabens. A large (2 km), and extremely steep, basement slope then dips 35° towards the east. This structure lies along the continuation of the 172° trend of the margin seen on the northern lines, and is steeply onlapped by sediments lacking a divergent nature. The similar steep slope, sedimentation history, and the along-strike alignment of this structure with the basement slope seen farther north suggests a genetic relationship between them. Seaward of this slope, the top basement can be seen to gain a smooth character, possibly indicating the presence of oceanic crust. This smooth character continues eastwards of the DFZ. The DFZ at this location is expressed by a positive flower structure, indicating a compressional component to the strike-slip tectonics along it. Moho reflections beneath the DFZ, which are stronger on the eastern flank, define a crustal thickness of over 3 s TWTT, attesting to the transpressional nature of the DFZ in this location. On the western flank of the DFZ, westward-dipping low angled reflectors can be seen to cut across the crust and are associated with a slight shallowing of the basement and counter-clockwise rotation of the upper crust. These structures are associated with crustal thickening around the DFZ and may represent thrust faults that developed in response to the compression. A similar structure, not cutting the entire crustal section, also offsets the Moho to the east of the DFZ and is again associated with a thickening of the crust. In this region, strong Moho reflections define a crustal thickness of generally between 2.2 and 1.7 s TWTT, and a more seismically transparent nature of the crust is seen to the east of the DFZ, indicative of oceanic crust.

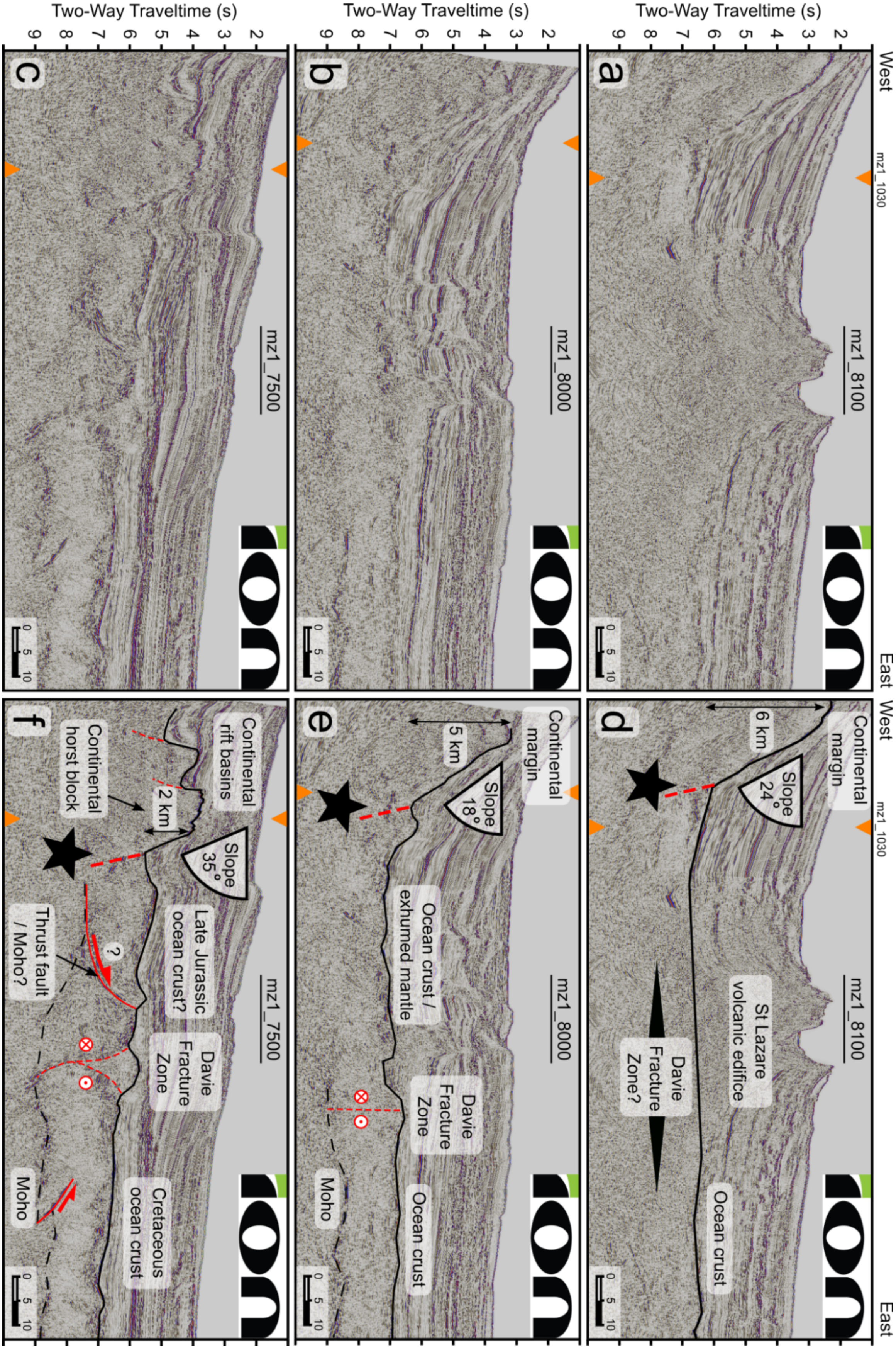

Two-Way Traveltime (s)
West
East
a
b
c
d
e
f
mz1_1030
mz1_8100
mz1_8000
mz1_7500
Continental margin
Slope 24°
6 km
St Lazare volcanic edifice
Davie Fracture Zone?
Ocean crust
Slope 18°
5 km
Ocean crust / exhumed mantle
Davie Fracture Zone
Moho
Continental rift basins
Continental horst block
2 km
Slope 35°
Late Jurassic ocean crust?
Thrust fault / Moho?
Cretaceous ocean crust

Figure 3.5. ION seismic reflection profiles crossing the continental margin are shown unmarked (a-c) and interpreted (d-f). Line intersections with the perpendicular mz1-1030 profile are marked by orange triangles. For the location of the seismic lines, see Figure 3.3a. (d-f) The basement interfaces are marked as solid black lines and highlight the steep continental margin. Basement slopes across the margin are labelled, as is the depth-converted vertical offset from top to bottom. Possible Moho reflections are indicated by dashed black lines. Positions of the base of the margin slope as interpreted from seismic are shown as black stars.

3.4.1.4. Mz1_1030

Running perpendicular to the above seismic lines, and at a highly oblique angle to the trend of the identified basement slope, line mz1_1030 also crosses the continental margin (Figure 3.6.). A deep set of strong reflections, with a southerly apparently dip, lie well below the top basement and are interpreted as the Moho. At the southern edge of the line these reflections lie at a depth of ~30 km. Moving northwards, the reflections rise consistently shallower to where they outcrop at the basement surface just north of line mz1_8000. To the north of this outcrop, exhumed mantle may therefore form the basement surface.

The rise of the Moho reflections northward indicates that the transition from continent to ocean occurs in this direction. In map view, the Moho reflections are oriented at 176 (i.e. almost due N-S, see Figure 3.3a). To transition from continent to ocean in a northerly direction, the margin must trend more NW-SE than the seismic line (i.e. <176°). Onshore, the basement outcrop along the southern Rovuma Basin has a trend of 172°, the same as the basement trend of the slope identified from margin-perpendicular seismic lines. Therefore, assuming a margin trend of 172°, we can correct the apparent dip of the Moho slope from line mz1_1030 to its true dip. This shows that it dips extremely steeply at ~74° towards the continent.

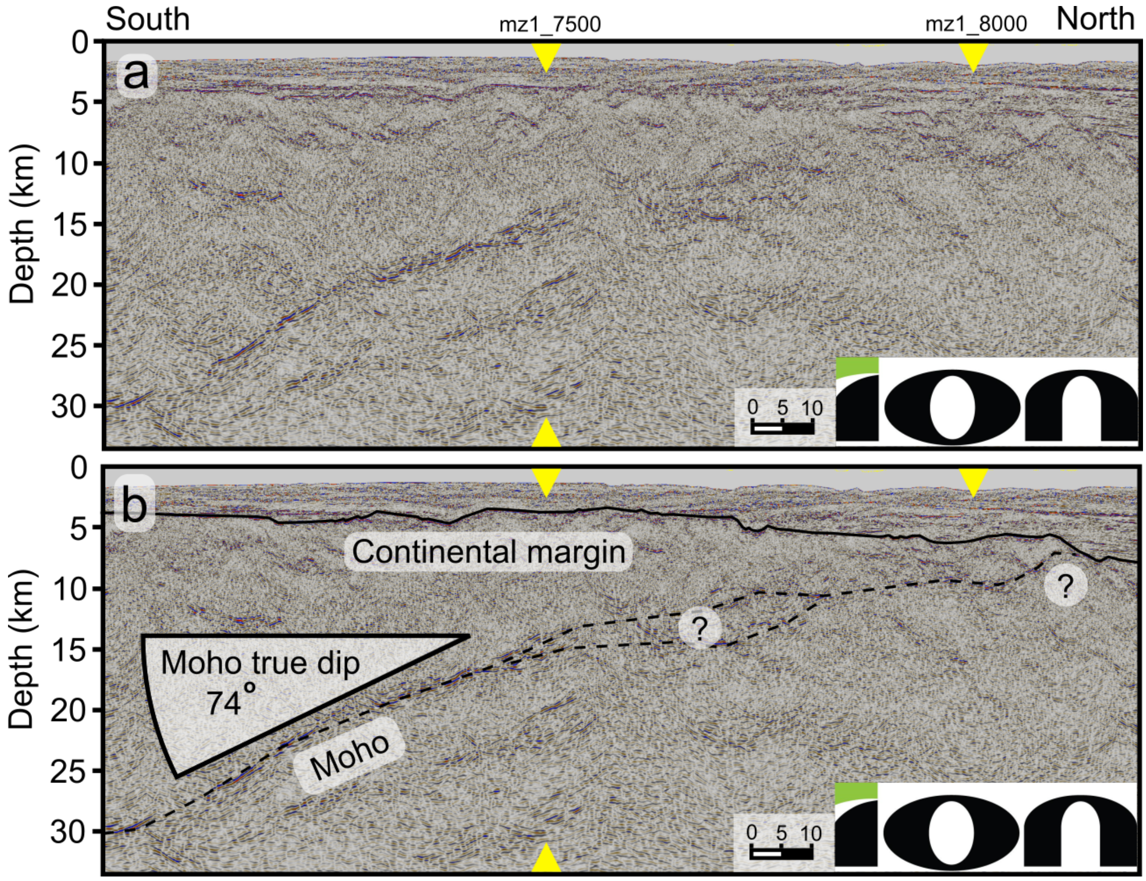

Figure 3.6. Depth-converted ION seismic reflection profile mz1_1030, crossing the margin at a highly oblique angle. Basement and Moho interfaces are marked as for Figure 3.5 and intersections with perpendicular seismic lines are marked by yellow triangles. For location, see Figure 3.3a. The true dip of the Moho, after correction for the obliquity of the profile to the margin trend, is 74°. The downward dip of the Moho reflections to the south indicates that the margin must trend in a more NW-SE direction than the seismic profile.

3.4.2. Gravity

3.4.2.1. Model type 1: Best fit ramp-style Moho geometries across the margin

Using constraints on the remaining density interfaces, gravity profiles with coincident seismic data crossing the margin are used to systematically determine best fit Moho geometries across the margin. An initial set of models is used to test a range of continental crustal thicknesses and consistently shows minimum RMSD fits to gravity data for 29 km thick continental crust. Visual best fits of the landward trend of the calculated gravity anomaly to data also consistently use a crustal thickness of 29 km. This value is in close agreement with Globig et al., (2016) and all final models therefore use a 29 km thick continental crust.

Model sensitivity to the geometry of the basement interface within the unconstrained region, between the basement outcrop and the onset of seismic constraint (e.g. Figure 3.3b), is also tested by the introduction of basins and ridges. Whilst the inclusion of basins sometimes results in lower RMSDs, it has little impact on the best fit Moho geometry. The introduction of complexities in this region is therefore unnecessary to determine best fits for the Moho, and is thus avoided.

All three profiles (mz1_8100, mz1_8000, and mz1_7500) show a similar pattern of results with a strong preference for steep Moho slope angles (15-85°) and a relatively narrow band (~15-30 km) of acceptable slope locations (Figure 3.7). The arcuate pattern of low RMSD fits reflects the natural trade-off between these two parameters in achieving a good model fit to the gravity data.

The northernmost profile with coincident seismic data, profile 3 (mz1_8100), is well constrained by type 1 modelling. Only Moho slopes greater than 25° result in low RMSD fits and the top of the Moho slope location is also constrained to within a 15 km band, centred on 107.5 km from the profile's western edge. Minimum RMSD values are achieved using an extremely steep Moho slope of 69° and a top of Moho slope location 105 km from the start of the profile. The top of the best-fit Moho slope is located 9.5 km to the west of the bottom of the basement slope identified in seismic data.

Profile 2 (mz1_8000) shows similarly well constrained Moho interface. Again, only Moho slopes greater than 25° result in low RMSD fits and the top of the Moho slope location is also constrained to within 15 km, centred on 102.5 km from the profile's western edge. Minimum RMSD values are again achieved using an extremely steep Moho slope of 65°, with a top of Moho slope location 99 km from the start of the profile. This places the top of the Moho slope 6.5 km to the west of the bottom of the basement slope identified in seismic data.

Profile 1 (mz1_7500) is the least well constrained of the three profiles by type 1 modelling and yet low RMSD fits are still only achieved using Moho slopes of 15° or greater. A 30 km band of low RMSD fits is achieved using Moho slope locations centres around 95 km from the profile's western edge. Minimum RMSD values are achieved for this profile using steep Moho slopes of 28°, with the top of the slope positioned at 95 km from the start of the profile. This places the top of the Moho slope 6 km to the east of the bottom of the basement slope identified in seismic data.

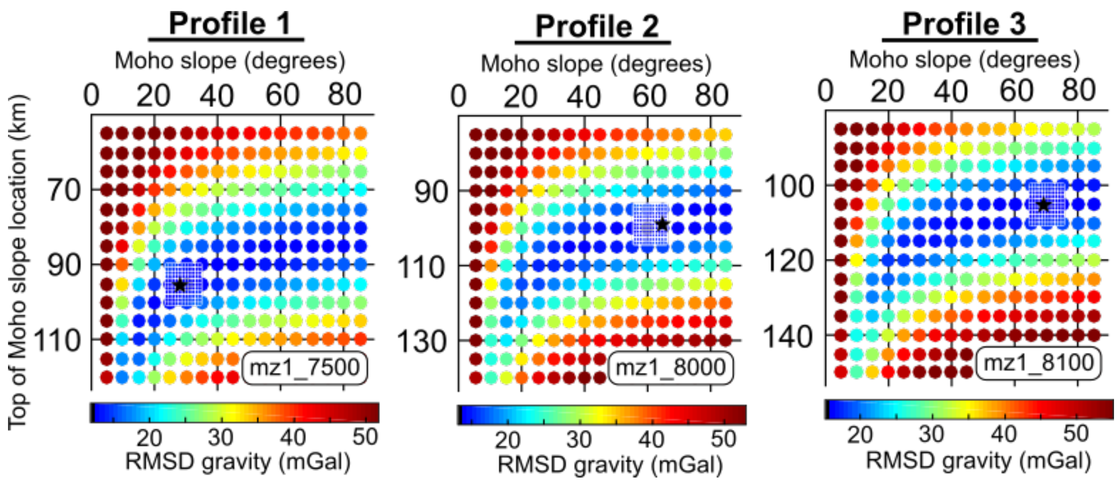

Figure 3.7. RMSD fits of Moho location and angle configurations for gravity profiles 1-3 as determined from type 1 modelling. All profiles show a similar trend, with the majority of the preferred parameter space covering steeper Moho slopes. Initial models at 5° and 5 km intervals are followed by models at 1° and 1 km intervals around the best-fitting parameter space determined during 5° and 5 km modelling. The minimum RMSD combination for each profile is marked by a black star.

3.4.2.1.1. Comparison of crustal thickness profiles to a global compilation of margins

Using the best fit Moho parameters for the three lines we generate crustal thickness profiles across the margin for comparison to global compilations of margin profiles by Harry et al., (2003) and Mercier de Lépinay et al., (2016) (Figure 3.8). All profiles fall firmly within the transform margin domain, with profiles 2 and 3 lying along its most extreme edge. These profiles are incompatible with observed profiles from rifted margins, and thus support an initial interpretation of the Rovuma Margin as a transform margin.

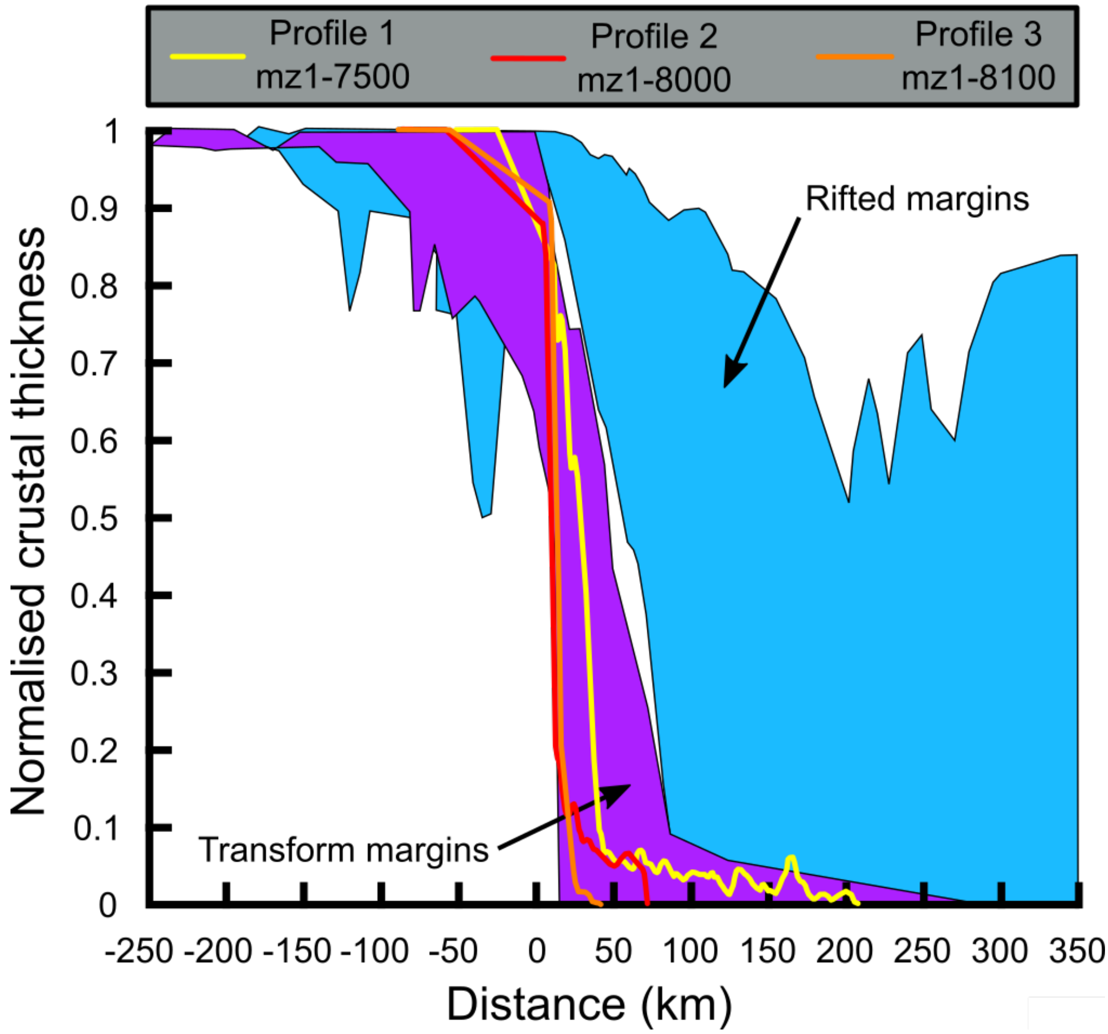

Figure 3.8. Normalised crustal thickness profiles across transform (purple) and rifted (blue) margins after Harry et al., (2003) and Mercier de Lépinay et al., (2016). Normalised crustal thickness profiles derived from type 1 modelling of gravity profiles 1, 2, and 3 are overlain. All profiles across the Rovuma margin lie within the transform margin domain.

3.4.2.2. Model type 2: Best-fit locations for average margin geometries and margin trend

We first test the search algorithm on profile 1, where it locates the bottom of the basement slope just 3.5 km seaward of its location in seismic data, despite the very different geometries of profile 1 and the average of profiles 2 and 3. The midpoint of the Moho slope is also in good agreement with that derived from type 1 modelling (Figure 3.9), validating the search algorithm's effectiveness. The resulting best fit gravity profile, however, differs substantially from the gravity data. This is due to complexities in the margin's real geometry not present in the tested average geometry. For the effectiveness of the model it is only required that the RMSDs of all tested locations are similarly affected by such complexities. Due to the simplicity of the input geometry this is to be expected and the only way to further remove the misfit between modelled and observed gravity profiles is to change the geometries in the gravity model (which will be the focus of modelling type 3).

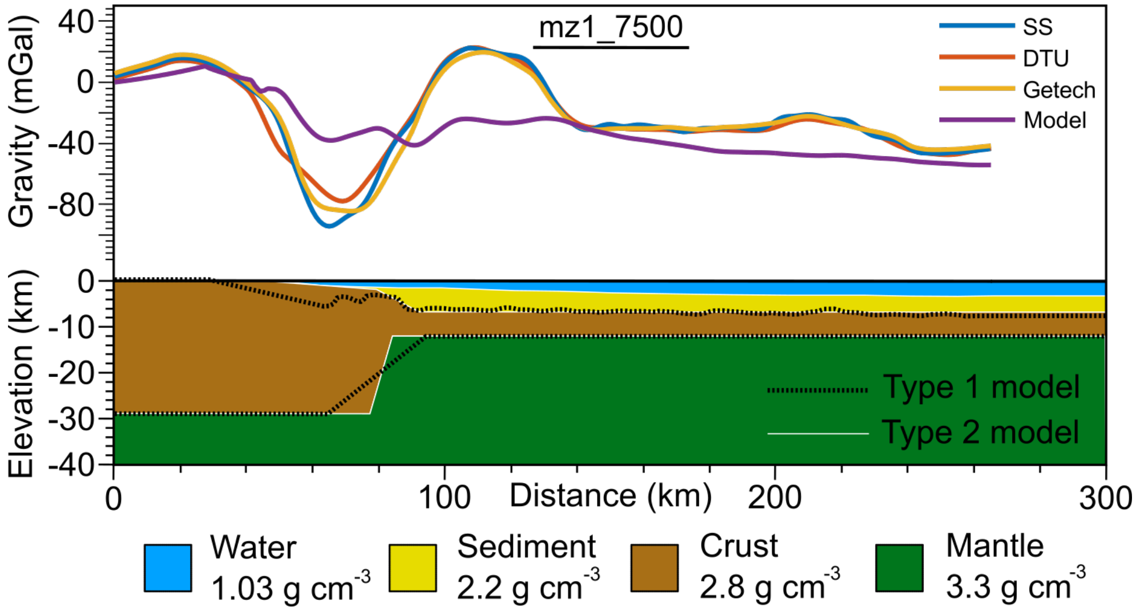

Figure 3.9. Calculated gravity profile (purple line) for the best fit location of the average margin geometry along profile 1 as determined from type 2 modelling. Despite the significant differences between the modelled average geometry and that determined from seismic data and type 1 modelling, there is a good agreement of the resulting margin locations. Misfits between the modelled gravity anomaly and data that result from simplifications in the modelled average geometry derived from the type-1 modelling, therefore, have not affected the model's ability to accurately locate the margin.

Application of the methodology on all profiles consistently results in a margin location with a sharp, single RMSD minimum (Figure 3.10), and defines a NNW-SSE trend of the margin. There is no indication that the continental margin follows the DFZ, and north of profile 3 the margin trends slightly more NW (at ~160°) than farther south (172°). The margin generally follows the trend of the basement outcrop on the western edge of the Rovuma Basin along its length. Small deviations in best fit locations of the margin from the average trend, of up to 25 km, may reflect complications in the margin structure and resulting shifts in the location predicted by the model. They may also be due to real variations in the margin's trend, and we note that the most significant deviation, across the border of Mozambique and Tanzania, is in alignment with the major Sea Gap Fault, which runs ~NNE-SSW through the TCB and may be related. Nonetheless, reasonable RMSD fits of the margin (RMSD <= 120% minimum RMSD) can be linked with a smooth curve through the margin, representing the margin's general trend.

Additional testing of the search algorithm's sensitivity to the input geometry is performed on all eight profiles. Steeper and shallower Moho slopes, of 87° and 47°, shift the predicted margin's location on average by 7.5 km landward and 8.5 km seaward, respectively. Seaward and landward shifts of the Moho slope location by 8 km relative to the basement slope shift the predicted margin's location by 16 km and 19 km, respectively. Whilst these variations are not insignificant, they are small compared to the length scale of the margin and do not affect the general interpretation of the margin's trend.

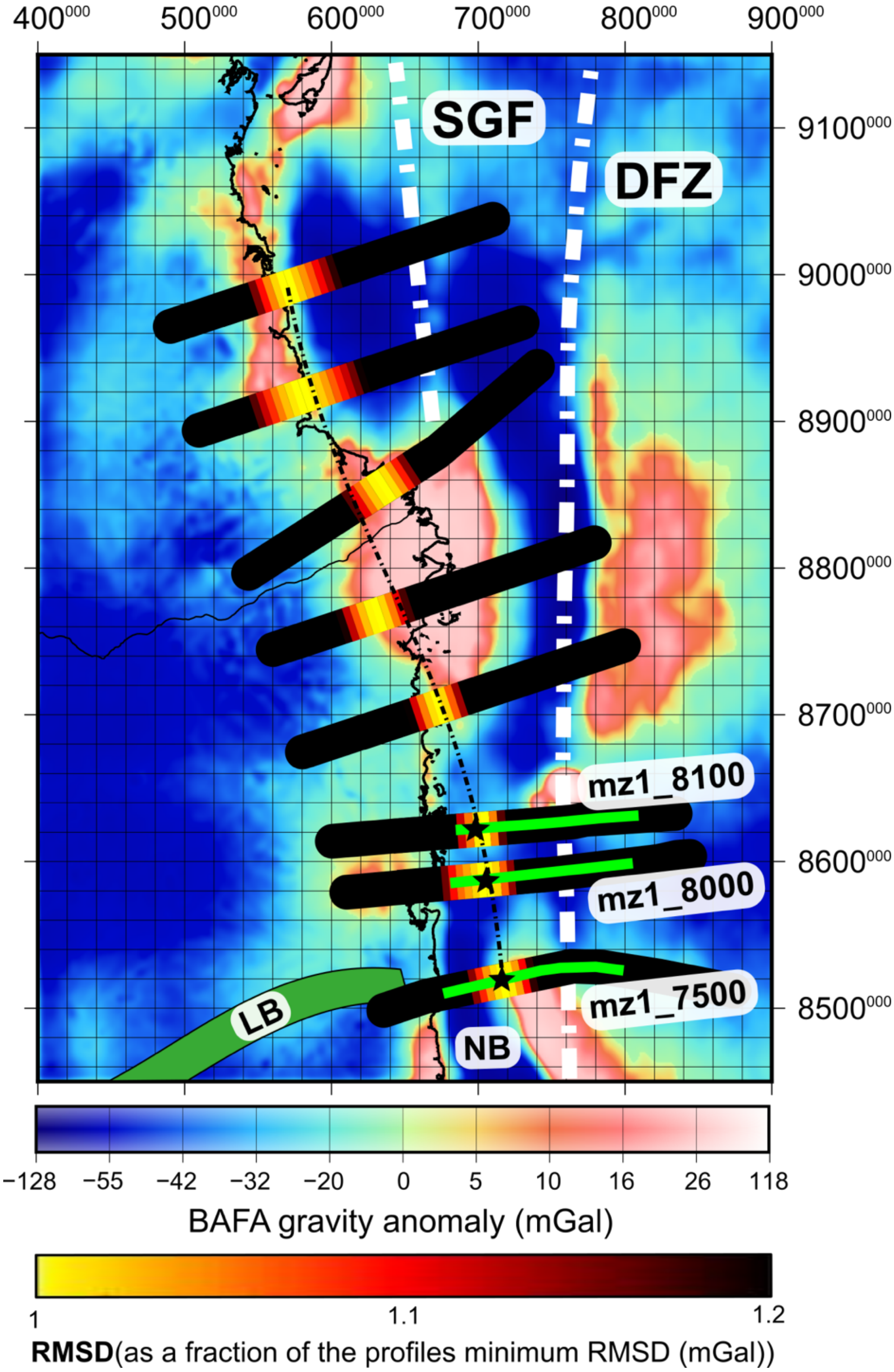

Figure 3.10. Sandwell and Smith free-air gravity anomaly map overlain with RMSD fits of the average margin geometry across the margin for profiles 1-8, as determined from type 2 modelling. RMSDs show a sharp convergence along each profile and define a NNW trend of the margin, marked by the dashed black line. The best fit locations are in close agreement with those determined from seismic data (black stars). The margin is significantly offset from the DFZ, which runs N-S farther to the east. Coincident seismic lines are shown in green. SGF; Sea Gap Fault.

3.4.2.3. Model type 3: Detailed 2D gravity modelling

We perform detailed 2D gravity modelling of profiles 1, 2, and 3, which have coincident seismic data to assist in constraining the seabed and top basement interfaces, using the software IX2D-GM (Figure 3.11). Using a layered sedimentary package and/or a density contrast between the upper and lower crusts has little impact on the final result, so we avoid unnecessary complication and use constant densities for the sediments and crust in our final models.

The resulting density models from all three profiles are in good agreement with the preliminary results of type 1 modelling and, in addition, reveal many more aspects of the margin structure that help to determine the margin type. Moho slope angles and locations follow the same pattern as seen from type 1 modelling, with extremely steep slopes of up to 82° and 83° for profiles 2 and 3 (mz1_8000 and mz1_8100), respectively, and a shallower Moho slope of up to 45° for the southernmost profile 1 (mz1_7500). The top of Moho slope locations can also be seen to lie slightly to the west of the bottom of the basement slope for profiles 2 and 3, and to the east for profile 1, similar to the type 1 models.

Profiles 2 and 3 again show a great similarity in their detailed structure. Both profiles require a deepening of the basement interface within the unconstrained region to the west of the basement slope, defining a marginal ridge structure. These profiles also show a downward flexure of the margin which increases seawards. This flexure is not only defined by the Moho architecture, but also by the down-flexed top basement interface. This basement is covered by an extensive (up to 50 km wide) thin sedimentary layer directly adjacent to the basement outcrop, which has been deposited within accommodation space generated by the flexure. On both of these profiles the basement slope is immediately bounded seaward by extremely thin crust, just 0-3 km thick, or exhumed mantle. This thin crustal layer extends seawards until the DFZ, although on profile 3 a slight thickening of the crustal layer to a consistent 4 km also occurs before the DFZ. This interpreted crustal thickening to 4 km is, however, beneath the St Lazare volcanic edifice, and may therefore be the influenced by intruded dense volcanic rocks above, which would require a low density crustal root to compensate them. Seaward of the DFZ, these two profiles show fairly consistent crustal thicknesses of ~6 km, likely representing oceanic crust of the WSB.

Profile 1 does not exhibit the same margin flexure as seen to the north. However, the fault-bounded blocks of continental crust landward of the basement slope do define a basement high that could be related to the marginal ridge seen on profiles 1 and 2. Seaward of the basement slope, the crust is ~4 km thick, thicker than the 0-3 km of profiles 2 and 3, but still slightly thinner than the 5.2 km typical of the WSB (Coffin et al., 1986). On this southernmost profile, significant crustal thickening to ~11 km, with a width of ~ 20 km, defines the DFZ. A slightly thicker than normal oceanic crust also extends ~ 50 km seawards of the DFZ on this profile, before normal crustal thickness values for the WSB return.

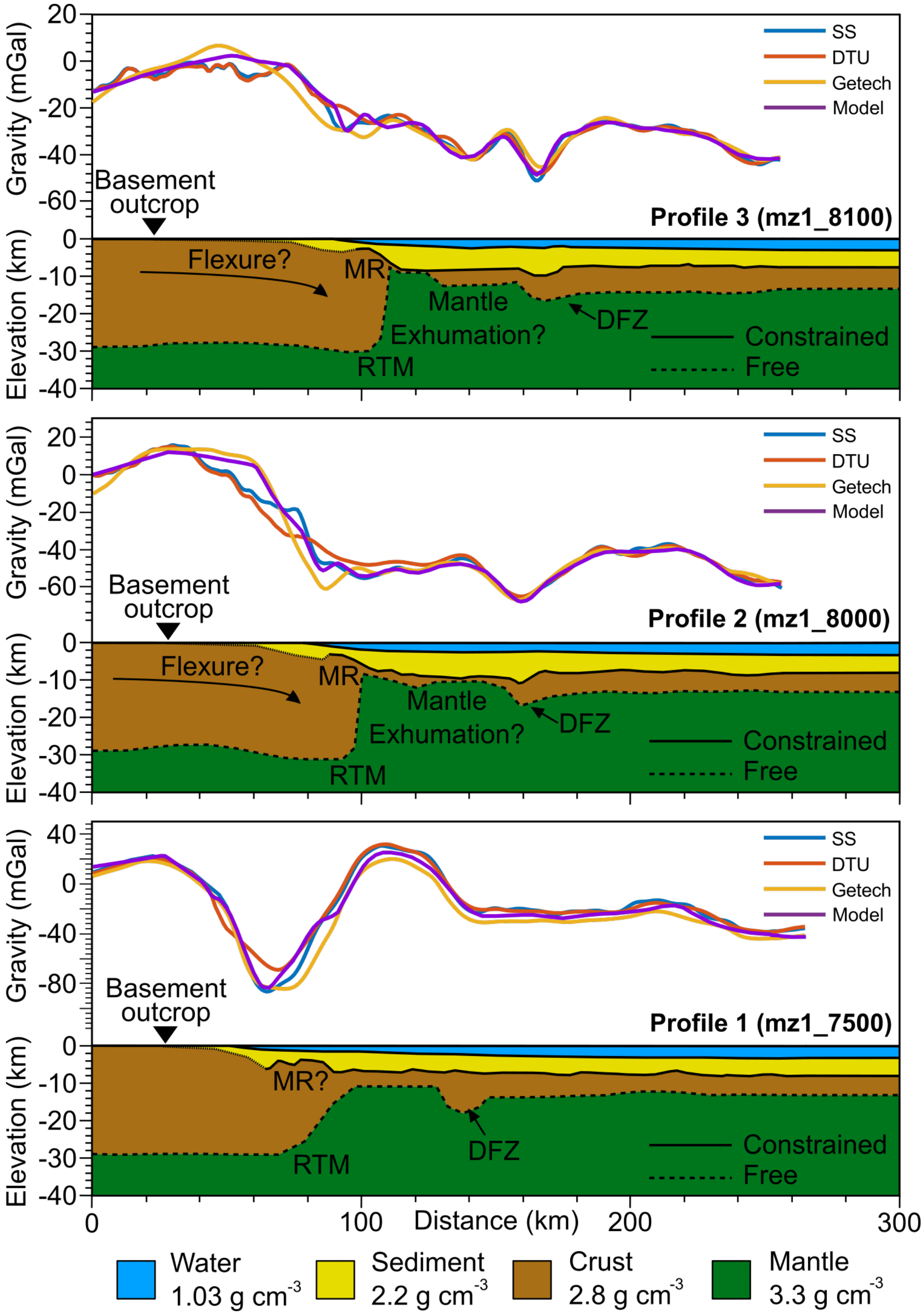

Figure 3.11. Detailed crustal structure as determined from type 3 modelling along profiles 1-3 with coincident seismic data. All profiles show possible marginal ridges adjacent to the margin. Profile 1 displays a large thickening of the crust around the DFZ. Profiles 2 and 3 indicate possible exhumation of the mantle immediately adjacent to the steep basement slope of the continental margin, which may have undergone downward flexure.

3.5. Discussion

3.5.1 The continental margin of northern Mozambique and southern Tanzania

Following type 1 gravity modelling, we generated crustal thickness profiles across the continental margin for comparison with the global compilation of Mercier de Lépinay et al., (2016; Harry et al., 2003). All three profiles fall well within the transform regime, and provide a robust and unbiased preliminary interpretation of the margin as a transform margin. Following this preliminary interpretation, we use additional observations from seismic reflection data and gravity modelling as an independent check.

Moho slopes across the necking zone identified in profiles 2 and 3 lie between 65-82°, with the more detailed type 3 modelling preferring the upper end of this estimate. These slope angles are steeper than any recorded from rifted margins across the globe, and comparably steep Moho slopes have, to date, only been inferred across the Côte d'Ivoire-Ghana transform margin, where they are thought to be sub-vertical (Sage et al., 2000). Along profile 1, type 1 modelling predicts Moho slope angles of an ambiguous 28°, which may be found across necking zones at both magma-poor divergent margins and transform margins. This simple ramp-style Moho geometry is, however, a simplification of true necking zone geometries. More detailed type 3 modelling of this profile reveals Moho slope angles possibly reaching up to 43°, with an average Moho slope of 32° across the necking zone. Such Moho slope angles are near to the upper limit of those found at divergent margins (Figure 3.2) yet lie well within those observed at transform margins worldwide. This supports the interpretation of this section of the margin as having strong transform affinities. However, the large reduction in Moho slope angles along profile 1, compared to profiles 2 and 3, may indicate a transition from transform to rifted margin at this location.

Steep basement slopes accommodating a large step in basement depth, without evidence for normal faulting, are common features of transform margins (e.g. Lorenzo and Wessel, 1997; Sage et al., 2000). These are identified in all three margin-perpendicular seismic lines and dip seaward at between 18° and 35°, similar to the equivalent slopes of the Northern and Newfoundland transform margins, respectively (Greenroyd et al., 2008; Keen et al., 1990).

Landward of the basement slopes identified in seismic data, marginal ridges, common features of transform margins (e.g. Bird, 2001), have also been identified. Along profile 1, this feature is represented by a continental horst block, as identified in seismic data (Figure 3.5f), rising ~1.5 km above continentward-dipping half grabens, which bound it to the west. Along profiles 2 and 3, the tectonic structure of the marginal ridge is unknown as identification is only possible through gravity modelling. It can, however, be seen to rise a similar 1-2 km above the basement to the west of the ridge. Seaward flexure of the margin, seen along profiles 2 and 3, is also indicative of transform margins. It probably developed as the result of mechanical coupling across the transform margin and thermal subsidence of the oceanic domain following the cessation of transform tectonics (Mercier de Lépinay et al., 2016).

Seaward of the marginal ridge and basement slope, thin crust and exhumed mantle is predicted by detailed 2D gravity modelling (type 3 models) and is supported by observations from seismic data. Line mz1_1030 shows the Moho outcropping at the surface in the vicinity of the base of the basement slope between profiles 2 and 3, and exhumed mantle is also consistent with the lack of Moho reflections adjacent to the basement slope along both of these profiles. Whilst exhumed mantle may be present at both magma-poor rifted margins and oceanic fracture zones (e.g. Doré and Lundin, 2015; Tucholke et al., 1998), the extremely narrow margin width of <50 km, predominantly lacking in rift structures, is incompatible with other observations of magma-poor rifted margins worldwide, supporting continent-ocean transform tectonics.

These observations overwhelmingly support the interpretation of the continental margin of Northern Mozambique and Southern Tanzania as a transform margin. Type 2 modelling and observations from seismic data constrain the trend of this margin as ~172° to the south of profile 3 and ~160° to the north. The margin follows the onshore trend of the Rovuma Basin's basement outcrop, and the northern section of the transform margin runs onshore, where it is enveloped beneath the Rovuma Delta which has prograded into the oceanic domain, similarly to the Niger Delta (e.g. Dickson et al., 2016).

In light of the margin's trend, and its newly recognised status, we term this margin the Rovuma Transform Margin (RTM) so that it may be distinguished from the DFZ. The DFZ is an ocean-ocean fracture zone that lies to the east of the RTM and is often coincident with the Davie Ridge. In the past, the DFZ and Davie Ridge have together been inferred to form the continental margin of the WSB (e.g. Coffin and Rabinowitz, 1987; Gaina et al., 2013).

3.5.2 Changes in margin style across the Lurio Belt

The RTM can be split into northern and southern sections, roughly bisected by the Lurio Belt, across which a change in margin geometry, trend, and adjacent ocean domain may occur. In the southern section, the Moho slope angle is much shallower, dipping at ~30° compared to ~70° farther north. The vertical offset across the margin's basement slope is also reduced, here only ~2 km compared with ~5 km farther north. Furthermore, continentward-dipping normal faults, forming syn-rift half grabens, also appear to the south of the Lurio Belt, and may form part of the Angoche Basin. The northward extent of this basin, however, is not delineated by seismic reflection data.

These observations suggest an increased extensional component may have been present during continental breakup south of the Lurio Belt, faulting and thinning this lithosphere prior to plate separation. This is consistent with the change in margin trend that occurs just to the north of the Lurio belt, in the vicinity of profiles 2 and 3. In this northern section of the margin, which trends at ~160°, the occurrence of dextral strike-slip tectonics would lead to highly oblique plate separation along the margin to the south of the Lurio Belt, which trends at 172°.

Therefore, during plate separation, strike-slip dominated transtensional rifting may have occurred along the Angoche Basin to the south of the Lurio Belt. This highly oblique southern section of the margin was likely linked to the RTM through horsetail splay faults, requiring normal faults along the edge of West Gondwana to dip towards East Gondwana. Subsequent isolation of these faults from West Gondwana during the onset of seafloor spreading and mid-ocean ridge propagation (e.g. Basile, 2015) in the Mozambique Basin may provide an explanation for the presence of continentward-dipping normal faults inboard of the margin slope in seismic line mz1_7500. In this case, this region of rifted continent between the transform margin and unrifted continental crust may represent a marginal plateau (e.g. Mercier de Lépinay et al., 2016). It should not be ruled out, however, that the continentward-dipping normal faults may have developed in response to volcanic rifted margin formation (e.g. Geoffroy, 2005) to the south within the Mozambique Basin (e.g. Mueller and Jokat, 2017).

Differences between the northern RTM (profiles 2 and 3) and the Angoche Basin (southern RTM; profile 1) also occur within the oceanic domain. The northern section of the RTM is immediately abutted by exhumed mantle or extremely thin crust, whereas to the south adjacent to the Angoche Basin, gravity modelling predicts crust ~4 km thick. The northern region also shows less crustal thickening in the vicinity of the DFZ, around ~0.5 s TWTT thickening, compared to seaward of the Angoche Basin where a larger crustal thickening of ~1 s TWTT around the DFZ is accompanied by compressional thrusting of the crust on either side. It should be noted, however, that observations of compressional tectonic structures are less likely in the north due to the obscuring of basement structures by post breakup volcanics and recent faulting.

Three scenarios may have led to exhumed mantle along the northern margin, yet 4 km thick crust adjacent to the continental margin along line 7500. Firstly, mantle exhumation may be local to profiles 2 and 3. This may be the case if oceanic core complexes have formed along the transform margin, as is common along ocean-ocean fracture zones. The scale of the exhumed mantle zone, ~50 km wide, is similar to core complexes found along fracture zones today.

Secondly, mantle exhumation may be widespread along the northern portions of the transform margin. In this case, the onset of oceanic crustal production along the COTM may be directly linked with the change in margin trend around the Lurio Belt and corresponding thinning of the continental lithosphere which occurred during rifting to the south of this feature. In this case, the lithospheric thinning may have increased heatflow from the mantle along the Angoche Basin, reducing the amount of heat lost from the MOR as it passed along the COTM, thereby allowing greater mantle melting and production of a thin oceanic crust.

Finally, it should be considered that the more intense manifestation of compressional tectonics to the south of the Lurio Belt may have acted to thicken any crust present. It may also have allowed the introduction of water into the mantle along thrust faults, resulting in its serpentinisation. The resulting reduction in mantle density at this location would thus result in the interpretation of a thicker crustal layer when using gravity methods. The top basement is, however, quite smooth and is not typical of exhumed mantle. Furthermore, the presence of a possible Moho reflection, although potentially also the manifestation of thrust faulting, also makes this final scenario is less likely.

3.5.3 Possible plate tectonic models

North of the Lurio Belt, the RTM appears to be void of extensional normal faults and forms a >400 km transform margin separating the highly oblique Angoche Basin from the TCB. This large offset between the TCB and Angoche Basin suggests that these rift segments did not overlap at their ends, and instead a transform fault would have been necessary to link the two from the onset of rifting (e.g. Basile, 2015). We therefore assume that the strike of this transform fault formed parallel to the initial extension direction between East and West Gondwana, supporting the initial SSE spreading direction proposed in Chapter 2, and, to a lesser extent, the NW-SE spreading directions of Klimke et al., (2017) and Reeves et al., (2016). This continental transform fault would go on to form the Rovuma Transform Margin following the passing of the southern Morondava Basin (Madagascar) along it to the SSE.

This initial phase of SSE drift, followed by a switch to a more southerly drift of East Gondwana, is also reflected in the outcrop pattern of the volcanic margin of Southern Mozambique. Here, the Lebombo Monocline shows a similar change in trend, which may in part have developed in response to the change in spreading direction at ~150 Ma. Furthermore, offshore of the Mozambique volcanic margin, a possible small microcontinent, the Biera High, has been identified (e.g. Mueller and Jokat, 2017). Several instances of microcontinent release have been documented during changes in plate motion, resulting from the build-up of transpressional stress along long-offset fracture zones (e.g. Schiffer et al., In Press; Whittaker et al., 2016). It is therefore possible that the cleaving of the Biera High microcontinent resulted from compressional stress build-up across left-stepping fracture zones during this clockwise plate rotation near the end of the Jurassic. Recent evidence for continental crust beneath the Comoros islands, through identification of Pan African age zircons (533 Ma) within xenoliths of the Grande Comore (e.g. Roach et al., 2017), points to the occurrence of a similar microcontient-cleaving event in the WSB, possibly driven by the same plate rotation.

The DFZ, which sits to the east of the Rovuma Transform Margin, also developed as the result of this plate rotation (e.g. Reeves et al., 2016; Chapter 2), and forms a major large-offset ocean-ocean fracture zone. The eastward offset of this structure from the RTM, and the presence of oceanic crust landward of this fracture zone within the TCB (e.g. Chapter 2; Sauter et al., 2016), preclude it from forming the COTM of the WSB. Loose-fit plate tectonic reconstructions, utilising the DFZ without an initial phase of SSE spreading, are therefore unable to predict the observations of this study.

3.5.4 Transform margin development and impacts

The RTM also crosscuts the pre-existing tectonic fabric of Gondwana (e.g. Reeves and de Wit, 2000; Windley et al., 1994) and whilst some Karoo-aged sedimentary deposits have been postulated to be present below parts of the Rovuma Basin (e.g. Salman and Abdula, 1995), these are not exposed at the surface as they are along the Kenya, Tanzania, and Madagascar margins. Late Triassic to Early Jurassic sediments, drilled within the Mandawa Basin (northernmost Rovuma Basin; Hudson and Nicholas, 2014), are thought to have been deposited in response to the Jurassic breakup of East and West Gondwana, and the oldest succession within isolated early rift grabens along the Rovuma Basin were found to be Jurassic in age (Smelror et al., 2008). This suggests that, whilst isolated Karoo basins may have been present beforehand, the development of the RTM was largely not controlled by pre-existing structures and instead formed as a new tectonic feature in direct response to the Jurassic breakup of Gondwana.

This new transform fault offset the volcanic Mozambique Basin (e.g. Leinweber et al., 2013) from the magma-poor Tanzania Coastal Basin (e.g. Chapter 2). Similar variations in magmatism between rift segments have been observed at other locations including: the Gulf of California (e.g. Lizarralde et al., 2007), the South Atlantic (e.g. Franke et al., 2007), and Central Afar (e.g. Stab et al., 2016). It is possible that a causal link between magmatism and margin segmentation exists. In the case of the Jurassic East Africa breakup, it may be postulated that the lack of lithospheric thinning along the RTM may have acted as a barrier to the lateral flow of anomalously hot mantle (postulated beneath the Mozambique basin due to the upwelling of the Bouvet mantle plume; e.g. Reeves, 2014) into the TCB, resulting in a lack of magmatism during the breakup of this basin.

Following breakup and an initial phase of SSE spreading, the change in plate motion near the end of the Jurassic would have resulted in transpression along the RTM. It is possible that these transpressional tectonics resulted in the development of the marginal ridge along the RTM inferred from gravity modelling. Such transpressional uplift has been found to control the development of marginal ridges elsewhere, such as at the Ivory Coast-Ghana transform margin (Huguen et al., 2001). Recent studies have also shown that a previously unexpected amount of along-strike variation in transform margin geometry may be common (Mercier de Lépinay et al., 2016). The basement slope angles and vertical offset across the margin seen on profiles 2 and 3, change from 18° and 5 km to 24° and 6 km, respectively, over a distance of ~50 km. Misfits between modelled gravity profiles and gravity data during type 2 modelling, which uses an average margin geometry, also suggest that variations in the margin geometry continue along strike, supporting the observations of Mercier de Lépinay et al., (2016). Such variations likely arise from small deviations in the margin trend along strike, leading to increased transpression and transtension, or from inherited features from the continental crust (e.g. Mercier de Lépinay et al., 2016). The seaward flexure of the margin supports suggestions that mechanical coupling between the continental and oceanic domains occurred post-transform motions. At this point, thermal subsidence of the oceanic domain would have induced the observed downward flexure of the continent adjacent to the margin, as seen along other COTMs (e.g. Lorenzo and Wessel, 1997).

3.6. Conclusions

Seismic reflection data reveal a newly identified COTM in the southern Rovuma Basin. The margin lies landward of the DFZ, which has previously been interpreted as the COTM of the WSB. We term this newly identified COTM the 'Rovuma Transform Margin' (RTM), to distinguish it from the DFZ.

The presence of a marginal ridge: steep (18° to 35°) basement slopes with large vertical offsets of up to 6 km, lacking evidence for internal rift structures; rapid crustal thinning from ~28 km to 2 km over a distances of less than 20 km; seaward flexure of the margin; extremely steep Moho slopes across the necking zone of up to 83°; and presence of exhumed mantle and thin oceanic crust adjacent to the margin support its interpretation as a transform margin. Furthermore, comparison of crustal thickness profiles across the margin to the global margin compilations of Mercier de Lépinay et al., (2016) confirms the transform nature of this continental margin.

Inverse gravity modelling shows that the RTM runs NNW-SSE along the Rovuma Basin, supporting an origin for Madagascar within the Tanzania Coastal Basin and tight-fit reconstructions of Gondwana fragments.

A slight change in the trend of the margin from 160° in the north to 172° in the south occurs approximately at the Lurio Belt. The slight bend in the margin controlled a change from pure transform tectonics to the north of the Lurio belt, to the highly oblique opening of the Angoche Basin to the south. The oblique nature of the margin is reflected by shallower Moho slopes across the necking zone and the appearance of half grabens in continental crust.

3.7. References

Barton, P.J., Owen, T.R.E., White, R.S., 1990. The deep structure of the east Oman continental margin: preliminary results and interpretation. Tectonophysics 173, 319–331. doi:10.1016/0040-1951(90)90227-Y

Basile, C., 2015. Transform continental margins - part 1: Concepts and models. Tectonophysics 661, 1–10. doi:10.1016/j.tecto.2015.08.034

Basile, C., Braun, J., 2016. The initiation of pull-apart basins and transform continental margins: Results from numerical experiments of kinematic partitioning in divergent settings. Terra Nov. 28, 120–127. doi:10.1111/ter.12198

Bird, D., 2001. Shear margins: Continent-ocean transform and fracture zone boundaries. Lead. Edge 20, 150. doi:10.1190/1.1438894

Coffin, M.F., Rabinowitz, P.D., 1987. Reconstruction of Madagascar and Africa: Evidence From the Davie Fracture Zone and Western Somali Basin 92, 9385–9406.

Coffin, M.F., Rabinowitz, P.D., Houtz, R.E., 1986. Crustal structure in the Western Somali Basin. Geophys. J. R. Astron. Soc. 331–369.

Dickson, W., Schiefelbein, C.F., Odegard, M.E., Zumberge, J.E., 2016. Petroleum systems asymmetry across the South Atlantic Equatorial Margins. Geol. Soc. London, Spec. Publ. 431, 219–233. doi:10.1144/SP431.13

Doré, T., Lundin, E., 2015. Hyperextended continental margins — Knowns and unknowns. Geol. 43, 95–96. doi:10.1016/0040

Ebinger, C., 2005. Continental break-up: the East African perspective. Astron. Geophys. 46, 2.16-2.21. doi:10.1111/j.1468-4004.2005.46216.x

Edwards, R.A., Whitmarsh, R.B., Scrutton, R.A., 1997. The crustal structure across the transform continental margin off Ghana, eastern equatorial Atlantic. J. Geophys. Res. 102, 747–772. doi:10.1029/96JB02098

Emmel, B., Kumar, R., Ueda, K., Jacobs, J., Daszinnies, M.C., Thomas, R.J., Matola, R., 2011. Thermochronological history of an orogen-passive margin system: An example from northern Mozambique. Tectonics 30. doi:10.1029/2010TC002714

Fairhead, J.D., Williams, S.E., Fletcher, K.M.U., Green, C.M., Vincent, K., 2009. Trident - A New Satellite Gravity Model for the Oceans. 71st EAGE Conf. Exhib. Amsterdam 1–5.

Franke, D., Jokat, W., Ladage, S., Stollhofen, H., Klimke, J., Lutz, R., Mahanjane, E.S., Ehrhardt, A., Schreckenberger, B., 2015. The offshore East African Rift System: Structural framework at the toe of a juvenile rift. Tectonics 34, 2086–2104. doi:10.1002/2015TC003922

Franke, D., Neben, S., Ladage, S., Schreckenberger, B., Hinz, K., 2007. Margin segmentation and volcano-tectonic architecture along the volcanic margin off Argentina/Uruguay, South Atlantic. Mar. Geol. 244, 46–67. doi:10.1016/j.margeo.2007.06.009

Gaina, C., Torsvik, T.H., van Hinsbergen, D.J.J., Medvedev, S., Werner, S.C., Labails, C., 2013. The African plate: A history of oceanic crust accretion and subduction since the Jurassic. Tectonophysics 604, 4–25. doi:10.1016/j.tecto.2013.05.037

Geiger, M., Clark, D.N., Mette, W., 2004. Reappraisal of the timing of the breakup of Gondwana based on sedimentological and seismic evidence from the Morondava Basin, Madagascar. J. African Earth Sci. 38, 363–381. doi:10.1016/j.jafrearsci.2004.02.003

Geoffroy, L., 2005. Volcanic passive margins. Comptes Rendus - Geosci. 337, 1395–1408. doi:10.1016/j.crte.2005.10.006

Globig, J., Fernàndez, M., Torne, M., Vergés, J., Robert, A., Faccenna, C., 2016. New insights into the crust and lithospheric mantle structure of Africa from elevation, geoid, and thermal analysis. J. Geophys. Res. Solid Earth 121, 5389–5424. doi:10.1002/2016JB012972

Greenroyd, C.J., Peirce, C., Rodger, M., Watts, A.B., Hobbs, R.W., 2008. Demerara Plateau - The structure and evolution of a transform passive margin. Geophys. J. Int. 172, 549–564. doi:10.1111/j.1365-246X.2007.03662.x

Harry, D.L., Londono, J., Huerta, A., 2003. Early Paleozoic transform-margin structure beneath the Mississippi coastal plain, southeast United States. Geology 31, 969–972. doi:10.1130/G19787.1

Hudson, W.E., Nicholas, C.J., 2014. The Pindiro Group (Triassic to Early Jurassic Mandawa Basin, southern coastal Tanzania): Definition, palaeoenvironment, and stratigraphy. J. African Earth Sci. 92, 55–67. doi:10.1016/j.jafrearsci.2014.01.005

Huguen, C., Guiraud, M., Benkhelil, J., Mascle, J., 2001. Synlithification deformation processes of the cretaceous sediments of the ivory coast-ghana transform margin: A way to detail the margin history. Tectonics 20, 959–975. doi:10.1029/2001TC900015

Keen, C.E., Kay, W.A., Roest, W.R., 1990. Crustal anatomy of a transform continental margin. Tectonophysics 173. doi:10.1016/0040-1951(90)90244-3

Klimke, J., Franke, D., Mahanjane, E.S., Leitchenkov, G., 2017. Tie-points for Gondwana reconstructions from a structural interpretation of the Mozambique Basin, East Africa, and the Riiser-Larsen Sea, Antarctica. Solid Earth Discuss. 1–28.

Leinweber, V.T., Klingelhoefer, F., Neben, S., Reichert, C., Aslanian, D., Matias, L., Heyde, I., Schreckenberger, B., Jokat, W., 2013. The crustal structure of the Central Mozambique continental margin - Wide-angle seismic, gravity and magnetic study in the Mozambique Channel, Eastern Africa. Tectonophysics 599, 170–196. doi:10.1016/j.tecto.2013.04.015

Lizarralde, D., Axen, G.J., Brown, H.E., Fletcher, J.M., González-Fernández, A., Harding, A.J., Holbrook, W.S., Kent, G.M., Paramo, P., Sutherland, F., Umhoefer, P.J., 2007. Variation in styles of rifting in the Gulf of California. Nature 448, 466–469. doi:10.1038/nature06035

Lorenzo, J.M., Wessel, P., 1997. Flexure across a continent-ocean fracture zone: the northern Falkland/Malvinas Plateau, South Atlantic. Geo-Marine Lett. 17, 110–118. doi:10.1007/s003670050015

Mahanjane, E.S., 2014. The Davie Fracture Zone and adjacent basins in the offshore Mozambique Margin - A new insights for the hydrocarbon potential. Mar. Pet. Geol. 57, 561–571. doi:10.1016/j.marpetgeo.2014.06.015

Mercier de Lépinay, M., Loncke, L., Basile, C., Roest, W.R., Patriat, M., Maillard, A., De Clarens, P., 2016. Transform continental margins – Part 2: A worldwide review. Tectonophysics 693, 96–115. doi:10.1016/j.tecto.2016.05.038

Mueller, C.O., Jokat, W., 2017. Geophysical evidence for the crustal variation and distribution of magmatism along the central coast of Mozambique. Tectonophysics 712–713, 684–703. doi:10.1016/j.tecto.2017.06.007

Parsiegla, N., Stankiewicz, J., Gohl, K., Ryberg, T., Uenzelmann-Neben, G., 2009. Southern African continental margin: Dynamic processes of a transform margin. Geochemistry, Geophys. Geosystems 10. doi:10.1029/2008GC002196

Pavlis, N.K., Holmes, S.A., Kenyon, S.C., Factor, J.K., 2012. The development and evaluation of the earth gravitational model 2008 (EGM2008). J. Geophys. Res. Solid Earth 117, 1–38. doi:10.1002/jgrb.50167,2013

Phethean, J.J.J., Kalnins, L.M., van Hunen, J., Biffi, P.G., Davies, R.J., McCaffrey, K.J.W., 2016. Madagascar’s escape from Africa: A high-resolution plate reconstruction for the Western Somali Basin and implications for supercontinent dispersal. Geochemistry, Geophys. Geosystems 17, 5036–5055. doi:10.1002/2016GC006624

Rabinowitz, P.D., Coffin, M.F., Falvey, D., 1983. The separation of Madagascar and Africa. Science (80-.). 220, 67–69. doi:10.1126/science.220.4592.67

Reeves, C., 2014. The position of Madagascar within Gondwana and its movements during Gondwana dispersal. J. African Earth Sci. 94, 45–57. doi:10.1016/j.jafrearsci.2013.07.011

Reeves, C., de Wit, M.J., 2000. Making ends meet-retracing the transformations of the Indian Ocean and reconnecting continental shear zones. Terra 12, 272–280.
Reeves, C. V, Teasdale, J.P., Mahanjane, E.S., 2016. Insight into the Eastern Margin of Africa from a new tectonic model of the Indian Ocean. Geol. Soc. London, Spec. Publ. 431, 1–24. doi:10.1144/SP431.12
Reston, T.J., 2009. The structure, evolution and symmetry of the magma-poor rifted margins of the North and Central Atlantic: A synthesis. Tectonophysics 468, 6–27. doi:10.1016/j.tecto.2008.09.002
Roach, P., Milsom, J., Toland, C., Matchette-Downes, C., Budden, C., Riaroh, D., Houmadi, N., 2017. New Evidence Supports Presence of Continental Crust beneath the Comoros. PESGB, 16th African E&P Conf. London.
Sage, F., Basile, C., Mascle, J., Pontoise, B., Whitmarsh, R.B., 2000. Crustal structure of the continent-ocean transition off the Cote d'Ivoire-Ghana transform margin: Implications for thermal exchanges across the palaeotransform boundary. Geophys. J. Int. 143, 662–678. doi:10.1046/j.1365-246X.2000.00276.x
Salman, G., Abdula, I., 1995. Development of the Mozambique and Ruvuma sedimentary basins, offshore Mozambique. Sediment. Geol. 96, 7–41. doi:10.1016/0037-0738(95)00125-R
Sandwell, D.T., Muller, R.D., Smith, W.H.F., Garcia, E., Francis, R., 2014. New global marine gravity model from CryoSat-2 and Jason-1 reveals buried tectonic structure. Science (80-.). 346, 65–67. doi:10.1126/science.1258213
Sauter, D., Unternehr, P., Manatschal, G., Tugend, J., Cannat, M., Le Quellec, P., Kusznir, N., Munschy, M., Leroy, S., de Lepinay, J.M., Granath, J.W., Horn, B.W., 2016. Evidence for magma entrapment below oceanic crust from deep seismic reflections in the Western Somali Basin. Geology 44, 407–410. doi:10.1130/G37747.1
Schiffer, C., Peace, A., Phethean, J., Gernigon, L., McCaffrey, K.J.W., Petersen, Kenni, D., Foulger, G., n.d. The Jan Mayen Microplate Complex and the Wilson Cycle. Geol. Soc. London, Spec. Publ.
Smelror, M., Key, R.M., Smith, R. a, Njange, F., 2008. Late Jurassic And Cretaceous Palynostratigraphy Of The Onshore Rovuma Basin, Northern Mozambique. Palynology 32, 63–76. doi:10.2113/gspalynol.32.1.63
Stab, M., Bellahsen, N., Pik, R., Quidelleur, X., Ayalew, D., Leroy, S., 2016. Modes of rifting in magma-rich settings: Tectono-magmatic evolution of Central Afar. Tectonics 35, 2–38. doi:10.1002/2015TC003893
Stenseng, L., Piccioni, G., Anderson, O.B., Knudsen, P., 2015. Sea surface retracking and classification of CryoSat-2 altimetry observations in the Arctic Ocean. Am. Geophys. Union, Fall Meet.
Todd, B.J., Reid, I., 1989. The continent - ocean boundary south of Flemish Cap: constraints from seismic refraction and gravity1. Can. J. Earth Sci. 26, 1392–1407.
Todd, B.J., Reid, I., Keen, C.E., 1988. Crustal structure across the Southwest Newfoundland Transform Margin. Can. J. Earth Sci. 25, 744–759. doi:10.1139/e88-070
Tucholke, B.E., Lin, J., Kleinrock, M.C., 1998. Megamullions and mullion structure defining oceanic metamorphic core complexes on the Mid-Atlantic Ridge. J. Geophys. Res. Solid Earth 103, 9857–9866. doi:10.1029/98JB00167
Tugend, J., Manatschal, G., Kusznir, N.J., Masini, E., 2015. Characterizing and identifying structural domains at rifted continental margins: application to the Bay of Biscay margins and its Western Pyrenean fossil remnants. Geol. Soc. London, Spec. Publ. 413, 171–203. doi:10.1144/SP413.3
Van Avendonk, H.J.A., Lavier, L.L., Shillington, D.J., Manatschal, G., 2009. Extension of continental crust at the margin of the eastern Grand Banks, Newfoundland. Tectonophysics 468, 131–148. doi:10.1016/j.tecto.2008.05.030
Wessel, P., Smith, W.H.F., Scharroo, R., Luis, J., Wobbe, F., 2013. Generic Mapping Tools: Improved Version Released. Eos, Trans. Am. Geophys. Union 94, 409–410. doi:10.1002/2013EO450001
Whittaker, J.M., Williams, S.E., Halpin, J.A., Wild, T.J., Stilwell, J.D., Jourdan, F., Daczko, N.R., 2016. Eastern Indian Ocean microcontinent formation driven by plate motion changes. Earth Planet. Sci. Lett. 454, 203–212. doi:10.1016/j.epsl.2016.09.019
Windley, B.F., Razafiniparany, A., Razakamanana, T., Ackermand, D., 1994. Tectonic framework of the Precambrian of Madagascar and its Gondwana connections: a review and reappraisal. Geol. Rundschau 83, 642–659. doi:10.1007/BF00194168

3.8. Supplementary material

3.8.1. Misfit between gravity datasets

Onshore, the difference between the bouguer anomaly generated from the World Gravity Map (WGM; used for the onshore SS and DTU anomalies) and Getech's Trident bouguer anomaly allows for an assessment of the data uncertainty (Figure S3.1). Gravity measurements included within the Getech Trident dataset are shown as white dots. Gravity profiles for 2D modelling are located to avoid areas of significant misfit between the datasets where possible. The largest disparity between the anomalies occurs onshore of the southern Rovuma Basin (500000-660000, 8450000-8620000). Here, the misfit exceeds 25 mGal over a distance of +100 km. The extent of this misfit coincides with a proprietary gravity survey included only within the Trident dataset and is therefore likely caused by this additional data. Therefore, where profile 1 cannot avoid the region of large disagreement between datasets, Getech data is used to replace data from the SS and DTU bouguer anomalies.

Offshore, comparison of the SS and DTU free-air anomalies is shown. Generally, misfits are concentrated in regions of shallow water along the coastline and are smaller than in the onshore regions. Nonetheless, where possible, profiles are located to avoid regions of larger disagreement.

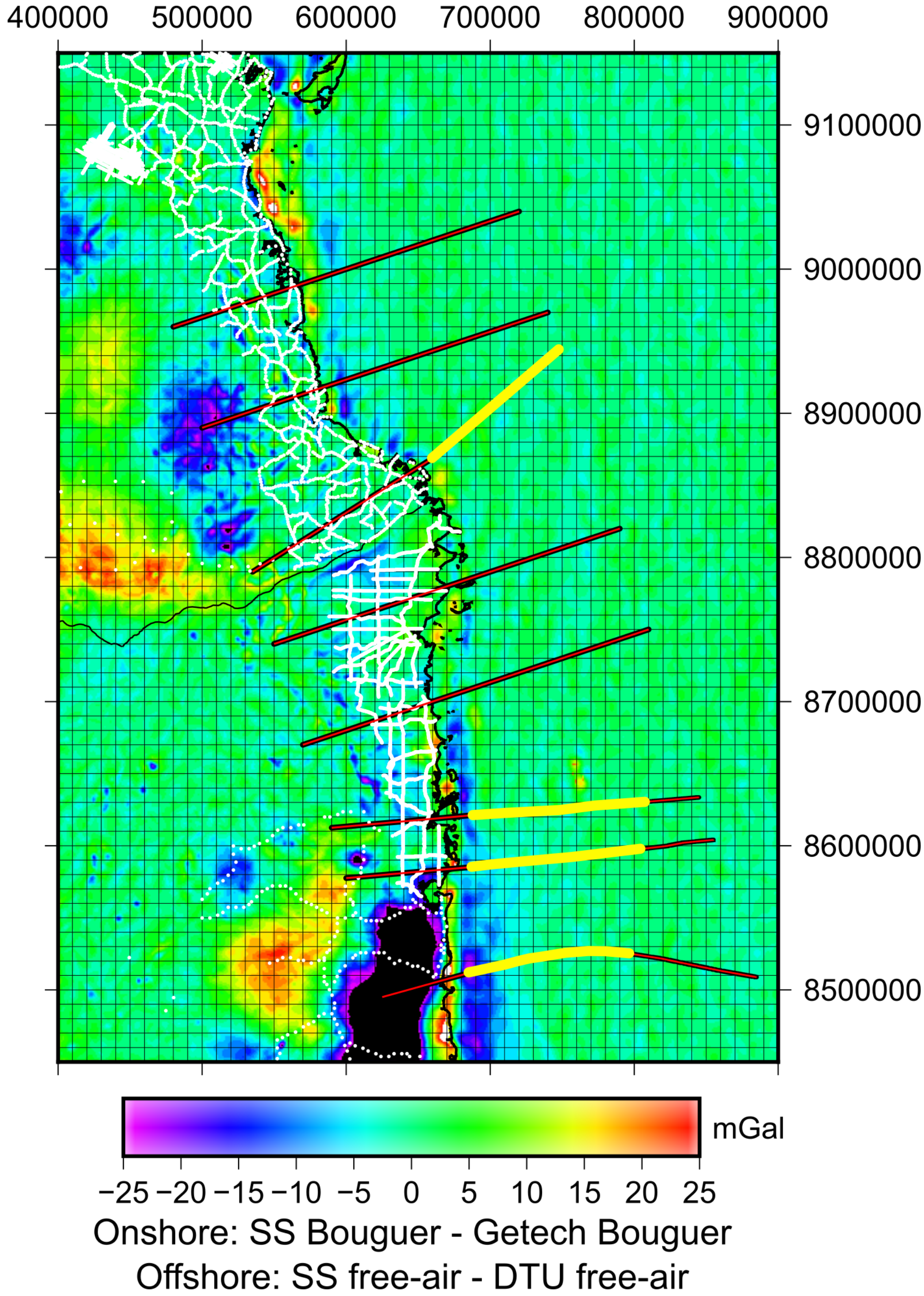

Figure S3.1. Comparison of different gravity datasets

3.8.2. Examples of seabed surfaces generated using alternative filter cut-off wavelengths

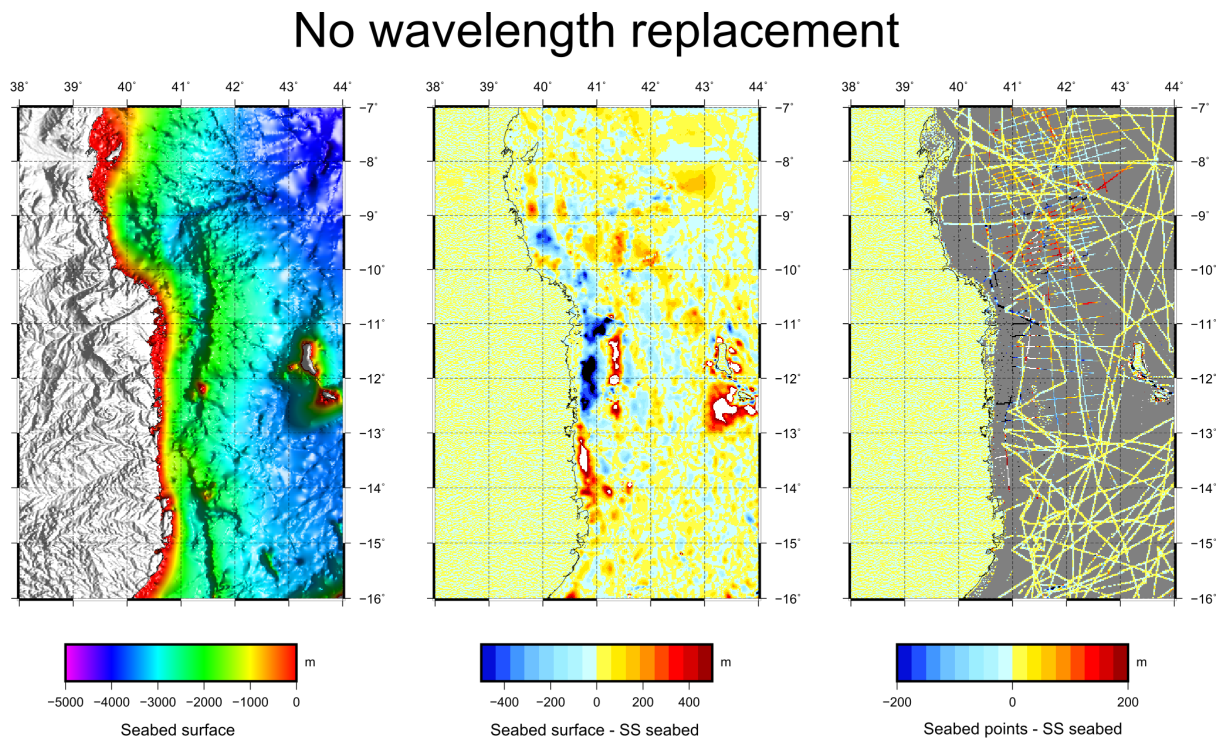

Figure S3.2. Seabed surface without short wavelength replacement. N.B. The panel on the right of this figure is not comparable with those in Figures S3.3-5.

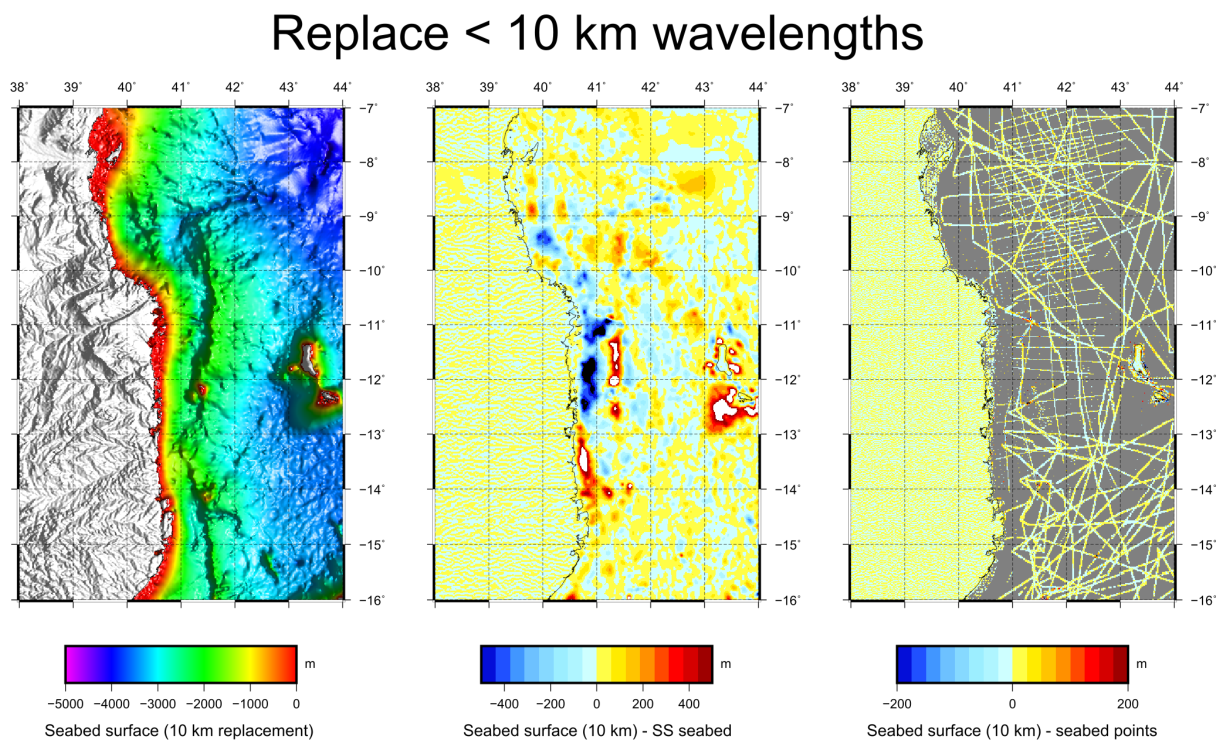

Figure S3.3. Seabed surface with replacement of wavelengths <10 km.

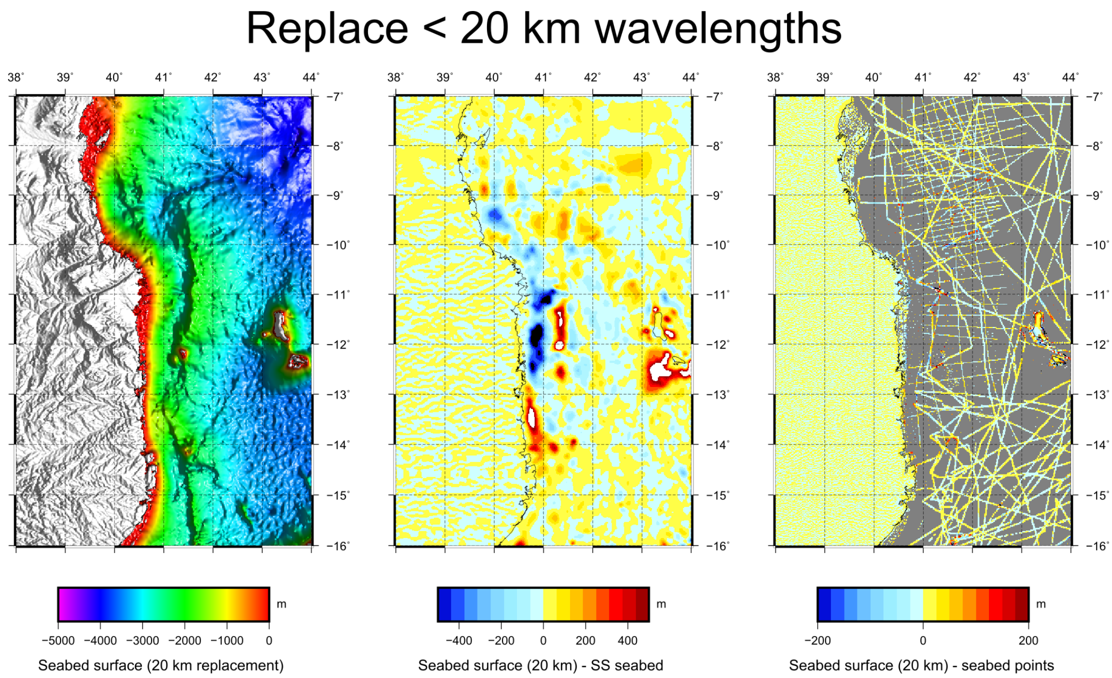

Figure S3.4. Seabed surface with replacement of wavelengths <20 km.

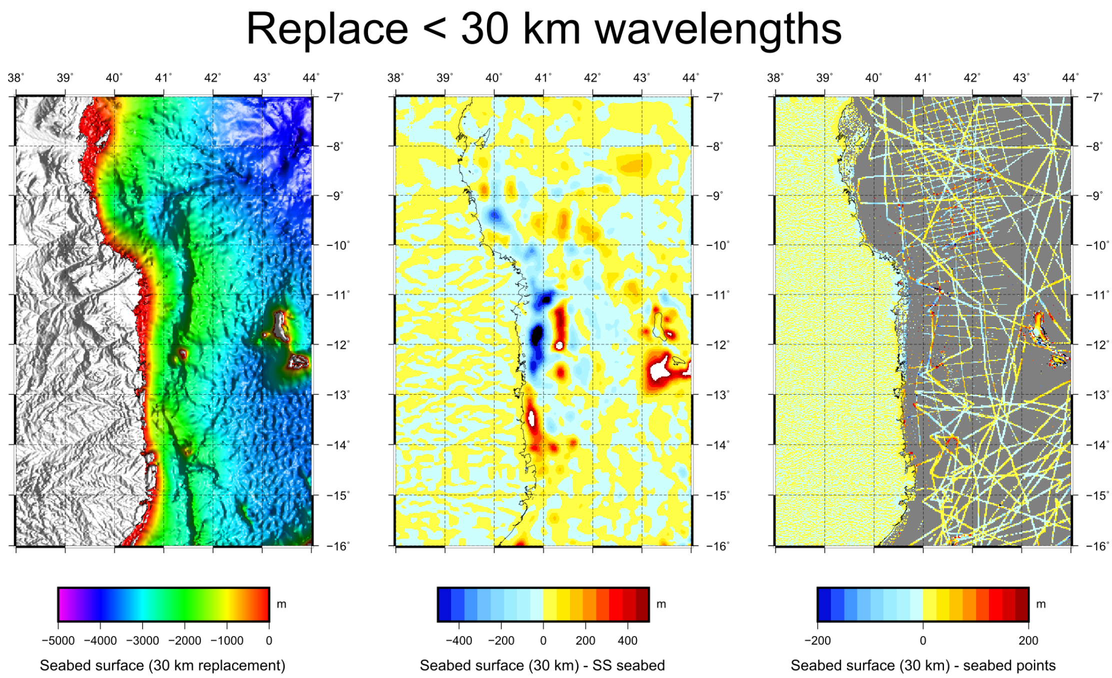

Figure S3.5. Seabed surface with replacement of wavelengths <30 km.

3.8.3. Deriving an average sediment density for the WSB for use in 2D gravity models

To constrain the density of the sediment layer we use coincident data from the DSDP 241 borehole and the 84v multichannel seismic reflection line shot during the R/V Vema leg 3618, providing a chance to quality-check derived seismic velocities and densities. Seismic velocities derived during post stack migration processing of line 84v envelope the velocities measured at DSDP 241 (Figure S3.6).

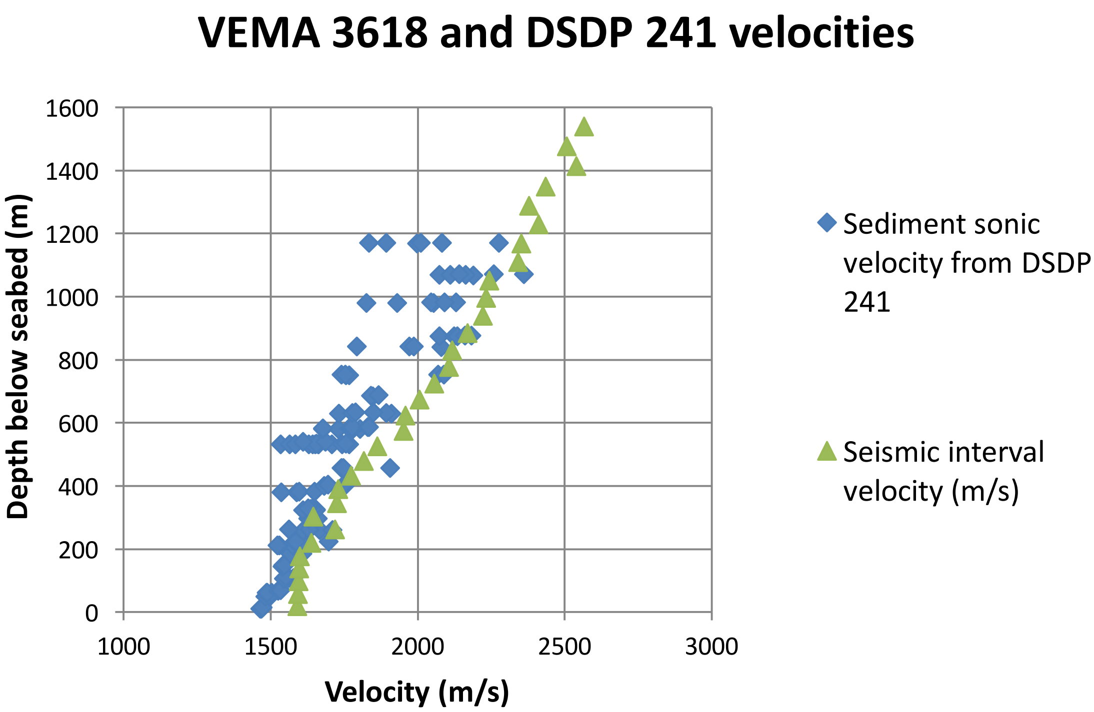

Figure S3.6. Measured and seismic-derived sediment velocities from DSDP 241.

We use the Nafe-Drake relationship between velocity and density to convert the seismic velocities (Figure S3.7) as it provides a superior fit to density data derived at DSDP 241 than Gardner's relationship.

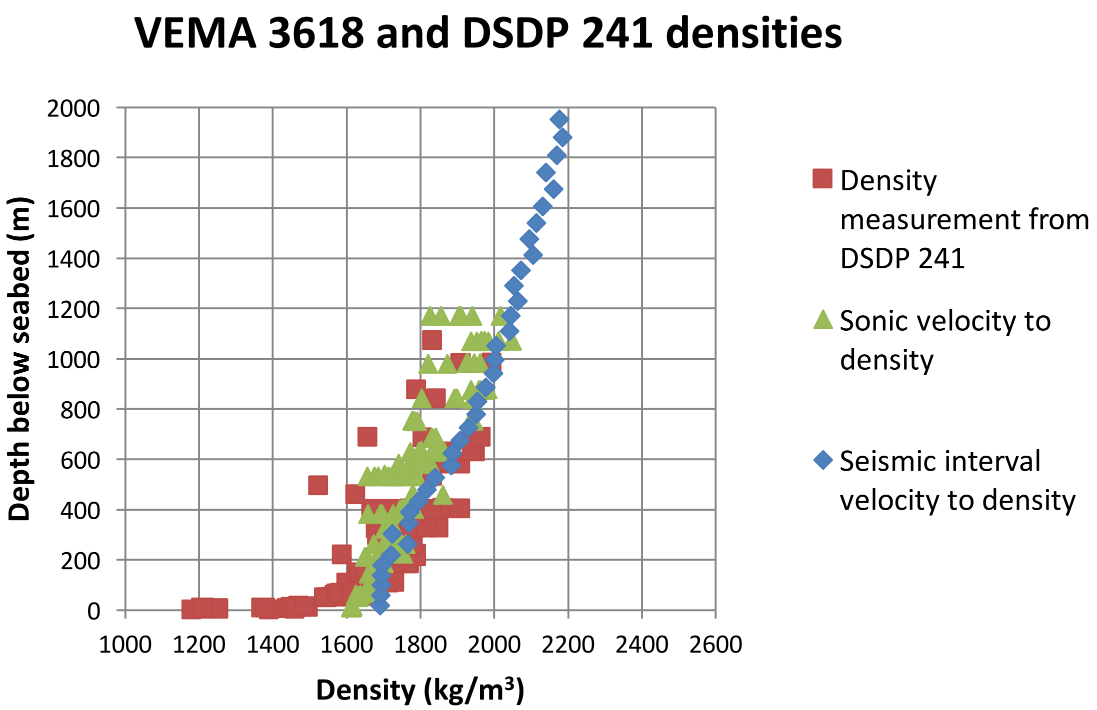

Figure S3.7. Measured and seismic-derived sediment densities at DSDP 241.

As the VEMA 3618 (84) line has similar sediment thicknesses to the ION PSDM lines used for gravity modelling, average sediment densities are calculated between the seabed and top basement using the entirety of the line (Figure S3.8). Densities range between 1.62 and 2.38 g cm^{-3}, with a mean value of ~2.2 g cm^{-3}.

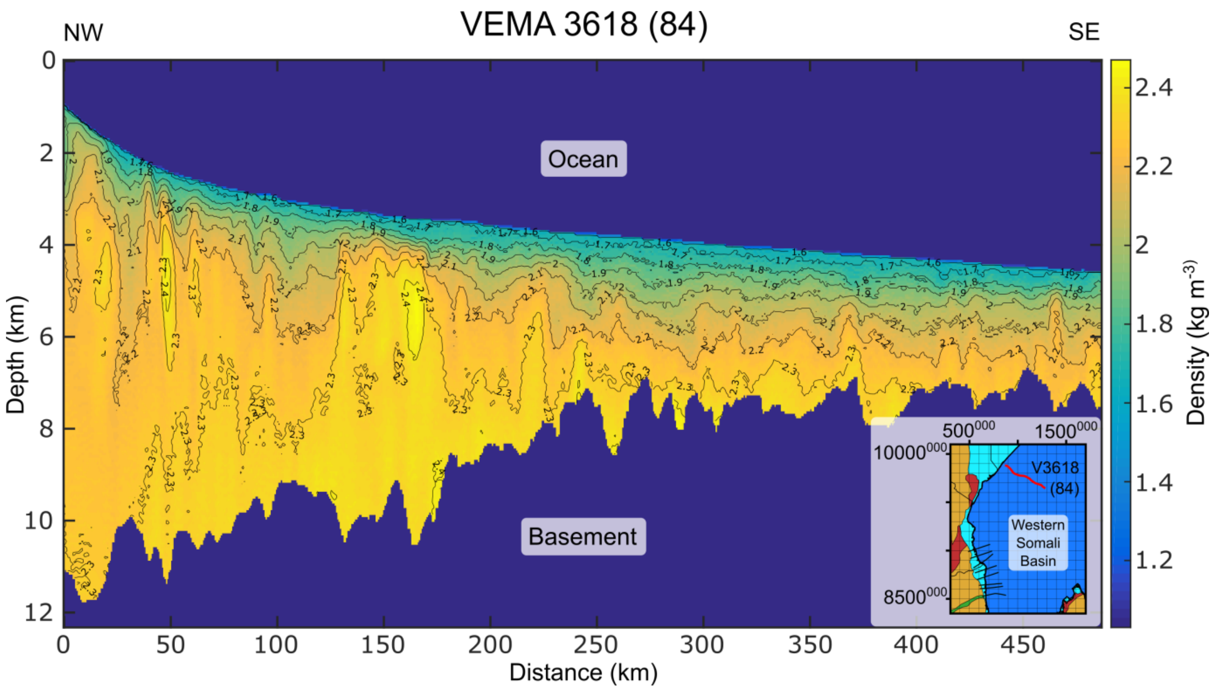

Figure S3.8. Seismic-derived sediment densities along seismic line V3618.

3.8.4. Determination of the thickness of continental crust

To determine the crustal thickness for use in all final models, phase 1 modelling was initially performed using crustal thicknesses between 20 and 35 km. A thickness of 29 km consistently resulted in the lowest RMSD was used in all final models (Figure S3.9).

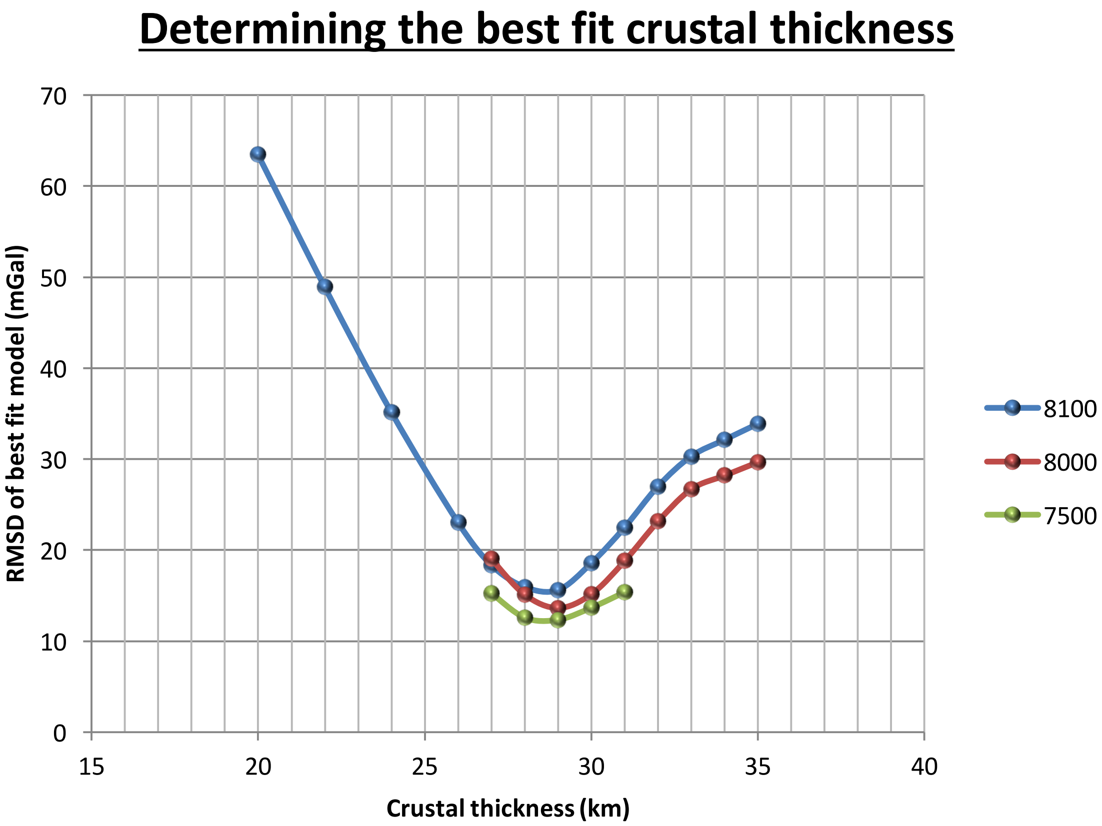

Figure S3.9. Type 1 modelling results using different thicknesses for the continental crust.

3.8.5. Resolving gravity misfits of type 2 models

IX2D-GM software was used to model misfits along profile 6 (in addition to profiles 1, 2, and 3) as it also had coincident seismic constraint on the top basement interface along a portion of its length (tz1_2000). Unfortunately, as the seismic line does not cross the continental margin, it was not suitable for type 1 or type 3 modelling.

In order to resolve the misfit inherent to models using the simple margin geometry, profiles 1, 2, and 3 commonly required modifications of the flat basement surface, introduction of a region of thin crust adjacent to the margin, and/or small adjustments to the slope angle of the Moho. No adjustment to the margin location as determined from type 2 modelling was necessary for any profile. Profile 6 (Figure S3.10) was no exception and only required simple adjustments of the basement interface to resolve the majority of misfit and modifications follow the basement interface where constrained by seismic data (Figure S3.11).

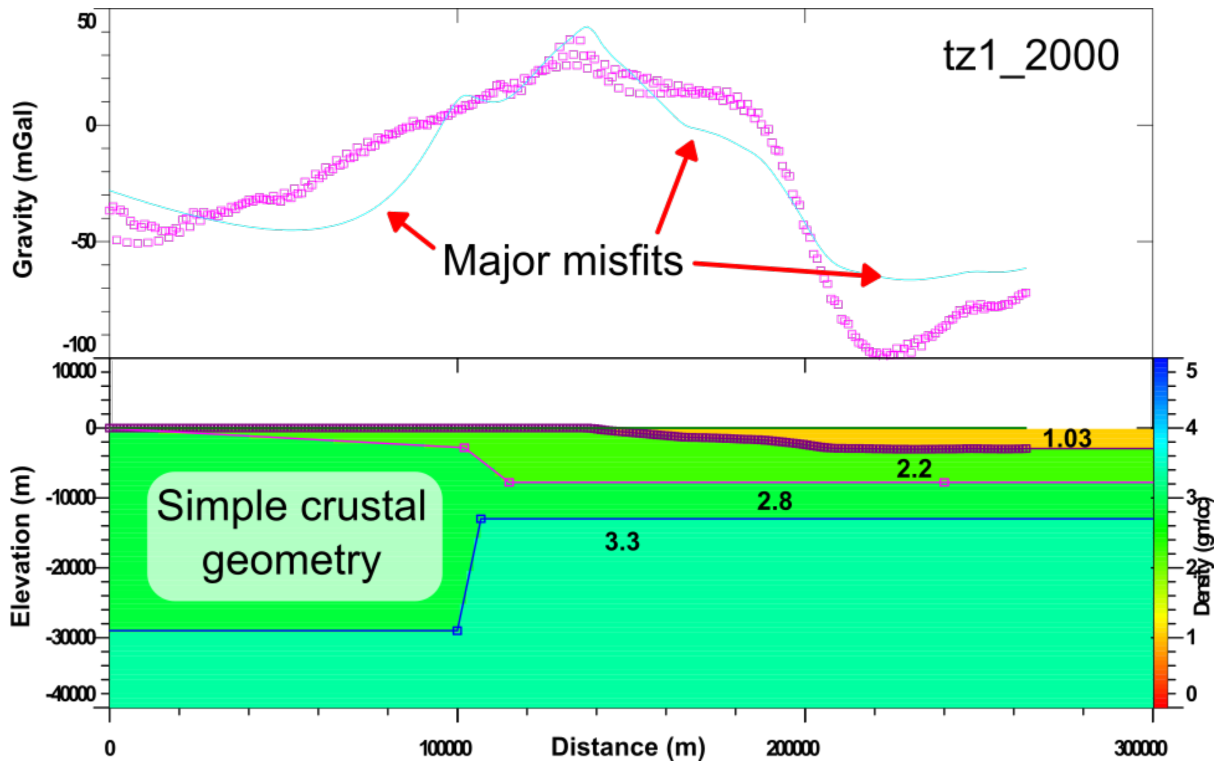

Figure S3.10. Best-fit result for profile 6 following Type 2 modelling.

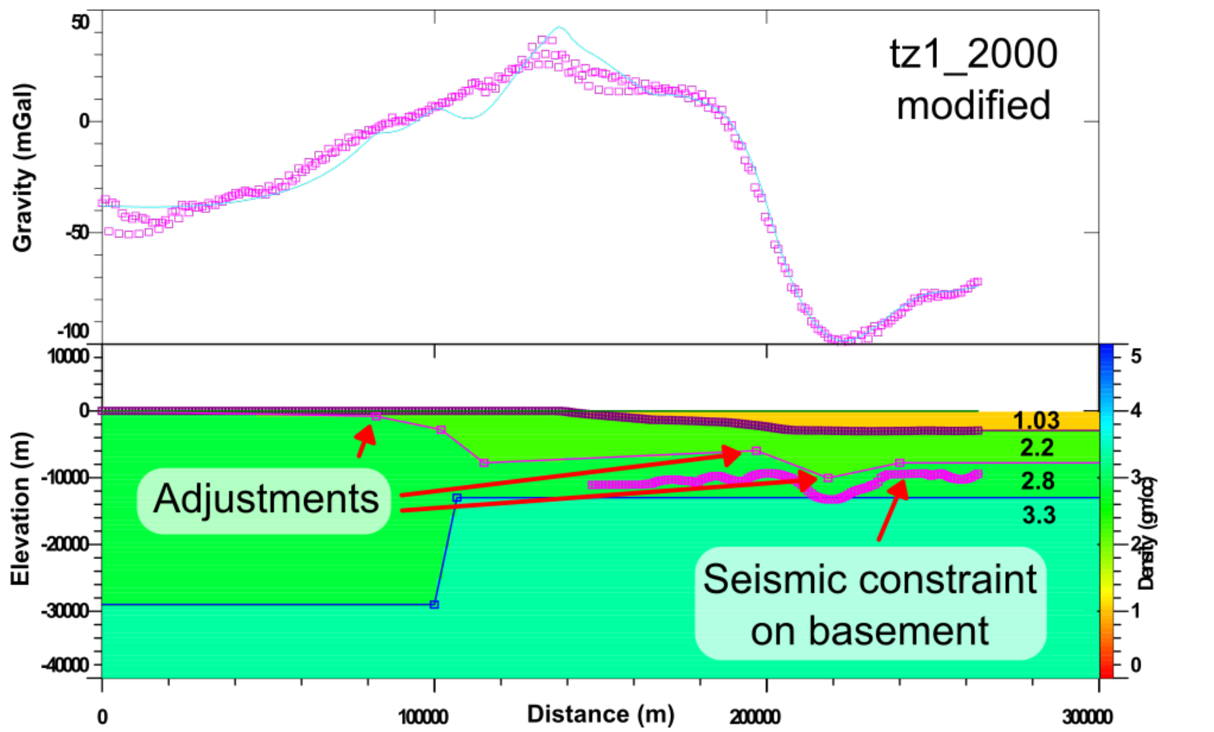

Figure S3.11. Small geologically plausible alterations are able to remove the majority of misfits and follow the trend of seismic constraints.

4. Compressional consequences of complex spreading: Formation of the Tanzania Coastal Basin and Davie Fracture Zone during the Mesozoic East Africa breakup

Abstract

Changes in plate motion often lead to transpressional deformation along oceanic fracture zones, due to their incompatibility with the new spreading direction. Here, we present evidence for compression, which localised along the trend of fracture zones, within the Tanzania Coastal Basin (TCB) that was coincident with a change in spreading direction near the end of the Jurassic. This compression of the TCB probably led to the extinction of mid-ocean ridge segments, development of the 250 km long Tanzania Coastal Basin thrust belt (TCBtb), and short wavelength (50 km) buckle folding within young (<3 Ma) oceanic crust.

We argue that this change in plate motion was triggered by a coincident alignment of weak lithosphere, in the form of rifted margins and mid-ocean ridge segments, along the future trend of the Davie Fracture Zone (DFZ), and was thus not driven by changes in plate driving forces, but by a reduction in resisting forces along the strong Rovuma Transform Margin. The cessation of compression within the TCB, possibly related to the development of the DFZ, migrated from south to north, suggesting a similar northward propagation of the 2000 km DFZ to join the spreading ridges of the Mozambique and Western Somali Basins. Since its formation, the DFZ was dominated by transpressional deformation, suggesting that the new plate motions were not fully aligned with plate driving forces. This supports the top-down concept that the DFZ formed where and when plate configurations 'allowed' it, as opposed to where and when plate driving forces 'preferred' it, indicating a first order control of lithospheric strength on plate motions.

The subsequent drift of East Gondwana along this 2000 km fracture zone led to the collision of southern Madagascar with the oblique rifted margin of northeast Mozambique, forming

the 'Davie Compression' and the 'Davie ridge'. The Davie Ridge has a similar geometry to the TCBtb and may also represent a rotated oceanic thrust.

4.1. Introduction

Changes in spreading direction have been attributed to both top-down (plate-derived; e.g. Anderson, 2001) and bottom-up (mantle flow-derived; e.g. King et al., 2002) driving mechanisms, and can result in transpression or transtension along existing fracture zones due to their incompatibility with the new spreading direction (Whittaker et al., 2016). Where strong, long offset transform boundaries exist between plates, plate motion may be restricted orthogonally to the transform due to the large force required to deform this lithosphere, and can lead to anisotropic coupling of the plates (Silver et al., 1998).

Where transpressional forces along fracture zones exceed the lithospheric strength, compressional forces may fold (e.g. McAdoo and Sandwell, 1985; Müller and Smith, 1993), and thrust (e.g Briggs et al., 2009a; Jiménez-Munt et al., 2010; Massell et al., 2000), oceanic crust, generally along pre-existing fracture zones (e.g. Briggs et al., 2009b). The strength of oceanic lithosphere is strongly age dependent, increasing approximately linearly with age (Mammerickx and Sandwell, 1986), due to cooling and accretion of thicker mantle lithosphere with time. After 20 Myr, it may be equal in strength to normal continental lithosphere; however, before this time it may also be preferentially susceptible to deformation (Vauchez et al., 1998). McAdoo and Sandwell (1985) demonstrated a strong rheological control on folding of the oceanic lithosphere, with the shortest wavelength folds occurring in the youngest oceanic lithosphere. Where thrusting occurs, it may be thin or thick-skinned, with detachment occurring at the Moho or deep in the mantle, respectively. Generally, the direction of overthrusting has been observed to be age-dependent, where thrusting exploits pre-existing fracture zones with an age offset across them, with the younger plate overriding the older (e.g. Gorringe Ridge; Owen Ridge).

If the new plate motion cannot be accommodated gradually by ocean spreading and the formation of progressively curved fracture zones, plate shearing may be favourable, and can lead to the calving of microplates and the formation of new spreading axes (e.g. Nunns, 1983; Schiffer et al., In Press; Whittaker et al., 2016). Due to thinning of the crust, associated development of structural weaknesses and fluid permeation, mechanical and thermal thinning of the lithospheric mantle, increases in the geotherm, and thermal blanketing by post-rift sedimentary sequences (Cloetingh et al., 2008), young (<25 Ma) rifted margins are also inherently weak, and may preferentially succumb to deformation.

The Early to Middle-Jurassic breakup of East and West Gondwana was coincident with the impact of the Bouvet plume and eruption of the Karoo Large Igneous Provence in SE Africa. Following breakup, oceanic spreading resulted in the drift of Madagascar to the SSE and the formation of the TCB (Tanzania Coastal Basin; Figure 4.1) (e.g. Phethean et al., Section 2), before a switch to N-S spreading around the end of the Jurassic resulted in the southward drift of East Gondwana, carrying Madagascar to its present day position (Reeves et al., 2016).

Here, we present evidence for an episode of NE-SW compressional deformation within the Tanzania Coastal Basin (TCB), which we interpret as the result of plate motion changes near the end of the Jurassic. Our findings present a rare glimpse into thrust tectonics within oceanic crust and provide an opportunity to further study controls on plate motion changes. They also have large consequences for our understanding of the tectono-thermal history of the TCB and adjacent basins, with widespread implications for paleo-heatflow and trap development within the associated petroleum province.

4.2. Database

The principal data used in this study consist of a subset of the ION East AfricaSPAN deep imaging seismic reflection dataset, including data from the ke1, tz1, tz3, tz4, and mz1 surveys. The data cover an area of ~450,000 km^2 from offshore Kenya to offshore north-east Mozambique, including much of the TCB and DFZ. In light of our findings, we also reinterpret seismic reflection data along the DFZ, immediately to the south of the East AfricaSPAN, which were presented in Mahanjane (2014). We also supplement our dataset with reprocessed seismic reflection data from the VEMA 3618 cruise, and two crustal thickness measurements from the TCB derived from sounobuoy data collected during this cruise. The locations of seismic sections and crustal thickness measurements, together with structural picks made from these data, are shown in Figure 4.1. Free-air gravity data, also shown in Figure 4.1 (SS24; Sandwell et al., 2014), are used for the identification of structural elements within the basin, and to assist in the determination of their strike and continuity where seismic data alone are insufficient.

Satellite imagery from the northern Morondava Basin, Madagascar, was used for the mapping, and determination of the origin of, structural lineaments within this basin. The geological maps of Besairie (1964) are used to determine the ages of these structures.

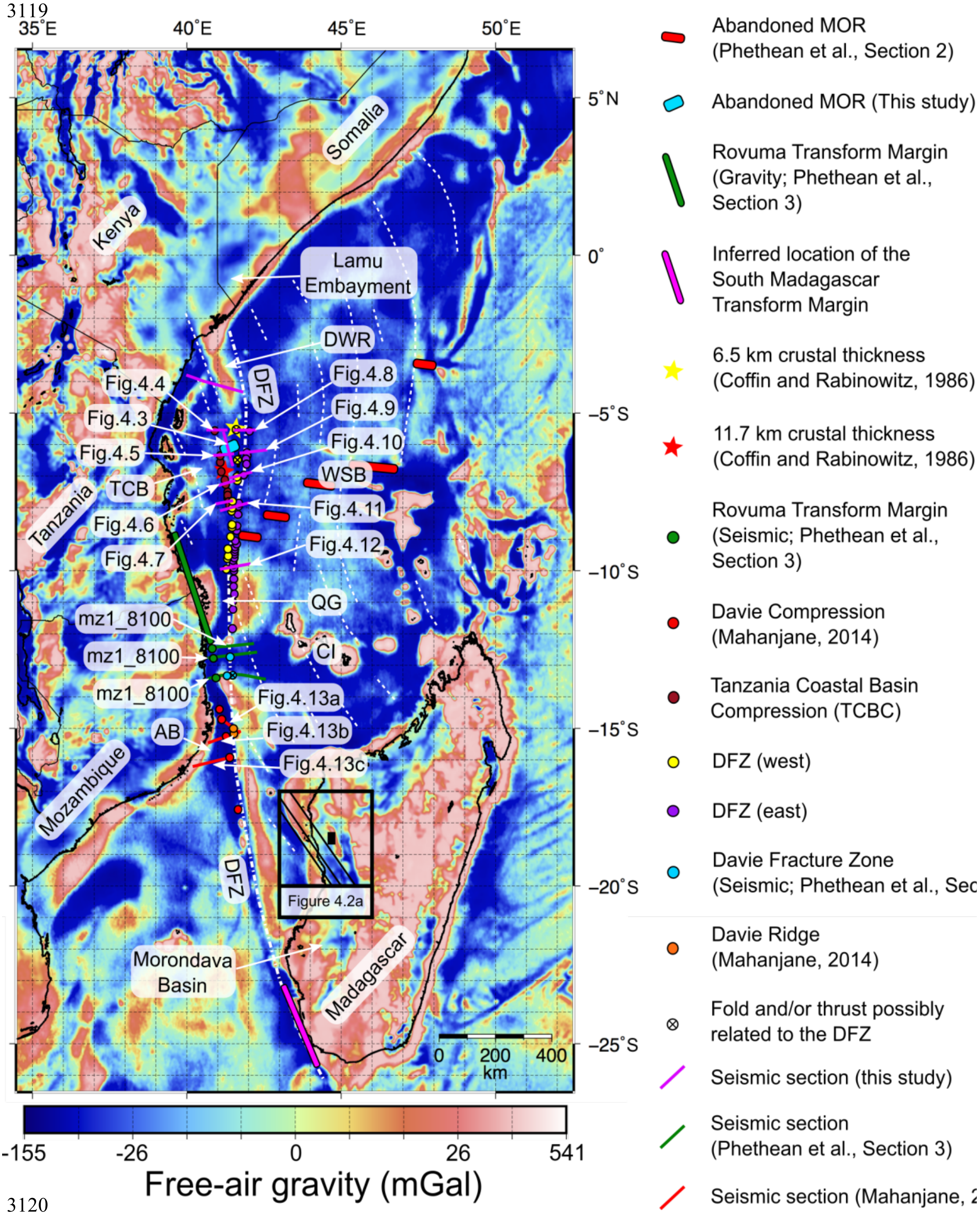
35°E
40°E
45°E
50°E
5°N
0°
−5°S
−10°S
−15°S
−20°S
−25°S
Somalia
Kenya
Lamu Embayment
DWR
DFZ
Fig.4.4
Fig.4.3
Fig.4.5
Fig.4.8
Fig.4.9
Fig.4.10
WSB
TCB
Tanzania
Fig.4.6
Fig.4.7
Fig.4.11
Fig.4.12
QG
mz1_8100
mz1_8100
mz1_8100
CI
Fig.4.13a
Fig.4.13b
Fig.4.13c
AB
Mozambique
Figure 4.2a
Morondava Basin
Madagascar
0 200 400
km
-155
-26
0
26
541
Free-air gravity (mGal)
Abandoned MOR (Phethean et al., Section 2)
Abandoned MOR (This study)
Rovuma Transform Margin (Gravity; Phethean et al., Section 3)
Inferred location of the South Madagascar Transform Margin
6.5 km crustal thickness (Coffin and Rabinowitz, 1986)
11.7 km crustal thickness (Coffin and Rabinowitz, 1986)
Rovuma Transform Margin (Seismic; Phethean et al., Section 3)
Davie Compression (Mahanjane, 2014)
Tanzania Coastal Basin Compression (TCBC)
DFZ (west)
DFZ (east)
Davie Fracture Zone (Seismic; Phethean et al., Sec
Davie Ridge (Mahanjane, 2014)
Fold and/or thrust possibly related to the DFZ
Seismic section (this study)
Seismic section (Phethean et al., Section 3)
Seismic section (Mahanjane, 2

Figure 4.1. Free-air gravity anomaly map of East Africa highlighting locations of figures and seismic lines used in this study. AB, Angoche Basin; DFZ, Davie Fracture Zone ; DWR, Davie-Walu Ridge ; QG, Quirimbas Graben; CI, Comoros Islands; TCB, Tanzania Coastal Basin; WSB, Western Somali Basin. Inset shows the location of Figure 4.2a, and within this, the internal solid black box shows the location of Figures 4.2b and c. Figure numbers to seismic references: 4.3, tz3_1300; 4.4, tz1_4000 (west); 4.5, tz3_3600 (west); 4.6, tz4_3300; 4.7, tz4_2950; 4.8, tz1_4000 (east); 4.9, tz3_3600 (east); 4.10, tz4_3350; 4.11, tz4_2850; 4.12, tz3_2101; 4.13a, Mahanjane_3a; 4.13b, Mahanjane_2c; 4.13c, Mahanjane_2b.

4.3. Pre-breakup position of Madagascar

The initial configuration of Gondwana fragments prior to supercontinent disassembly has been the source of much debate for over 30 years, and Madagascar forms a key piece in this puzzle. An accurate determination of the origin of this continental fragment has large repercussions for the fit of the surrounding continents due to its central position and the presence of several major intercontinental shear zones commonly used to align conjugate margins. Suggestions for the origin of Madagascar generally fall into one of two groups, and may be described as 'tight-fit' or 'loose-fit' reconstructions. Loose fit reconstructions assume that the N-S trending DFZ represents the continent-ocean transform margin, where to the west of this feature no oceanic spreading has occurred. These models use the DFZ to guide Madagascar back to a northern position seaward of the TCB. Tight-fit reconstructions, on the other hand, allow for an initial NNW-SSE phase of spreading before the formation of the DFZ and subsequent N-S drift. This results in an initial position of Madagascar within the TCB (Reeves et al., 2004). This latter model has recently been supported by the discovery of a transform margin along the Rovuma Basin and oceanic crust within the TCB, both inboard of the DFZ (Sauter et al., 2016; Chapter 2), which necessitates an initial phase of oceanic spreading to the west of the DFZ, and thus an origin for Madagascar within the TCB.

This initial phase of oceanic spreading within the TCB sent Madagascar in a SSE direction, constrained by the analysis of gravity lineaments related to spreading features (Phethean et al., 2016), and resulted in strike-slip tectonics between Southern Madagascar and Southern Tanzania/Northern Mozambique. This strike-slip motion led to the development of the Rovuma Transform Margin, the location of which has recently been accurately constrained through combined seismic reflection and gravity modelling studies (Chapter 3). This transform margin generally follows the trend of the onshore basement outcrop along the coastlines of the Southern TCB and the Rovuma Basin, and is located ~80 km seaward of the basement outcrop along its length.

The location and trend of this transform margin further constrains the initial motion of Madagascar relative to Africa, as the conjugate transform margin in southern Madagascar must have been in continuous contact along it during the active transform phase. Ascertaining the location and trend of the transform margin along southern Madagascar is, however, difficult due to tectonic overprinting and disruption of this margin during the formation of the DFZ at ~150 Ma (Reeves et al., 2016; Chapter 2). The present day location of the basement outcrop along southern Madagascar, however, is unlikely to have been affected by this tectonic overprinting. Therefore, we assume the transform margin of southern Madagascar also runs parallel to, and ~80 km seaward of, the basement outcrop as for the conjugate transform margin. This allows for an accurate reconstruction of Madagascar and Africa by aligning the two transform margins, which not only constrains the orientation of Madagascar relative to Africa, but also its south-westerly position. The north-westerly position may then be derived by aligning the eastern edges of the once-adjoining Selous and Morondava basins to give the absolute location of Madagascar relative to Africa prior to breakup. Imposing these simple constraints on the position and orientation of southern Madagascar results in a good alignment of structural features in northern Madagascar with those of the conjugate East African margin.

Newly recognised strike-slip faults are preserved in the syn-breakup Bajocian-Bathonian limestones of the northern Morondava Basin (the Karoo-recent aged basin spanning the entire west coast of Madagascar) and are highly oblique to the trend of this basin (Figure 4.2). The strike-slip nature of these faults is indicated by their highly linear nature and interlinking pull apart basins, which are similar to others found within Karoo aged deposits of the Morondava Basin (Schandelmeier, 2004) and indicate a dextral sense of motion across the faults. These faults closely follow the trend of NNW-SSE coastline segments (Figure 4.2a), and terminate at the End Bathonian boundary (blue line; Figure 4.2b), possibly indicating the localisation of strike-slip deformation onto oceanic transform faults at this time. Following the reconstruction of the southern Madagascar and Rovuma Transform Margins, these strike-slip faults are closely aligned with the SSE trend of the Davie-Walu ridge (DWR), a prominent gravity high just offshore the conjugate Lamu Embayment (Figure 4.1). They define the same SSE initial plate motion constrained by the Rovuma Transform Margin, and together, these features provide an additional robust constraint on the Mid- to Late-Jurassic relative plate motions of East and West Gondwana.

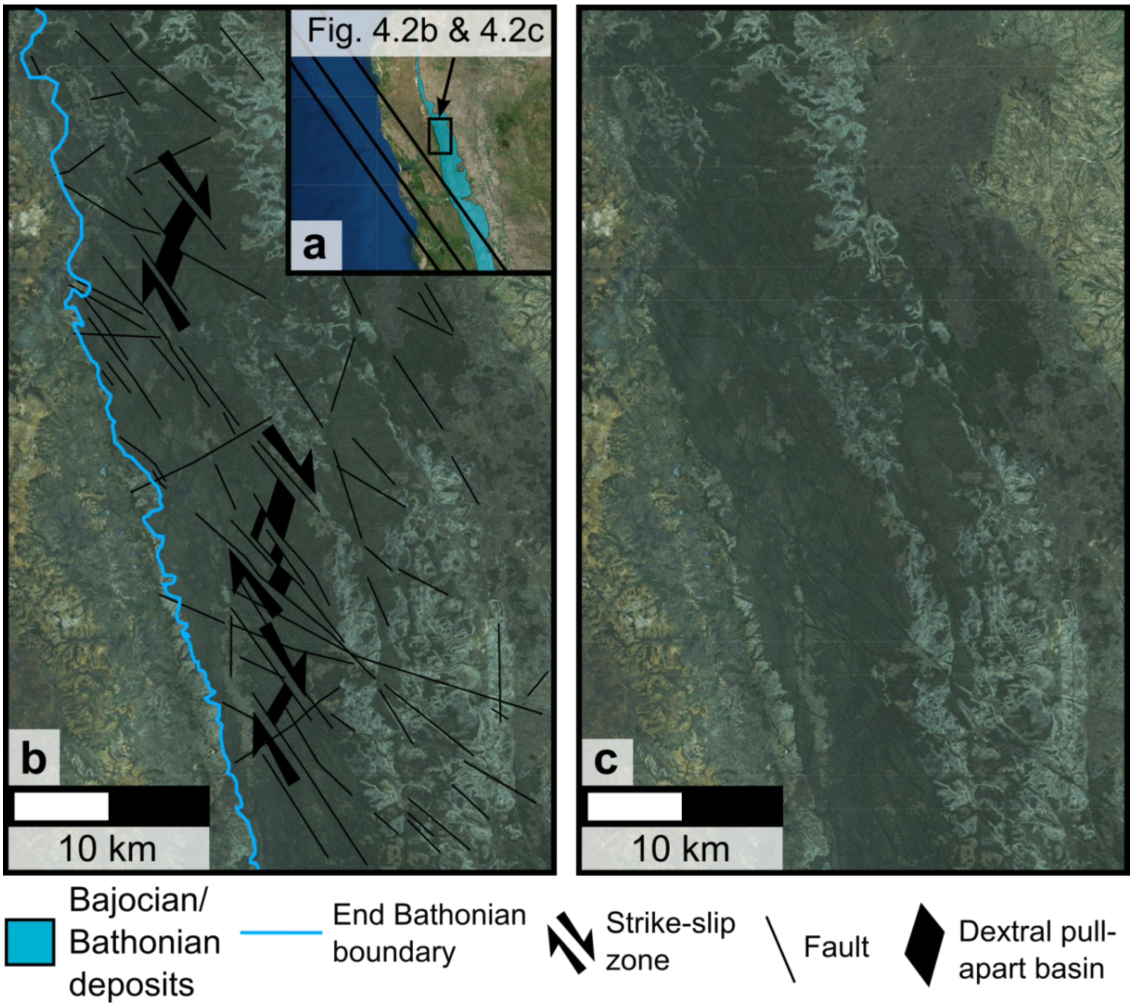

Figure 4.2. (a) Location of Figures 4.2b and c within the Morondava Basin. Black lines show the extrapolated trend of structures identified in Figures 4.2b and c. The extent of Bajocian/Bathonian deposits is taken from the geological maps of Besairie (1970). The location of Figure 4.2a is shown in Figure 4.1. (b) Landsat Satellite imagery of Bajocian-Bathonian syn-breakup deposits from the northern Morondava Basin, with fault lineament interpretation as black lines. (c) Figure 4.2b without fault interpretation. The location of the Morondava Basin is shown in Figures 4.1 and 2.1.

4.4. Major tectonic signatures of the TCB, DFZ, and Western Somali Basin

The interpretation of seismic reflection data from the Western Somali Basin (WSB) and surrounding coastal basins of East Africa reveals evidence for several major tectonic events. Here, we assess the nature of these events and constrain them in relation to the plate tectonic framework of (Chapter 2).

4.4.1. Cessation of spreading in the TCB

Within the TCB, at 6.2°S 41.4°E, the SSE trending tz3_1300 line displays a change in character of the oceanic crust (Figure 4.3; location shown in Figure 4.1). The northernmost section of the line displays a smooth and continuous top basement reflector, which changes southwards to a rough and internally reflective layer. Coincident with this change, the mid-lower crustal layers become more seismically transparent, and the onset of extensional faulting of the basement, which generates tilted half grabens that dip symmetrically about a central graben, also occurs. Some of these normal faults offset the Moho by up to 0.5 s TWTT. In the northern and southern regions of Figure 4.3, Moho reflections define a crustal thickness of ~2.1 s TWTT, and in places bound the base of the seismically transparent crust. Where Moho reflections are faint or not present, the base of the seismically transparent body is, therefore, taken as an indication of the Moho level. This and the high amplitude reflections of the top basement allow the definition of a roughly symmetrical thinning of the crust from ~2.1 s at the edges of the central graben to ~ 1 s TWTT at the graben's centre over a distance of ~ 40 km.

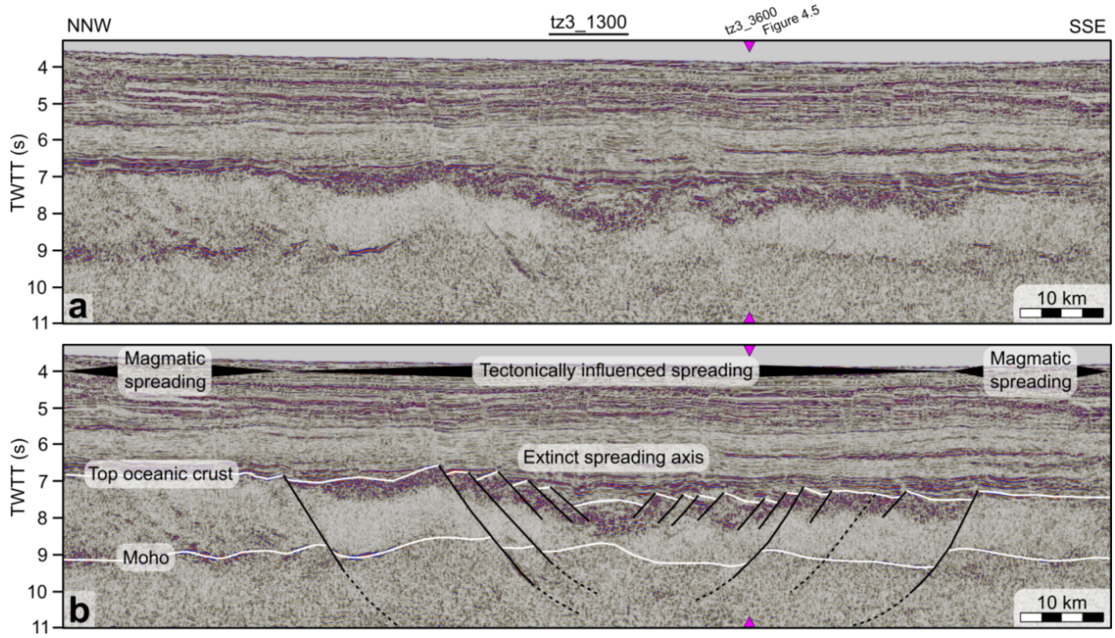

Figure 4.3. Extinct ocean spreading segment identified within the TCB. (a) Uninterpreted section. (b) Interpreted section. Extensional faults (black lines) sometimes offset the Moho and become increasingly dominant approaching the spreading centre. The crustal thickness decreases from ~2.1 s TWTT outside of the axial rift, to ~1 s TWTT at the rift centre. An associated change in the character of the top basement (top white line) occurs alongside crustal thinning. Moho reflections and the basal termination of the seismically transparent crust define the base of the oceanic crust (bottom white line). Location shown in Figure 4.1.

Smooth oceanic crust is generated by magmatically dominated spreading, whereas rough oceanic crust results from an insufficient supply of melt to the spreading axis and the onset of tectonically accommodated plate separation (Louden et al., 1996; Smith, 2013). As melting at mid-ocean ridge (MOR) systems is primarily controlled by spreading rate, where slower spreading results in greater conductive cooling of the upwelling mantle and therefore less melt production, lower melt supplies generally reflect lower spreading rates (White et al., 1992). Mid to lower oceanic crust may display a transparent character in seismic reflection data (e.g. Bécel et al., 2015; Morris et al., 1993), and half grabens within oceanic crust have been shown to generally dip towards the spreading centre about which they form (Behn and Ito, 2008). The axial valleys at such spreading centres generally range in width from 16-62 km, averaging at 35 km (Malinverno, 1990), as measured along the Mid-Atlantic Ridge.

On line tz3_1300, the reduction in crustal thickness from ~2.1 s to ~ 1 s TWTT over similar distances to the width of axial spreading valleys and the symmetrical dip of half grabens about this thinning suggest that this structure represents an abandoned spreading centre within the TCB. Similar observations of crustal thinning and an associated broad zone of rotated fault blocks have been observed at the extinct Labrador spreading centre (Louden et al., 1996). Therefore, a reduction in spreading rate probably occurred in the lead up to the extinction of the spreading centre, resulting in greater cooling of the upwelling asthenosphere and less melt production (e.g. Niu and Hékinian, 1997). The resulting deepening of the brittle-ductile transition may also have allowed normal faults to extend into the upper mantle (e.g. Harper, 1985), offsetting the Moho.

The abandoned spreading centre is situated ~ 210 km away from the coastline in the paleo spreading direction; according to the plate tectonic model of (Chapter 2), this places the age of abandonment at ~150 Ma, close to the end of the Jurassic. At roughly the same time, a major clockwise rotation of East Gondwana relative to West Gondwana, and the subsequent formation of the DFZ, occurred (Reeves et al., 2016). Subsequent oceanic spreading between 150 and 125 Ma, forming the Western Somali Basin, transposed the remaining MOR segments farther south offsetting the abandoned ridges of the Tanzania Coastal Basin and younger Western Somali Basin.

4.4.2. Compression post SSE spreading

Several E-W trending seismic lines within the TCB show evidence for crustal thickening and compression of the basement, and are described from north to south below.

4.4.2.1. Line tz1_4000 (west)

The central and eastern portions of Figure 4.4 display a smooth top basement and clear Moho reflection, defining oceanic crust with a uniform thickness of ~ 2.2 s TWTT. This crust forms an open buckle fold, which has a trough to trough wavelength of ~35 km. The crest of the buckle fold sits at a depth of 6.6 s TWTT, and the troughs at 7.3 s TWTT. Overlying the buckle fold, sedimentary packages onlap, and then overlap, the folded crust, and diverge towards the troughs of the fold.

At the western edge of the buckle fold, reflections from the sediments, top basement, and Moho, are bent sharply upwards before terminating abruptly in a steep west dipping line, perpendicular to the folded crust. To the west, an adjacent basement block with sporadic internal westward dipping reflections sits at a depth of 5.4 s TWTT. This block has been uplifted by at least 1.2 s TWTT relative to the surrounding crust, and the rotated internal reflections are truncated by an erosion surface along the top of the eastern flank that continues to form top of the divergent sedimentary fill to the east. Above the western side of this block, toplap of sedimentary packages against the same erosion surface also occurs, but diminishes westward (Figure 4.4). Between the west-dipping uplifted block, and west-dipping upper crustal reflectivity at the far west of the line, an ~10 km wide block of east-dipping upper crustal reflectivity is present, and is delineated by offsets in the higher amplitude top basement reflections.

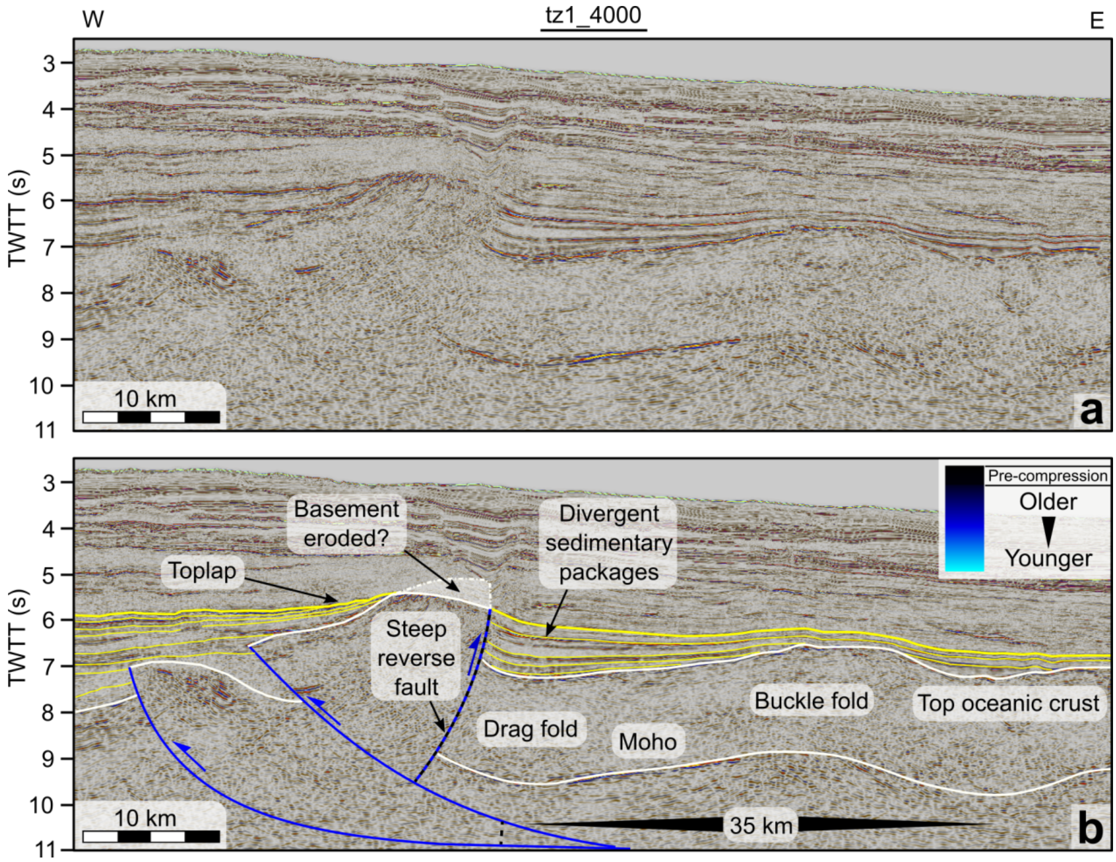

Figure 4.4. Thrusting and folding of the basement along seismic line tz1_4000 (west) in response to compression. (a) Uninterpreted section. (b) Interpreted section. Yellow lines show the top (thick lines) and internal structure (thin lines) of syn-compressional sediments. Upper white lines indicate the top basement, where dashes indicate eroded sections, and the lower white line indicates the Moho. The interpreted relative ages of faults in this section are shown in the key. Location shown in Figure 4.1.

The buckle fold in the eastern half of Figure 4.4b likely developed in response to compression, and the divergence of overlying sedimentary packages towards the troughs of the buckle suggests that they were deposited syn-compression. The onlap of sediments against the crest of the buckle suggests either 1) the presence of an original basement high, or 2) the onset of deposition after the onset of compression (e.g. Burbank and Vergés, 1994). Assuming a predominantly terrestrial sedimentary source, this onlap and the subsequent sedimentary overlap of the fold suggest that uplift rates of the fold crest were less than the rate of sedimentary deposition.

To the west of the buckle fold, the uplift and rotation of the basement block has resulted in crustal thickening from 2.2 s up to 3.5 s TWTT where it overlies the edge of the buckle fold. This crustal thickening also strongly supports compressional tectonics. The abrupt termination of sedimentary, top basement, and Moho reflections against the western end of the buckle fold, and the upward bending of reflections immediately before their termination, suggest reverse faulting in this location (Figure 4.4b). The orthogonality of the reverse fault to the restored basement section indicates the reactivation of a sub-vertical structure during compression, and the folding associated with this faulting is therefore interpreted as drag folding as opposed to fault propagation folding associated with thrust fault initiation. Erosion of the tip of the uplifted block and toplap of sedimentary packages against this erosion surface (which may represent a depositional surface farther to the west) suggest that uplift of this block was faster than the rate of sedimentary deposition (Burbank and Vergés, 1994; Hardy and Ford, 1997). Near the western edge of Figure 4.4, the rotation and offset of basement reflections may be the result of low angle thrust faulting during the compression, which allows for the uplift of the basement block along the steep reverse fault.

4.4.2.2. Line tz3_3600 (west)

Similar crustal geometries to those along tz1-4000 (west) are seen 90 km to the SSE in Line tz3_3600 (west), and are shown in Figure 4.5. The eastern half of this figure crosses the heavily faulted extinct spreading centre of the TCB (i.e. Figure 4.3) at a highly oblique angle (see Figure 1 for line locations), possibly resulting in the sporadic reflective character of the top basement and lack of clear Moho reflections in this region. Identification of the geometry of the top basement, by enveloping top of basement reflections, reveals a possible folding of the crust, the top of which sits at a depth of 7.2 s TWTT. Above the western flank of the fold, the sedimentary sequence can be seen to thicken into the trough, although the internal structure of these sediments is poorly defined and does not allow for an analysis of their possibly divergent nature.

Before the top basement reflections terminate abruptly to the west, they bend back upwards. Immediately west of this, a rotated and uplifted basement block sits at a depth of 6 s TWTT, and west-dipping top basement and upper crustal reflections define its western limb. Strong Moho reflections, which have been similarly tilted, define the base of the crust, and bend sharply downwards before their abrupt termination at the eastern edge of the block. Farther west, east-dipping top basement and upper crustal reflections define a second crustal block, along the eastern flank of which reflections bend back upwards, as can be seen particularly clearly in the overlying sedimentary packages (Figure 4.5). West of this block, close to the western edge of the figure, reflections from the upper crust and top basement are sub-horizontal.

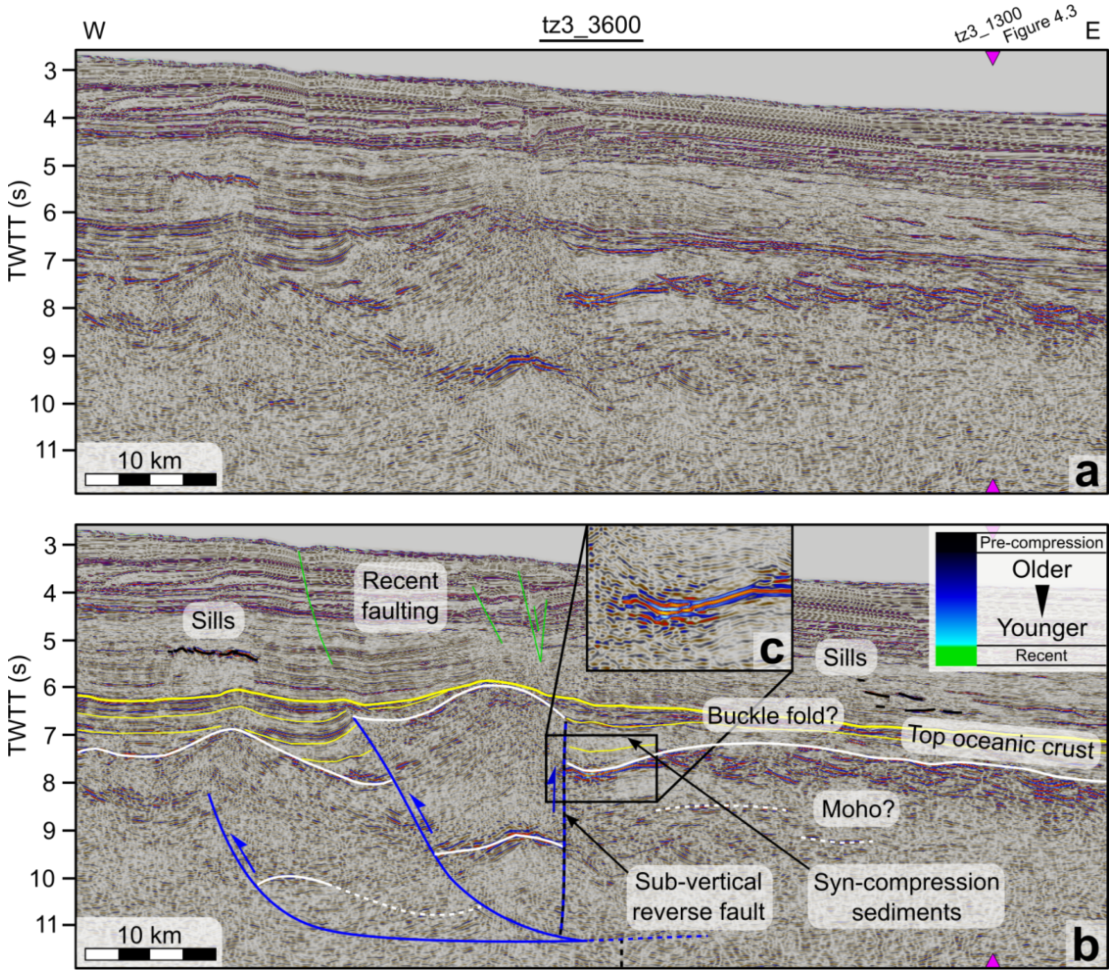

Figure 4.5. Thrusting and folding of the basement along seismic line tz3_3600 (west) in response to compression. (a) Uninterpreted section. (b) Interpreted section. (c) Close up of the inset region without interpretation showing the curved top basement reflections. Line descriptions are as for Figure 4.4. The interpreted relative ages of faults in this section are shown in the key and continuation of the structures at depth is speculative. Location shown in Figure 4.1.

The overall geometry of line tz3_3600 (west) is similar to that seen along line tz1_4000 (west), despite the 90 km offset between the two lines, and may be interpreted in a similar way. Again, buckling and thrusting of the crust have occurred in response to compression, and in places the resulting crustal thickness may reach 4 s TWTT. In tz3_3600, the sudden termination of reflections against the eastern edge of the uplifted basement block defines another sub-vertical reverse fault, similar to the one seen in tz1_4000, again possibly reactivating a pre-existing structure. Drag folds have developed along this reverse fault and are defined by the top basement reflections to the east, and Moho reflections to the west. Similarly to line tz1_4000 (west), uplift along this reverse fault was probably facilitated by the development of thrusts to the west, which have also rotated and uplifted the crust in this location.

4.4.2.3. Line tz4_3300

Another basement high is imaged within the TCB another 100 km farther to the SSE. Here, smooth top basement reflections, underlain by a more transparent mid-crust and strong Moho reflections, are prevalent over the west and east portions of the section (Figure 4.6). They define a crustal thickness of between 1.7 s and 2.3 s TWTT within undeformed regions, generally sitting at a depth of around 7.3 s TWTT. The smooth top basement of the eastern portion of Figure 4.6 shows slight bulges on an approximately 10 km length scale, and the tips of bulges are commonly aligned with dipping reflections within the crust, and sometimes also offsets in the Moho. In this eastern portion of the line, a pair of reflective bands is sometimes present instead of a single band of Moho reflections. Both bands are offset in several locations, show a similar seismic waveform and amplitude, and do not always have a consistent vertical separation from one another.

In the central region of the line, the top of the basement has been uplifted to a depth of ~ 6.4 s TWTT, and in places the crust possibly thickens to 3.7 s TWTT. Below and to the east of the crest of this basement uplift, reflections within the crust dip gently eastwards, whereas below and to the west of the basement's crest, an ~ 5 km wide block of seismically transparent crust sits directly above a band of east-dipping high amplitude reflections. Strong Moho reflections are sparse in the central region, but a short high amplitude reflector dips eastward ~3.5 s below the crest of the thickened crust. Above the basement, the deep sedimentary section, correlating to the folded and divergent packages of the syn-compressional sediments along lines tz1_4000 (west) and tz3_3600 (west), shows little sign of deformation, and follows the regional sedimentary tilt of the basin. On this line, unlike along lines tz1_4000 (west) and tz3_3600 (west), no buckle folding has occurred adjacent to the crustal thickening.

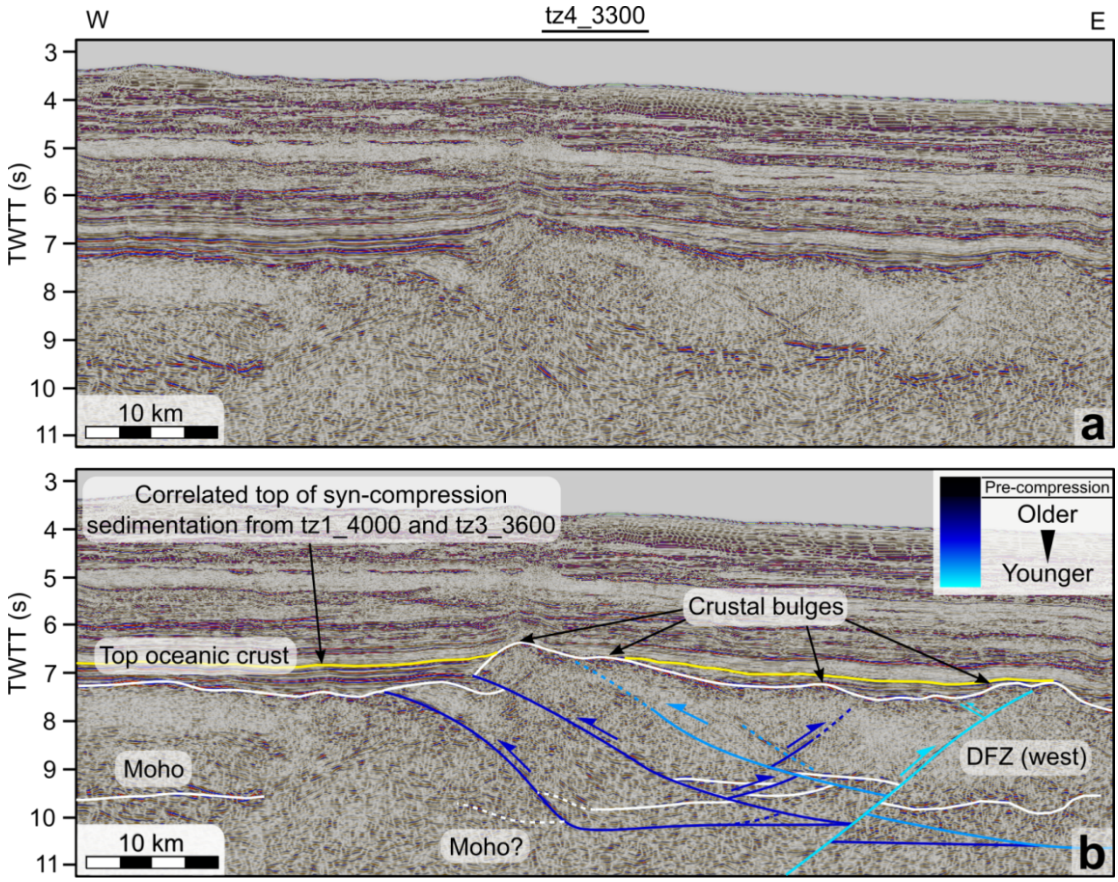

Figure 4.6. Thrusting of the basement along seismic line tz4_3300 in response to compression. (a) Uninterpreted section. (b) Interpreted section. Dual reflector bands around the depth of the Moho result from Moho stacking in response to thrusting and backthrusting. Line descriptions are as for Figure 4.4, where the top of the syn-compressional sediments is now interpreted to correlate with the top of deformed sediments on lines tz1_4000 (west) and tz3_3600 (west). The interpreted relative ages of faults in this section are shown in the key and continuation of the structures at depth is speculative. Location shown in Figure 4.1.

Along line tz4_3300, the clear Moho reflections on either side of the crustal thickening, the smooth character of the top basement, the undeformed crustal thickness of ~ 2 s TWTT, and the seismically more transparent mid-crust indicate oceanic crust. As this oceanic crust surrounds, and therefore likely also comprises, the region of uplifted basement, tectonic thickening of the crust is likely the cause of the basement uplift. Beneath this, the eastward-dipping reflections within the crust and the juxtaposition of crustal blocks, which sometimes have seismically transparent internal characteristics, suggest repeated stacking of the crust along eastward-dipping thrust faults (Figure 4.6b). The short, high amplitude reflector, seen below the crest of the crustal thickening, may therefore form a faulted contact between crust and mantle rocks, where shearing of this boundary may have increased its reflectivity.

To the east, bulges in the top basement, as well as east- and west-dipping reflections within the crust and offsets in the Moho (where offsets occur with the top to both the east and west), suggest further thrust and back-thrust development in this region. The complex geometry of the pair of Moho reflection bands in the east may therefore be the result of Moho stacking along such thrusts (Figure 4.6b). It should be considered, however, that the lower band of reflections may also have developed in response to early thrusting at this level, which was subsequently offset by later thrusts. This interpretation is presented in the supplementary material, but, without sufficient justification for the abandonment of an early detachment fault in favour of developing a new deeper one, this scenario is less attractive.

Above the thrust stack, sediments correlating to the syn-compressional sedimentary packages seen farther north along lines tz1_4000 (west; Figure 4.4) and tz3_3600 (west; Figure 4.5) have been identified (yellow line, Figure 4.6b). These sediments onlap both the basement thrust stack and the DFZ (west), and show little sign of deformation beyond the regional background, following the same tilt as the overlying strata. This suggests that either, 1) the stratigraphic correlation of the sediments does not correspond to a temporal correlation, or 2) the sediments were deposited following thrusting and development of the DFZ, in which case the cessation of thrusting and formation of the DFZ must have occurred earlier farther south.

At the eastern edge of the line, a west-dipping thrust (cyan colour on Figure 4.6b) offsets the Moho by +0.5 s TWTT, and the lack of counter-clockwise rotation of Moho reflections within the hanging wall suggests that the thrust does not curve and sole out in the immediate vicinity. This fault may therefore cut the older west verging thrusts, in which case it would be younger. This fault tips out in the DFZ (west), where it contributes to crustal thickening.

4.4.2.4. Line tz4_2950

Approximately 65 km farther to the SSE, just before intersecting the main trace of the DFZ, basement uplift and folding of the crust has again occurred, and is shown in Figure 4.7. Here, as to the north, smooth and high amplitude reflections define the top and bottom of oceanic crust, which also commonly displays a seismically transparent mid-crust. In the western part of the section, the crust forms an open buckle fold, with a trough to trough wavelength of ~40 km. The crest of the buckle fold sits at a depth of 7.6 s TWTT, and the troughs at ~8 s TWTT. At the eastern edge of the buckle fold, the east-dipping smooth top basement reflections, low reflectivity mid-crust, and Moho reflections step down, and a sharp change to a westward dip of these reflections occurs. It should be noted, however, that below 10 s TWTT, patches of west-dipping reflections occur sporadically in several places on this line, and may interfere with the Moho interpretation. Less than 10 km to the east, the west-dipping top basement reflections are tightly folded to dip back eastwards, before terminating abruptly ~6 km on. The basement topography immediately above the tight fold has been partially filled by a layer of discontinuous, moderate to high amplitude reflections, which roughly follow the dip of the top basement.

Along the eastern edge of the line, a block of uplifted basement sits at 7.2 s TWTT, and clear top basement and Moho reflections dip eastwards. Between this uplifted block, and the tightly folded crust to the west, additional east-dipping reflections are slightly offset below the trend of Moho reflections beneath the uplifted block. These reflections are bounded above by a region of reduced reflectivity, and below by chaotic reflections.

Similarly to line tz4_3300, sediments that correlate with deformed or divergent sedimentary packages farther north (along lines tz1_4000 (west) and tz3_3600 (west)), onlap the basement and do not form large divergent growth wedges as seen farther north. They have also not been subject to deformation beyond the regional background, and follow the same trend as the overlying strata.

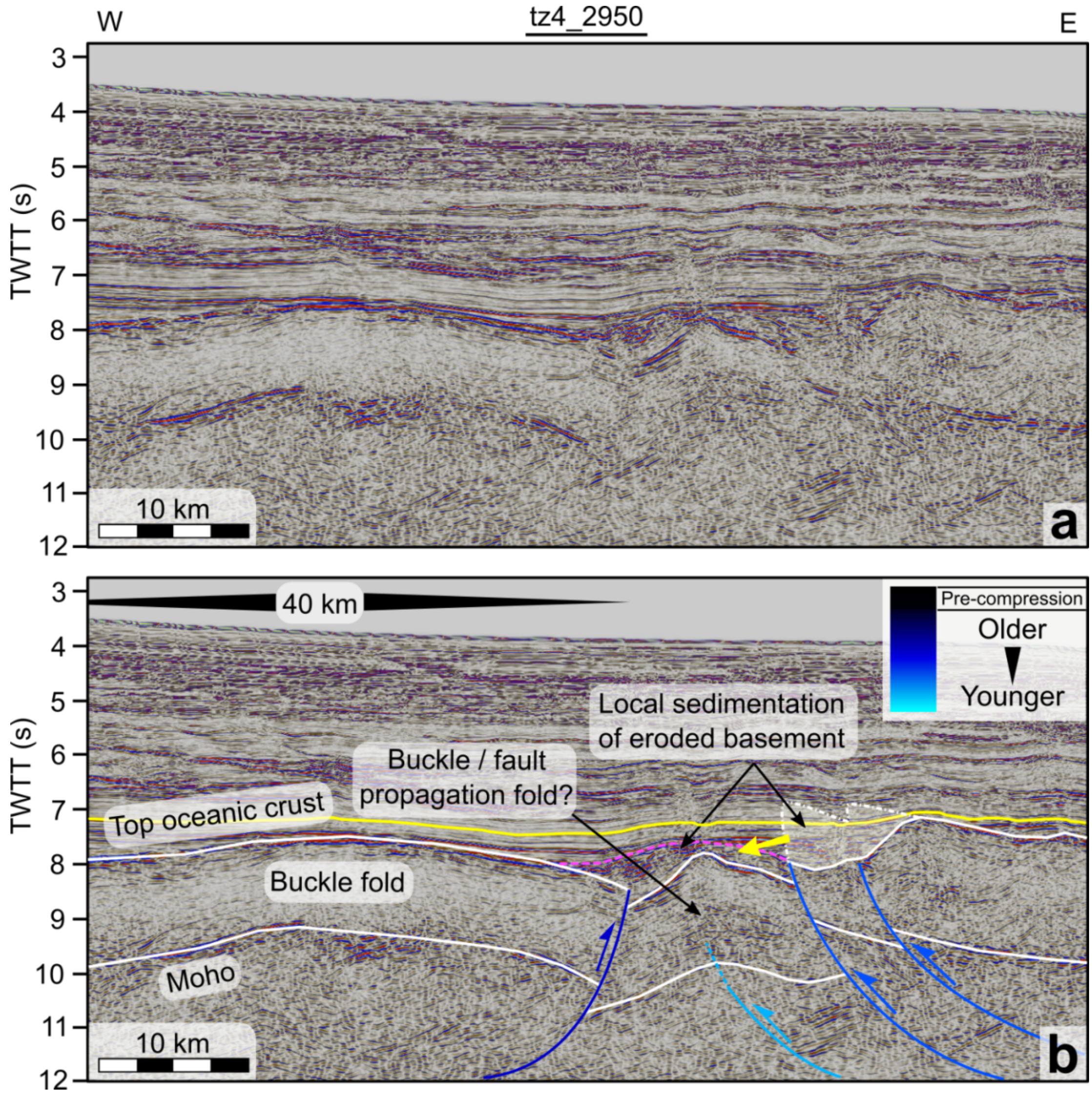

Figure 4.7. Folding and thrusting of the basement along seismic line tz4_2950 in response to compression. (a) Uninterpreted section. (b) Interpreted section. Line descriptions are as for Figure 4.4, where the top of the syn-compressional sediments is now interpreted to correlate with the top of deformed sediments on lines tz1_4000 (west) and tz3_3600 (west), and the dashed pink line shows the top of locally sourced sediments deposited during compression. The interpreted relative ages of faults in this section are shown in the key. Location shown in Figure 4.1.

The termination and step down of top basement and Moho reflections at the eastern end of the buckle fold imply a faulted contact between the buckle fold and the tight fold to the east. The eastward step from the Moho terminations to the top basement terminations suggests this fault is west-dipping and, therefore, a reverse fault, consistent with other observations of basement compression. The sharp folding of oceanic crust immediately to the west is uncharacteristic of the buckle folding elsewhere, and may have required the influence of a propagating fault to localise the deformation.

Immediately east of the fault-propagation fold, the presence of a lower reflectivity area above the east-dipping reflections is compatible with the interpretation of these reflections as the Moho, with overlying seismically transparent oceanic crust. The relative uplift of this basement during compression, with top to the east offset, implies the presence of east-dipping thrusts, as interpreted elsewhere along the compressional structures of the TCB. To the east, Moho reflections of the uplifted block are offset slightly upwards. A second thrust fault, offsetting the Moho and further uplifting the eastern block, is therefore likely. Between the uplifted block and the fault-propagation fold, the shallow level of the Moho and relatively low top basement, therefore, imply a large amount of erosion of this crust during, and following, its uplift. It is possible that local deposition of the derived sediment occurred above the developing limbs of the fault-propagation fold, where continuous steepening of the fold limbs resulted in deformation and re-deposition of these sediments, resulting in their chaotic nature. The later deposition of onlapping and undeformed sediments, which correlate to syn-compressional sediments in the north of the basin, may again support the earlier cessation of compression in this more southern location, as compared to the north of the TCB.

4.4.2.5. Summary of compressional deformation within the TCB

Regions of highly tilted and uplifted basement associated with 1) coincident offsets in the Moho, 2) thickening of oceanic crust, and 3) in some cases, large adjacent drag folds provide strong evidence of thrust tectonics within the TCB. Furthermore, the development of buckle folds is compatible with these observations of compressional tectonics.

Observations of crustal thickening from Figures 4.4 - 4.7 suggest that the crust has been locally thickened from approximately 2 s TWTT to, from north to south, 3.5 s, 4.0 s, 3.7 s, and, before significant erosion, 3.3 s TWTT. This thickening is very similar to a crustal thickness measurement of 3.6 s TWTT (converted here to TWTT assuming a crustal velocity of 6.5 km/s) performed by Coffin et al., (1986), which sits between the observed thrusts on seismic lines tz3_3600 (west) and tz4_3300, and independently confirms the observations from seismic reflection data.

This similar level of crustal thickening across each of the thrust structures, with an apparent continuity between seismic observations; consistent west vergence of thrust structures; and alignment of all thrust structures along a SSE trending gravity anomaly that also follows other gravity lineaments within the TCB (Figure 4.1) suggest that the observed thrusting within the TCB may all form part of a single structure. This structure, which we term the Tanzania Coastal Basin thrust belt (TCBtb), runs from at least 5.5°S to 7.8°S along a SSE trend, spanning over 250 km. This makes the TCBtb, to the best of our knowledge, the longest intraplate oceanic thrust complex known on the globe. Its SSE trend, similar to the Rovuma Transform Margin, spreading lineaments of the TCB, and strike-slip faults related to initial plate separation in Madagascar, in conjunction with evidence for the reactivation of sub-vertical faults during thrusting and termination of an extinct MOR segment against this structure suggests that the TCBtb developed along a pre-existing fracture zone in the oceanic lithosphere of the TCB.

Buckle folds that have developed alongside the TCBtb have short wavelengths, between 35 and 40 km. As the wavelength of buckle folds in oceanic lithosphere is strongly dependent on the age of the lithosphere, where younger lithosphere results in shorter fold wavelengths, the compression of the TCBtb must have occurred < 3 Myr after of the formation of the buckled crust (McAdoo and Sandwell, 1985). This may account for the cessation of buckle folding on the east of the TCBtb with increasing lithospheric age to the south of the extinct MOR. The appearance of buckle folds to the west of the TCBtb yet farther south may therefore indicate an approach towards an offset MOR segment, which lay in the vicinity of the present day DFZ.

The distance between the abandoned MOR of the northern TCB (Figure 4.3), and the northernmost observed buckle folding along line tz1_4000 (west; Figure 4.4), is ~80 km. Assuming a palaeospreading rate of ~ 20 mm/y (half rate; Phethean et al., Section 2), a rough relative age of this crust may be calculated, which is ~ 4 Myr older than the extinct MOR. This suggests that the compression of this basin predated and overlapped the abandonment of spreading. Due to several assumptions made during this calculation (i.e. wavelength of folding not affected by decoupling along thrusts, constant spreading rate before extinction, etc.), however, we prefer to simplify this finding to say that the compressional event and extinction of the MOR occurred at roughly the same time.

As changes in plate motion can lead to the build-up of transpressional stress along fracture zones (Section 4.1), which is seen in the TCB, we propose that the plate motion change near the end of the Jurassic (e.g. Chapter 2; Reeves et al., 2016) may have been the ultimate cause of compression along the TCBC. This change may have also resulted in the extinction of MOR segments incompatible with the new spreading direction, accounting for the contemporaneity of compression and MOR extinction. The absence of a sedimentary record of the compressional event along the southern TCBtb, despite the presence of sediments equivalent to those that record such a compression farther north along this structure, suggests diachronous cessation of compression from south to north.

4.4.3. The DFZ

The DFZ forms the eastern boundary of the TCB, and is readily recognisable in free-air gravity data as an arcuate low gravity anomaly, which spans from just offshore Kenya at ~5°S, to the southwestern tip of Madagascar at -25°S (Figure 4.1). This large-offset fracture zone separates the Jurassic oceanic crust of the TCB from the younger crust of the central WSB. The DFZ developed in response to a change in plate motion from NNW-SSE spreading to ~N-S spreading near the end of the Jurassic, after which East Gondwana was translated southwards along this major transform fault (e.g. Chapter 2; Reeves et al., 2016). To the north of the WSB's spreading centre, which was abandoned when Madagascar reached its present day latitude at ~125 Ma, the DFZ experienced a variable cumulative offset along its length. This is due to the cessation of transform motions following the southward passage of the MOR, which means that the cumulative dextral offset along the DFZ to the north of the extinct spreading centre increases from north to south.

4.4.3.1. Line tz1_4000 (east)

Near the northern limit of the TCB, just to the south of the Davie-Walu Ridge, line tz1_4000 (east) crosses the DFZ (Figure 4.8). Smooth or hummocky top basement reflections and high amplitude Moho reflections define crustal thicknesses of between 1.5 s and 2.4 s TWTT in regions of undeformed crust. To the west of the DFZ, within the TCB, the crust has been folded and buckled, sometimes in association with offsets in the top of the basement and Moho. High amplitude convex downward reflections, which are also present beneath the level of Moho reflections, are aligned with basement offsets and the steepening of crustal folds. Above the basement, sedimentary deposits that correlate with syn-deformational sediments elsewhere along line tz1_4000 (west; i.e. Figure 4.4), show both onlap and toplap relationships, and diverge into the trough of the central fold. In the centre of this trough, a small step up in the basement occurs moving east and above this the layered reflections of the sedimentary package has been disrupted. Both of the edges of the disrupted region dip to the east, but the eastern edge propagates farther through the stratigraphy than the western, which is onlapped by later deposits. East of this, a block of uplifted crust in the shape of an inverted triangle sits adjacent to a small basin on the east, and is shown in detail in Figures 4.8c and d. The western edge of this crustal block is defined by reflections in the mid crust which become more steeply dipping downwards, and may align with the offset in the top of the basement along the eastern edge of the disrupted sediments. The eastern edge of the block is defined by the termination of top basement and mid-crustal reflections from the east, and may also steepen downwards to align with an offset of Moho reflections. An erosion surface, truncating the sedimentary packages that overlie the uplifted block, bounds local deposits to the east of the block, which have a high amplitude reflectivity (Figure 4.8c and d). Above this erosion surface, sedimentary deposits onlap the palaeobathymetric high, and a small normal fault has developed along the edge of the uplifted block. East of the uplifted block, the Moho locally deepens before flattening to the east, and the top basement surface does the same. This crust, to the east of the DFZ, shows a slightly more seismically transparent nature than crust to the west, and, away from the DFZ, remains at a relatively consistent depth.

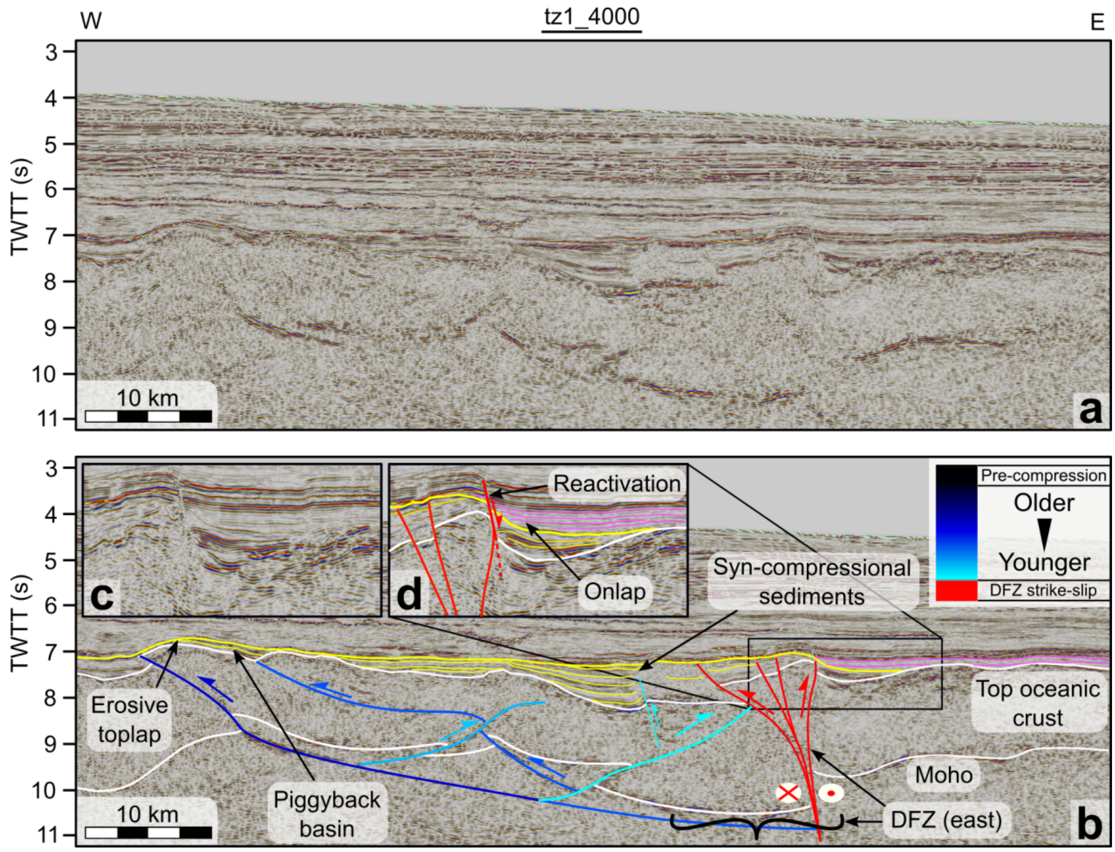

Figure 4.8. Folding, thrusting, and strike slip deformation along seismic line tz1_4000 (east) in response to compression and development of the DFZ. (a) Uninterpreted section. (b) Interpreted section. (c) Close up of the inset region without interpretation. (d) Close up of the inset region with interpretation. Line descriptions are as for Figure 4.4, and pink lines depict the structure of the post-deformation sequences. The relative ages of the faulting are shown in the key and continuation of the structures at depth is speculative. Location shown in Figure 4.1.

The thickness of the crust, and smooth high amplitude top basement reflections, indicate an oceanic nature of the basement in this region. To the west of the DFZ, within the TCB, the folding of crust and offsets in the top basement and Moho reflections are similar to observations along the TCBtb. In Figure 4.8, as along the TCBtb, buckle folding and thrusting have accommodated compressional deformation, resulting in some crustal thickening, particularly around the DFZ. The tightening of the folding to the west of the DFZ, resulting in the deepening of the central syn-deformation basin, is coincident with a convex downward reflector in the mid crust, and is likely influenced by a propagating thrust. The western edge of the band of disrupted stratigraphy in the middle of this basin is coincident with an offset in the top of the basement, and likely results from back thrusting along a large Moho-offsetting thrust. The matching tops of divergent sedimentary packages here, and syn-compressional stratigraphies elsewhere in the north of the TCB, suggests that compression occurred at the same time here as farther west around the northern TCBtb.

The western fault boundary of the uplifted triangular block crosscuts the entire overlying syn-compressional sedimentary sequence, and is therefore one of the latest structures to form in this region. The downward steepening of these reverse faults is characteristic of positive flower structure geometries that develop during transpression, suggesting strike-slip deformation across this structure. These observations are consistent with satellite gravity data that suggest that the DFZ passes through this region, and the change in the character of the oceanic crust across the strike-slip zone further supports the presence of a major crustal discontinuity. Crust to the east of the DFZ has, therefore, only been accreted adjacent to the DFZ following the passing of the MOR and cessation of strike-slip deformation. The very limited and localised deposition of sediments below the erosional surface bounding the syn-deformation sedimentary packages on the east of the DFZ (Figure 4.8c and d) suggests that this crust formed after, or at a similar time to, the cessation of compressional deformation. It is likely that these localised deposits were sourced from the eroding DFZ flower structure, and rapidly deposited in new accommodation space being generated at the passing spreading centre. In this case, the intercalation of these sediments with volcanic deposits at the MOR may have resulted in their high amplitude nature, and the loading of this zero-age crust may have contributed to the local subsidence and depression of the Moho. Following this, further loading of this crust by post-compressional sediments, which onlap the unconformity bounding the syn-deformation sediments, and thermal subsidence may have resulted in the partial reactivation of the DFZ as a normal fault (Figure 4.8d).

4.4.3.2. Line tz3_3600 (east)

75 km to the south, line tz3_3600 (east) crosses the DFZ and two other deviations of the top basement interface (Figure 4.9). At the western end of the section, the top basement, upper crustal reflections, and a band of less reflective mid-lower crust dip to the west, defining a small (~15 km) fold, which uplifts the top basement at its crest by 0.2 s TWTT. The top of

this fold is onlapped by the syn-compressional sediments identified to the west (i.e. Figure 4.5). The available data do not constrain the continuation of this package to the east; however, there is little evidence that it continues to the east of the DFZ, with the possible exception of local deposits as seen in Figure 4.8. Just east of the fold, the crust, which has a thickness of approximately 2.3 s TWTT, has flat top basement and Moho reflections until near the DFZ. At this point, a thickening of the crust to 3.2 s TWTT occurs as the top basement becomes tilted to the west and the Moho dips to the east, and the reflective nature of the upper crust becomes subdued. On the other side of the DFZ, the opposite occurs, returning the crust to a normal thickness.

Beneath, and to the east, of the DFZ, straight low-angle reflections of low-mid amplitude are common in the crust and mantle. Within the crustal thickening of the DFZ, however, a high amplitude convex downward reflector dips to the west, and may coincide with an offset in the Moho. The upper termination of this reflector coincides with the downward continuation of an east dipping reflector that steepens downwards.

Crust to the east of the DFZ shows a generally consistent thickness, with flat Moho and top basement interfaces spanning ~50 km. The eastern limit of this flat crust is defined by an offset in the top of the basement down to the east and an ~3 km wide inverted triangular trough, containing flat-lying reflective material, which separates it from more flat-lying oceanic crust to the east.

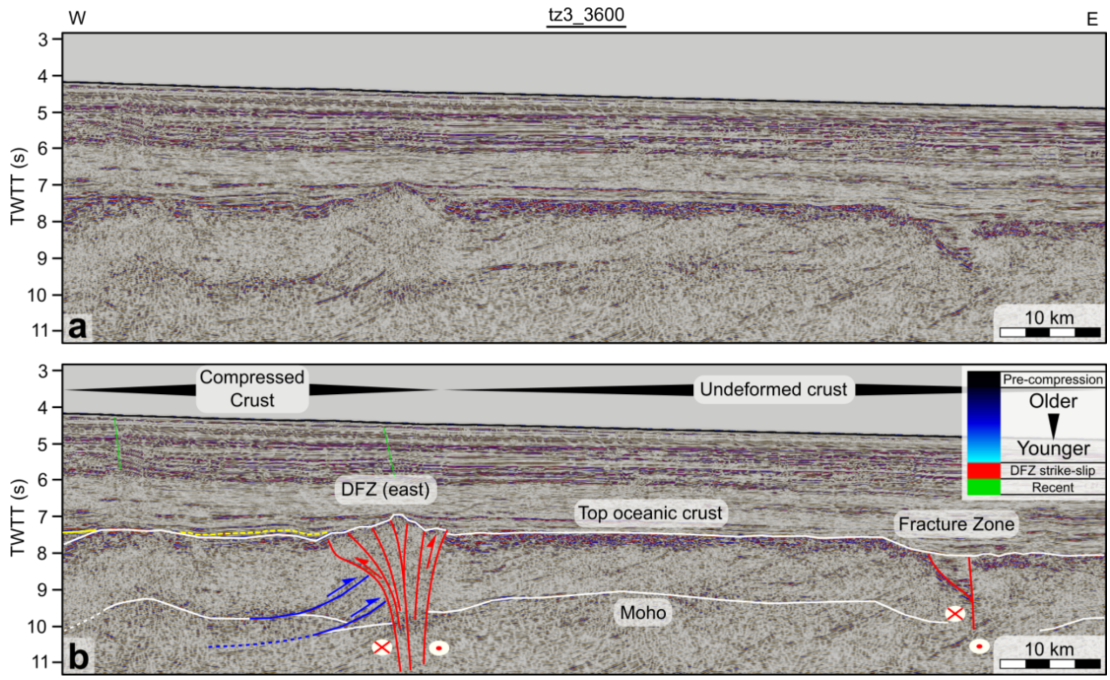

Figure 4.9. Folding, thrusting, and strike slip deformation along seismic line tz3_3600 in response to compression and development of the DFZ. (a) Uninterpreted section. (b)

Interpreted section. Line descriptions are as for Figure 4.4, where the dashed yellow line is the inferred top of syn-compressional sediments. The relative ages of the faulting are shown in the key. Location shown in Figure 4.1.

The small fold at the western end of the profile, with a slightly uplifted crest, is to the west of the DFZ, and therefore within the TCB. The same compressional event that resulted in the thrusting and folding of the basement elsewhere within the TCB may, therefore, have also generated this fold structure. The wavelength of the fold is shorter than other buckle folds seen within the TCB, and may have been influenced by a propagating thrust fault, as thought to result in tighter folds elsewhere within the TCB. The lack of clear Moho reflections, however, precludes the determination of any Moho offsets that would confirm this interpretation. The oceanic crust adjacent to this fold has a thickness typical of that elsewhere in the TCB, at ~2.3 s TWTT, and does not appear to have been thickened. Approaching the DFZ, however, the tilting of the crust and the presence of high amplitude convex downward reflections, which may correspond to sheared crust and the sheared crust-mantle boundary, suggest that east verging thrusts have developed in this location and contribute to the crustal thickening of the DFZ. The truncation of these thrusts by later faults that steepen downwards and have contributed to the uplift of the top basement interface suggests that a positive flower structure developed at a later stage in response to an increasing strike-slip component of deformation here. These steeply dipping strike-slip faults may have destroyed the initially reflective structure of the upper oceanic crust within the DFZ.

To the east of the DFZ, the flat oceanic crust has a thickness of ~1.8 s TWTT, typical for the oceanic crust of the WSB (Coffin et al., 1986). This crust shows no sign of compressional deformation, despite the transpression experienced locally along the DFZ here, and farther north along line tz1_4000 (east). This suggests that this crust formed later than both the compressional episode that affected the TCB and the transpression along the DFZ, and is consistent with its accretion on the north of the MOR in the WSB.

As line tz3_3600 (east) is oriented perpendicular to the palaeo-spreading direction of the WSB, and would therefore be expected to crosscut fracture zones related to oceanic spreading, the step down in the top of the oceanic crust farther east and accompanying basin likely represent a locally transtensional fracture zone that developed between spreading segments of the WSB.

4.4.3.3. Line tz4_3350

Approximately 80 km farther south, seismic line tz4_3350 images both the DFZ and the SSE trending TCBtb as they come into proximity (Figure 4.10). At the western edge of the section, the basement has been uplifted to ~6.5 s TWTT, above the adjacent crust at 7.7 s TWTT, and forms part of the TCBtb. On the eastern flank of the TCBtb, an ~0.2 s TWTT offset in the top basement uplifts crust to its east. This offset may align with east dipping reflections in the mantle via a disrupted zone of Moho reflectivity, across which the Moho is possibly offset, and weak east dipping reflections within the crust. In the same location, mid and low amplitude reflections in the crust and mantle, respectively, may be aligned and dip to the west, but are not associated with any resolvable offset. In this western region of Figure 4.10, clear top basement and Moho reflections and a seismically transparent mid crust define an oceanic crustal thickness of ~1.7 s TWTT. Moving eastwards, the crust thickens to 2.7 s TWTT and mid-crustal reflectivity increases. The top basement and Moho reflections form a bulbous shape, similar to that which forms the DFZ (east) farther north. This thickened crust contains several prominent crosscutting reflections, dipping to both the east and west, which may align with hummocks in the top of the basement. This crustal thickening is offset to the west of the trend of the DFZ (east) by ~20 km.

East of the thickened crust, a sharp onset of chaotic and high amplitude reflections in the top of the crust and seismic transparency in the mid-lower crust occurs across a sub-vertical boundary, which possibly also connects offsets in the top basement and Moho. East of this boundary, a clear Moho reflection defines the base of flat lying oceanic crust. The top of this crust lies at a depth of 7.7 s TWTT and has a thickness of 1.8 s TWTT. This crustal strip, with a width of approximately 10 km, loses its character to the east beneath an intruded sill, which disrupts imaging of the basement structures. A rise in the top basement to 7.5 s TWTT, however, is imaged just to the east of the sill. This basement uplift has a width of between 10 and 15 km, similar to the bulbous crustal thickening to the west and the DFZ (east) to the north (i.e. Figure 4.9). It is also aligned with the trend of the DFZ (east) as derived from lines tz1_4000 and tz3_3600. Beneath, and on either side of, the uplifted top basement interface, mid-crustal reflections bend upwards before terminating against boundaries that possibly steepen downwards. To the east of this uplifted basement, an intruded sill complex obscures detailed investigation of the basement structures.

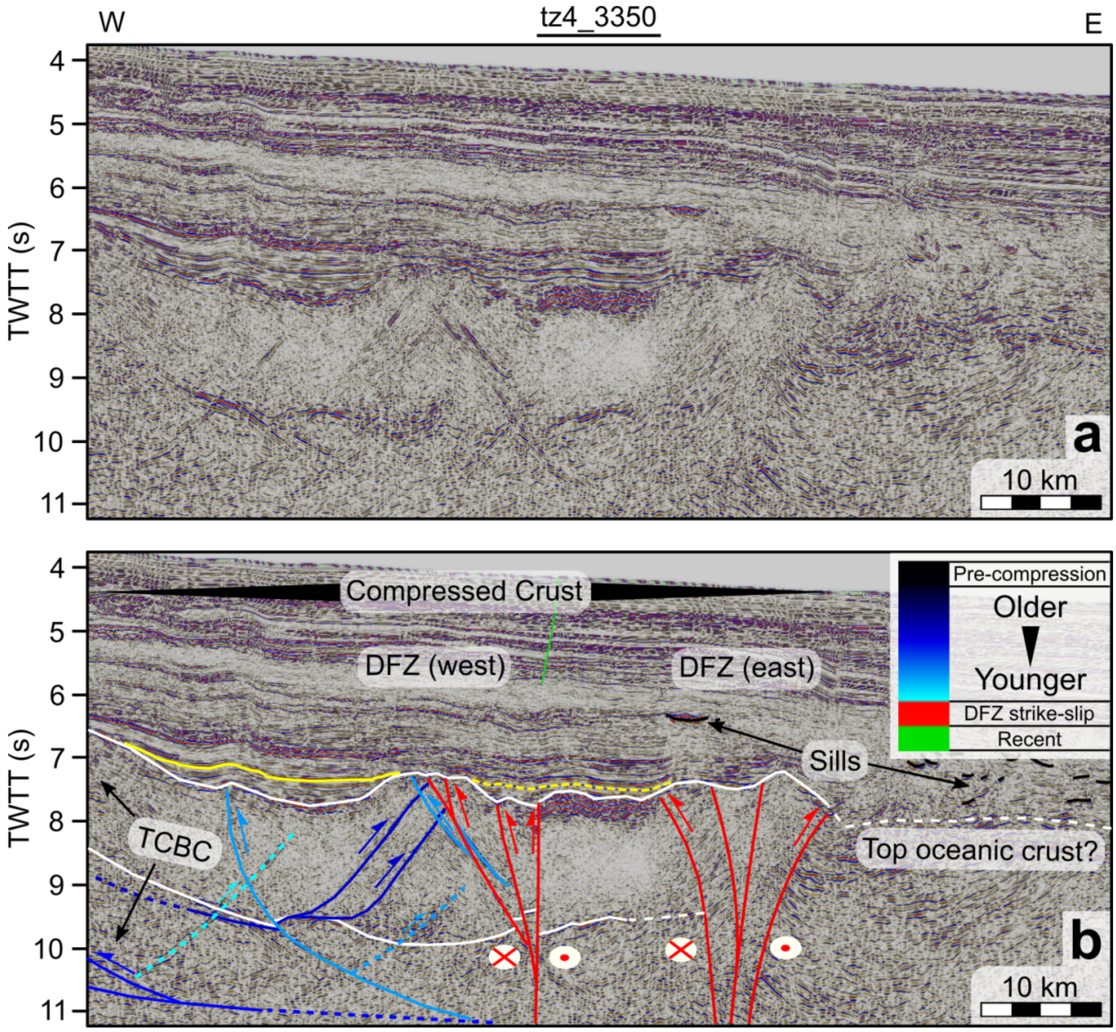

Figure 4.10. Folding, thrusting, and strike slip deformation along seismic line tz4_3350 in response to compression and development of the DFZ. (a) Uninterpreted section. (b) Interpreted section. Line descriptions are as for Figure 4.4, where the top of the syn-compressional sediments is now interpreted to correlate with the top of deformed sediments on lines tz1_4000 (west) and tz3_3600 (west) and the dashed yellow line is inferred. The relative ages of the faulting are shown in the key. Location shown in Figure 4.1.

The TCBtb, at the western edge of Figure 4.10, has a similar geometry to the TCBtb in Figure 4.6, located 10 km to the south, and likely formed in a very similar way. The top basement offset in its flank, coincident with dipping reflections in the crust and mantle and a possible offset in the Moho, likely developed in response to a west verging thrust. As this structure does not offset crosscutting, east verging reflections, it likely developed at an earlier stage. The bulbous crustal thickening in the western half of Figure 4.10 contains dipping reflections that may be coincident with hummocks in the top of the basement, and likely results from thrusting of the crust, similar to that seen along line tz3_3600 (east). Possible offsets of the dipping reflections may indicate a time progression of thrusting. Sub-vertical faults, offsetting the basement and bounding areas of different crustal characteristics, likely separate the crustal thickening from undeformed crust to the east and offset earlier thrusts. The steepness of these faults and inconsistent offsets of Moho and top basement interfaces along them indicate a strike-slip nature. These faults may therefore form part of a transform system related to, but offset from, the DFZ (east), which we therefore term the DFZ (west). 20 km to the east, the second crustal thickening, with reflections possibly dragged upwards into it along downward steepening faults, likely forms part of the DFZ (east). This is supported by its similar positive flower geometry and alignment with the trend of this structure. The two branches of the DFZ are separated by a thin 10 km strip of undeformed oceanic crust.

4.4.3.4. Line tz4_2850

Another 110 km to the south, the DFZ nearly intersects the TCBtb (Figure 4.11). In the west, folded top basement and Moho interfaces are separated by a seismically transparent mid crust. This oceanic crust has a thickness of 1.8 s TWTT. The eastern termination of the fold is marked by the termination of upper crustal reflectivity and mid crustal seismic transparency along a sub-vertical boundary. A sudden flip in the dip angle of the top basement, which is also possibly upthrown on the east, occurs just above this and lies along the trend of the TCBtb. In this location, beneath the west dipping top basement, short, segmented mid-crustal reflections also dip to the west.

To the east by ~10 km, the top basement interface and internal reflections of the crust are segmented and folded on a short (~1-3 km) length scale. Beneath this and to the east, segmented and offset Moho reflections, which dip to the east before reversing to dip to the west, define the base of a bulbous or lens-shaped thickening of the crust. Several offsets and hummocks in the top of the basement also define this crustal thickening, which in places reaches a thickness of ~2.4 s TWTT. This structure lies ~20 km to the west of the trend of the DFZ (east), and, as seen farther north, therefore likely represents the DFZ (west). Along the trend of the DFZ (east), a second lens-shaped segment of thickened crust is present, likely representing this fracture zone. Along the top basement interface of the DFZ (east), variations in reflector amplitude, dip, and continuity, occur. Below this, reflections which dip into the central region of the DFZ (east) may align with some of these variations in the top of the basement. Between the two regions of thickened crust, the structure of the basement is obscured by sills intruded into the overlying sediments, which precludes a determination of the crustal thickness in this region. East of the DFZ (east), within the WSB, strong top basement reflections are underlain by a reflective crustal layer, below which a high amplitude reflector, possibly the Moho, defines a thin (~1.1 s TWTT) oceanic crust.

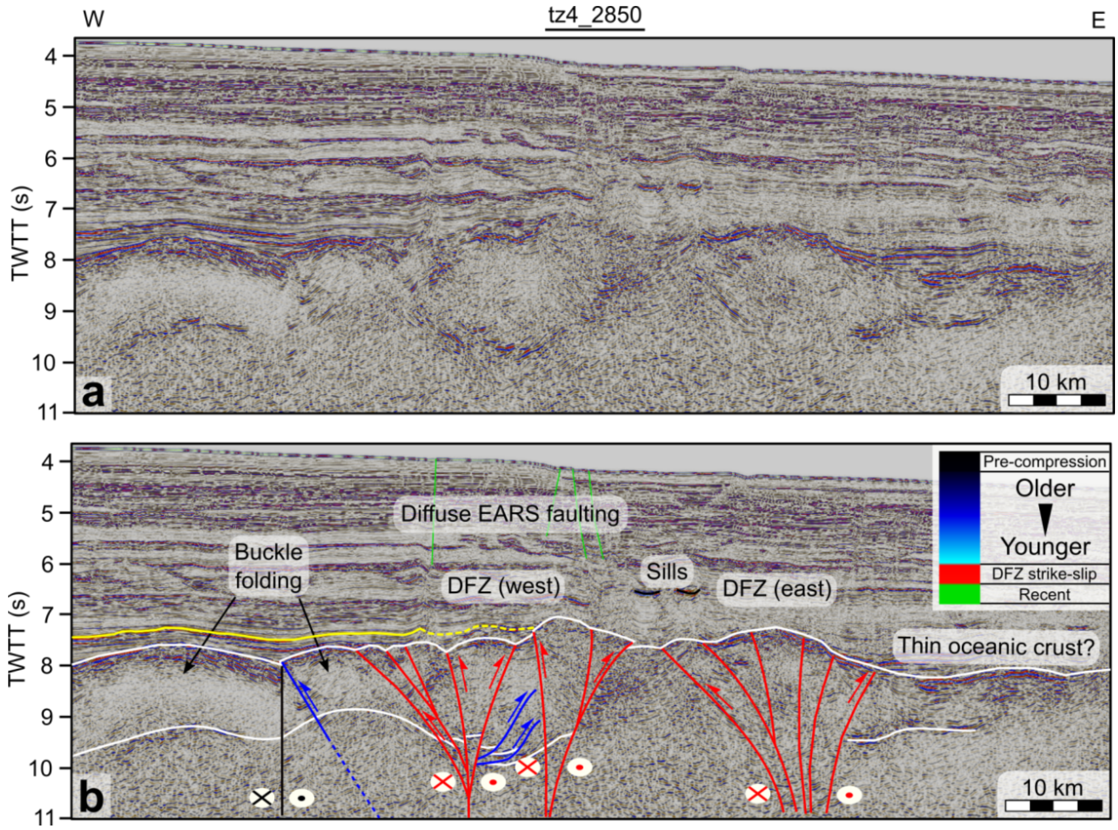

Figure 4.11. Folding, thrusting, and strike slip deformation along seismic line tz4_2850 in response to compression and development of the DFZ. (a) Uninterpreted section. (b) Interpreted section. Line descriptions are as for Figure 4.4. The relative ages of the faulting are shown in the key. Location shown in Figure 4.1.

In the western part of Figure 4.11, the sudden change in the dip of the top basement at the eastern end of the fold suggests a decoupling of the fold from crust to the east. This may have occurred along the sub vertical boundary between zones of different crustal reflectivity, and/or east dipping thrust faults, which may have also offset and folded the top basement interface and mid crustal reflections. These thrust faults lie along the trend of the TCBtb and likely form part of this structure. Here, however, at this southern limit of the TCBtb, very little crustal thickening has occurred. This is consistent with an earlier cessation of compression in the south, as inferred from the deformation of sedimentary packages overlying the TCBtb (i.e. Section 4.4.2.5), which would result in less crustal thickening in this southern location. The presence of a buckle fold to the west of the TCBtb, is consistent with earlier observations of a swap from the development of buckles on the east of the TCBtb in the north to on the west in the south, likely related to the age of the crust before deformation.

Slightly to the east, the folded and offset segments of crust that form part of the DFZ (west) may be bounded by discontinuities that dip towards the centre of the lens-shaped area of thickened crust, defining a positive flower structure. In the central region of the DFZ (west), thrust faults, which stack and thicken the crust, may also present. In this interpretation, these gently dipping faults have been cut by later, steeper, strike-slip faults, consistent with the onset of strike-slip deformation after thrusting, as inferred elsewhere along the DFZ (e.g. tz3_3600 (east)). The DFZ (east), which likely also forms a positive flower structure, is again offset from the DFZ (west) by ~20 km, suggesting that these features run parallel to each other. This is confirmed by observations made at several other locations as summarised in Figure 4.1.

4.4.3.5. Line tz3_2101

Line tz3_2101 intersects the DFZ some 215 km to the south of the previous line. It is located to the south of the extinct spreading centre of the WSB (Chapter 2), and shows elements of the Quirimbas Graben (Franke et al., 2015). This recent extension is related to the East African Rift System and overprints deformation associated with the DFZ (Figure 4.12). Nonetheless, at the western edge of the section beneath the Quirimabas Graben, top basement reflections are identifiable and step down to the west across normal faults. Approximately 20 km from the western edge of Figure 4.12, normal faulting becomes reduced and a horst structure forms a relatively uplifted area of seafloor. Beneath the horst, segmented, but high amplitude, basement reflections define a generally domed shape of the top basement, which sits nearly along the trend of the DFZ (west). To the east, a subsidiary basin separates this basement dome from a second region of uplifted basement, which sits at depths as shallow as 5.3 s TWTT, as much as 1.7 s TWTT above the surrounding basement. Beneath this basement uplift, which sits nearly along the trend of the DFZ (east), a diffuse band of east dipping, mid-high amplitude, reflections sits at a depth of ~6.9 s. Below this, at depths of 9.3 s and 9.8 s TWTT, other reflections also dip gently to the east or lie sub-horizontal. These may define an offset in the Moho, which has been upthrown on the east. Inspection of crosslines to tz3_2101 along the western edge of this uplifted crust reveals that the faults, with a generally E-W strike, bend northwards as they approach the western edge of the uplift.

To the east of this belt of crustal thickening, top basement and Moho reflections have been folded, and define a buckle fold with a wavelength of ~50 km that has developed in the oceanic crust. Near the eastern edge of Figure 4.12, a step up in the top of the basement is aligned with a high amplitude east dipping reflector in the mid crust.

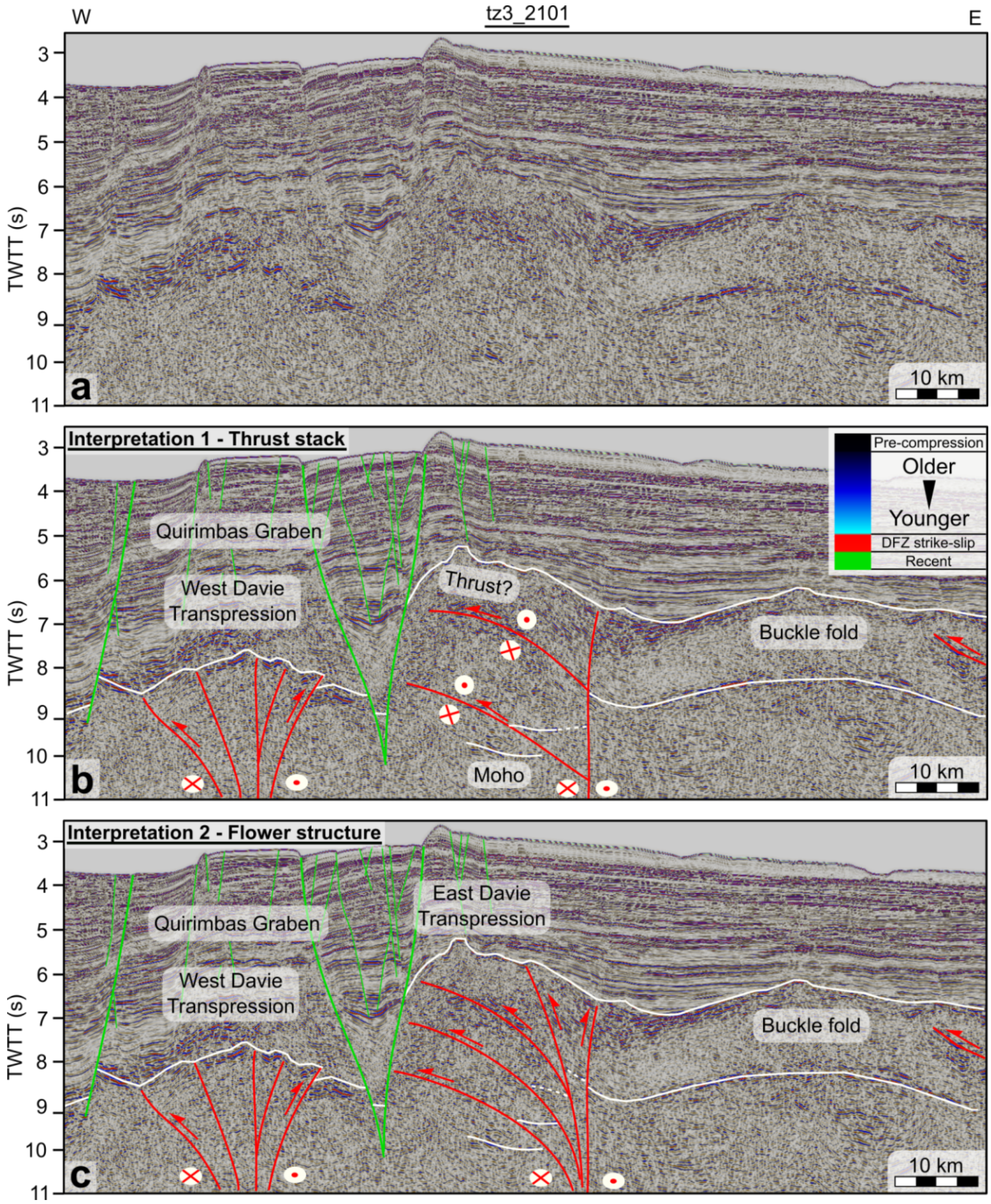

Figure 4.12. Folding, thrusting, and strike-slip deformation along seismic line tz3_2101 in response to compression and development of the DFZ, and graben formation in response to extension across the Quirimbas Graben. (a) Uninterpreted section. (b) Interpreted section based on the transportation of thrust sheets along the strike of the DFZ (east). (c) Interpreted section based on flower structure development along the DFZ (east). Line descriptions are as for Figure 4.4. The relative ages of the faulting are shown in the key. Location shown in Figure 4.1.

The uplift of the top basement beneath the horst block within the Quirimbas graben is not wholly accounted for by the reduced extension across this structure, and may therefore indicate a relative thickening of the crust in this region. To the east, top basement and Moho reflections record a crustal thickening to 4.7 s TWTT, more than twice the original crustal thickness. Allowing for 5 – 12 km of recent extension across the DFZ (Franke et al., 2015), the two regions of thickened crust in Figure 4.12 are closely aligned with the trends of the large offset DFZ (east) and DFZ (west), suggesting that they are the southern continuations of these structures.

The geometry of the top of the basement around the DFZ (west) is consistent with a compressional flower structure, as seen elsewhere along this fracture zone. The amount of crustal thickening recorded at the DFZ (east), however, is greater than anywhere else along this structure. Eastward dipping reflections within the crust and an offset in the Moho imply a general tilting of the crust to the east due to east dipping compressional faults. The detailed nature of the crustal structure is, however, not well constrained by the data, and in Figure 4.12 b and c, we therefore present two scenarios that are consistent with the main observations. Interpretation 1 (Figure 4.12b) employs a sequence of stacked thrusts sliding along each other, into the plane of Figure 4.12, to achieve greater than twice the original crustal thickness in this location. Interpretation 2 (Figure 4.12c) employs steeper faults, within a large flower structure, to achieve a similar effect.

The cause of this possible change in style and amount of crustal thickening in this location may be revealed by the presence of E-W trending faults that bend northwards as they approach the western boundary of the DFZ (east). Ordinarily, normal faults generated at an oceanic spreading centre near to a MOR transform offset bend in the direction of the adjacent spreading centre (Davies et al., 2005). This is caused by a rotation of σ_1 on approach to the transform fault due to the local influence of opposing plate motions across the fault. Within the WSB, MOR segments have a left lateral offset (e.g. Cochran, 1988; Chapter 2), and the adjacent MOR segment across the DFZ lies in the Mozambique basin. Ordinarily, therefore, faults within the WSB adjacent to the DFZ should bend to the south, opposite to the observed trend. Faults that develop along the borders of transpressional stepover basins, however, can show the opposite trend (e.g. (McClay and Bonora, 2001)). A step to the east, when moving south along the DFZ (east), would result in such a transpressional push-up structure, with faults within the WSB bending to the north adjacent to the DFZ (east). The large offset across the DFZ would likely supply a large amount of crust into this transpressional zone, allowing a large amount of observed crustal thickening. Both low-angled thrusts and steep faulted flower structures have been shown to develop under such transpressional conditions from analogue modelling (e.g. McClay and Bonora, 2001), and it is likely that a combination of these structures, from both Figure 4.12b and c, contributed to the crustal thickening of the DFZ (east).

Recent extension across the Quirimbas Graben is localised along the flanks of the DFZ (east and west), and likely reactivates these structures, resulting in the development of a horst above the DFZ (west). The northward termination of extension associated with the Quirimbas Graben coincides with the extinct MOR system of the WSB. It is possible, therefore, that coupling across the DFZ to the north of the Quirimbas Graben due to the passing of a spreading centre and associated magmatism stopped the extensional reactivation of the DFZ farther north.

East of the DFZ, a buckle fold and thrust fault, which results in a step in the top of the basement on the east flank of the fold, have developed. These observations oppose those from farther north along the DFZ, where to the east of the DFZ (east), the oceanic crust shows little sign of compressional deformation. Figure 4.12, however, is located to the south of the MOR system of the WSB, which may provide an explaination for the observed compressional deformation in this location. To the north of the MOR, no relative motion occurrs across the DFZ subsequent to the formation of adjacent oceanic crust. To the south of the MOR, however, this is no longer true. Oceanic crust accreted to the south of the MOR, and adjacent to the DFZ, formed part of the East Gondwana plate. This crust will have, therefore, subsequently undergone a protracted history of transportation along the transpressional DFZ, until the final cessation of spreading in the WSB at ~125 Ma. This transpression may have resulted in the observed buckle folding and compressional deformation of Figure 4.12. Transpression of this crust would have begun immediately after its formation at the MOR, and is consistent with the short 50 km wavelength of the buckle fold, which must have formed in extremely young oceanic lithosphere.

4.4.3.6. South of the Quirimbas Graben

To the south of the Quirimbas Graben, gravity modelling and investigation of seismic reflection lines mz1_8100, mz1_8000, and mz1_7500, has been performed in Chapter 3 (Figures 3.5 and 3.11). Along line mz1_8100, The DFZ is obscured by the St Lazare volcanic edifice, but lines mz1_8000 and mz1_7500 are clear of volcanics, and allow for an investigation of basement structures associated with the DFZ. Along the trend of the DFZ (east), line mz1_8000 displays a thickening of the crust from 2 s TWTT to 2.5 s TWTT. To the west of the DFZ (east), a zone of possible exhumed mantle exists, which may result in the lack of observed crustal thickening along the trend of the DFZ (west). The amount of crustal thickening along the DFZ (east) is similar to observations along the northern DFZ, and the large amount of crustal thickening observed along line tz3_2101, possibly associated with a transpressional stepover basin along the DFZ (east), does not continue to this point. 380 km to the south of this, line mz1_7500 displays a well-developed positive flower structure along the approximate trend of the DFZ (west), and a 20 km wide zone of 3.3 s TWTT thick crust has developed. However, 20 km to the east no evidence for strike-slip tectonics along the trend of the DFZ (east) is present and instead a thrust fault, which offsets the Moho, thickens the crust in this location.

The Rovuma Transform Margin (Figure 4.1, dark green symbols) has also been identified along these three seismic and gravity profiles (Chapter 3), and runs in a SSE direction. It is aligned with the Davie Compression (Figure 4.1, red circles), a SSE trending fold and thrust belt composed predominantly of Jurassic and basement rocks (Mahanjane, 2014; Figures 4.13a, b, and c). The natural prolongation of the large offset Rovuma Transform Margin into the trend of the Davie Compression (Figure 4.1), suggests a genetic relationship between these two features, and we propose that the Davie Compression forms the transform continent-ocean boundary along the eastern edge of the Angoche basin.

To the east of the SSE trending Davie Compression, the Davie Ridge, an ~N-S trending prominent basement high which generally protrudes 2-3 s TWTT above the surrounding basement (Figure 4.13a and b), forms the natural extension of the DFZ farther north (Figure 4.1). This uplifted basement structure has previously been interpreted as a rift shoulder uplift (e.g. Mahanjane, 2014), similar to the uplifted flanks of the Quirimbas Graben farther north. However, dredge samples recovered from the DFZ show a metamorphic P-T path associated with compressional tectonics, (Bassias, 1992). The geometry of the Davie Ridge, visible in published seismic sections (e.g. Mahanjane, 2014), shares characteristics with thrusts observed along the TCBtb. To the east of the Davie Ridge, flexure of the basement has led to the development of a sedimentary basin and, approaching the ridge, the top basement is bent upwards towards the uplifted basement. An erosion surface has developed along the top of the highly rotated basement of the Davie Ridge, and possibly bounds syn-compressional sediments deposited in the adjacent basin (Figure 4.13.a and b). This is similar to the geometries that developed along the TCBtb in response to compressional flexure, thrust faulting, and associated fault drag folding. We therefore tentatively suggest that the Davie Ridge may, in fact, be composed of oceanic crust and meta-sediments, compressed and uplifted by thrusting. If the Davie Ridge is such a thrust structure, it likely developed in response to the compressional stresses that led to the development of the Davie Compression, or during the compression near the end of the Jurassic, when this crust may have been attached to East Gondwana, conjugate to the compressed crust within the TCB.

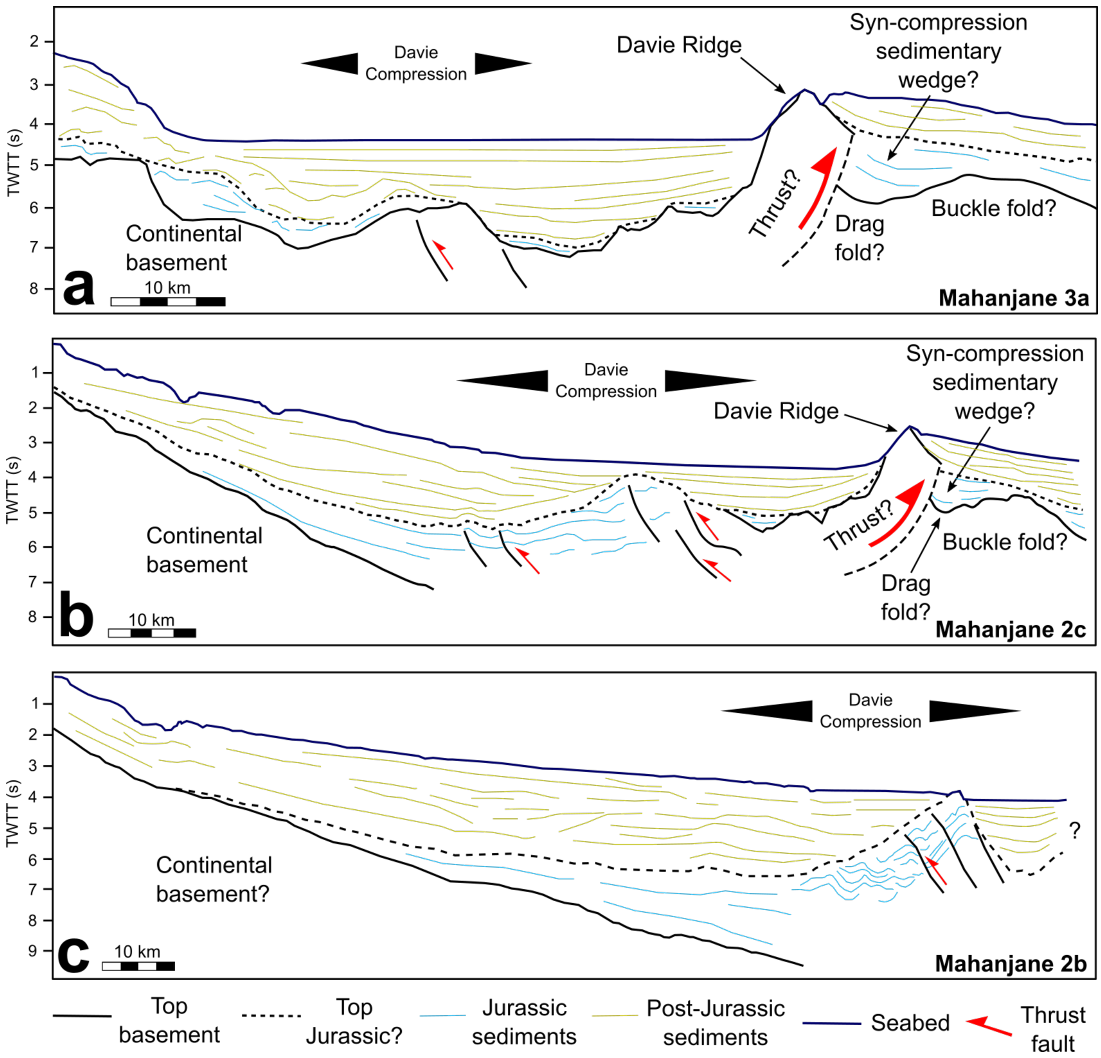

Figure 4.13. Line drawings of seismic reflection data from Mahanjane (2014), which have been re-interpreted in this study. (a) Figure 3a of Mahanjane (2014). (b) Figure 2c of Mahanjane (2014). (c) Figure 2b of Mahanjane (2014). Location shown in Figure 4.1.

4.4.3.7. Summary of the DFZ formation

Bounding the eastern edge of the TCB and the Mozambique Basin, the DFZ appears as a 2000 km arcuate free-air gravity low between -5°S and -25°S (Figure 4.1), following a single small circle with the pole of rotation at 10.15 S, 74.30 E. Our interpretation of seismic reflection data supports the presence of steep strike-slip faults and transpressional flower structures along the DFZ, and different tectonic crustal histories on either side of the DFZ. This combined evidence supports the interpretation of this structure as a large-offset fracture zone along which East Gondwana was transported southwards. Along the majority of the DFZ, crustal thickening, generally to ~2.8 s TWTT, but possibly of up to 4.7 s TWTT, results from thrusting and the development of transpressional flower structures. Faults associated with strike-slip motion and flower development generally cut older thrust faults, possibly reflecting a shift from compression to transpression over time. In general, deformation along the DFZ has been dominated by transpression throughout its history, and little evidence for transtension is present.

Along most of the length of the WSB, the DFZ is comprised of a pair of transpressional fracture zones, which run parallel to each other from 7°S to just below the Comoros Islands c. 13°S. North and south of these latitudes, evidence for strike-slip motion only exists along the trends of the DFZ (east) and DFZ (west), respectively, with a termination of strike-slip deformation along the trend of the other DFZ branch. The northern termination of the DFZ (west), however, lies at the intersection of a SSE trending fold and thrust belt within the TCB (Figure 4.1). Given that SSE trending thrust belts within the TCB seem to have developed along pre-existing fracture zones, the initiation of the DFZ (west) at an intersection with such a thrust belt may indicate a genetic link between these two structures. In the south, along the trend of the DFZ (east) on line mz1_7500, the presence of a thrust, but no indication of strike-slip motion, may suggest a similar termination of the DFZ (east) into a pre-existing SSE trending FZ. Whether such a join between the DFZ and SSE trending fracture zones occurred gradually, through the formation of arcuate fracture zones, or suddenly, through the development of crosscutting faults, is not constrained by the available data. However, the lack of bending of the southern TCBtb into the DFZ suggests that any previous fracture zone in this location was cut by the DFZ, rather than merging with this structure. This is supported by the extinction of the MOR to the NE of the TCBtb (Figure 4.3), suggesting a sudden abandonment of the spreading configuration, as opposed to a gradual change in spreading directions, which might have allowed this spreading centre to remain active.

Formation of the DFZ, whether gradual or sudden, resulted from a change in plate motion near the end of the Jurassic (e.g. Reeves et al., 2016; Chapter 3), when an alignment between the obliquely rifted northeast Mozambique margin and southern Morondava margin occurred (Figure 4.14). To the north of these juxtaposed margins, plate tectonic modelling (e.g. Phethean et al., 2016) predicts a series of left-stepping spreading centres running north-south, close to the eastern edge of the present day TCB. The presence of an extinct MOR segment near to the DFZ in the north of the TCB, and the occurrence of short wavelength buckle folds, which are associated with young (< 3 Myrs) oceanic crust, close to the DFZ on the SW side of the TCBtb, is consistent with this prediction. This alignment of weak rifted margins and young oceanic lithosphere (Figure 4.14) may have influenced the timing of the plate rotation, and the location of the DFZ development. The plate rotation, near the end of the Jurassic, likely resulted in transpression along incompatible fracture zones in the TCB, and presents a possible driving mechanism for the compression seen there. Development of the DFZ, which was compatible with the new plate motion, however, would remove this driving mechanism of compression within the TCB. As the sedimentary record along the TCBtb suggests an earlier cessation of compression along the south of this structure, compared to north, it may also be the case that the DFZ developed from the south, propagating northwards to form the edge of the TCB.

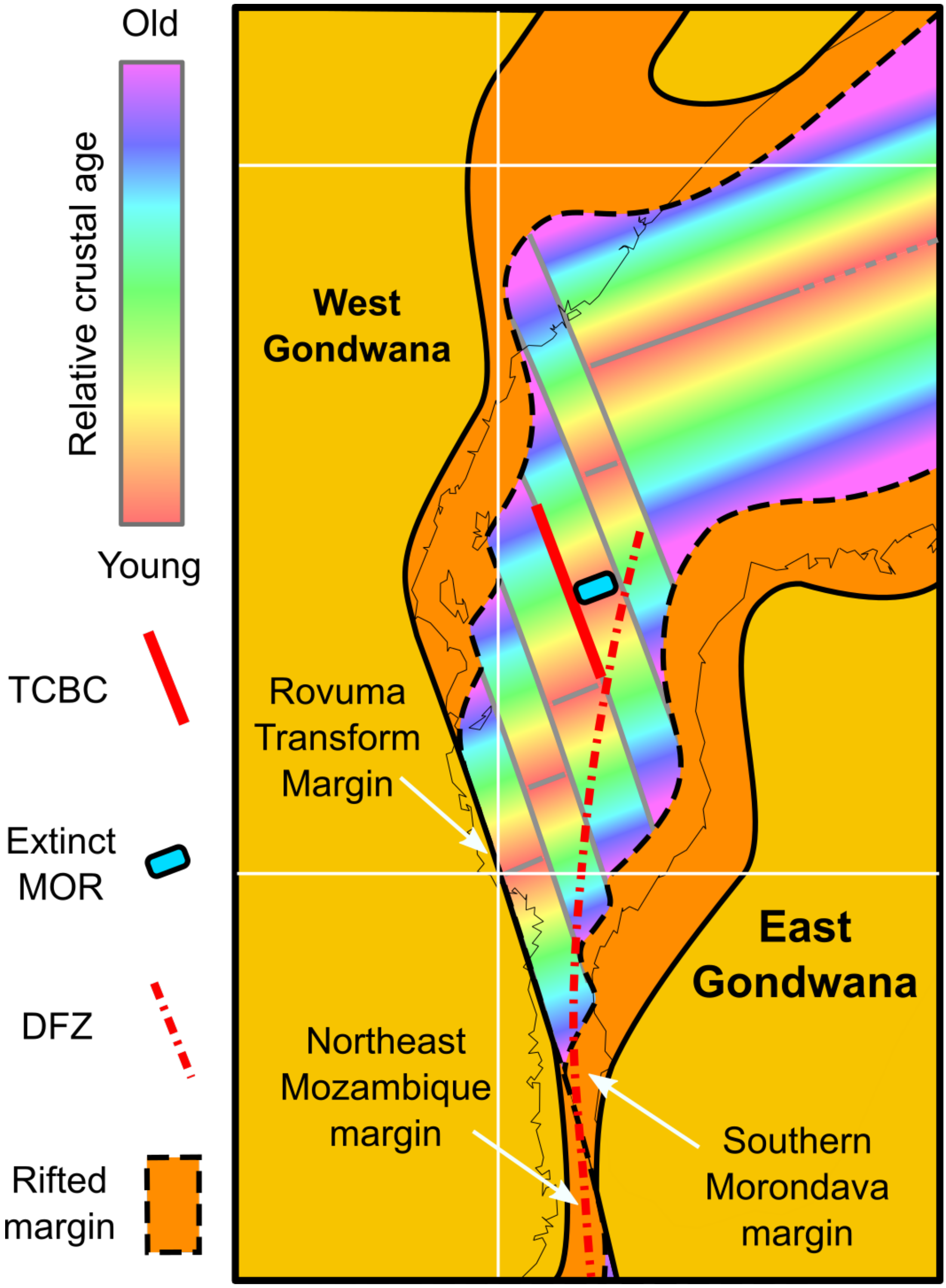

Figure 4.14. Plate configuration around the end of the Jurassic. Transformation of East Gondwana along the Rovuma Transform Margin has led to the alignment of the southern Morondava and north-east Mozambique oblique rifted margins, and release of East Gondwana from the constraints of strong lithosphere along this transform boundary. A contemporaneous alignment of young oceanic crust to the north may have influenced the location at which the DFZ developed.

4.5. Regional tectonic interpretation

Observations of compression within the TCB, followed by strike-slip and transpression along the DFZ, likely result from the change in plate motions of East Gondwana relative to West Gondwana during plate separation. These observations are, therefore, tied to this broader regional tectonic context below:

- Following a tight initial fit of Madagascar within Africa (Section 4.3), rifting between East and West Gondwana began at ~182 Ma (Figure 4.15a; Geiger et al., 2004), coincident with the eruption of the Karoo large igneous province in Mozambique (e.g. Riley and Knight, 2001). This resulted in oblique margin formation along northeastern Mozambique and the Southern Morondava Basin in Madagascar (Chapter 3).
- Following continental breakup at ~170 Ma (e.g. Chapter 2), an initial phase of SSE plate separation translated Southern Madagascar (attached to East Gondwana) along the Rovuma Transform Margin of Northern Mozambique (Figure 4.15a-b; Chapter 3). Due to the large offset of the Angoche Basin and Tanzania Coastal Basin across the Rovuma Transform Margin (Chapter 3), these basins are unlikely to have overlapped and were, therefore, likely connected by transform faults at the onset of rifting (Section 1.2.2.1). This means no rifting of the lithosphere along the Rovuma Transform Margin would have occurred prior to strike-slip motions, maintaining the thickness and strength of this lithosphere.
- At ~150 Ma, an alignment of the obliquely rifted margins of northeastern Mozambique and the Southern Morondava Basin occurred across the Rovuma Transform Margin (Figure 4.15b). Around this time, MOR segments to the north within the TCB were also aligned with these opposed rifted margins (Figure 4.14). The timing of this alignment, near the end of the Jurassic, was coincident with a change in plate motion from SSE to N-S, (Figure 4.15b-c) and it is possible that the alignment of weaker lithosphere, along the rifted margins and MOR segments, influenced this change.
- This new southerly plate motion was incompatible with SSE trending fracture zones within the TCB, and resulted in the build-up of transpressional deformation along these structures (Figure 4.15c), leading to thrusting of oceanic crust along pre-existing fracture zones and short wavelength buckle folding of young (<3 Ma) oceanic crust (Figure 4.15d). The extinction of spreading centres within the TCB at the same time as the onset of compression was probably ultimately caused by this change in spreading direction. A prediction of this model, which may be tested in

future as more widespread data becomes available, is that this compressional event will have also affected the Jurassic oceanic crust to the west and northwest of Madagascar, which at the time was attached to East Gondwana.

- This compression, which continued for longer in the north of the basin, was most likely ended by the development of the DFZ, which propagated northwards and accommodated the new plate motion (Figure 4.15e). This fracture zone was, nonetheless, dominated by transpression throughout its history.
- Subsequent to the formation of the DFZ at ~ 150 Ma, the southward drift of East Gondwana led to the overlap of the East and West Gondwana plates across the southern Rovuma Transform Margin (Figure 4.15f), and thus the collision of south Madagascar with the obliquely rifted margin of northeast Mozambique (red area, Figure 4.15f). The Davie Compression, a thrusted and inverted sequence of Jurassic and basement rocks along the eastern edge of the Angoche Basin (Mahanjane, 2014), likely resulted from this plate collision (Figure 4.15g), and may therefore represent the continent-ocean boundary in this region. The Davie Ridge, which may be a highly rotated oceanic thrust, may have also developed during this collision. This is supported by the metamorphic P-T paths from along this structure, which show a pattern generally associated with collisional settings (Bassias, 1992).

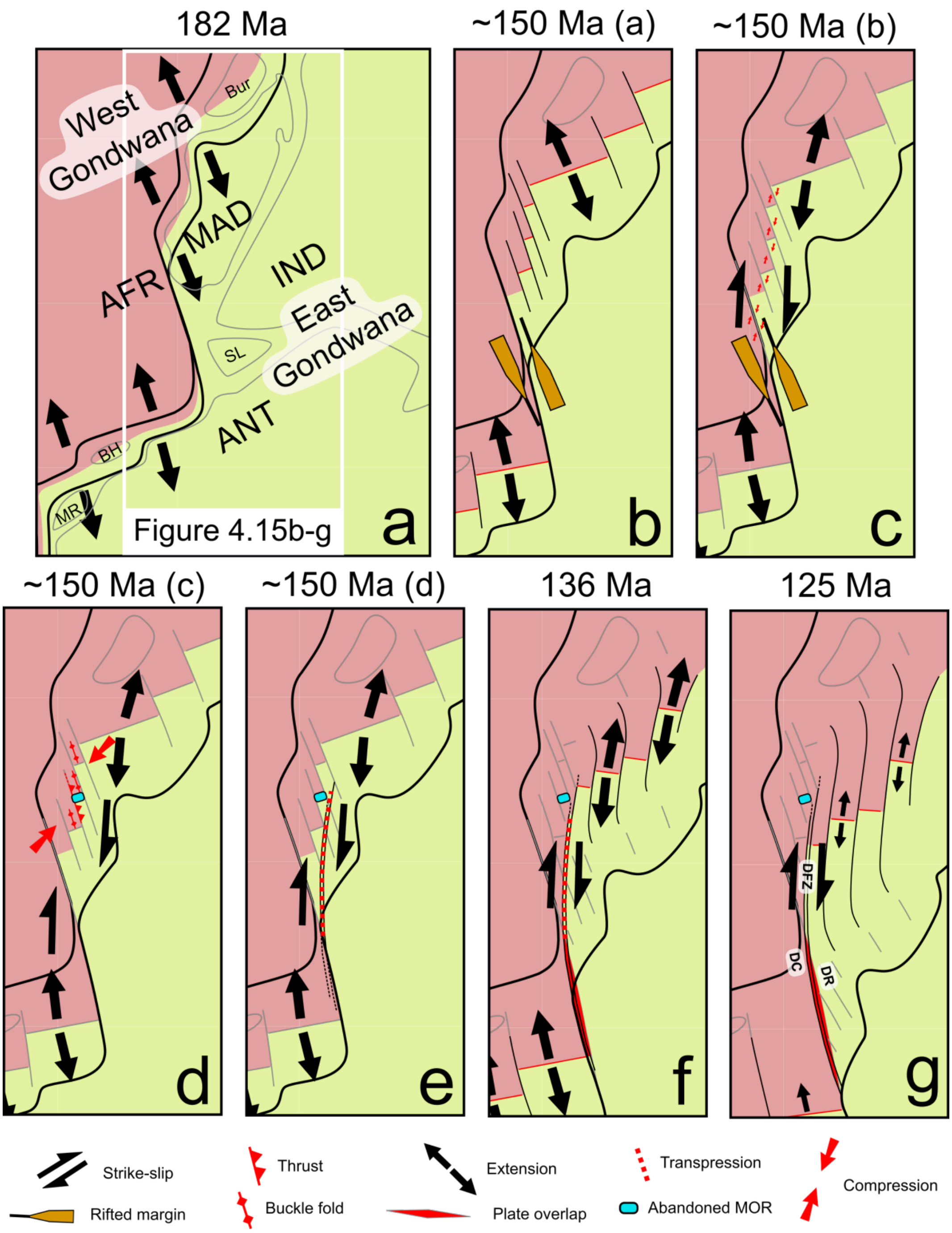

Figure 4.15. Plate tectonic model showing the change in plate motion between West Gondwana (pink) and East Gondwana (green) at ~ 150 Ma, possibly influenced by the alignment of rifted margins offshore Mozambique and Madagascar, and of MOR segments in the north. This plate motion change may have resulted in compression within the TCB, extinction of MOR segments within the TCB, and development of the DFZ. Subsequently, the collision of southern Madagascar with the oblique rifted margin of northeast Mozambique during the southward drift of East Gondwana may have led to the development of the Davie Compression and Davie Ridge. AFR, Africa; ANT, Antarctica; BH, Biera

High; Bur, Bur High; DC, Davie Compression; DR, Davie Ridge; IND, India; MAD, Madagascar; MR, Mozambique Rise; SL, Sri Lanka.

4.6. Implications for plate motion controls

Plate motions are classically inferred to be controlled by a number of driving forces originating from the lithosphere and mantle, including: mantle convection (e.g. Ziegler, 1993); slab-pull (Lithgow-Bertelloni, 2014); ridge-push (e.g. Mahatsente and Coblentz, 2015); orogenic collapse (e.g. Rey et al., 2001); and mantle plumes (e.g. Larson, 1991). The largest change in plate driving forces within the basins surrounding Gondwana was the onset of subduction along the NeoTethys. However, this was before the Late Jurassic change in plate motions (Stampfli, 2000). The diachronous subduction of the NeoTethys spreading ridge, however, may have still been occurring at the time of plate motion changes (e.g. Stampfli and Borel, 2002). However, the sharp change in spreading direction, indicated by the cutting of the TCBtb by the DFZ, would be unlikely to have been generated by this gradual subduction process. In contrast, the alignment of the obliquely rifted northeast Mozambique margin and Southern Morondava margin with young oceanic spreading centres farther north occurred relatively rapidly, and at the moment of plate motion change. Furthermore, following plate rotation and the formation of the DFZ, this large-offset fracture zone was dominated by transpression throughout its history, suggesting it did not form in perfect alignment with plate driving forces.

We therefore argue that this change in plate motion was not ‘driven’ by alterations to plate driving forces, but was partly the consequence of a reduction in resisting forces along the Rovuma Transform Margin. This reduction was the caused by the alignment of weak, rifted and/or young, lithosphere along the N-S trend of the future DFZ, which provided a new alternate pathway for East Gondwana that was more, but not perfectly, compatible with plate driving forces. In this case, prior to the end of the Jurassic, the driving forces required for a more southerly drift of East Gondwana would have already been active, but were resisted by plate boundary forces along the strong Rovuma Transform Margin, resulting instead in the slip of East Gondwana along the trend of this margin. This would have led to transpression along the Rovuma Transform Margin, and so structural investigations along this margin could be used to test this model.

4.7. Conclusions

A change in the plate motion of East Gondwana near the end of the Jurassic from SSE to southwards drift led to build-up of transpressional forces along SSE trending fracture zones within the TCB. This resulted in the onset of compressional tectonics within this basin, including the development of the SSE trending TCBtb, possibly along a pre-existing fracture zone, and short wavelength buckle folds, possibly associated with young oceanic crust in proximity to MOR segments. At the same time, the extinction of spreading centres within the TCB likely also resulted from the change in spreading direction. This model for the onset of compression within the TCB predicts that crust that lay conjugate to the TCB, now situated offshore northern and western Madagascar, would also have been affected by compression, allowing it to be tested when data becomes available in these regions.

The onset of this plate motion change was coincident with the passing of southern Madagascar beyond the strong lithosphere of the Rovuma Transform Margin and the alignment of weak and/or young lithosphere, associated with rifted margins and oceanic spreading centres, along the future trend of the DFZ. This reduction in lithospheric strength may have triggered the change in plate motion and would imply first-order control of resisting forces along transform plate boundaries on the motions of plates during the dispersal of Gondwana. In this case, prior to the change in plate motions, the Rovuma Transform Margin may have been under transpression; therefore, structural analyses of this margin could test this hypothesis.

The development of the DFZ likely ended compression within the TCB, and the earlier cessation of compression in the south of the basin, as compared to the north, may represent a south to north propagation of the DFZ along what was to become the eastern boundary of the TCB. The subsequent drift of East Gondwana along this 2000 km fracture zone was dominated by transpression, and led to the collision of southern Madagascar with the oblique rifted margin of northeast Mozambique, forming the Davie Compression, which may represent the continent-ocean boundary in this region. The Davie Ridge, which may be a rotated oceanic thrust, may have also developed during this collision.

4.8. References

Anderson, D.L., 2001. Plate Tectonics as a Far- From- Equilibrium Self-Organized System. Plate Bound. Zo. doi:10.1029/GD030p0411

Bassias, Y., 1992. Petrological and geochemical investigation of rocks from the Davie fracture zone (Mozambique Channel) and some tectonic implications. J. African Earth Sci. 15, 321–339. doi:10.1016/0899-5362(92)90018-8

Bécel, A., Shillington, D.J., Nedimović, M.R., Webb, S.C., Kuehn, H., 2015. Origin of dipping structures in fast-spreading oceanic lower crust offshore Alaska imaged by multichannel seismic data. Earth Planet. Sci. Lett. 424, 26–37. doi:10.1016/j.epsl.2015.05.016
Behn, M.D., Ito, G., 2008. Magmatic and tectonic extension at mid-ocean ridges: 1. Controls on fault characteristics. Geochemistry, Geophys. Geosystems 9. doi:10.1029/2008GC001965
Besairie, H., 1964. Carte Géologique de Madagascar, Service Géologique de Madagascar, scale 1:1000000.
Briggs, S.E., Cartwright, J., Davies, R.J., 2009a. Crustal structure of the deepwater west Niger Delta passive margin from the interpretation of seismic reflection data. Mar. Pet. Geol. 26, 936–950. doi:10.1016/j.marpetgeo.2008.07.003
Briggs, S.E., Davies, R.J., Cartwright, J., Morgan, R., 2009b. Thrusting in oceanic crust during continental drift offshore Niger Delta, equatorial Africa. Tectonics 28, 1–16. doi:10.1029/2008TC002266
Burbank, D.W., Vergés, J., 1994. During Active Thrusting. J. Geophys. Res. 99, 20281–20297.
Cloetingh, S., Beekman, F., Ziegler, P.A., van Wees, J.-D., Sokoutis, D., 2008. Post-rift compressional reactivation potential of passive margins and extensional basins. Geol. Soc. London, Spec. Publ. 306, 27–70. doi:10.1144/SP306.2
Cochran, J.R., 1988. Somali Basin, Chain Ridge, And Origin Of The Northern Somali Basin Gravity And Geoid Low. J. Geophys. Res. 93, 11985–12008. doi:10.1029/JB093iB10p11985
Coffin, M.F., Rabinowitz, P.D., Houtz, R.E., 1986. Crustal structure in the Western Somali Basin. Geophys. J. R. Astron. Soc. 331–369.
Davies, R.J., MacLeod, C.J., Morgan, R., Briggs, S.E., 2005. Termination of a fossil continent-ocean fracture zone imaged with three-dimensional seismic data: The Chain Fracture Zone, eastern equatorial Atlantic. Geology 33, 641–644. doi:10.1130/G21530.1
Franke, D., Jokat, W., Ladage, S., Stollhofen, H., Klimke, J., Lutz, R., Mahanjane, E.S., Ehrhardt, A., Schreckenberger, B., 2015. The offshore East African Rift System: Structural framework at the toe of a juvenile rift. Tectonics 34, 2086–2104. doi:10.1002/2015TC003922
Geiger, M., Clark, D.N., Mette, W., 2004. Reappraisal of the timing of the breakup of Gondwana based on sedimentological and seismic evidence from the Morondava Basin, Madagascar. J. African Earth Sci. 38, 363–381. doi:10.1016/j.jafrearsci.2004.02.003
Hardy, S., Ford, M., 1997. Numerical modeling of trishear fault propagation folding. Tectonics 16, 841–854. doi:10.1029/97TC01171
Harper, G.D., 1985. Tectonics of slow spreading mid-ocean ridges and consequences of a variable depth to the brittle/ductile transition. Tectonics 4, 395–409. doi:10.1029/TC004i004p00395
Jiménez-Munt, I., Fernàndez, M., Vergés, J., Afonso, J.C., Garcia-Castellanos, D., Fullea, J., 2010. Lithospheric structure of the Gorringe Bank: Insights into its origin and tectonic evolution. Tectonics 29, 1–16. doi:10.1029/2009TC002458
King, S.D., Lowman, J.P., Gable, C.W., 2002. Episodic tectonic plate reorganizations driven by mantle convection. Earth Planet. Sci. Lett. 203, 83–91. doi:10.1016/S0012-821X(02)00852-X
Larson, R.L., 1991. Geological consequences of superplumes. Geology 19, 963–966. doi:10.1130/0091-7613(1991)019<0963:GCOS>2.3.CO
Lithgow-Bertelloni, C., 2014. Driving Forces: Slab Pull, Ridge Push BT - Encyclopedia of Marine Geosciences, in: Harff, J., Meschede, M., Petersen, S., Thiede, J. (Eds.), . Springer Netherlands, Dordrecht, pp. 1–6. doi:10.1007/978-94-007-6644-0_105-1
Louden, K.E., Osler, J.C., Srivastava, S.P., Keen, C., 1996. Formation of oceanic crust at slow-spreading rates: New constraints from an extint spreading center in the Labrador Sea. Geology 24, 771–774.
Mahanjane, E.S., 2014. The Davie Fracture Zone and adjacent basins in the offshore Mozambique Margin - A new insights for the hydrocarbon potential. Mar. Pet. Geol. 57, 561–571. doi:10.1016/j.marpetgeo.2014.06.015
Mahatsente, R., Coblentz, D., 2015. Ridge-push force and the state of stress in the Nubia-Somalia plate system. Lithosphere 7, 503–510. doi:10.1130/L441.1
Malinverno, A., 1990. A QuantitativeS tudyo f the Axial Topographyo f the Mid-Atlantic Ridge. J. Geophys. Res. 95, 2645–2660.
Mammerickx, J., Sandwell, D., 1986. Rifting of old oceanic lithosphere. J. Geophys. Res. 91, 1975. doi:10.1029/JB091iB02p01975
Massell, C.G., Coffin, M.F., Mann, P., Mosher, S., Frohlich, C., Schuur, C.L., Karner, G., Ramsay, D., Lebrun, J.-F., 2000. Neotectonics of the Macquarie Ridge Complex, Australia-Pacific plate boundary. J. Geophys. Res. 105, 13,457-13,480. doi:10.1029/1999JB900408

McAdoo, D.C., Sandwell, D.T., 1985. Folding of Oceanic Lithosphere. J. Geophys. Res. 90, 8563–8569.

McClay, K., Bonora, M., 2001. Analog models of restraining stepovers in strike-slip fault systems. Am. Assoc. Pet. Geol. Bull. 85, 233–260. doi:10.1306/8626C7AD-173B-11D7-8645000102C1865D

Morris, E., Detrick, R.S., Minshull, T.A., Mutter, J.C., White, R.S., Su, W., Buhl, P., 1993. Seismic Structure of Oceanic Crust in the Western North Atlantic. J. Geophys. Res. 98, 13879–13903. doi:10.1029/93JB00557

Müller, R.D., Smith, W.H.F., 1993. Deformation of the oceanic crust between the North American and South American Plates. J. Geophys. Res. Solid Earth 98, 8275–8291. doi:10.1029/92JB02863

Niu, Y., Hékinian, R., 1997. Spreading-rate dependence of the extent of mantle melting beneath ocean ridges. Nature. doi:10.1038/385326a0

Nunns, A.G., 1983. Plate Tectonic Evolution of the Greenland-Scotland Ridge and Surrounding Regions BT - Structure and Development of the Greenland-Scotland Ridge: New Methods and Concepts, in: Bott, M.H.P., Saxov, S., Talwani, M., Thiede, J. (Eds.), . Springer US, Boston, MA, pp. 11–30. doi:10.1007/978-1-4613-3485-9_2

Reeves, C.V., de Wit, M.J., Sahu, B.K., 2004. Tight Reassembly of Gondwana Exposes Phanerozoic Shears in Africa as Global Tectonic Players. Gondwana Res. 7, 7–19. doi:10.1016/S1342-937X(05)70302-6

Reeves, C. V, Teasdale, J.P., Mahanjane, E.S., 2016. Insight into the Eastern Margin of Africa from a new tectonic model of the Indian Ocean. Geol. Soc. London, Spec. Publ. 431, 1–24. doi:10.1144/SP431.12

Rey, P., Vanderhaeghe, O., Teyssier, C., 2001. Gravitational collapse of continental crust: definitions, regimes, mechanisms and modes. Tectonophysics 342, 435–449.

Riley, T.R., Knight, K.B., 2001. Age of pre-break-up Gondwana magmatism. Antarct. Sci. 13, 99–110. doi:10.1017/S0954102001000177

Sandwell, D.T., Muller, R.D., Smith, W.H.F., Garcia, E., Francis, R., 2014. New global marine gravity model from CryoSat-2 and Jason-1 reveals buried tectonic structure. Science (80-.). 346, 65–67. doi:10.1126/science.1258213

Sauter, D., Unternehr, P., Manatschal, G., Tugend, J., Cannat, M., Le Quellec, P., Kusznir, N., Munschy, M., Leroy, S., de Lepinay, J.M., Granath, J.W., Horn, B.W., 2016. Evidence for magma entrapment below oceanic crust from deep seismic reflections in the Western Somali Basin. Geology 44, 407–410. doi:10.1130/G37747.1

Schandelmeier, H., Bremer, F., Holl, H.G., 2004. Kinematic evolution of the Morondava rift basin of SW Madagascar - From wrench tectonics to normal extension. J. African Earth Sci. 38, 321–330. doi:10.1016/j.jafrearsci.2003.11.002

Schiffer, C., Peace, A., Phethean, J., Gernigon, L., McCaffrey, K.J.W., Petersen, Kenni, D., Foulger, G., In Press. The Jan Mayen Microplate Complex and the Wilson Cycle. Geol. Soc. London, Spec. Publ.

Silver, P.G., Russo, R.M., Lithgow-Bertelloni, C., 1998. Coupling of South American and African Plate Motion and Plate Deformation. Science (80-.). 279, 60–63. doi:10.1126/science.279.5347.60

Smith, D., 2013. Tectonics: Mantle spread across the sea floor. Nat. Geosci. 6, 247–248. doi:10.1038/ngeo1786

Stampfli, G.M., 2000. Tethyan oceans. Geol. Soc. London, Spec. Publ. 173, 1–23. doi:10.1144/GSL.SP.2000.173.01.01

Stampfli, G.M., Borel, G.D., 2002. A plate tectonic model for the Paleozoic and Mesozoic constrained by dynamic plate boundaries and restored synthetic oceanic isochrons. Earth Planet. Sci. Lett. 196, 17–33. doi:10.1016/S0012-821X(01)00588-X

Vauchez, A., Tommasi, A., Barruol, G., 1998. Rheological heterogeneity, mechanical anisotropy and deformation of the continental lithosphere. Tectonophysics 296, 61–86. doi:10.1016/S0040-1951(98)00137-1

White, R.S., McKenzie, D., O'Nions, R.K., 1992. Oceanic crustal thickness from seismic measurements and rare earth element inversions. J. Geophys. Res. 97, 19683–19715. doi:10.1029/92JB01749

Whittaker, J.M., Williams, S.E., Halpin, J.A., Wild, T.J., Stilwell, J.D., Jourdan, F., Daczko, N.R., 2016. Eastern Indian Ocean microcontinent formation driven by plate motion changes. Earth Planet. Sci. Lett. 454, 203–212. doi:10.1016/j.epsl.2016.09.019

Ziegler, P.A., 1993. Plate-moving mechanisms: their relative importance. J. Geol. Soc. London. 150, 927–940. doi:10.1144/gsjgs.150.5.0927

4.9. Supplementary material

4.9.1. Alternative interpretation of seismic line tz4_3300

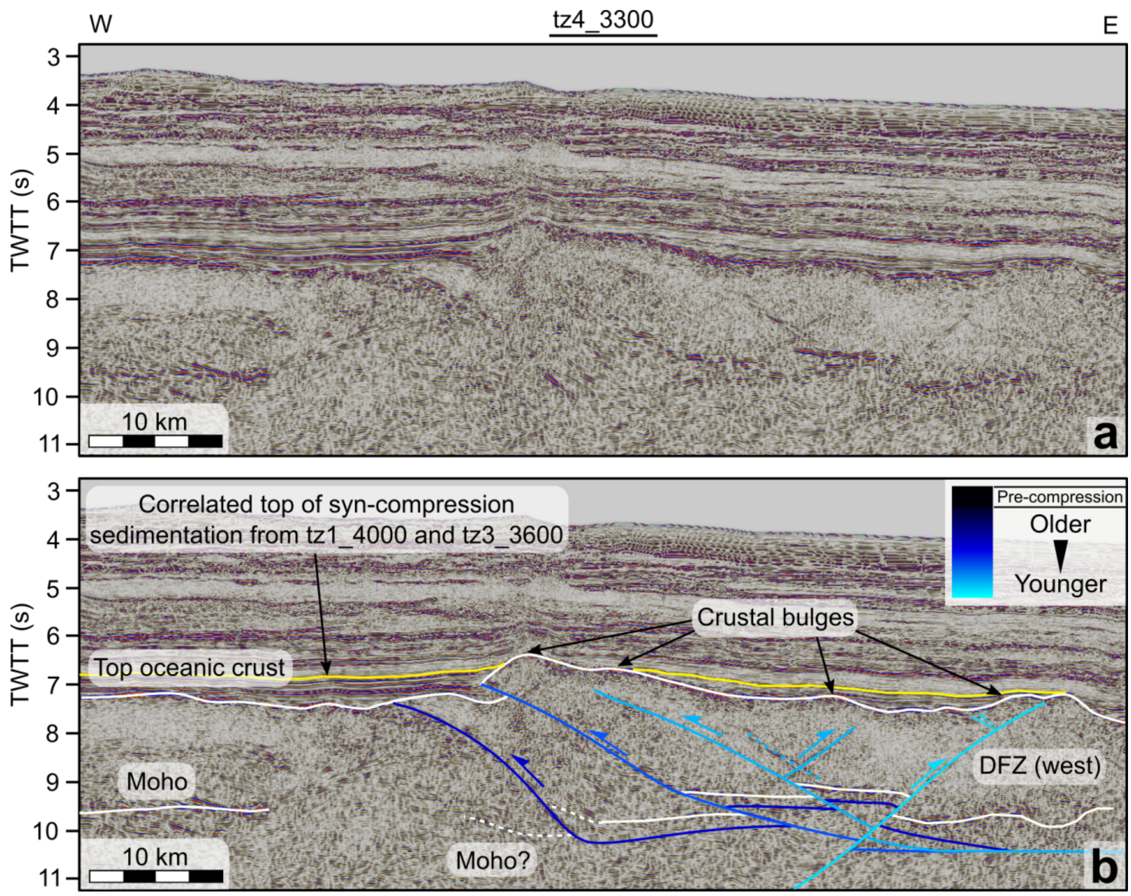

Figure S4.1. The lower of the dual bands of reflections around the level of the Moho may alternatively represent a shear boundary, which has been subsequently offset. The continuation of the structures at depth is speculative.

5. Discussion, conclusions, and future work

Plate tectonic modelling of the WSB, based on the analysis of gravity lineaments related to ocean spreading features, shows that two phases of spreading led to the development of this basin. The more recent phase, between the Late Jurassic (~150 Ma) and Aptian (~125 Ma), involved a simple north-south translation of East Gondwana along the DFZ, and has been recognised previously (e.g. Coffin and Rabinowitz, 1987; Gaina et al., 2013). The Earlier phase between Middle Jurassic (~170Ma) and Late Jurassic, however, deviates from the previous academic consensus for the region and involves a NNW-SSE motion of East Gondwana. This motion places the origin of Madagascar within the TCB, inboard of the DFZ, which is supported by the identification of oceanic crust inboard of the DFZ. The initial SSE motion also predicts the existence of a SSE trending transform margin along the Rovuma Basin (Chapter 2). Subsequent identification of the Rovuma Transform Margin using seismic and gravity methods (Chapter 3), confirms this controversial phase of NNW-SSE spreading during the Jurassic. This changes the interpretation of the DFZ, previously thought to be a continent-ocean fracture zone, to an ocean-ocean fracture zone and consequently shifts the location of the continent-ocean transition landward within the TCB. This changes our understanding of the crustal affinity within the TCB, and the hydrocarbon industry should now consider that significant portions of the TCB may be oceanic in nature. This may affect the likelihood of source rock presence in these regions and should also be taken into account during paleoheatflow modelling.

The origin of Madagascar within the TCB also supports a tight initial fit of Gondwana fragments (Chapter 2), which, combined with the newly determined initial SSE drift of East Gondwana, has large implications for the types of margins that surround the WSB. The northern margins of the WSB likely developed roughly orthogonal to the extension direction and may therefore be interpreted as rifted margins. The western margins, however, developed at an oblique angle to the extension direction and are therefore likely highly segmented and/or obliquely rifted margins (Chapter 2). Between these two margins an offset is required along the western border of the Lamu Embayment to satisfy the fit of Madagascar within this basin. The offset has a similar trend to the Rovuma Transform Margin and suggests the presence of another transform margin in this region. This is supported by the observation of strike-slip faults within the conjugate Bajocian deposits of Madagascar (Chapter 4). The formation of these different types of margin surrounding the

WSB may have been facilitated by several mechanisms suggested to assist continental rupture. The northern margins follow branches of the Karoo rift system and pre-existing lithospheric weaknesses may therefore have influenced continental breakup (e.g. Audet and Bürgmann, 2011). The western margins of the WSB and TCB also follow the pre-existing Karoo rift system, and additionally have undergone oblique rifting, both of which may have facilitated breakup (e.g. Brune et al., 2012). The Rovuma Transform Margin, however, did not follow any apparent pre-existing rift system, but was highly oblique (Chapter 3). Rifting in the Mozambique basin to the south was contemporaneous with large amounts of volcanism and, therefore, thermal weakening due to magmatism may have played an important role in facilitating continental breakup in this basin (e.g. Buck, 2007). This suggests that a collaboration of different rifting facilitators led to the breakup of Gondwana. The prolonged and episodic phase of Karoo rifting prior to volcanism in Mozambique and subsequent Gondwana dispersal may reflect this necessity for interplay of mechanisms to achieve successful supercontinent breakup (Chapter 2). Chapter 4 shows that the change in spreading direction during the Late Jurassic may have been triggered by the alignment of lithospheric weaknesses along the future trend of the DFZ. This suggests that plate motion changes are not necessarily driven by changes in bottom-up driving forces, and, consequently, that plate motions may not purely reflect such driving forces but are also subject to top-down controls on plate motion of a first-order significance (e.g. Brune et al., 2016). This questions whether observations of plate motions may be used to make inferences about dynamic processes in the mantle which are thought to drive plate tectonics, and therefore has large consequences for future academic studies in this field (e.g. Becker and Faccenna, 2011).

The change in plate motions during the Late Jurassic (Chapters 2 and 4) led to the formation of the DFZ, yet contradictory evidence exists as to whether this occurred sharply by the cutting of new faults, or gradually by the formation of curved fracture zones. Chapter 2 shows that curved gravity lineaments from the northern and southern regions of the WSB are best accounted for by a gradual plate rotation. Chapter 4, however, presents evidence for the crosscutting of a SSE trending fracture zone (the TCBtb) by the DFZ suggesting a sharp plate motion change in this region. Two important factors allow for these observations to be reconciled. Firstly, in Chapter 4, a significant amount of internal plate deformation within the TCB is also observed, which, despite local manifestation as sharp crosscutting indicators of plate motion, could allow for gradual plate motion changes away from this deformation. This emphasises the importance of introducing such internal plate deformation (e.g. Eakin et al., 2015) into future generations of plate tectonic models. Secondly, Chapter 3 contains suggestions that the recent discovery of Pan African age (533 Ma) zircons within the xenoliths of Grande Comore may indicate a microcontinent cleaving event during the Late Jurassic change in plate motions (Roach et al., 2017). Such a cleaving event would allow for a period of simultaneous ocean spreading along two overlapping MOR systems within the WSB. Whilst the same total amount of extension in the WSB would result as predicted in Chapter 2, the gradual reduction in spreading and eventual extinction of the original MOR system at the expense of increased spreading along the propagating (cleaving) MOR system would lead to the development of arcuate fracture zones and the abandonment of a triangular ocean basin (Figure 5.1; e.g. Nunns, 1983). The Comoros Basin, between the Comoros island chain and the northern margin of Madagascar, has such a triangular geometry (e.g. Figure 2.4) and this scenario is thus worthy of further investigation. Microcontinent release during such plate motion changes possibly offers a new mechanism to explain the large numbers of enigmatic microntinents being discovered within oceanic domains (e.g. Whittaker et al., 2016). These continental fragments, e.g. the recently interpreted Biera High microcontinent offshore Mozambique (e.g. Mueller et al., 2016), may offer new prospective zones for hydrocarbon exploration, and understanding their development is crucial for locating potential future resource exploration opportunities.

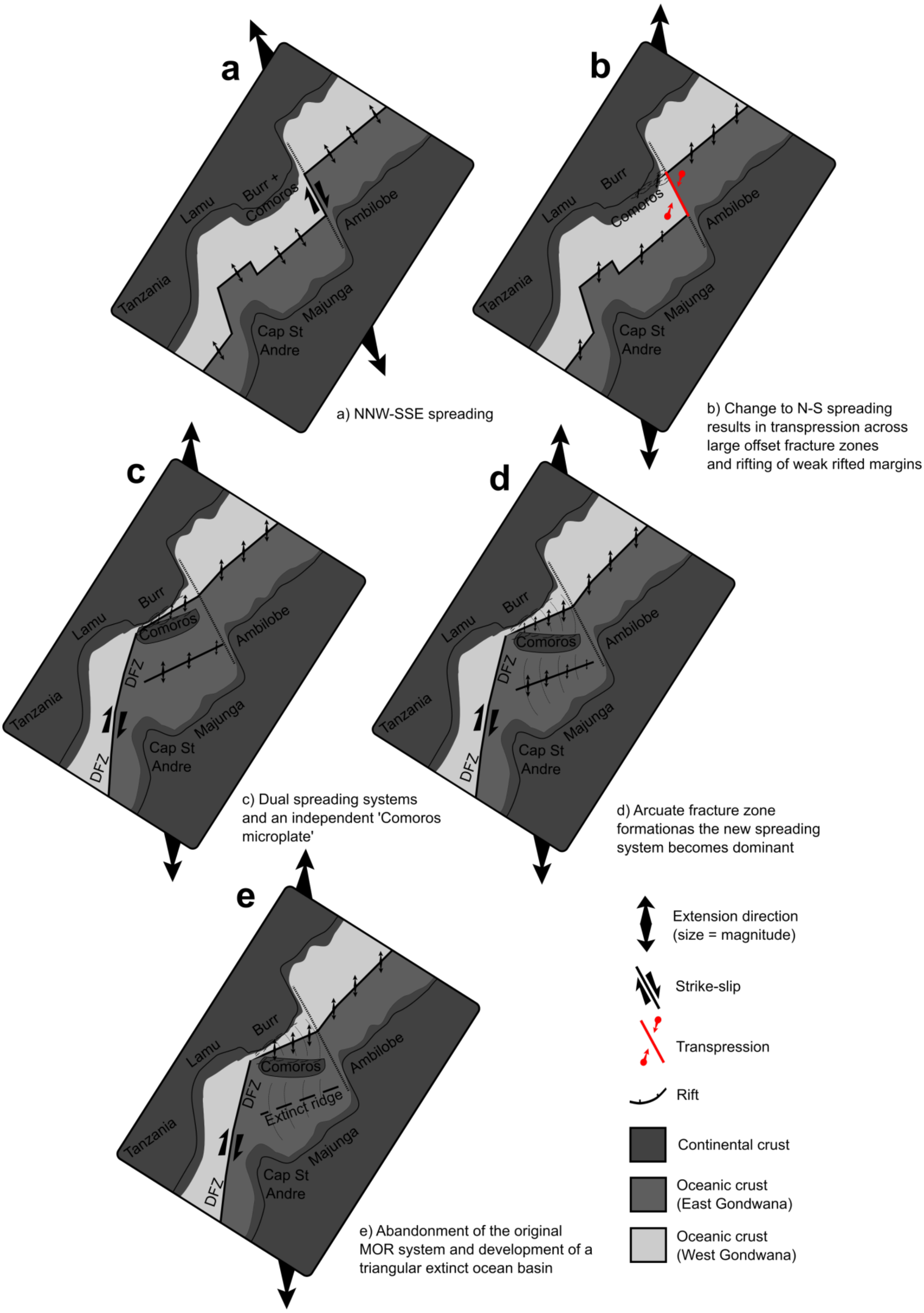

Figure 5.1. Schematic of the proposed 'Comoros Microcontinent' cleaving during the Late Jurassic change in plate motions. The sudden change in plate motion may form arcuate fracture zones due to the development of a second spreading axis which gradually takes over from the first.

5.1. References

Audet, P., Bürgmann, R., 2011. Dominant role of tectonic inheritance in supercontinent cycles. Nat. Geosci. 4, 184–187. doi:10.1038/ngeo1080

Becker, T.W., Faccenna, C., 2011. Mantle conveyor beneath the Tethyan collisional belt. Earth Planet. Sci. Lett. 310, 453–461. doi:10.1016/j.epsl.2011.08.021

Brune, S., Popov, A.A., Sobolev, S. V., 2012. Modeling suggests that oblique extension facilitates rifting and continental break-up. J. Geophys. Res. Solid Earth 117, 1–16. doi:10.1029/2011JB008860

Brune, S., Williams, S.E., Butterworth, N.P., Müller, R.D., 2016. Abrupt plate accelerations shape rifted continental margins. Nature 536, 201–204. doi:10.1038/nature18319

Buck, W.R., 2007. Dynamic Processes in Extensional and Compressional Settings: The Dynamics of Continental Breakup and Extension. Treatise Geophys. 335–376.

Coffin, M.F., Rabinowitz, P.D., 1987. Reconstruction of Madagascar and Africa: Evidence From the Davie Fracture Zone and Western Somali Basin 92, 9385–9406.

Eakin, C.M., Long, M.D., Scire, A., Beck, S.L., Wagner, L.S., Zandt, G., Tavera, H., 2015. Internal deformation of the subducted Nazca slab inferred from seismic anisotropy. Nat. Geosci. 9, 56–59. doi:10.1038/ngeo2592

Gaina, C., Torsvik, T.H., van Hinsbergen, D.J.J., Medvedev, S., Werner, S.C., Labails, C., 2013. The African plate: A history of oceanic crust accretion and subduction since the Jurassic. Tectonophysics 604, 4–25. doi:10.1016/j.tecto.2013.05.037

Mueller, C., Jokat, W., Schreckenberger, B., 2016. The crustal structure of Beira High, central Mozambique—Combined investigation of wide-angle seismic and potential field data. Tectonophysics 683, 233-254.

Nunns, A.G., 1983. Plate Tectonic Evolution of the Greenland-Scotland Ridge and Surrounding Regions BT - Structure and Development of the Greenland-Scotland Ridge: New Methods and Concepts, in: Bott, M.H.P., Saxov, S., Talwani, M., Thiede, J. (Eds.), . Springer US, Boston, MA, pp. 11–30. doi:10.1007/978-1-4613-3485-9_2

Roach, P., Milsom, J., Toland, C., Matchette-Downes, C., Budden, C., Riaroh, D., Houmadi, N., 2017. New Evidence Supports Presence of Continental Crust beneath the Comoros. PESGB, 16th African E&P Conf. London.

Whittaker, J.M., Williams, S.E., Halpin, J.A., Wild, T.J., Stilwell, J.D., Jourdan, F., Daczko, N.R., 2016. Eastern Indian Ocean microcontinent formation driven by plate motion changes. Earth Planet. Sci. Lett. 454, 203–212. doi:10.1016/j.epsl.2016.09.019